RIPARIAN WETLANDS: HYDROLOGY MEETS BIOGEOCHEMISTRY

Interactions between hydrology and biogeochemistry within riparian wetlands

Potential implications for internal biogeochemical process distributions and solute exports

Dissertation zur Erlangung des Grades Doktor der Naturwissenschaften (Dr. rer. Nat.)
an der Fakultät Biologie/Chemie/Geowissenschaften der Universität Bayreuth

Vorgelegt von
Sven Frei
Geb. am 21. Juni 1979 in Augsburg

Vollständiger Abdruck der von der Fakultät für Biologie, Chemie und Geowissenschaften der Universität Bayreuth genehmigten Dissertation zur Erlangung des akademischen Grades eines Doktors der Naturwissenschaften (Dr. rer. nat.).

Dissertation eingereicht am: 05.10.2012

Zulassung durch die Prüfungskommission: 17.10.2012

Wissenschaftliches Kolloquium: 28.03.2013

Amtierender Dekan: Prof. Dr. Beate Lohnert

Prüfungsausschuss:

Dr. Jan H. Fleckenstein (Erstgutachter)

Prof. Dr. Stefan Peiffer (Zweitgutachter)

Prof. Dr. Michael Hauhs (Vorsitz)

Prof. Dr. Bernd Huwe

Prof. Dr. Egbert Matzner

RIPARIAN WETLANDS: HYDROLOGY MEETS BIOGEOCHEMISTRY

Interactions between hydrology and biogeochemistry within riparian wetlands

Potential implications for internal biogeochemical process distributions and solute exports

Vorfluternahe Feuchtgebiete: Hydrologie trifft Biogeochemie

Interaktionen zwischen Hydrologie und Biogeochemie in vorfluternahen Feuchtgebieten

Potentielle Auswirkungen für die interne biogeochemische Prozessverteilung und auf den Export gelöster Stoffe

Extended Summary

Acknowledgements

Table of Contents

List of Figures

List of Tables

Summary

Interactions between hydrology and biogeochemistry at various spatio-temporal scales are important control mechanisms within terrestrial and aquatic ecosystems and exist among different compartments and transition interfaces. Understanding the fundamental mechanistic couplings between hydrological and biogeochemical processes and how these couplings feed back into ecosystem services and functions is an interdisciplinary challenge that must be addressed especially in the context of humanly mediated climate change. Riparian wetlands, as a transition zone between terrestrial and aquatic ecosystems, occupy large fractions of terrestrial ecosystems and provide important ecohydrological services. Due to their anoxic environments, riparian wetlands are able to store significant amounts of carbon as peat and act as an effective nutrient sink e.g. for sulfur, phosphorous and nitrogen. Riparian wetlands are characterized by highly dynamical interactions between hydrologically controlled transport mechanisms and biogeochemically controlled substrate availability, which governs nutrient cycling as well as the sink and source functions of wetlands. Generally, these interactions and their potential implications on ecosystem functions are only poorly understood. The representation of the tight couplings between hydrology and biogeochemistry in mechanistic models is a very challenging task because they have revealed a complexity which is often beyond the capabilities of current models. The objective of this thesis is to investigate interactions between hydrology and biogeochemistry in riparian wetlands and to understand their potential implications for internal biogeochemical process distributions and solute mobilization. Additionally, one major focus of the thesis is the attempt to represent such fundamental couplings in a process-based, hydrological/biogeochemical modeling approach. To this end, this thesis uses a combination of field and virtual experiments, as well as catchment-scale numerical modeling, performed for the Lehstenbach catchment, which was exemplarily chosen as main study site.

Results from the virtual experiments show very complex small-scale hydrological dynamics within the riparian areas. Here, runoff generation processes are strongly influenced by the spatial structure of the wetland-typical micro-topography (hummocks and hollows). Surface flow is episodically generated by a highly dynamical, threshold-controlled process where extended surface flow networks drain large fractions of the wetland's area. During intensive rainstorm events these surface flow networks, which contribute to stream discharge due to a fill and spill mechanism, dominate runoff generation. These fast flow components are characterized by very low residence times (minutes to hours) and once they are activated, the surface flow networks are able to rapidly mobilize large amounts of solutes, like nitrate or dissolved organic carbon (DOC), out of the wetlands by bypassing deeper anoxic layers. The importance of fast flow components for the catchment-scale mobilization of DOC was further confirmed by field investigations and catchment-scale numerical modeling. High frequency measurements of DOC in runoff of the Lehstenbach catchment revealed that DOC export is

subject to substantial short term variations at an hourly to daily timescale. During intense rainstorms, DOC concentrations are up to ten times higher (up to 40 mg/L) compared to low flow conditions (~3-5 mg/L). Short term variations together with the dramatic rise of DOC concentrations in runoff during rainstorms can be explained by the episodically activation of fast flow components in the wetland areas. At the catchment-scale, application of a hydraulic mixing-cell (HMC) methodology in combination with numerical modeling has revealed that fast flow components like saturated overland flow are exclusively generated in the wetland areas during intensive rainstorm events. On an annual basis, exemplarily for the hydrological year 2001, the HMC analysis quantified the relative contribution of saturated overland flow related to the total discharge with 19.5%, which highlights the importance of riparian wetlands for catchment-scale runoff generation.

Virtual experiments, additionally show that distinct shifts between surface and subsurface flow dominance, as a result of small-scale micro-topographic driven runoff generation in the wetlands, are responsible for very complex three-dimensional subsurface flow patterns showing a wide range of subsurface residence times. To investigate how these micro-topography induced subsurface flow patterns, together with the non-uniform hydrological and biogeogeochemical boundary conditions, affect the internal re-distribution and transformation of redox-sensitive species (like nitrate, sulfate or iron) a coupled hydrological/biogeogeochemical model was developed. In the model, wetland-typical biogeochemical processes are represented in a sequential stream tube approach where redox-sensitive processes are implemented as kinetic reactions. Simulations show the formation of local hot spots for redox-sensitive processes within the subsurface as a result of the complex subsurface flow paths and the transport-limited availability of electron acceptors and donors. Formation of hot spots was simulated for all key reduction processes including iron(III)-/sulfate reduction and denitrification as well as for the corresponding re-oxidation processes. These results offer a new perspective on hydrologically controlled biogeochemical transformation processes in riparian wetlands, which provides a dynamic framework to explain process heterogeneity in wetland soils and variability in process rates over space and time.

Findings from this thesis clearly prove how useful interdisciplinary approaches are in understanding processes and mechanisms in ecosystems and how important functions of ecosystems are affected by couplings among those. However, a lot of knowledge gaps still exist in understanding the nature of dependency between water and nutrient cycles across scales and how these interacting cycles feed back into humanly-mediated climate change in ecosystems. Development of new interdisciplinary methodologies and frameworks as well as an integrated way of thinking across the boundaries of the different environmental disciplines is necessary to address the grand challenges associated with climate change.

Zusammenfassung

Interaktionen zwischen hydrologischen und biogeochemischen Prozessen, auf unterschiedlichen zeitlichen und räumlichen Skalen, sind wichtige Steuermechanismen in terrestrischen und aquatischen Ökosystemen. Diese Interaktionen existieren für unterschiedliche Komponenten in Ökosystemen sowie für ökosystemverbindende Schnittstellen. Die Erforschung dieser Interaktionen und inwiefern sich gekoppelte Prozesse auf ökosystemare Funktionen und Dienstleistungen auswirken, stellt eine interdisziplinäre Herausforderung dar, der sich die Ökosystemforschung, vor allem im Kontext des globalen Klimawandels, stellen muss. Vorfluternahe Feuchtgebiete sind Schnittstellen zwischen terrestrischen und aquatischen Ökosystemen und üben durch ihre besonderen hydrologischen und biogeochemischen Eigenschaften wichtige ökohydrologische Funktionen aus. Durch ihr sauerstoffarmes, anoxisches Milieu sind Feuchtgebiete in der Lage große Mengen an Kohlenstoff in Form von Torf langfristig zu speichern und gelten als effiziente Nährstoffsenken wie etwa für Sulfat, Phosphat oder Stickstoff. Diese Gebiete zeichnen sich durch komplexe, hoch dynamische Kopplungen zwischen hydrologisch-physikalisch kontrollierten Transportprozessen und biogeochemisch kontrollierter Stoff- und Substratverfügbarkeit aus. Die enge Verschränkung zwischen hydrologischen und biogeochemischen Prozessen steuert, in vorfluternahen Feuchtgebieten, systeminterne Stoffflüsse sowie wichtige Quell- und Senkenfunktionen. Bisher sind diese Interaktionen, sowie deren potentielle Auswirkungen auf ökosystemare Funktionen von Feuchtgebieten, nur sehr wenig erforscht. Die Übertragung der Interaktionen zwischen Hydrologie und Biogeochemie in mechanistische Modelle ist äußerst schwierig, da die Komplexität die Fähigkeiten aktueller Modelle oft übersteigt. Ziel dieser Arbeit ist die Untersuchung hydrologisch-biogeochemischer Interaktionen in vorfluternahen Feuchtgebieten sowie deren Einfluss auf das systeminterne biogeochemische Prozessgefüge und die Stoffmobilisierung. Ein Schwerpunkt dieser Arbeit ist die Entwicklung eines kombinierten hydrologisch-biogeochemischen Modellansatzes, um mechanistisch die engen funktionalen Kopplungen zwischen Hydrologie und Biogeochemie in Feuchtgebieten zu untersuchen. Zu diesem Zweck benutzt diese Arbeit eine Kombination aus Feld- und virtuellen Experimenten sowie nummerischer Einzugsgebietsmodellierung, angewendet auf das Einzugsgebiet des Lehstenbaches, das exemplarisch als Hauptuntersuchungsgebiet ausgewählt wurde.

Ergebnisse der kleinskaligen virtuellen Experimente zeigen eine hoch komplexe hydrologische Dynamik, bei der abflussgenerierende Prozesse innerhalb der Feuchtgebiete, insbesondere von der Mikro-topographie, beeinflusst werden. Intensiver Niederschlag führt zur Ausprägung von ausgedehnten Abflussnetzwerken, die weite Bereiche der Feuchtgebiete oberflächlich entwässern. Die episodische Aktivierung dieser Netzwerke erfolgt dabei durch einen schwellenwert-gesteuerten Prozess in Abhängigkeit von den hydrologischen und meteorologischen Randbedingungen. Während Niederschlagsereignissen, dominieren diese Netzwerke im hohen Maße die Abflussgenerierung gegenüber anderen Abflusskomponenten. Diese schnellen Abflusskomponenten zeichnen sich durch

sehr kurze Verweilzeiten (Minuten - Stunden) aus. Sobald es zur Aktivierung der Abflussnetzwerke kommt, sind diese in der Lage in sehr kurzer Zeit große Mengen an gelösten Stoffen (z.B. Nitrat oder DOC) unter Umgehung tiefer anoxischer Bereiche aus den Feuchtgebieten zu mobilisieren. Die Bedeutung schneller Abflusskomponenten für die Freisetzung von DOC auf Einzugsgebietsebene wurde durch Feldmessungen sowie hydrologische Einzugsgebietsmodellierung bestätigt. Zeitlich hoch aufgelöste Messungen der DOC Konzentrationen im Abfluss des Lehstenbaches zeigen, dass der DOC Export kurzfristigen Schwankungen im Bereich von Stunden bis Tagen unterliegt. Bei Starkniederschlägen sind die DOC Konzentrationen zeitweilig bis auf das Zehnfache (bis zu 40 mg/L) gegenüber Niedrigabflussbedingungen (ca. 3-5 mg/L) erhöht. Die kurzfristigen Konzentrations-schwankungen zusammen mit dem dramatischen Anstieg der DOC Konzentrationen im Abfluss lassen sich durch die episodische Aktivierung schneller Abflusskomponenten in den Feuchtgebietszonen des Einzugsgebietes erklären.

Virtuelle Experimente zeigen zusätzlich, dass es aufgrund der durch die mikro-topographie-induzierten Verschiebungen der Dominanz zwischen Oberflächen- und Grundwasserabfluss auf der kleinen Skala, zur Ausprägung komplexer dreidimensionaler Fließmuster im Untergrund kommt. Die Erforschung inwiefern sich diese Muster, zusammen mit den wechselnden hydrologischen und biogeochemischen Randbedingungen, auf die interne Umverteilung und Transformation redox-sensitiver Stoffe (Nitrat, Sulfat und Eisen(III)) auswirken, war die Motivation für die Entwicklung eines gekoppelten hydrologisch-biogeochemischen Modellansatzes. Hier werden, für Feuchtgebiete, typische biogegeochemische Prozesse simuliert, wobei die einzelnen Prozesse als kinetische Reaktionen implementiert wurden. Ergebnisse dieser Simulationen zeigen die Ausprägung räumlich eng begrenzter Bereiche mit hoher Prozessaktivität ("hot spots"), als Folge des komplexen Fließfeldes und der transport-limitierten Verfügbarkeit von Elektronenakzeptoren und Donoren. Die Generierung von "hot spots" konnte sowohl für reduktive Prozesse (Eisen(III)-/Sulfatredution und Denitrifikation) als auch für entsprechende Reoxidationsprozesse simuliert werden. Ergebnisse dieses Modellierungsansatzes tragen im Wesentlichen zum Verständnis bei, inwiefern sich beobachtete räumliche und zeitliche Heterogenität im biogeochemischen Prozessgefüge von Feuchtgebieten durch das dynamische Zusammenspiel zwischen hydrologischen und biogeochemischen Prozessen erklären lassen.

Darüber hinaus zeigt diese Arbeit wie nützlich interdisziplinäre Forschungsansätze sein können, um Prozesse und Mechanismen in Ökosystemen zu verstehen und um die Auswirkungen von Prozessinteraktionen auf wichtige Ökosystemfunktionen zu erforschen. Dennoch existieren immer noch viele Wissenslücken welche Art von Abhängigkeiten zwischen Wasser- und Stoffkreisläufen skalenübergreifend in Ökosystemen existieren und inwiefern sich der anthropologisch verursachte Klimawandel auf diese Abhängigkeiten auswirkt. Die Entwicklung neuer interdisziplinärer Methoden und Forschungsansätze als auch eine fachübergreifende Denkweise ist Notwendig um die großen Herausforderung des globalen Klimawandels für die Ökosystemforschung anzugehen.

1   Introduction

1.1   Interactions between hydrology and biogeochemistry - an interdisciplinary challenge

Interactions between hydrology and biogeochemistry are important control mechanisms for functions and services of ecosystems. Such fundamental couplings were reported for different compartments and among different transition interfaces of terrestrial ecosystems (Lohse et al., 2009). Hydrological and biogeochemical processes interact at the land-atmosphere interface (e.g. Chapin, 1991; Schimel et al., 1997; Crockford and Richardson, 2000; Shaw et al., 2002), within soils (e.g. Kalbitz et al., 2000; D'odorico et al., 2003; Rodriguez-Iturbe, 2003; Porporato et al., 2004) in groundwater (e.g. McMahon et al., 1999; Hill et al., 2000; McMahon, 2001), streams (e.g. Minshall et al., 1985; Fisher et al., 1998; Fisher et al., 2004) and the corresponding transition zones between the different compartments like for example the hyporheic zone (e.g. Jones Jr. et al., 1995; Jones et al., 1995; Dent and Grimm, 1999; Dent et al., 2001). For the different compartments and interfaces hydrological/biogeochemical interactions occur at different spatio-temporal scales. Couplings at the land-atmosphere interface, such as the physiochemical reaction of a plant individual on changing hydrological and meteorological boundary conditions, can proceed very fast, within seconds to minutes restricted to a very small-scale (centimeters to meters), whereas coupled processes within the groundwater, e.g. conversion of DOC (dissolved organic carbon) to DIC (dissolved inorganic carbon) via mineral weathering, can occur over years to decades and over large spatial scales (catchment to regional scale) (Lohse et al., 2009). Traditionally, hydrologists and biogeochemists individually developed their own perspectives on how nutrients like carbon or nitrogen are being transported, processed and transformed within terrestrial ecosystems (Figure **1**). Conceptual frameworks in hydrology traditionally have focused on physical controls on transport and reactions, whereas those developed by biogeochemistry emphasized substrate and enzymatic constraints on reaction potential (Lohse et al., 2009). Additionally, both disciplines often operate on different spatial scales. The area of interest for micro-biologists or soil ecologists was or is often restricted to a very small scale e.g. micro- or mesocosm experiments. Such scales are rarely addressed by hydrologists, who primarily work at larger scales of transects, hill slopes or catchments. However, gradually various studies have shown that hydrological and biogeochemical processes are tightly coupled across scales (Doran and Linn, 1984; Schimel et al., 1997; Cirmo and McDonnell, 1997) which demands a combined perspective and an interdisciplinary approach if one wants to better understand potential feedbacks and control mechanisms between hydrology and biogeochemistry within terrestrial ecosystems. Such profound process knowledge is especially essential in the context of climate change, where responses of ecosystems to changing hydro-meteorological boundary conditions, as predicted by climate models (Parry, 2007), will fundamentally affect local-to-regional hydrologic cycles, biogeochemical cycles, as well as

interactions and feedbacks among them (Lohse et al., 2009). The importance to understand the nature of dependency between water-, C and N cycles across scales and how these interacting cycles feed back into humanly-mediated climate change was postulated to be one of the eight grand challenges in environmental science (National Research Council: Committee on Grand Challenges in Environmental Sciences, 2001).
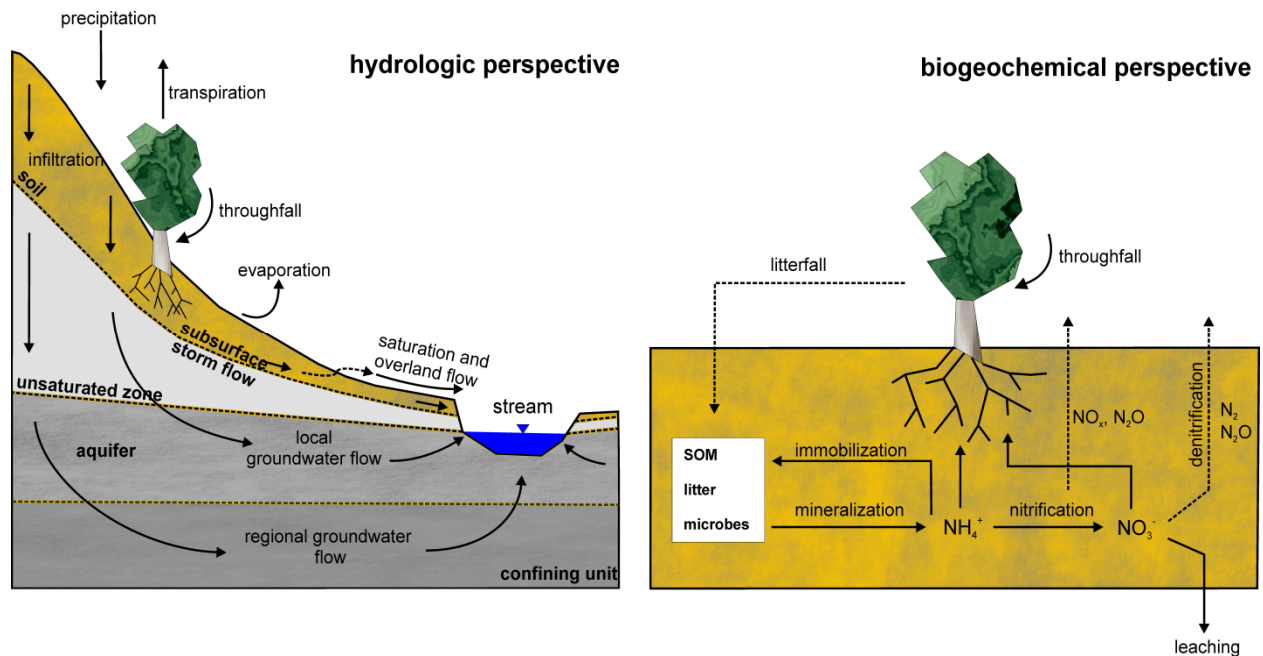
Figure 1: *Traditional hydrologic and biogeochemical perspective on transport and reaction. Hydrologists traditionally focus on physical transport aspects of water as precipitation, evapotranspiration, infiltration, local/regional groundwater flow and overland/stream flow. Biogeochemists emphasize reaction potential and substrate availability as shown exemplarily for the simplified N-cycle (adapted and modified from Lohse et al. (2009)).*

In recent years, many interdisciplinary studies started to investigate such fundamental couplings and researchers began to understand how feedback mechanisms between hydrology and biogeochemistry affect nutrient cycling (e.g. carbon or nitrogen) within terrestrial or stream ecosystems (reviews about this topics are given in Reich et al. (2006) and Lohse et al. (2009)). However, a lot of knowledge gaps still exist, especially the relevance of interactions between hydrology and biogeochemistry on scales which are important to ecosystem functions and human interactions remains a challenging field of research (Hyvönen et al., 2007). An interim objective for ecosystem research should be to develop and establish interdisciplinary tools and frameworks, such as combined modeling approaches, in which feedback mechanisms and interactions between hydrology and biogeochemical cycling are accounted for and which can be used for a better understanding of how nutrients within ecosystems are being processed. Once established, such frameworks ultimately can be used to address the challenges associated with climate change and its impact on functions and services of ecosystems.

1.2   Riparian Wetlands: Complex hydrology meets complex biogeochemistry

Riparian wetlands are peculiar landscape elements. They are preferentially located in areas where different hydrological flow paths are converging (e.g. at bottoms of basin shaped catchments, local hollows or around major streams or rivers) and represent interfaces between hillslopes and stream channels (Cirmo and McDonnell, 1997). Riparian wetlands, at the landscape scale, can be regarded as *"hot spots of mixing"* similar to the hyporheic zone. Here different waters, originating from different source areas, each with a different chemical signature (nutrient loadings or redox-sate) and subsurface residence time, meet and are intensively mixed (Stumm and Morgan, 1996; Cirmo and McDonnell, 1997). Despite various studies that have focused on investigating riparian wetlands and their hydrology, the significance of flow path mixing, the internal runoff generation processes and their responses and dynamics to changing meteorological boundary conditions are generally still poorly understood (Bishop et al., 2004; Vidon and Hill, 2004).

Runoff generation in wetlands has been shown to be highly dynamic and controlled by distinctly different runoff generation processes with shifts between subsurface and surface flow dominance for low and high flow events (Kværner and Kløve, 2008). During intensive rainstorms, fast flow components like surface or shallow subsurface flows typically dominate runoff generation in wetlands (Devito and Hill, 1997; Lischeid et al., 2007). Non-linear relationships between riparian water table depths and stream flow have often been observed (Branfireun and Roulet, 1998; Fraser et al., 2001; Molenat and Gascuel-Odoux, 2002; Seibert et al., 2003) in riparian wetlands. For wetlands dominated by matrix flow, these relationships have been attributed to the *"transmissivity feedback"* mechanism (Bishop, 1991; Bishop et al., 2004; Seibert et al., 2009) where stream flow originating from matrix flow increases exponentially when the water table rises into soil layers with progressively increasing lateral hydraulic conductivity (Bishop et al., 2004; Seibert et al., 2009). Runoff generation and interactions between surface-, subsurface- and stream-water in riparian areas are often controlled by storage threshold processes, which in the literature are reported to be related to (1) the retention of surface flow due to micro-topography (Antoine et al., 2009; Fiedler and Ramirez, 2000), (2) the retention of sub-surface flow due to sub-surface micro-topography, the so called *"fill and spill mechanism"* (Tromp-van Meerveld and McDonnell, 2006a; Tromp-van Meerveld and McDonnell, 2006b) and (3) the capacity of the near-stream zone to store floodwaters (bank-infiltration) over periods of weeks to years (Brooks and Lemon, 2007; Baillie et al., 2007; Meixner et al., 2007).

Wetlands are typically anoxic environments where shallow groundwater levels restrict the availability of atmospheric oxygen (O_2) up to the most superficial layers. With increasing water filled pore space oxygen availability decreases and microbial communities switch to anaerobic heterotrophic processes where microorganisms, after O_2 is depleted, first use nitrate (NO_3^-) > manganese(IV) > iron(III) (Fe_3^+) > sulfate (SO_4^{2-}) > CO_2 as the preferred electron acceptors (Stumm and Morgan, 1996; Hunter et al., 1998). With the premise that an organic carbon source, as the preferred electron donor, is available

these reduction processes occur sequentially, known as the microbially influenced redox chain (Zehnder, 1988). The location of the redox-cline in wetlands, as the defined boundary between the reduced and oxidized environment, is tightly coupled to the location of the local water-table (Cirmo and McDonnell, 1997). Rapid fluctuations of the water table in response to onset of rainfall are a commonly observed phenomenon in wetland system (Cirmo and McDonnell, 1997; Devito and Hill, 1997; Devito and Hill, 1997). The rapid response of the water-table to rainfall is discussed in the literature as an effect of a large capillary fringe in near- surface layers of soil or peat, where small amounts of rainfall or snowmelt may result in rapid upward movement of the water-table (Gillham, 1984; Heliotis and DeWitt, 1987). Water level manipulation experiments in the field (Knorr et al., 2009; Knorr and Blodau, 2009) have demonstrated that fluctuations of the water-table are directly linked to rapid changes in the predominant redox processes (i.e. iron(III) reduction, sulfate reduction and methanogenesis), the location of the redox-cline and the mineralization of organic material.

At the landscape scale wetlands are commonly assumed to be effective sinks for solutes like sulfate or nitrate, because anaerobic conditions and large carbon supplies enhance reductive biogeochemical transformations like denitrification or sulfate reduction (Johnston, 1991). However, this perspective neglects that physically-controlled transport and biogeochemical transformation processes within wetlands are not static. Hydrology, biogeochemistry and their interactions are dynamic processes, especially in wetlands or riparian areas, which are frequently affected by rapid fluctuations in hydrological and meteorological boundary conditions (Cirmo and McDonnell, 1997; Knorr et al., 2009; Knorr and Blodau, 2009). Short and long term fluctuations of the hydrological and meteorological drivers have the potential to alter internal biogeochemical processes, which may constrain the sink and source functions of wetlands for certain minerals, gases and solutes (Knorr et al., 2009). Devito and Hill (1997) have shown that wetlands are an efficient net sink for sulfate during high flow conditions where high water tables and anoxic conditions enhance reductive transformation processes e.g. denitrification or sulfate reduction. However, during extended drought periods and dropping water tables, redox conditions within wetlands change as wetland layers are being aerated, leading to increased mineralization and re-oxidation of reduced species like sulfide or ammonium, which are being flushed during storm runoff. Under these conditions, wetlands can turn into an episodic source for nitrate or sulfate (Devito and Hill, 1997).

In catchments, upland areas and riparian wetlands are usually connected hydrologically, meaning that water originating from upland areas has to pass through the riparian wetlands first before it can reach the streams or rivers via subsurface flow. Groundwater from upland areas usually has a very different chemical signature compared to the pore water of the wetland. In comparison, pore water in the wetlands groundwater from upland areas is often enriched in oxidized species like sulfate, nitrate or oxygen, whereas in contrast to wetland areas carbon loadings are usually low. Along flow paths, where upland groundwater is exposed to the anoxic conditions within wetlands, compounds like nitrate or sulfate can be reduced efficiently (Hill et al., 2000; McMahon, 2001). However, intensive

rainfall or snowmelt may result in the generation of very fast flow components like surface or shallow subsurface flow ((Devito and Hill, 1997; Lischeid et al., 2007) within riparian wetlands. These fast flow components have very low subsurface residence times and the potential to rapidly transport water originating from hillslope areas to the streams by short-circuiting or bypassing the anoxic areas of wetlands (Wigington et al., 1990; Murdoch and Stoddard, 1992; Stoddard, 1994; DeWalle and Swistock, 1994). Under such conditions, the sink function of wetlands for nitrogen or sulfur can be deactivated temporarily.

Attempts to describe and represent the complex processes and couplings between the hydrology and biogeochemistry of wetlands in mechanistic models is a challenging task, as processes and couplings are commonly at a level of complexity that is beyond the capabilities of current models (Hill, 1993; Waddington et al., 1993; Eshleman et al., 1994; Richardson et al., 2007a). Often, below ground processes within wetlands are treated as a *black box* (Kettunen et al., 1999; Updegraff et al., 2001; Chimner and Cooper, 2003) where only the transfer characteristics between input and output variables are being considered, neglecting underlying physical laws that govern system-internal hydrological and biogeochemical processes. To "*unlock the black box*" (Walling, 1983), it is necessary to gain an improved understanding of system-internal process mechanisms and fundamental mechanistic couplings between physical transport and biogeochemical reactions (Burt and Pinay, 2005), especially in such complex environments as riparian wetlands. This requires spatially-explicit, physically-based model structures (Burt and Pinay, 2005; Richardson et al., 2007b; Boano et al., 2010) which represent processes based on their actual governing physical laws and which, by definition, account for spatial organization of relevant hydrologic and biogeochemical parameters. Although fully distributed approaches have been heavily criticized because of the difficulties in adequately defining process equations and a unique, problem-specific parameterization (the "*equifinality problem*" presented in Beven, (1989) and Beven, (1993)), they offer flexible and extensive possibilities to test certain hypotheses (the "*virtual experiment*" concept presented in Weiler and McDonnell (2004)), which are related to the nature of interactions between hydrology and biogeochemistry in wetland systems. These approaches can be used to partially elucidate the black box and investigate the fate of those elements and solutes, which are affected by physical transport and biogeochemical transformation in wetland ecosystems. This thesis contributes to this line of work.

2   Research Objectives and Hypotheses

This thesis aims at investigating fundamental interactions between hydrology and biogeochemistry in wetland ecosystems with the purpose to gain a better understanding of how nutrient cycling, internal biogeochemical process distributions, solute mobilization and solute export are affected by such interactions. A major focus of this thesis is to establish an interdisciplinary modeling framework where hydrological and biogeochemical processes are addressed equally and where fundamental interactions and feedback mechanisms between a wetland's hydrology and biogeochemistry can be represented in a physically-based model. The five studies, which are presented as part of this thesis, use a combination of field investigations, virtual experiments and catchment scale numerical modeling to address the different research objectives and hypotheses.

Study 1 focuses on the effects of surface micro-topography on hydrological process dynamics and interactions that govern surface-subsurface exchange and runoff generation in riparian wetlands. Specifically, study 1 uses a virtual experiment approach to investigate: (1) the role of a hummocky topography of wetlands on stream discharge generation; (2) the effect of micro-topography on typically-observed non-linear relationships between discharge and water table depth and (3) the connection between surface flow generation and climatic and hydrological boundary conditions. In study 2, the previously presented virtual wetland model, is subsequently used to develop a coupled hydrological/biogeochemical model which is being used in another virtual experiment to investigate how subsurface flow patterns, induced by micro-topography, affect hydrological transport and biogeochemical transformation processes of redox-sensitive solutes within wetlands. The main research hypothesis of study 2 is to explore whether a complex, three-dimensional subsurface flow field, as a result of micro-topography controlled surface/subsurface flow exchange, creates biogeochemical conditions that facilitate the formation of local process hot spots for wetland-typical redox reactions, even in soils with uniform soil properties.

Representing small-scale interactions between hydrology and biogeochemistry of wetland ecosystems, as presented in study 2, in a coupled physically-based modeling approach has proven to be computationally very demanding, resulting in low computational efficiencies and extremely long simulation times. The main objective of study 3 therefore is to develop a technique how effects of micro-topography on sub-surface flow patterns, runoff generation and biogeochemical process patterns can be represented more efficiently in physically-based models. Once established, such an alternative representation can be used to account for effects of micro-topography in larger scale models like in watershed or regional models. Study 4 is mainly based on data from a field campaign on DOC export of a small forested watershed with riparian wetlands. The impacts of short term fluctuations in hydrological and meteorological boundary conditions on DOC variations in runoff are investigated. Here, the main research objectives are (1) to identify the spatial origin of DOC in runoff,

(2) to identify hydrological flow paths which are important for DOC mobilization and (3) to investigate implications of short term variations of DOC in runoff for the calculation of annual DOC export rates.

Runoff generation mechanisms at the catchment scale are investigated in study 5, where a "*Hydraulic Mixing-Cell*" methology (HMC) is used to track overland and stream runoff generation mechanisms to attain a meaningful separation of streamflow hydrograph for the Lehstenbach. Objectives of study 5 are (1) to test whether the HMC method, developed and presented earlier by Partington et al. (2011), can principally be used in general to identify and quantify relevant runoff generation mechanisms in complex numerical flow models and more specifically (2) to investigate the spatial origin and relative contribution of different runoff components in the Lehstenbach catchment.

3 Materials and Methods

3.1 Study Site

Field experiments and numerical modeling were carried out in the Lehstenbach catchment. The catchment is located close to the city of Weisenstadt in north eastern Bavaria, Germany (50°08'38''N, 11°51'41''E). Elevations for the site vary between 877m above sea level for upslope areas and 690m above sea level for the outlet of the catchment. Mean annual precipitation, for the 4.2 km² large Lehstenbach catchment, is around 1150 mm with a mean temperature of ~5°C (Gerstberger, 2001). The main regional aquifer of the Lehstenbach catchment (around 40 m thick) is made up of regolithic material originating from weathering of the granitic bedrock (Lischeid et al., 2002). Hydrologically, the catchment can be separated into two distinct units as illustrated in Figure 2: Nearly one-third of the total area of the catchment can be classified as riparian wetlands surrounding all major streams. Peat forming wetlands have predominately developed in the topographic depressions towards the center of the bowl-shaped catchment, where converging groundwater flow (Figure 2) favors conditions that lead to the accumulation of peat. For the main wetlands, average peat thickness varies between 0.3m and 1.2m. The wetlands are locally separated from the deeper groundwater system by a basal clay layer of variable extent. Annual fluctuations of groundwater levels in the wetland's main zones are limited to the upper 0.2 m, but may increase down to 0.8m below soil surface during very extended drought periods. Water content of the variably saturated zone within the wetlands is comparably high, which favors anoxic conditions (above 80% water saturation according to Paul et al. (2006), Estop-Aragonés et al. (2012) and Estop-Aragonés and Blodau (2012)). Extended areas of the wetlands, especially in the lower parts of the catchment close to the outlet (Schlöppnerbrunnen II), are characterized by a pronounced micro-topography (Figure 3); sequences of hollow and hummock structures, built by the wetland's typical vegetation (*Carex rostrata, C. Canesccens, Eriophorum vaginatum, Nardus stricta, Molinia coeruela, Agrostis sp., Sphagnum fallax, Brachythecium rivulare* and *Atrichum undulatum* according to Knorr et al. (2008)). Such hummocky topographies are quiet common in peatlands (Nungesser, 2003) and evidence from chrono-stratigraphic studies indicates that such structures (hummocks and hollows) may persist relatively unchanged for centuries or even millennia (Godwin and Conway, 1939; Conway, 1948; Tolonen, 1971; Barber, 1981). Previous studies performed in the Lehstenbach catchment indicated that important mechanisms and processes controlling stream flow generation and solute export are located in the near-stream wetland areas (Lischeid et al., 2002; Alewell et al., 2007; Lischeid, 2008).

Around two-thirds of the area of the Lehstenbach catchment is covered by forest (mainly Norway Spruce populations, (Gerstberger, 2001)). Hydrologic conditions in the forested areas, located mainly in the upslope areas of the catchment (Figure 2), clearly differ from those within the riparian wetlands. Long term groundwater observations for the upslope areas show permanently deep

[17]

groundwater levels, 5-10m below the land surface and an extended unsaturated zone with comparably low water contents. In contrast to the water saturated conditions within the wetlands, the upslope areas can be classified as aerated forest soils. The forested areas represent the main recharge zones for the deeper groundwater system, as reflected by downward hydraulic gradients in the unsaturated zone. There is no clear evidence for pronounced lateral flows above the groundwater table (interflow) in these areas with deep water table.
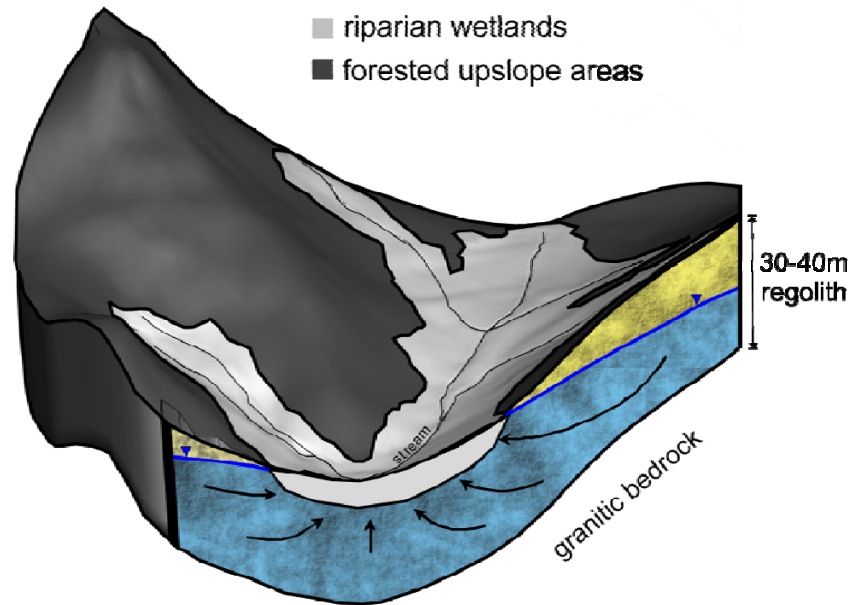
Figure 2: *Conceptual model of the Lehstenbach catchment. The overall hydrology of the catchment is controlled by the structure of the basin. Dark grey areas represent forested zones and light grey areas wetlands, which occupy almost 1/3 of the 4.2 km² catchment area.*

Figure 3: Picture of the Schlöppnerbrunnen II field site (located in the lower part of the catchment, close to the catchment's outlet) taken during a storm flow event in spring 2009. The Schlöppnerbrunnen II site is characterized by a pronounced micro-topography (hollow and hummock structures) and belongs to the core wetland areas of the Lehstenbach catchment.

3.2 Hydrological Modeling

Hydrological modeling as part of this thesis was performed using a spatially-explicit, physically-based modeling concept, where surface and subsurface hydrology is represented using the code HydroGeoSphere (**HGS**, presented in Therrien et al. (2008)). HGS is a fully-integrated finite element surface-subsurface flow model. Variably saturated subsurface flow in porous media is simulated by solving the Richards equation in three dimensions (3D):

$$-\nabla(w_m q) + \sum \Gamma_{ex} \pm Q = w_m \frac{\partial}{\partial t}(\theta_s S_w) \quad \textit{Eq. 1}$$

$$q = -K_{sat} k_r \nabla(\psi + z) \quad \textit{Eq. 2}$$

Where $\boldsymbol{w_m}$ [-] represents the volumetric fraction of the total porosity occupied by the primary continuum (porous or fractured medium) and **q** [LT⁻¹] the fluid flux. $\boldsymbol{\Gamma_{ex}}$ [L³ L⁻³T⁻¹] represents the volumetric fluid exchange between the subsurface domain and all other types of domains supported by the model (e.g. surface domain). Fluid exchange with the outside of the simulation domain is represented by **Q** [L³ L⁻³T⁻¹], which is a volumetric flux per unit volume representing source (positive) and sinks (negative). $\boldsymbol{\theta_s}$ [-] and $\boldsymbol{S_w}$ [-] represent the saturated water content and the degree of saturation respectively. Furthermore, the fluid flux **q** is given by Eq. 2 where $\boldsymbol{k_r}$ [-] represents the relative permeability of the medium as a function of the water saturation $\boldsymbol{S_w}$, K_{sat} [LT⁻1] is the saturated hydraulic conductivity of the medium, $\boldsymbol{\psi}$ [L] is the pressure head and **z** [L] the elevation. For representation of variably saturated flow, commonly used functions incorporated into HGS are those presented in Van Genuchten (1980b) and Brooks and Corey (1964) or alternatively, soil retention characteristics can also be handled through the use of tabular data input if field measurements are available (Therrien et al., 2008). Overland- or stream flow in 2D is represented by the diffusion wave approximation to the depth-averaged dynamic wave equations (Therrien et al., 2008):

$$-\nabla(d_o q_o) - d_o \Gamma_o \pm Q_o = \frac{\partial \phi_o h_o}{\partial t} \quad \textit{Eq. 3}$$

Within the diffusive wave equation, here written in vectorial notation, **d₀** [L] represents the surface flow water depth; **q₀** [LT⁻¹] the water flux on the surface; $\boldsymbol{\Gamma_o}$ [T⁻¹] the fluid exchange rate with the subsurface; **Q₀** [LT⁻¹] the volumetric flow rate per unit area representing external sinks (negative) or sources (positive); $\boldsymbol{\phi_o}$ [-] the surface porosity and **h₀** [L] the water surface elevation. Surface–subsurface coupling is implemented using the conductance concept:

$$d_o \Gamma_o = \frac{k_r K_{zz}}{l_{exch}}(h - h_o) \quad \textit{Eq. 4}$$

The conductance concept assumes that the exchange flux between the surface and the subsurface Γ_o [T^{-1}] depends on the gradient across a coupling interface $\mathbf{h}$-$\mathbf{h_o}$ [L] ($\mathbf{h}$ [L] represents the subsurface water head and $\mathbf{h_o}$ [L] the water surface elevation), the thickness of the interface l_{exch} [L] (coupling length), its relative permeability k_r [-] and the vertical saturated hydraulic conductivity K_{zz} [LT^{-1}] (Therrien et al., 2008). All governing equations for surface- and subsurface flow are solved simultaneously via a control volume, finite-element approach (Therrien et al., 2008). HGS has been applied over a wide range of spatial scales ranging from plot and river reach scales (Jones et al., 2006; Brookfield et al., 2009) over the scale of watersheds (Jones et al., 2008; Li et al., 2008) up to the scale of continents (Lemieux et al., 2008a; Lemieux et al., 2008b; Lemieux et al., 2008c). As part of this thesis, HGS was used to simulate hydrological flow processes and surface/subsurface flow interactions on two different scales: On the plot scale numerical flow modeling (using HGS) was used to represent the highly dynamic flow processes within the riparian wetlands (study 1, 2, 3) of the Lehstenbach catchment. An integrated perspective on hydrological flow processes, relevant for the catchment scale runoff generation and solute exports, was the motivation for setting up a numerical catchment scale flow model of the Lehstenbach area (study 4+5).

3.2.1 *Virtual Wetland Modeling (Study 1, 2 and 3)*

The conceptual idea behind the plot scale modeling is similar to the virtual experiments proposed by Weiler and McDonnell (2004). The objectives of the studies 1-3 are addressed through virtual modeling experiments. The numerical model is used as a virtual wetland, in which perfect process knowledge is assumed (see e.g. Zehe et al. (2005)). Virtual wetland modeling involves more than only one numerical flow model: Study 1 and 2 use different model scenarios with different, geostatistically generated 3D realizations of the hummocky micro-topography. Study 3 involves geostatistically derived, 2D representations of micro-topography, which were used in subsequent model scenarios. All numerical flow models (study 1-3) as part of the virtual wetland modeling approach were set up for the same spatial model domain (set up for a 10m x 20m x 2m plot) representing a synthetic section of a riparian wetland draining into a nearby stream segment (Figure 4). Virtual wetland modeling is described in detail in the method section of study 1 and only a brief summary about the applied techniques and methods is given in this section.
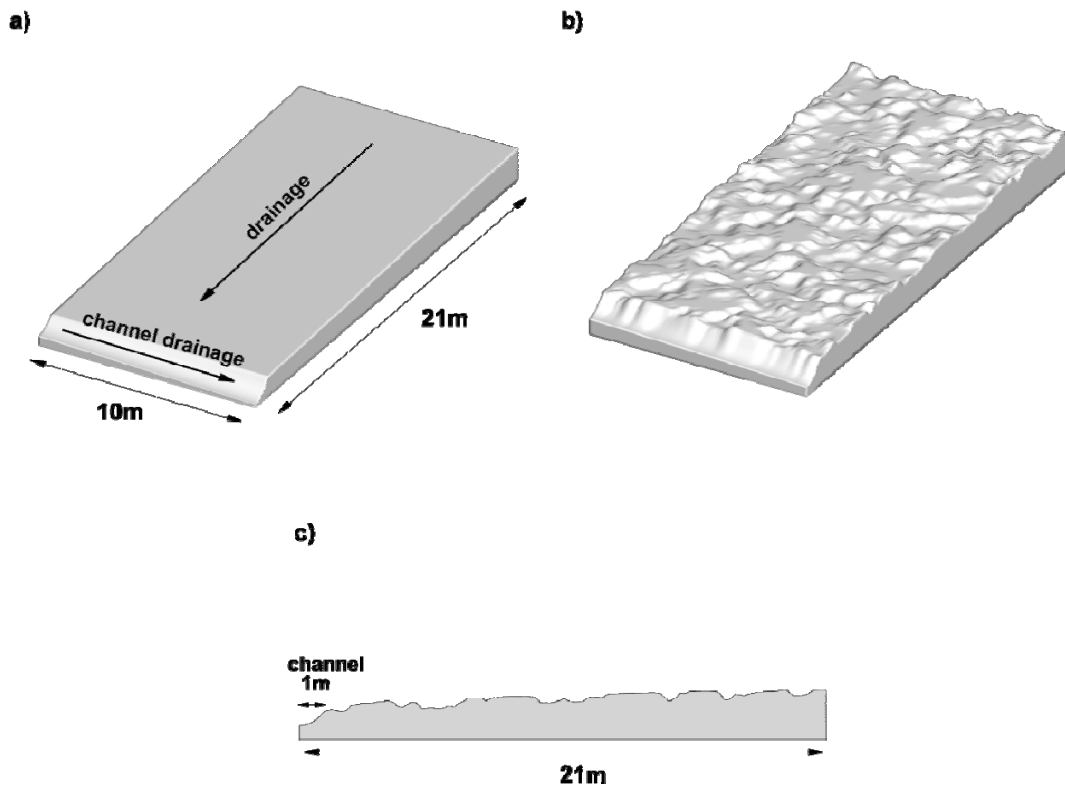
Figure 4: *Geometry of the virtual wetland segment: a) planar reference model showing the main drainage direction and channel location; b) smoothed realization of the wetlands hummocky micro-topography; c) cross section (Y=5m) of the micro-topography model.*

Representation of Micro-topography

The spatial structure of the micro-topography for a typical wetland in the Lehstenbach catchment was represented using geostatistical indicator simulations based on Markov Chain models of transition probabilities (TPROGS-*T*ransition *PRO*bability *G*eostatistical *S*oftware presented in Carle and Fogg (1996)). The method was originally developed to realistically represent aquifer heterogeneity with discrete transitions between different hydrofacies (Carle and Fogg, 1996). TPROGS has been widely applied for groundwater flow and transport problems (e.g. Weissmann, 1999; Fleckenstein et al., 2006; Lee et al., 2007; Frei et al., 2009). For a realistic representation of micro-topography, the geostatistical model was conditioned with field data derived from several surveyed transects taken within a 30m x 30m plot of the Schlöppnerbrunnen II site located in the Lehstenbach catchment. The output of the indicator simulations was transferred into an artificial digital elevation model (DEM) by assigning the different indicators to certain elevation classes. The resulting DEM mimics the spatial structures of the wetlands micro-topography. The application of geostatistical simulations provided the possibility to work with multiple realizations of micro-topography based on either the same or different structural properties. A detailed description of the used geostatistical approach is given in the methods chapter of study 1. Study 1 and 2 use model scenarios where micro-topography is actually

[21]

represented using a three-dimensional DEM. Study 3 introduces a technique where micro-topography can be represented by two dimensional, spatially distributed zones of rill storage heights. Rather than to transform the spatial indicator field, derived from the geostatistical simulations, into a three-dimensional DEM, the spatial indicators in study 3 were used to define two-dimensional rill storage height zones.

Surface/Subsurface Flow Simulation

The geostatistically generated realizations of micro-topography were used to set up different model scenarios, where the artificial three-dimensional DEM and the rill storage zones were superimposed onto an inclined (slope of 0.03m/m) surface plane of the HGS model grid. The resulting flow models consist of 210,000 grid nodes with a nodal spacing of about 0.1m in X, Y and Z directions. The channel (Figure 4) is represented by a parabolically shaped cross section (1 m in diameter) draining into the Y direction with a constant slope of 0.03 m/m. For comparison, a model with a planar surface was used as a reference model to simulate hydrological dynamics without micro-topographical structures. The peat body of the synthetic wetland was assumed to be homogenous and isotropic in all simulations. Heterogeneity was intentionally excluded to clearly separate micro-topographical effects from effects induced by material heterogeneity. The saturated hydraulic conductivity of the peat was estimated at 0.2 m/d, which is in the range of values reported for the filed site (Hauck, 1999) and for typical peat soils in general (Kruse et al., 2008; Schlotzhauer and Price, 1999). Parameterization for the variably saturated flow characteristics are based on field measurements taken from Price et al. (2010) for similar peatlands in Alberta, Canada (soil retention functions for the swamp areas are shown in Figure A1 in the appendix). On the surface, water is only allowed to leave the model domain at the channel's outlet which was accomplished due to a critical depth boundary condition. All other boundary conditions were set to now flow boundaries with exception of the upper model surface where variable rainfall rates were applied. Hydrology, as part of the virtual wetland modeling, was simulated based on daily precipitation values measured for the hydrological year 2000 (November 1999 to October 2000) estimated for the Lehstenbach catchment.

3.2.2 *Catchment Scale Modeling (Studies 4 + 5)*

Spatial Discretization, Boundary and Initial Conditions

A hydrological model for the entire Lehstenbach catchment was set up using HGS. An earlier version of the catchment model had been set up as part of a diploma thesis at the Department of Hydrology (Werb, 2009). Later, the model was modified and adapted to the needs of the thesis objectives by the author. A DEM with a spatial resolution of 5m x 5m of the Lehstenbach area was used to represent the bowl shaped surface topography of the catchment. Vertically, the model is discretized into two main layers of variable thickness to represent major soil types and subsurface geology of the Lehstenbach catchment. The uppermost layer (1m thick) represents the organic peat soils of the wetland areas. This upper layer was subdivided into 10 sub-layers, each with a thickness of 0.1m, to assure that the vertical resolution is fine enough to adequately capture the highly non-linear processes within the variably saturated zone and to prevent numerical problems associated with simulation of variably saturated flow (Kinzelbach and Rausch, 1995). Below the upper layer, a ~40m thick layer was implemented within the model to represent the regolithic aquifer that was formed by weathering of the granitic bedrock. Horizontally, the model uses a finite element discretization scheme with variable mesh resolution. Because surface/subsurface flow interactions in the proximity of the streams and within the riparian wetlands are usually are highly dynamic including short term fluctuations and associated short term changes of hydraulic connectivity as opposed to areas distant from the stream, the nodal density was gradually increased towards the stream segments (as shown in Figure 5).
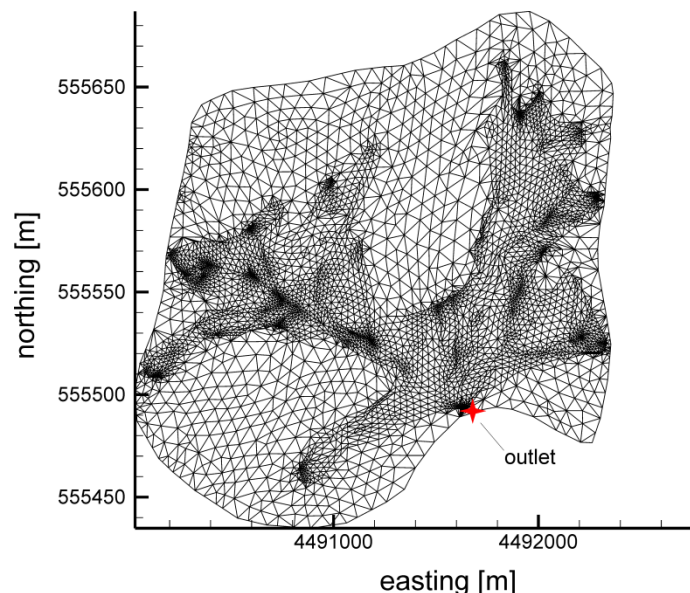
Figure 5: *Finite element grid of the Lehstenbach catchment model. Wetland areas were set up using a finer spatial resolution compared to forested areas. Further, nodal spacing gradually was increased towards the stream segments.*

[23]

Boundary conditions for the subsurface flow domain were set to now flow boundaries at the base of the model representing an impermeable granitic bedrock. To the sides of the subsurface flow domain no flow boundaries were used because it was assumed that there is no exchange of groundwater with areas located outside of the surface watershed of the Lehstenbach catchment. The upper boundary representing the land surface uses a combination of variable rainfall inputs, interception and evapotranspiration as upper boundary conditions. In HGS, interception and evapotranspiration are simulated as mechanistic processes governed by plant and climatic conditions based on Kristensen and Jensen (1975) and Wigmosta et al. (1994). A detailed description of the implemented interception/evapotranspiration routine is given in the manual of HGS (Therrien et al., 2008). Daily rainfall inputs observed for the hydrologic year 2001 (11/1/2000 – 31/10/2001) in the Lehstenbach catchment were used as climatic forcing for the model. As HGS currently does not provide a snow routine, rainfall rates had to be manually adapted to represent snow accumulation and melting during the winter and spring time (Werb, 2009). In the current version of HGS the locations of streams cannot be pre-defined by line boundaries, which means it is not possible to assign certain nodes/elements and define them as stream nodes where channel flow exclusively occurs. Streams or rivers, in the used version of HGS, develop from the 2-dimensional solution of the overland flow equations out of the model's geometry and topography (Therrien et al., 2008). Because the used DEM was too coarse to adequately resolve differences in elevation between the narrow stream channels (typically less than 1m in width) and their immediate surroundings, the elevation of the surface nodes which coincides with the stream locations were manually lowered (1m). The edges of the surface flow domain use a critical depth boundary to allow surface water to flow out of the model domain. Because of the bowl shaped geometry of the catchment, the only location where surface water actually is able to leave the model is at the catchment outlet (as shown in Figure 5). As initialization, the model was run to a quasi steady state by applying a constant rainfall rate of 1.5 mm/d, which represents the mean annual precipitation rate for the Lehstenbach catchment (Werb, 2009). The resulting steady state solution was later used as an initial condition for the yearly simulations with variable rainfall inputs.

Parameterization, Model Calibration and Validation

In the wetlands, the saturated hydraulic conductivities for the upper ten sub-layers were varied exponentially (K_{sat}-values decrease exponentially with depth) according to the *"transmissivity feedback"* mechanism as proposed by Bishop et al., (2004). The K_{sat} for the peat layers ranged between 200 m/d for the uppermost sub-layer, representing fresh, less decomposed and less compacted organic material, and 8.64×10^{-3} m/d for the basal peat layer (Figure A2, shown in the appendix). K_{sat} values used to represent the wetland areas are based on the study of Jacks and Norrström (2004), who performed *"slug tests"* for similar wetlands located in the Luntoma catchment in south western Sweden. K_{sat} for the regolithic aquifer was optimized during model calibration where ranges of isotropic/an-isotropic values for K_{sat} were tested (Werb, 2009). Best results were achieved

assuming an isotropic regolithic aquifer with a K_{sat} value of 0.24 m/d. This value was uniformly assigned to the lower model layer.

Soil retention functions used to represent variably saturated flow are based on the model proposed by Van Genuchten (1980a) and are shown in the supplement (Figure A1 shown in the appendix). Soil retention functions for the wetland layers are based on field measurements performed by Price et al. (2010) for similar wetlands in Alberta, Canada and are identical to those functions used for the virtual wetland model. For the main regolithic aquifer, a Van Genuchten model was adapted to field measurements performed in the Lehstenbach catchment (unpublished data from Gunnar Lischeid). The friction slope for surface flow simulations within HGS is described using Manning's equation (Therrien et al., 2008). Manning's roughness coefficients for the peat surface were uniformly assigned as 0.03 $m^{-1/3}$s for x and y; a value reported for high grass (Shen and Julien, 1993). Friction slopes for the forested upslope areas were uniformly assigned to 1.9×10^{-6} $m^{-1/3}$s, which represents areas with minor ground vegetation (Shen and Julien, 1993). Results from study 1 show that micro-topography is responsible for complex surface flow generation processes ("*fill and spill*" mechanism see study 1) and flow retention due to depressional storage. To account for the storage effects caused by micro-topography, the catchment scale model was set up using different zones of rill storage heights which were randomly distributed to the wetland's surface grid (used rill storage heights are shown in Table A1 in the appendix). This approach, although applied to a much larger catchment-scale model, follows the concepts that are described in study 3, where rill storage variations were used to mimic effects of micro-topography in the virtual wetland segment. The model was calibrated by comparing simulated versus observed discharge values measured at the catchment's outlet for the hydrological year 2001 (1.11.2000 – 31.10.2001, as shown in Figure 6). For the calibration period a Nash-Sutcliffe efficiency (Nash and Sutcliffe, 1970) of 0.70 could be achieved for the catchment scale model. Model validation, based on the parameters estimated as part of the calibration process, was performed for the hydrological years 2002 to 2005 (11/01/2001 – 10/31/2005). Nash-Sutcliffe efficiency for the validation period was 0.51.
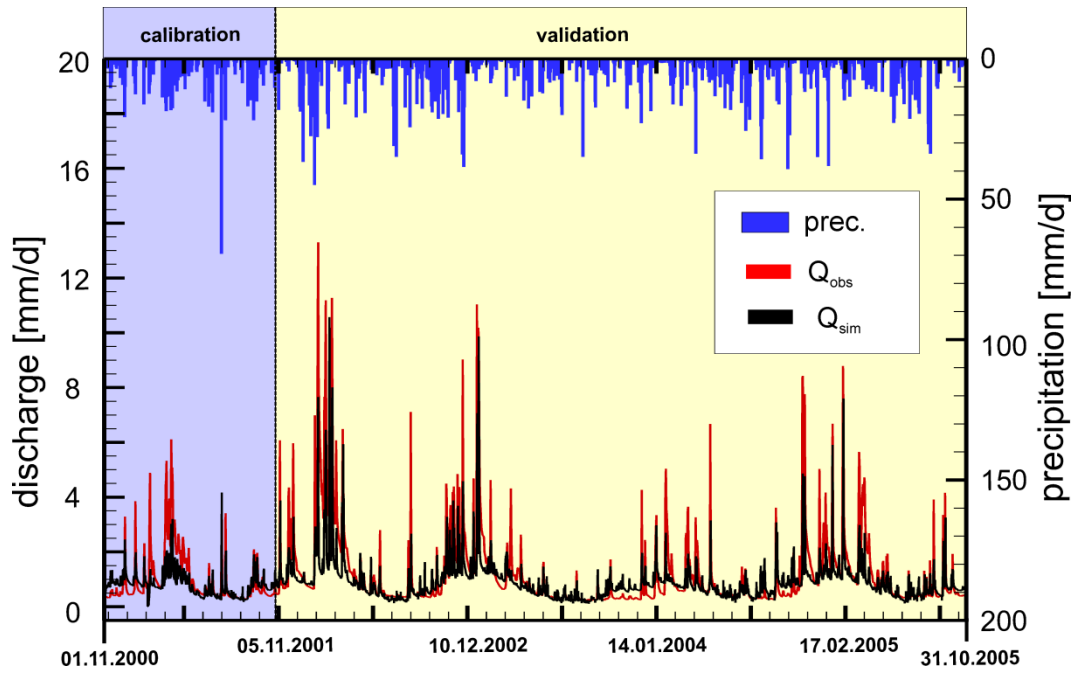
Figure 6: *Observed and simulated discharge values (estimated at the catchment outlet) for the calibration and validation periods of the catchment scale model. Calibration was performed for the hydrological year 2001 (11/01/2000 – 10/31/2001) with a Nash-Sutcliffe efficiency of 0.70. The model was validated for the hydrological years 2002 to 2005 (11/01/2001 – 10/31/2005) achieving a Nash-Sutcliffe efficiency of 0.51.*

3.3 Biogeochemical Modeling (Studies 2 + 3)

To investigate interactions and feedback mechanisms between hydrology and biogeochemistry, a coupled biogeochemical/hydrological model was developed. The used approach for coupling biogeochemistry and hydrology follows a stream tube concept where it is assumed that subsurface flow and transport occurs along defined stream tubes. The stream tube approach used here assumes that there is no mixing between different stream tubes due to hydrodynamic dispersion (mechanic dispersion + diffusion). Stream tubes or subsurface flow paths were isolated using advective particle tracking, which was applied to the transient model output of the virtual wetland model. Key biogeochemical processes were simulated along individual subsurface flow path lines, depending on the hydrological and biogeochemical boundary conditions, using the geochemical model PHREEQC (Parkhurst, 1995). The main concepts and limitations of this approach are described in detail in the method section of study 2 and are only briefly summarized here.

3.3.1 *Coupling Hydrology and Biogeochemistry*

For the virtual wetland model (study 1) transient model output for subsurface flow exist for the hydrologic year 2000. Model output includes spatial pressure/total head distributions and Darcy flow velocities in X, Y and Z, transiently calculated for the whole model domain of the virtual wetland. Advective particle tracking for the transient velocity fields from the flow model was implemented using the *Tecplot 360* post-processing software (Bellevue, 2003). The particle tracking routine calculates subsurface flow paths for hypothetical, mass less particles based on an existing transient subsurface flow velocity field. For each realization of the virtual wetland model (two realizations of micro-topography + planar reference case) 21,000 individual subsurface flow paths were isolated by using particle tracking. Particle tracking simulations were performed for a 25 year simulation period by sequentially repeating the model output for the hydraulic year 2000 twenty-five times. This ensured that every particle actually leaves the subsurface model domain and that a continuous subsurface flow path exists from infiltration to exfiltration. According to Figure 7, each subsurface flow path is split into different sub-sections. A sub-section represents a small reach of a flow path for which constant hydrological boundary conditions (pressure heads and subsurface flow velocities) are assumed. For each sub-section, *PHREEQC* was used to simulate the redox chemical evolution of water volume, which carries redox-sensitive solutes, for the time it resides within this sub-section. Between consecutive sub-sections redox-sensitive solutes are exchanged, which means that sub-section *i* uses the final solute composition of the *i-1* sub-section as initialization. The entire sequence of different sub-sections, each belonging to one subsurface flow path, represents a continuous simulation of the redox-chemical evolution of a hypothetical volume of water carrying redox-sensitive solutes from its moment of infiltration until it leaves the subsurface flow domain due to exfiltration (Figure 7). For all of the 21,000 isolated flow paths per flow model, the above-mentioned approach

[27]

was used to represent the whole 3D domain of the virtual wetland model, which resulted in ~1.450.000 different PHREEQC sub-section simulations per flow model.
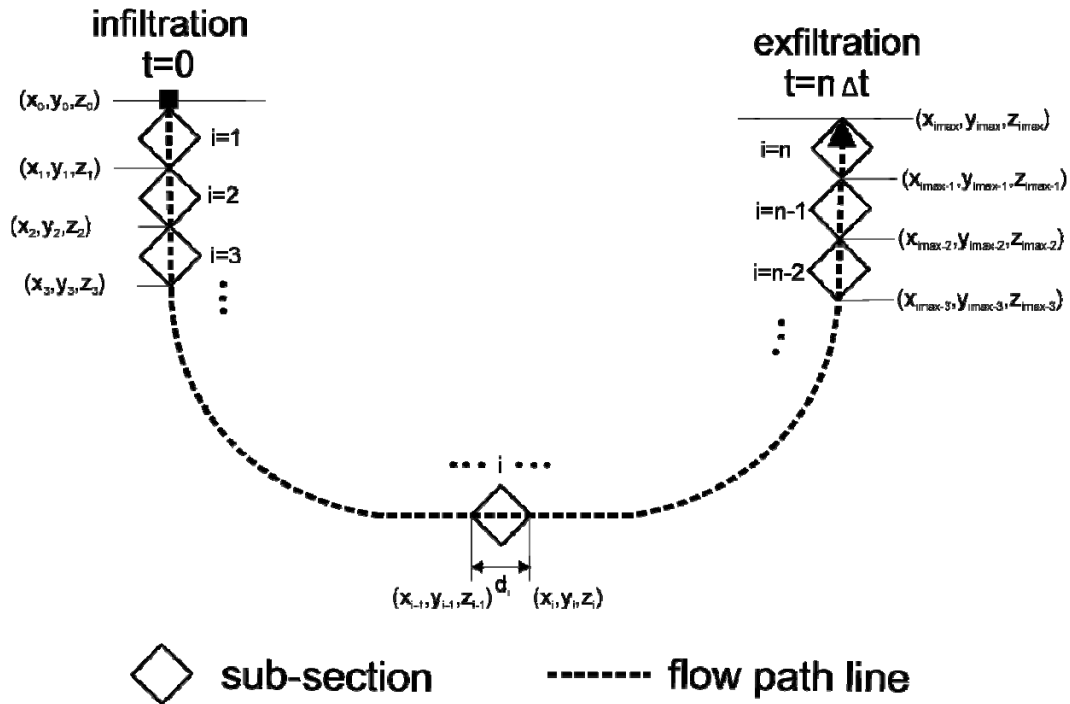
Figure 7: *Concept of the applied stream tube approach for representation of biogeochemistry along isolated subsurface flow paths (dashed line). An isolated flow path is split into n different sub-sections. Each sub-section i represents a small reach of the flow path, for which the biogeochemical evolution, depending on the hydrological/biogeochemical boundary conditions, is simulated using PHREEQC (Parkhurst, 1995). Boundary and initial conditions are individually assigned for each PHREEQC sub-section simulation. Between consecutive sub-sections, redox-sensitive solutes are exchanged were the ith sub-section uses the final redox chemical composition of the i-1th sub-section as initial condition. X, Y and Z represent the spatial coordinates at the beginning and the end of a sub-section; Δt represents the sub-section's residence time.*

3.3.2   *Implemented Reaction and Boundary Conditions*

The biogeochemical model represents wetland-typical, redox-sensitive processes, which are implemented using different kinetic reactions. In particular, the following redox-sensitive processes are being simulated: aerobic respiration, denitrification, iron(III) reduction, sulfate reduction, iron(II) oxidation, ammonium oxidation, aerobic and anaerobic sulfide oxidation. Kinetics for all reduction processes (aerobic respiration, denitrification, iron(III) reduction, sulfate reduction) where microorganisms use different electron acceptors (oxygen, nitrate, iron(III) and sulfate) for turnover of organic material are formulated based on Monod kinetics (Monod, 1949). For reactions following Monod kinetics, as shown in Eq. 5, the kinetic rate R_k [ML^{-3}T^{-1}] is calculated as a function of the solutes concentration c_k [ML^{-3}] and the reaction specific constants μ_{max} [ML^{-3}T^{-1}] and $K_{s,k}$ [ML^{-3}].

$$R_k = \frac{dc_k}{dt} = \mu_{max} \frac{C_k}{K_{s,k} + C_k} \quad \textit{Eq. 5}$$

In the model, Monod kinetic constants for the different reduction processes are based on laboratory studies of biodegradation of organic chemicals (references are listed in Table 2 of study 2) and were adjusted as part of the calibration process. Finally, calibrated coefficients are listed in Table 2 of study 2. Oxidation processes (iron(II) oxidation, ammonium oxidation, anaerobic and aerobic sulfide oxidation) were formulated using higher order reaction kinetics as listed in Table 2 of study 2. In redox controlled systems like wetlands, reduction processes occur sequentially where microorganisms use oxygen as primary electron acceptor first, before nitrate, iron(III) and sulfate are being used. To represent this sequential behavior within the biogeochemical model, different conditions were formulated for which the different reduction processes are being initiated. In the approach presented here, these conditions are represented by critical concentrations for redox-sensitive solutes which control whether a redox process is initiated or not. For the different reduction processes, controlling critical concentrations are listed in Table 1. Table 1 must be red row-wise, where entries ">0" mean that the corresponding redox-sensitive reactant (column) must be available and "-" means that this process does not depend on the presence of the redox-sensitive compound. For example iron(III) reduction in the biogeochemical simulation is only initiated if: (1) Dissolved oxygen concentrations fall below $Ccrit_{O_2}$; (2) Most of the nitrate is already depleted and actual concentrations fall below $Ccrit_{NO_3^-}$; and (3) The electron acceptor iron(III) is available.

Table 1: *Critical concentrations which are controlling the sequential initialization of the redox sequence. Values were derived from field observations. Table must be read row-wise (e.g. denitrification is initiated if 1) oxygen contents drop below C_{crit} for oxygen and 2) if nitrate is present). $Ccrit_{O_2}$ = 5.0 x 10^{-6} mol/L; $Ccrit_{NO_3^-}$ = 4.0 x 10^{-7} mol/L; $Ccrit_{Fe_{3+}}$ = 5.0 x 10^{-6} mol/L.*

	oxygen	nitrate	iron(III)	Sulfate
aerobic respiration	>0	-	-	-
denitrification	$< Ccrit_{O_2}$	>0	-	-
iron(III) reduction	$< Ccrit_{O_2}$	$< Ccrit_{NO_3^-}$	>0	-
sulfate reduction	$< Ccrit_{O_2}$	$< Ccrit_{NO_3^-}$	$< Ccrit_{Fe_{3+}}$	>0

The critical concentrations were formulated based on evaluation of depth profiles for redox-sensitive solutes which were taken at the Schlöpnerbrunnen II site in the Lehstenbach catchment (Knorr and Blodau, 2009; Knorr et al., 2009). Intervals for the activation of redox processes are overlapping, meaning that multiple processes can occur simultaneously which can be approved under laboratory as well as under field conditions (Knorr and Blodau, 2009; Knorr et al., 2009).

Availability of oxygen can be seen as a key component, controlling the process composition within wetland ecosystems. Processes like aerobic respiration or nitrification only occur if oxygen is

[29]

available. Other processes, like denitrification iron(III)- or sulfate-reduction are only initiated under anoxic conditions where oxygen concentrations are very low. Along a subsurface flow path, availability of oxygen varies as the hydrological boundary conditions change. Within the unsaturated zone, depleted oxygen is being replaced by diffusion of atmospheric oxygen and availability of oxygen for microbial catalyzed reactions is high. In the saturated zone dissolved oxygen concentrations are low because the resupply by diffusion is being inhibited by pore water, which acts as an effective diffusion barrier. Therefore, in the biogeochemical model oxygen availability was used as a key variable that either triggers or suppresses redox-sensitive processes. Along a sub-surface flow path, availability of oxygen was coupled to the transient pressure heads which were available as part of the virtual wetland modeling. For each PHREEQC sub-section simulation of a sub-surface flow path, the corresponding pressure head was estimated for the start location of the sub-section. Pressure heads were related to a certain oxygen concentration according to Figure 8. If the pressure head of the sub-section is located within zone 1 (unsaturated zone with negative pressure heads), the oxygen availability is at a maximum due to the uninhibited diffusion of atmospheric oxygen. Within zone 2 (saturated zone with positive pressure heads), oxygen contents are decreasing with increasing pressure heads representing increasing inhibition of oxygen diffusion with depth. Oxygen concentrations in sub-section simulations that are located either within zone 1 or 2 were set to a constant value reflecting that rapid resupply of oxygen prevents its depletion by oxygen consuming processes. For sub-sections that are located within zone 3 (deeper saturated zone with pressure heads above 0.25 m) oxygen is not assigned as a constant boundary condition. Instead, oxygen is set as an initial condition where the residual oxygen contents of the preceding sub-section are used as initialization. Within zone 3, where atmospheric diffusion is disrupted, oxygen can be totally depleted due to oxygen consuming processes. The relationship shown in Figure 8 was derived from observed oxygen-depth profiles taken at the Schlöppnerbrunnen II site in the Lehstenbach catchment (Knorr et al., 2009). Aside from an adequate electron acceptor (e.g. oxygen, nitrate, iron(III) or sulfate), microbial catalyzed reduction processes require a carbon source that is available to microorganisms. For the carbon rich systems studied here unlimited availability of carbon was assumed.
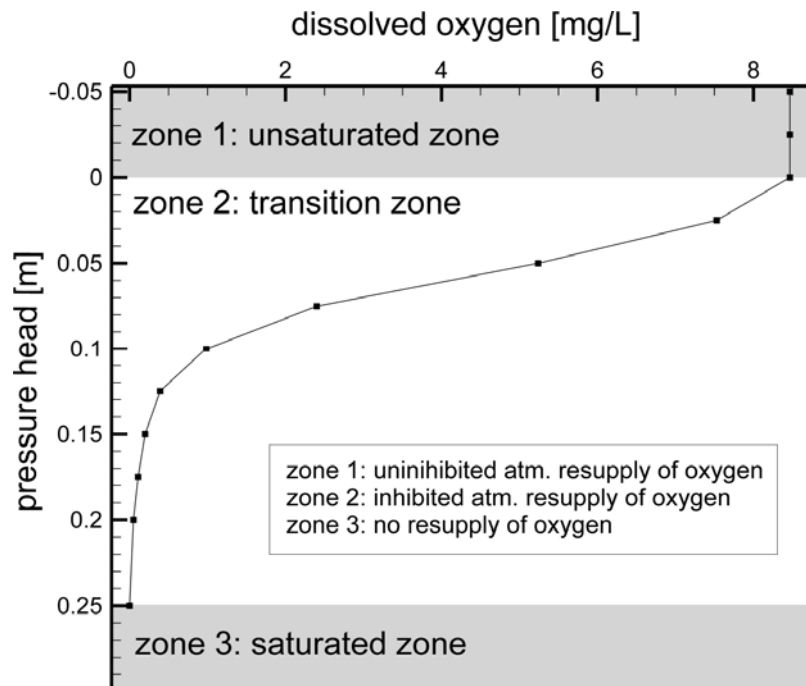
Figure 8: *Typical oxygen depth profile observed for a wetland site of the Lehstenbach catchment. Profile was used to assign oxygen boundary conditions to the different PHREEQC sub-section simulations based on transient model output of the virtual wetland model.*

4 Results and Discussion

4.1 Effects of micro-topography on surface-subsurface exchange and runoff generation in a virtual riparian wetland (Study 1)

Results from the virtual wetland modeling indicate that hydrological dynamics and runoff generation processes within the riparian wetland are significantly affected by the wetland's hummocky topography. Surface and subsurface runoff generation are influenced by distinct shifts between surface and sub-surface flow dominance resulting from the interplay between rainfall-induced fluctuations of the shallow water table and the surface micro-topography. Surface flows are characterized by a fill and spill mechanism, similar to what has been described for shallow subsurface drainage of hillslopes (Hopp and McDonnell, 2009). Here, surface depressions (hollows) are filled with water as soon as the groundwater level intersects with the land surface (e.g. during intensive rainstorm events).With increasing rainfall intensity ponded depressions start to interconnect, forming distinct surface flow networks which develop independently in space and time (as shown in Figure 9). These networks can rapidly drain large areas of the wetlands and at times (during very intensive rainstorm events) contribute up to 80% of the total discharge that is generated from wetlands.
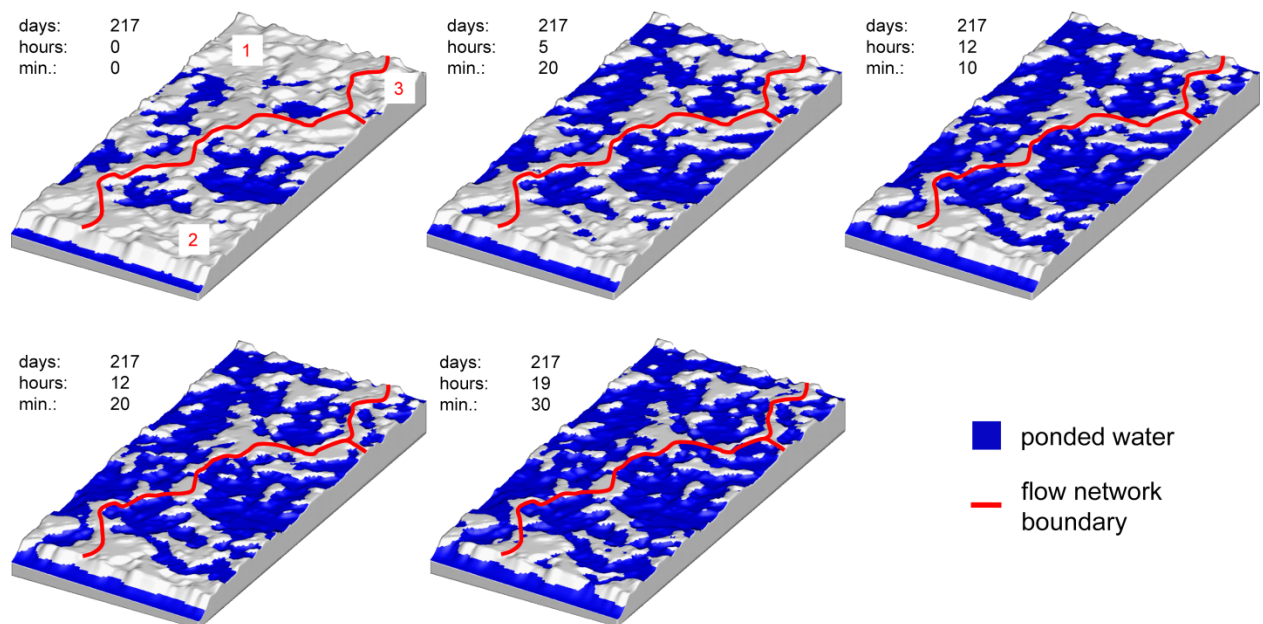
Figure 9: *Six consecutive snapshots of the evolving surface flow networks during the largest flow event of the year (day 217 to day 218). The red lines separate different flow networks (1-3) that developed independently from each other.*

However, whether such surface flow networks develop in space and time and whether surface runoff is generated in the wetlands depends on the history of the system. For rainstorms occurring after extended dry periods in summer, surface flow networks may not be generated because groundwater levels in the wetland are too far below the land surface to generate surface ponding. On the contrary, a

rainstorm of the same or even lesser intensity may cause the generation of significant surface runoff if it occurs with wet preconditions. The simulated runoff dynamics can also explain observed non-linear and hysteretic relationships between the riparian groundwater level in the wetlands and discharge being generated from it (Figure 10). The dynamic runoff generation mechanism, which is controlled by micro-topography where the system rapidly shifts between surface and subsurface flow dominance, was identified as a main driver for the observed non-linear dynamics. Similar non-linear relationships between water table and discharge have been reported for wetlands and riparian zones in other parts of the world (e.g. Fitzgerald et al. (2003)).

Understanding the mechanisms that govern hydrologic flow paths and stream flow generation in riparian zones is important, because nutrient transformation and export are integrally related to the hydrological dynamics (Gillham, 1984; Devito and Hill, 1997; Vidon and Hill, 2004; Lischeid et al., 2007). Although mobilization of solutes has not been explicitly simulated in study 1, the micro-topographic controlled runoff generation can have significant implications for the export of solutes (e.g. DOC, nitrate or sulfate) from the wetlands. Fast flow components like rapid surface drainage due to the extensive surface flow networks or shallow subsurface flow have the potential to quickly (within minutes to hours) mobilize solutes from the uppermost layers (10 to 20 cm) of the wetlands. Field observations (Knorr and Blodau, 2009; Knorr et al., 2009) for the Lehstenbach catchment have shown that these superficial layers, which are typically unsaturated, are rich in oxic species that accumulate during drier periods such as nitrate or sulfate. During rainstorms, which trigger generation of rapid surface and shallow subsurface drainage, these species can be flushed from the system. Along these very fast flow pathways nitrate and/or sulfate are not being reduced because deeper, anoxic layers are being bypassed by the superficial runoff components. In its effect on the mobilization of redox-sensitive solutes, this mechanism operates the same way as other bypassing processes that have been described for the Lehstenbach catchment (Lischeid et al., 2007) and for other comparable ecosystems (Curtis et al., 2011). Similar dynamics apply to the mobilization of DOC because its concentrations are also highest in the uppermost layers where fresh organic material is available and the peat is less decomposed than in deeper layers (Clemens, 2011).

The mechanistic understanding on how runoff is being generated on the small scale in the wetland areas and how the different flow components with their individual response and residence times contribute to stream flow generation is crucial to identify which flow pathways are important for solute mobilization. Findings from study 1 were subsequently used to develop a catchment-scale conceptual model for DOC mobilization presented as part of study 4. Moreover, findings that surface flow generation in the wetland areas is strongly influenced by micro-topography are important to simulate the catchment-scale hydrological dynamics (study 5), because rather than as sheet flow, surface flow in the catchment is generated in discrete surface flow networks in a threshold-controlled process, which must be accounted for in larger scale models (study 5). This was done by applying the rill storage concept developed as part of study 3.
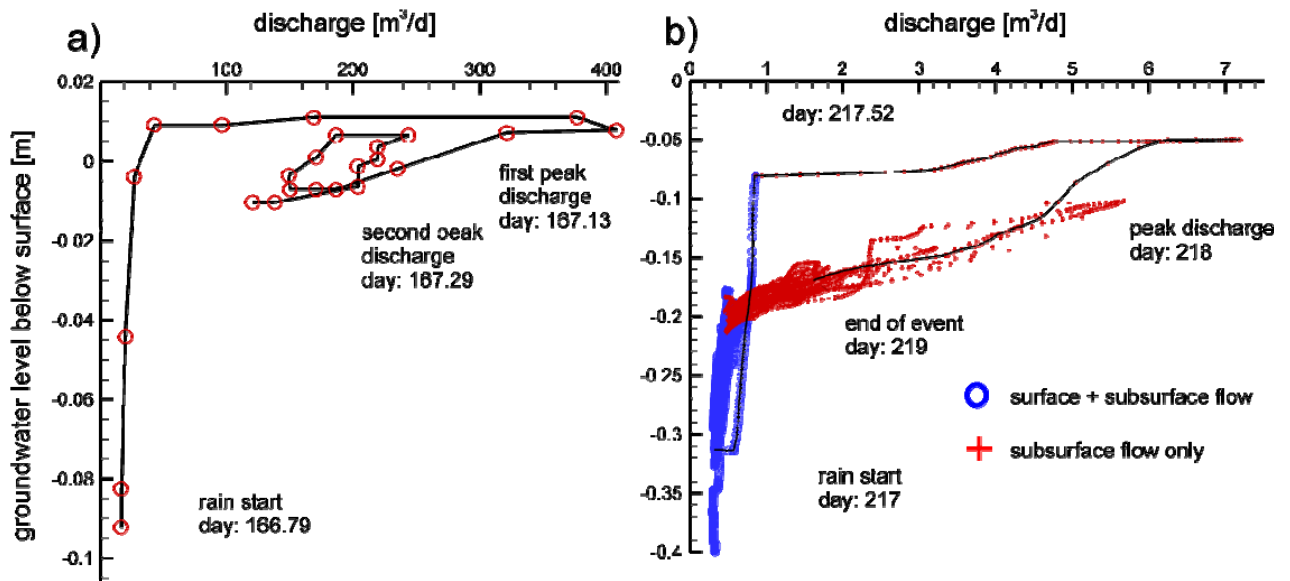
Figure 10: **a)** *Relationship between discharge and groundwater level for two peak flow events, observed for a small catchment located in British Colombia, Canada (modified after Fitzgerald et al. (2003)).***b)** *Simulated relationship between groundwater level and channel discharge for the micro-topography model. Blue filled circles represent times when no surface drainage occurs, red open circles represent conditions when surface drainage is being generated; different scales are used on the x-axis for better visibility of hysteretic behavior during low discharges; the sequence of days 217 to 219, representing an intense rain storm, is depicted by a line.*

4.2 Surface micro-topography causes hot spots of biogeochemical activity in wetland systems – a virtual modeling experiment. (Study 2)

Results from particle tracking show that superficial micro-topographical structures of the wetland cause a complex subsurface flow field with shallow and deeper flow cells that transport water and solutes across the model domain (Figure 11 A). The spatial distribution of high points (hummoks) and depressions (hollows) results in small-scale patterns of in- and exfiltration. Hummocks generally represent areas of preferential infiltration and hollows zones of preferential exfiltration (Figure 11 A). The coexisting deep and shallow flow system shows distinctly different flow velocities and subsurface residence times (Figure 11 B). The resulting complex redistribution of water in the subsurface and residence times, ranging from a few days to years, have significant effects on biogeochemical process patterns and the spatial distribution of redox-sensitive compounds in the wetlands. Biogeochemical simulations show the formation of local hot spots for redox processes within the wetlands. They are the result of the complex subsurface flow paths and the transport-limited availability of electron acceptors and donors. Hot spots for reduction of redox-sensitive species (e.g. denitrification, iron(III)- and sulfate reduction) are preferentially generated below local hummocks (Figure 11 C), whereas oxidation hot spots form in zones of upwelling water below hollows where older, reduced groundwater gets in contact with atmospheric oxygen (Figure 11 D).

Findings from study 2 mechanistically prove the existence of localized zones of higher reactivity (hot spots) where most of the biogeochemical turnover is accomplished within wetland system. This has been observed before in various field studies (e.g. Jacks and Norrström, 2004; Paul et al., 2006; Knorr, 2009). Typically, the generation of such hot spots has been explained by the heterogeneous distribution of static, physical-chemical properties of the soil (Reeve et al., 2001; Holden and Burt, 2003) or labile carbon input in the rhizosphere (Crow and Wieder, 2005). However, results from the biogeochemical simulations in this study demonstrate that the occurrence of reactivity hot spots does not need to be associated with static physical-chemical soil heterogeneities a priori. Results have shown that hot spots could theoretically develop even in homogenous peat soils due to a highly dynamic flow system with (1) complex surface/subsurface flow interactions, where surface micro-topography induces a subsurface flow field that defines a small-scale zonation of in- and exfiltration areas and (2) a hydrological control of the biogeochemical boundary conditions that either facilitated or suppressed redox processes in ex- and infiltration areas.

These results present a new perspective on biogeochemical transformation processes in riparian wetlands, which provides a dynamic framework to explain process heterogeneity in wetland soils and variability in process rates over space and time. Formation of biogeochemical hot spots as a result of the mechanisms presented in this study may furthermore explain how material heterogeneity is being generated within the subsurface. Biogeochemical hot spots may have the potential to alter the hydrodynamic properties of the peat or wetland soils. The precipitation of iron oxides for example,

which preferentially occurs at oxidation hot spots, can lead to a reduction of the effective porosity and a lower hydraulic conductivity, providing a negative feedback on oxygen penetration.

Future work will have to address under which climatic conditions the simulated biogeochemical hot spots are stable, because shifts in climatic forcing due to climate change will probably affect the in study 1 simulated surface/subsurface flow interactions as well as the sub-surface flow field. This will in turn affect the oxygen availability and the biogeochemical process distributions within the wetlands. During extended drought periods for example, which are predicted by climate models for the temperate zones (McCarty et al., 2001), biogeochemical hot spots are likely to vanish as the system gradually shifts towards a more homogenous process distributions. Here, the dropping groundwater may be responsible for the reversal of the hydraulic gradients under depressions, switching from upwelling to infiltrating conditions. In turn oxidation hot spots will diminish because resupply of reduced species from upwelling groundwater is disrupted.

The effect of the biogeochemical process patchiness on solute exports (e.g. nitrate or sulfate) out of the wetland areas has also to be investigated further. Because of model limitations it was so far not possible to link the internal biogeochemical process distributions to the runoff generation mechanisms presented in study 1 in order to explicitly simulate solute exports under conditions of hot spot formation. Such an integrated simulation would also help to further improve the in study 4 presented conceptual model on catchment-scale solute mobilization.
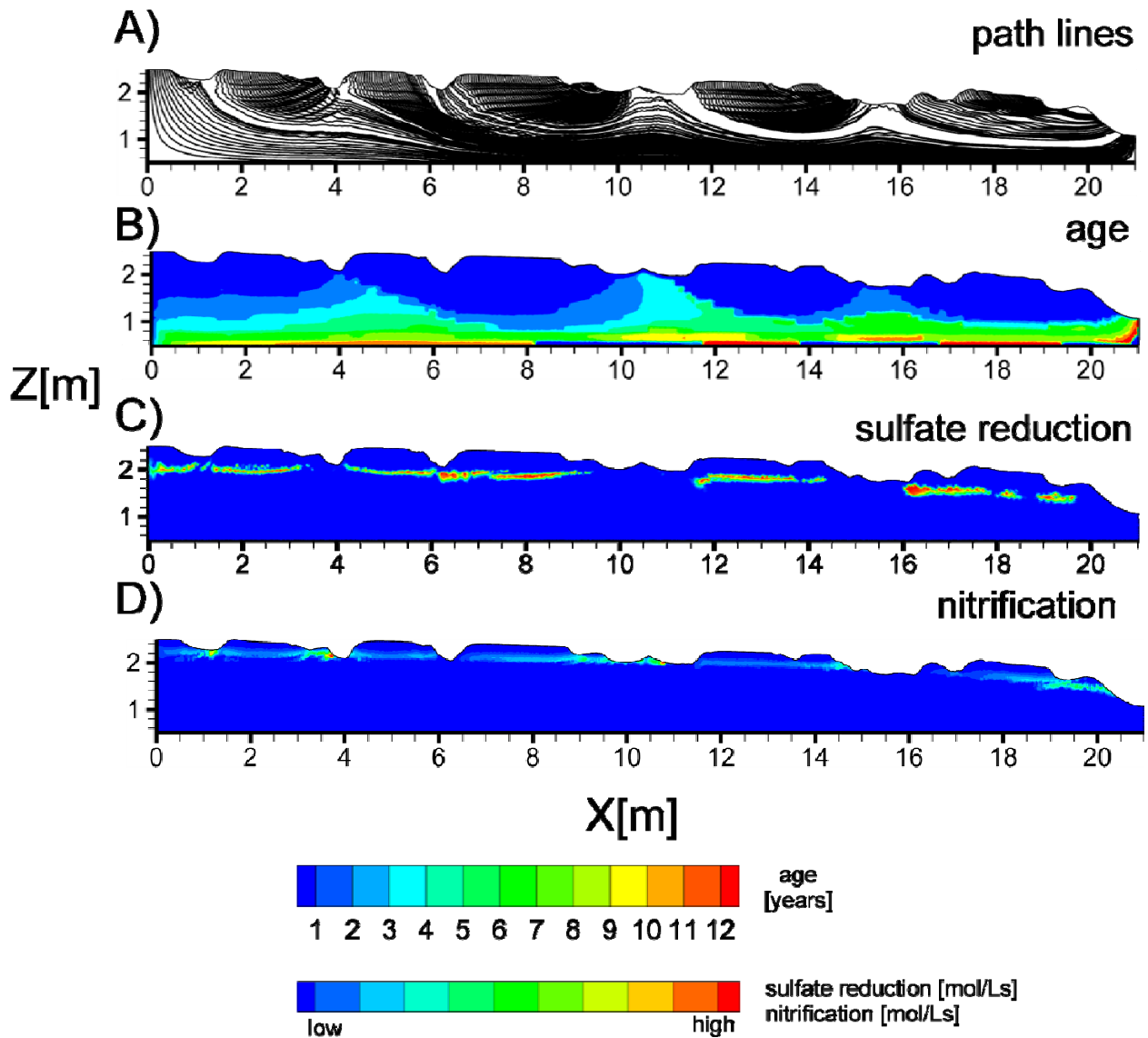
Figure 11: *Results of the biogeochemical simulations shown for the sulfate reduction process of the micro-topography scenario with the mean length 0.5m. PHREEQC simulations were performed along the flow paths shown in A. Results were interpolated into the 2D cross sections. B shows the age distribution in years of subsurface flow derived from backward particle tracking. C represents process activity of sulfate reduction (kinetic rate in mol/Ls). Hot spots for reduction processes preferentially develop below local hummock structures for infiltration conditions. D represents process activity of nitrification (kinetic rate in mol/Ls), exemplarily for oxidation processes. Hot spots for oxidation processes preferentially develop below local depressions for upwelling conditions.*

4.3 Representing effects of micro-topography on runoff generation and sub-surface flow patterns by using superficial rill storage height variations (Study 3).

Results from study 1 and 2 show that micro-topography is directly or indirectly responsible for: (1) Complex runoff generation processes during rainstorms where saturated overland flow occurs in defined surface flow networks and micro-channels. (2) Characteristic subsurface flow patterns as a result of micro-topography moderated surface/subsurface flow interactions. (3) Formation of biogeochemical hot spots as a result of the interactions between micro-topography moderated surface/subsurface flow and biogeochemical processes in the subsurface. However, virtual wetland modeling also demonstrated that the representation of small scale hydrological and biogeochemical processes in spatially-explicit models can be computationally demanding, resulting in very long simulation times. This computational effort restricts the application of such models to small scales. However, beyond the plot-scale, e.g. in catchment-scale models, it might be important to represent small-scale variations in topography to adequately predict runoff generation (Bronstert and Plate, 1997; Sharratt et al., 1999; Nakayama and Watanabe, 2006,). To accomplish this, an approach is needed that simplifies the representation of micro-topography in numerical flow models in order to reduce the computational burden of spatially-explicit models.

Replacing the small scale DEM with two dimensional spatially distributed rill storage height zones to represent micro-topography allows to use a coarser numerical mesh, which significantly decreases computational demands. By using the rill storage concept to represent micro-topography computation times could be reduced to 0.63 days from the 48 days necessary for the original micro-topography model. At the same, time important aspects of micro-topography-induced hydrologic dynamics are being maintained: (1) Surface runoff during intensive rainstorms occurs in discrete micro-channels, forming extended surface flow networks similar to those observed for the original micro-topography model (Figure 12). (2) The typical micro-topography-induced subsurface flow patterns as a result of the small scale variations in in- and exfiltration as identified in study 2. (3) The formation of biogeochemical hot spots, as presented in study 2, as a result of complex interactions between the subsurface flow field, biogeochemical processes and non-uniform hydrological and biogeochemical boundary conditions, as well as (4) the power law distribution of subsurface residence times that is associated with the micro-topography induced subsurface flow field. However, results also demonstrate that models that use superficial rill storage height variations often fail to adequately simulate the exact timing of surface flow network activation, mainly because it is very hard to represent the exact amount of threshold storage capacities with the rill storage approach. Furthermore, it has to be mentioned that surface runoff in the micro-topography model is predominantly generated due to saturation excess where the local groundwater level rises to the land surface. Whether the rill storage concept can also be applied to systems with micro-topography where surface runoff is

generated due to infiltration excess, like for example in arid system as described by Solé-Benet et al. (1997), remains to be tested.
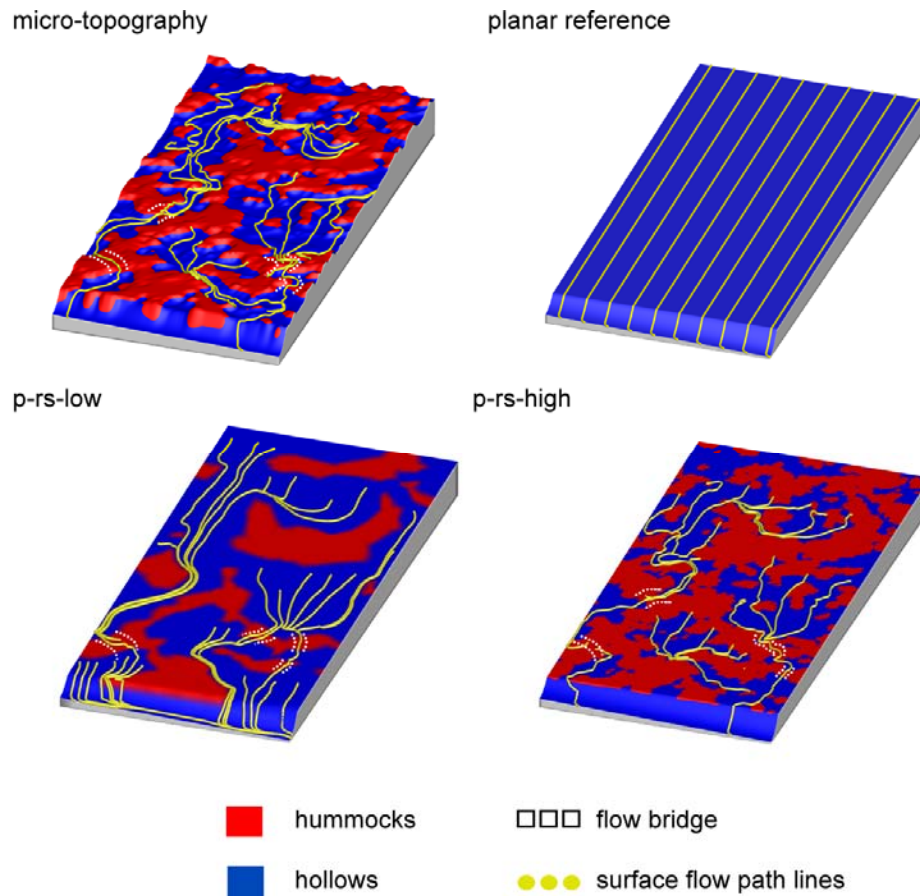
Figure 12: *Snap shots taken at the end of a steady rainfall simulation showing the fully developed surface flow networks (yellow) which are generated in the micro-topography model as well as in the models with rill storage height variations (p-rs-low and p-rs-high) yet not for the planar reference case. Surface flow networks dynamically develop out of inter-connected, ponded depression areas. Flow bridges (white squares) belong to hummock zones were the inter-connection between ponded depressions occurs by overspilling.*

Results show that the rill storage concept can be an efficient way to represent the impact of micro-topography on hydrological processes. As shown exemplarily for the virtual wetland model, grid resolution can be reduced by the factor ten by using the rill storage concept while preserving important aspects of micro-topography driven hydrological processes. Because simulation times drop very dramatically if the rill storage concept is being applied on the plot scale, future simulations addressing open research questions of study 1 or 2 can be carried out much more efficiently. For example, the investigation of the impact of climate change on the stability of biogeochemical hot spots in hummocky wetlands (see preceding chapter) would require a large amount of simulations to represent different climate change scenarios. Such Monte Carlo approaches are only possible if the individual simulation runs can be solved in manageable time scales.

On the small scale, results of study 1 have shown that runoff generation in the wetland areas is

significantly affected by micro-topography. However these processes, that control runoff generation on the small scale may also be important on the larger scale, but cannot easily be transferred into watershed or catchment-scale models because grid resolutions are too coarse to explicitly account for micro-topography. Here, the rill storage concept provides a viable means to account for effects of micro-topography beyond the plot scale. First results along those lines look promising where the rill storage concept was used to account for the threshold-controlled surface flow generation mechanism as part of the catchment-scale modeling of study 5. However, further work is needed to test more rigorously, which aspects of micro-topography driven surface and subsurface flow processes can be adequately mimicked at larger scales by applying the rill storage concept and which ones can not.

4.4 Concentrations and fluxes of dissolved organic carbon in runoff from a forested catchment: insights from high frequency measurements (Study 4)

High frequency measurements of DOC concentrations in runoff of the Lehstenbach catchment revealed that DOC export is subject to substantial short term variations at an hourly to daily time scale, with concentrations ranging from 3-34 mg/L. In general, DOC concentrations at the lower end occurred at baseflow conditions and highest concentrations were measured during highflow events. The relationship between DOC and discharge followed counter-clockwise hysteretic loops, as shown in Figure 13 (dt = 15 min). These loops had different shapes at different times of the year. Such hysteretic relationships between DOC concentrations and discharge have been reported for different catchments (e.g. Andrea et al., 2006; Hood et al., 2006; Raymond and Saiers, 2010). Furthermore, results from the high frequency measurements showed that the observed hysteretic loops are dynamic where single events have unique trajectories (Figure 13 dt =15 min) in the concentration/discharge relationship. However, to capture the progression of the rising and falling limps for single storm flow events correctly, a high sampling frequency is necessary. Lower sampling frequencies can result in a miss-interpretation of the hysteretic relationships as exemplarily demonstrated in Figure 13. Weekly or monthly sampling frequencies, as suggested by Koehler et al. (2009), would be far too low to reveal the short term variations in DOC concentrations in runoff of the Lehstenbach and would result in massive errors in DOC export calculations.

Short term variations of DOC in runoff have been related to changing water flow paths, which are mainly originating from the wetland areas of the Lahstenbach catchment. Forested sites can be ruled out as a potential source for DOC because percolating water at forested areas is low in DOC concentrations (1-3 mg/L), mainly due to sorption and decomposition (Schulze et al., 2011). Results from numerical modelling and field observations point to the riparian wetland soils as the major source of DOC in runoff. Field observations have shown that the highest DOC (up to 40 mg/L) concentrations are found in the upper layers of the wetland soils while concentrations are low in deeper layers. In the wetlands, mobilization of DOC is likely controlled by the so-called "*transmissivity feedback*" mechanism (Bishop, 1991; Bishop et al., 2004 and Seibert et al., 2009) which is caused by a decrease in the lateral saturated hydraulic conductivity with depth in the riparian wetland soils. Hydraulic conductivities in the deeper layers are lower due to the compacted and more decomposed organic material than in the porous and less decomposed shallow layers. The differences in hydraulic conductivities between deeper and shallow layers of wetland soils can be several orders of magnitude (Jacks and Norrström, 2004), causing shallow layers to drain much more effectively than the deeper soil layers. The shallow layers of the riparian wetland soils typically contain more DOC than deeper soil layers. Once the water table rises, layers of high DOC concentrations and high conductivity are drained causing the strong response of DOC in runoff. The DOC pool available for mobilization in the riparian wetland soils seems to be large (Worrall et al., 2008) in wetland

ecosystems. In this study no decrease in maximum DOC concentrations could be observed during series of consecutive rain events.
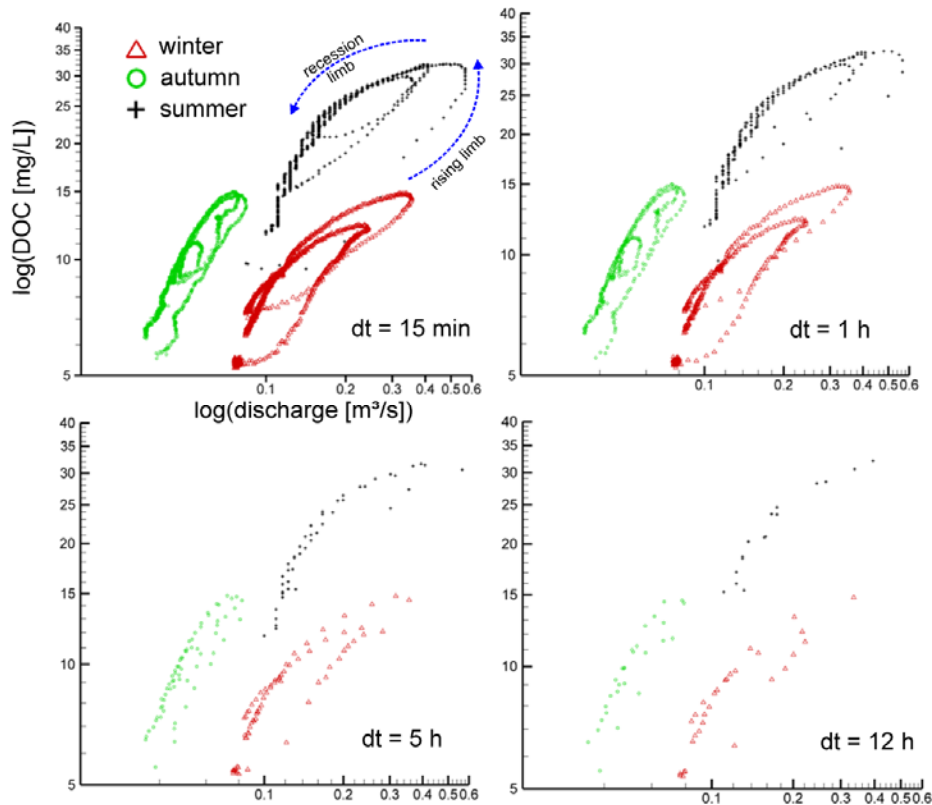
Figure 13: *Typical non-linear and hysteretic relationships between observed DOC concentrations in runoff and discharge. Original measurement resolution was dt = 15 min. Trajectories of the rising and falling limps are unique for different rainfall events and general patterns of the relationship show a seasonal variation. A correct interpretation of the trajectory e.g. for annual export calculations requires a high sampling resolution. Sampling resolution was artificially lowered to dt = 1, 5 and 12 hours, respectively, to mimic the impact of lower sampling resolutions. Trajectories for sampling resolutions above 5 h do not show the characteristic progression of the rising limb anymore, with the result that such a relationship easily can be misinterpret as a linear relationship, leading to massive errors in annual export calculations for DOC*

Comparing the findings of study 1 and 4, two different mechanisms were identified that can explain non-linearities in the concentration vs. discharge (study 4)/groundwater depth vs. discharge relationships (study 1). Results from this study suggest the transmissivity feedback mechanism as the potential driver for the non-linear relationship, whereas study 1 ascribes the non-linear response to effects induced by micro-topography. In reality, probably both mechanisms operate jointly. We suspect that in such cases transmissivity feedback will control non-linear response in the low to moderate stream flow range, whereas micro-topography induced dynamics will dominate the upper stream flow range when surface flow has already been initiated, sine then flow to the stream is no longer constrained by porous media flow. However, should the uppermost soil layers be so conductive to allow very large lateral subsurface flows to the streams, it is unlikely that ponding will occur as infiltrating water is quickly moved away laterally. In this case the effects of micro-topography on the non-linear runoff response will be minimal.

[43]

4.5 Interpreting flow generation mechanisms from integrated surface water-groundwater flow models of a riparian wetland and catchment (Study 5).

The Hydraulic Mixing-Cell (HMC) methodology (Partington et al., 2011 and Partington et al., 2012) has proven to be a useful tool for assessment of catchment functioning and separation of flow hydrographs. Applied to the catchment scale model of the Lehstenbach, the HMC method elucidated the complexity in the spatiotemporal distribution of the different runoff generation mechanisms. The different flow components which were identified to dominate runoff generation for the Lehstenbach catchment are, (1) groundwater discharge to the stream network (GW-CH), (2) direct rainfall entering the streams (RF-CH) and (3) stream inputs due to saturated overland flow from the wetland areas. Overland flow from the riparian wetlands was further sub-divided into a surface flow fraction originating from groundwater exfiltration (GW-WL) and overland flow generated from rainfall falling onto entirely water saturated areas of the wetlands (RF-WL). Relative contributions of the five different runoff generation mechanisms are tracked in time and space by the HMC routine. The HMC routine was applied for a large storm event (13th- 21st July, 2001) as well as for the entire 2001 hydrological year (11/01/2000 – 10/31/2001). Results for the storm event are shown in Figure 14. The GW-CH component (panel A) dominates runoff generation over large areas of the stream network prior to the storm event during low flow conditions. At the peak of the storm, GW-CH generation is of minor importance as other generation mechanisms are activated (RF-CH, GW-WL and RF-WL in panel B, C and D, respectively). Most overland flow that contributs to stream discharge during the storm event is generated due to rainfall, which is directly falling onto the fully water saturated wetland areas as indicated by the high relative fraction of the RF-WL component in panel B. On an annual basis, total stream water leaving the catchment at the outlet (shown in Figure 5), according to the HMC analysis, consists of 67.9% of water originating from groundwater inputs (GW-CH), 12.6% of direct rainfall to the stream network and 19.5% of saturated overland flow from the wetland areas (GW-WL + RF-WL). However, overland flow was identified to be only relevant during very intensive rainstorm events and is only generated in significant proportions in the areas of wetland that are close to the catchment outlet. According to the HMC analysis, no overland flow is generated in the forested areas because rainfall quickly infiltrates there and recharges the underlying regolithic aquifer.
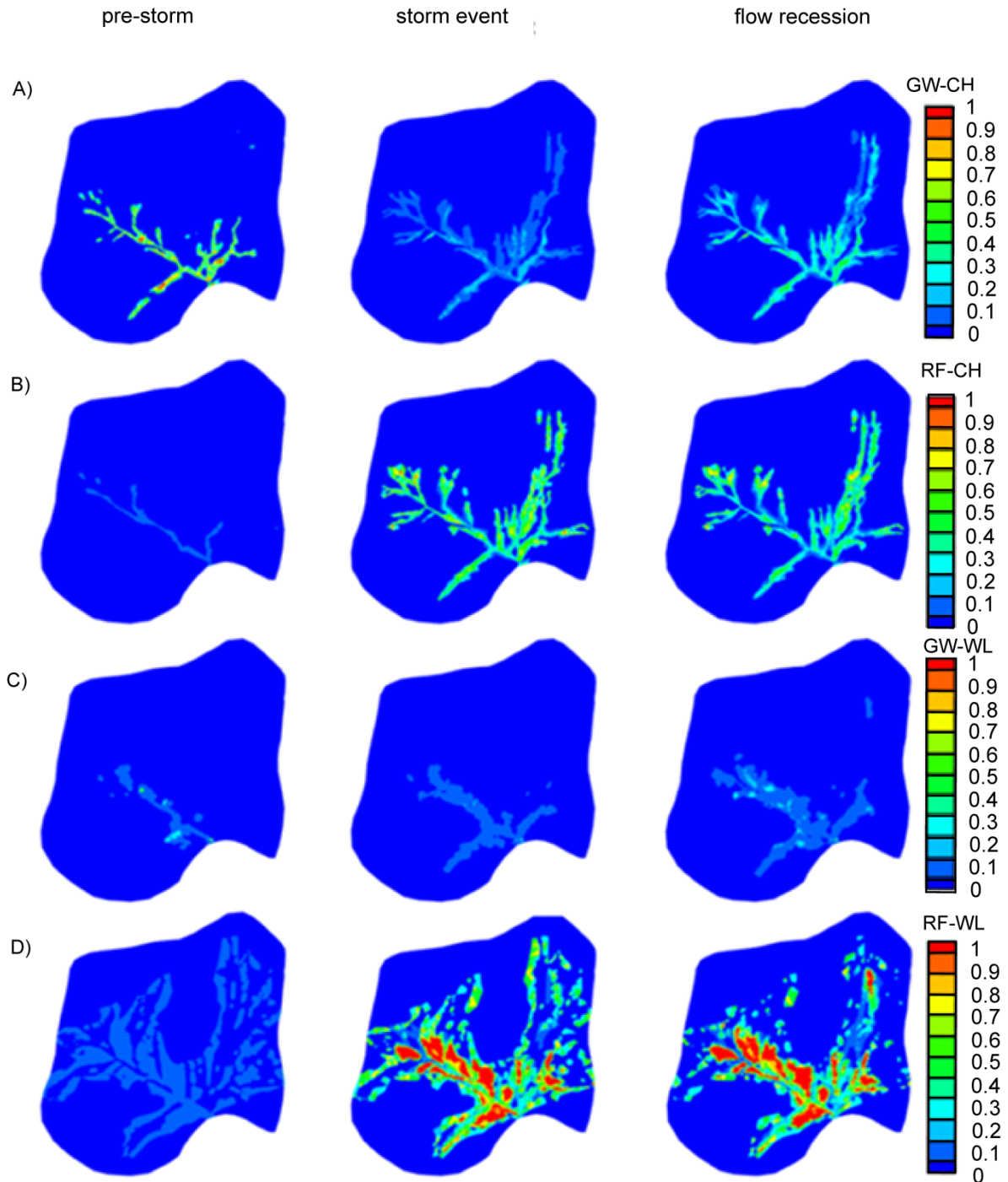
Figure 14: *Calculated stream and overland flow generation, estimated by applying the "hydraulic mixing-cell" methodology to the Lehstenbach catchment model. The flow generation components tracked are: a) groundwater discharge to the channel (GW-CH), b) rainfall to the channel (RF-CH), c) groundwater discharge to the wetlands (GW-WL), and d) rainfall to the wetlands (RF-WL). Relative contributions (colored scales ranging from 0 to 1) were tracked for a typical storm flow event.*

However, the response times of subsurface flow entering the stream network (GW-CH) to rainfall seems to be very fast. This can be explained by the *"pressure wave propagation"* mechanism (Germann et al., 1990; Lischeid, 2008), where increasing hydraulic pressure in the upslope areas mobilizes groundwater further downslope (e.g. in the center of the bowl-shape catchment). Interestingly, surface flow components from the wetland areas (GW-WL + RF-WL), which are usually regarded as very fast flow components, show a clearly delayed response to rainfall inputs. This can partly be explained by the threshold-controlled *"fill and spill"* surface flow generation mechanisms described in study 1 where small scale depressions first have to be filled with water before any surface flow towards the stream is generated. The threshold-controlled surface flow generation caused by the micro-topography has been accounted for in the catchment-scale model by applying the rill-storage height concept presented in study 3.

Whether simulated fluxes from the individual runoff generation processes as estimated by the HMC analysis actually match with the more complex reality is questionable due to simplifications in the model. For example, direct rainfall inputs to the stream network are presumably negligible as streams cover only a minor fraction of the catchment area (Lischeid, 2008). In the catchment scale model, however, stream segments occupy comparatively large fractions of the total area because the resolution of the numerical mesh was too coarse to adequately represent the narrow stream channels. This explains the large fractions of the RF-CH component (12.6% of total discharge per year) in the simulated discharge. Nevertheless, the HMC method in combination with numerical modeling provides a valuable tool to assess whether or not a catchment model behaves in the expected way or, more importantly, the way the catchment processes are conceptualized. In that sense it is a promising and useful tool for a *"soft calibration"* based on understanding of catchment functioning from real observations.

A future application of the HMC method in combination with the catchment-scale model of the Lehstenbach area could be to separate runoff components originated from forested sites and wetland areas. Water originating from the wetlands and forested sites have very different chemical signatures (e.g. oxygen saturation, redox states or DOC loadings) which are being mixed within the stream or the hyporheic zone. Applying the HMC analysis to track how much water in stream runoff is originated from the wetlands and forested sites would improve our understanding on the relative contributions of different flow paths to stream discharge and solute exports.

5 Conclusions and Outlook

Findings from this thesis have shown that the combination of field investigations, virtual experiments and catchment scale numerical modeling has proven to be a very useful combination to investigate and explore scale-dependent runoff generation processes and couplings between hydrology and biogeochemistry. On the catchment scale, couplings between hydrology and biogeochemistry were identified to be very important for the mobilization of DOC. Flow components, relevant for the generation of runoff in the Lehstenbach catchment, contribute differently to the mobilization of DOC. Deep groundwater flow originated from the forested upslope areas was identified to be generally low in DOC, mainly because percolating water for forested sites is being efficiently depleted in DOC due to sorption and biogeochemical decomposition processes. Fast flow components like surface flow or interflow, which would have the ability to bypass soil layers where sorption and decomposition occur, could not be verified for the forested areas, neither in field investigations nor in numerical simulations.

Field investigations and numerical modeling indicate that the potential for DOC mobilization is highest for flow components located within the riparian wetlands. Mobilization of DOC within the riparian wetlands is controlled by the interplay of **(1)** the *transmissivity feedback* mechanism controlling the depth dependent dynamics and timescales of subsurface transport, **(2)** a threshold-controlled surface flow generation where, episodically, large amounts of surface water are rapidly being mobilized in extended surface flow networks and **(3)** the depth dependent availability of DOC caused by the lateral variation of DOC production and the non-uniform biogeochemical transformation and degradation processes. Episodically, the activation of fast flow components in shallow layers and/or on the surface is responsible for the mobilization of large amounts of DOC, which can explain observed short term variations of DOC concentrations in runoff.

This conceptual view on how DOC is being mobilized at the catchment-scale relates physical controlled mobilization pathways to the biogeochemical substrate availability and includes scale-bridging insights on DOC mobilization and runoff production. Hydrological and biogeochemical process interactions, identified to be relevant for the mobilization of DOC in the Lehstenbach catchment, are, in our opinion, of general significance and can be transferred to similar ecosystems. However, this conceptional view on how DOC is being mobilized in the Lehstenbach catchment has to be further improved and verified. Recent field investigations (Knorr, 2012) e.g. show that timescales of complexation and de-complexation of DOC with dissolved iron in addition to iron reduction/oxidation cycles significantly control the availability of DOC, especially in the superficial layers of the wetlands. This so far has not been accounted for in the developed conceptual model. Also, the significance of the interplay between different hydrological flow paths with their individual response and residence times combined with the spatial heterogeneity of biogeochemical conditions

(forested sites vs. wetlands) on nutrient cycling and solute mobilization is, in general, so far only still poorly understood and must be further addressed in future work. First preliminary results for nitrate (unpublished data) for example hint that the mobilization processes across the catchment differ significantly from those identified for DOC, mainly because spatial sources of nitrate and biogeochemical transformation processes along the flow paths are different for nitrate compared to DOC.

On the small scale, results from the developed hydrological and biogeochemical model, where sub-surface transport processes and kinetically controlled redox-sensitive reactions are represented equally, highlight how complex couplings between hydrology and biogeochemistry can be within wetland ecosystems. One of the most interesting results of this thesis is that biogeochemical hot spots can form even in homogenous peat or wetland soils, simply as a result of the interactions between a highly dynamic, three-dimensional subsurface flow system induced by micro-topography and the hydrologically controlled biogeochemical boundary conditions that either facilitate or suppress redox-sensitive processes. Results from this modeling approach offer a new perspective on biogeochemical transformation processes in riparian wetlands which provides a dynamic framework to explain process heterogeneity in wetland soils and variability in process rates over time and space.

A next step would be to approve that the simulated mechanisms and interactions between hydrology and biogeochemistry actually can result in the formation of biogeochemical hot spots under field conditions. This is a challenging task because characterization of subsurface flow patterns in situ, necessary to investigate interactions between hydrology and biogeochemistry, is very difficult and would require improved experimental settings. However, the framework presented as part of this thesis may be helpful to develop such novel in situ experiments. Because of various limitations and simplifications, the hydrological/biogeochemical modeling approach so far is restricted to relative simple test case scenarios. Future work will have to address these shortcomings and improve the modeling framework stepwise in order for it to be applied to more realistic systems and to address topics like the interplay between different static (e.g. soil properties, vegetation patterns) and dynamic controls (e.g. flow, temperature and vegetation dynamics) of spatial and temporal variations in biogeochemical process activities in wetlands.

Finally, this thesis has shown that interdisciplinary research efforts, combining the knowledge of hydrologists and biogeochemists, offer new perspectives on how ecosystems are functioning. However, a lot of knowledge gaps still exist and in order to fill these gaps and to improve our understanding on how nutrients and elements are cycled at various scales within ecosystems, it is necessary to further organize "*joint task forces*" among the different disciplines to develop new interdisciplinary approaches where hydrological and biogeochemical methods and perceptions are being exchanged and adopted.

6   References

Alewell, C., Paul, S., Lischeid, G., Storck, F.R., 2007. Co-regulation of redox processes in freshwater wetlands as a function of organic matter availability? Science of the Total Environment 404 (2-3), 335–342. doi:10.1016/j.scitotenv.2007.11.001.

Andrea, B., Francesc, G., Jérôme, L., Eusebi, V., Francesc, S., 2006. Cross-site comparison of variability of DOC and nitrate c–q hysteresis during the autumn–winter period in three Mediterranean headwater streams: a synthetic approach. Biogeochemistry 77 (3), 327–349.

Antoine, M., Javaux, M., Bielders, C., 2009. What indicators can capture runoff-relevant connectivity properties of the micro-topography at the plot scale? Advances in Water Resources 32 (8), 1297–1310. doi:10.1016/j.advwatres.2009.05.006.

Baillie, M., Hogan, J., Ekwurzel, B., Wahi, A., Eastoe, C., 2007. Quantifying water sources to a semiarid riparian ecosystem, San Pedro River, Arizona. Journal of Geophysical Research 112 (G3), G03S02.

Barber, K., 1981. Peat stratigraphy and climatic change: a palaeoecological test of the theory of cyclic peat bog regeneration. Balkema, Rotterdam.

Bellevue, W., 2003. Tecplot User's Manual. Amtec Engineering Inc.

Beven, K., 1989. Changing ideas in hydrology - The case of physically-based models. Journal of Hydrology 105 (1-2), 157–172.

Beven, K., 1993. Prophecy, reality and uncertainty in distributed hydrological modelling. Advances in Water Resources 16 (1), 41–51.

Bishop, K., 1991. Episodic increase in stream acidity, catchment flow pathways and hydrograph seperation. Ph.D. thesis, Cambridge University, Cambridge, UK.

Bishop, K., Seibert, J., Köhler, S., Laudon, H., 2004. Resolving the Double Paradox of rapidly mobilized old water with highly variable responses in runoff chemistry. Hydrol. Process 18 (1), 185–189.

Boano, F., Demaria, A., Revelli, R., Ridolfi, L., 2010. Biogeochemical zonation due to intrameander hyporheic flow. Water Resources Research 46 (2), W02511.

Branfireun, B., Roulet, N., 1998. The baseflow and storm flow hydrology of a precambrian shield headwater peatland. Hydrological Processes 12 (1), 57–72.

Bronstert, A., Plate, E., 1997. Modelling of runoff generation and soil moisture dynamics for hillslopes and micro-catchments. Journal of Hydrology 198 (1-4), 177–195.

Brookfield, A.E., Sudicky, E.A., Park, Y.J., Conant Jr., B., 2009. Thermal transport modelling in a fully integrated surface/subsurface framework. Hydrological Processes (23), 2150–2164. 10.1002/hyp.7282.

Brooks, P., Lemon, M., 2007. Spatial variability in dissolved organic matter and inorganic nitrogen concentrations in a semiarid stream, San Pedro River, Arizona. Journal of Geophysical Research 112 (G3), G03S05.

Brooks, R., Corey, A., 1964. Hydraulic properties of porous media. Hydrology Papers, Colorado State University (March).

Burt, T.P., Pinay, G., 2005. Linking hydrology and biogeochemistry in complex landscapes. Progress in Physical Geography 29 (3), 297–316.

Carle, S., Fogg, G., 1996. Transition Probability-Based Indicator Geostatistics. Mathematical Geology 28 (4), 453–476.

Chapin, F., 1991. Integrated responses of plants to stress. BioScience 41 (1), 29–36.

Chimner, R., Cooper, D., 2003. Influence of water table levels on CO_2 emissions in a Colorado subalpine fen: an in situ microcosm study. Soil Biology and Biochemistry 35 (3), 345–351.

Cirmo, C.P., McDonnell, J.J., 1997. Linking the hydrologic and biogeochemical controls of nitrogen transport in near-stream zones of temperate-forested catchments: a review. Journal of Hydrology 199 (1-2), 88–120.

Clemens, C., 2011. Biogeochemische Charakterisierung der Wiedervernässung eines Hangmoores im Fichtelgebirge. Master Thesis, University of Bayreuth, Bayreuth.

Conway, V., 1948. Von Post's work on climatic rhythms. New Phytologist 47 (2), 220–237.

Crockford, R.H., Richardson, D.P., 2000. Partitioning of rainfall into throughfall, stemflow and interception: effect of forest type, ground cover and climate. Hydrological Processes 14 (16-17), 2903–2920.

Crow, S., Wieder, R., 2005. Sources of CO_2 emission from a northern peatland: root respiration, exudation, and decomposition. Ecology 86 (7), 1825–1834.

Curtis, C., Evans, C., Goodale, C., Heaton, T., 2011. What Have Stable Isotope Studies Revealed About the Nature and Mechanisms of N Saturation and Nitrate Leaching from Semi-Natural Catchments? Ecosystems, 1–17.

Dent, C., Grimm, N., 1999. Spatial heterogeneity of stream water nutrient concentrations over successional time. Ecology 80 (7), 2283–2298.

Dent, C., Grimm, N., Fisher, S., 2001. Multiscale effects of surface-subsurface exchange on stream water nutrient concentrations. Journal of the North American Benthological Society 20 (2), 162–181.

Devito, K.J., Hill, A.R., 1997. Sulphate dynamics in relation to groundwater-surface water interactions in headwater wetlands of the southern Canadian Shield. Hydrological Processes 11 (5), 485–500.

DeWalle, D., Swistock, B., 1994. Causes of episodic acidification in five Pennsylvania streams on the northern Appalachian Plateau. Water Resources Research 30 (7), 1955–1963.

D'odorico, P., Laio, F., Porporato, A., Rodriguez-Iturbe, I., 2003. Hydrologic controls on soil carbon and nitrogen cycles. II. A case study. Advances in Water Resources 26 (1), 59–70.

Doran, J.W., Linn, D.M., 1984. Effect of water-filled pore space on carbon dioxide and nitrous oxide production in tilled and nontilled soils. Soil Science Society of America Journal 48 (6), 1267–1272.

Eshleman, K., Pollard, J., O'Brien, A., 1994. Interactions between groundwater and surface water in a Virginia coastal plain watershed. 1. Hydrological flowpaths. Hydrological Processes 8 (5), 389–410.

Estop-Aragonés, C., Blodau, C., 2012. Effects of experimental drying intensity and duration on respiration and methane production recovery in fen peat incubations. Soil Biology and Biochemistry 47, 1–9.

Estop-Aragonés, C., Knorr, K., Blodau, C., 2012. Controls on in situ oxygen and dissolved inorganic carbon dynamics in peats of a temperate fen. Journal of Geophysical Research 117 (G2), G02002.

Fiedler, F.R., Ramirez, J.A., 2000. A numerical method for simulating discontinuous shallow flow over an infiltrating surface. International journal for numerical methods in fluids 32 (2), 219–239.

Fisher, S., Grimm, N., Martí, E., Holmes, R., Jones, J.J., 1998. Material spiraling in stream corridors: a telescoping ecosystem model. Ecosystems 1 (1), 19–34.

Fisher, S., Sponseller, R., Heffernan, J., 2004. Horizons in stream biogeochemistry: flowpaths to progress. Ecology 85 (9), 2369–2379.

Fitzgerald, D.F., Price, J.S., Gibson, J.J., 2003. Hillslope-swamp interactions and flow pathways in a hypermaritime rainforest, British Columbia. Hydrological Processes 17 (15), 3005–3022. 10.1002/hyp.1279.

Fleckenstein, J., Niswonger, R., Fogg, G., 2006. River-Aquifer Interactions, Geologic Heterogeneity, and Low-Flow Managment. Groundwater 44 (6), 837–852.

Fraser, C.J., Roulet, N.T., Moore, T.R., 2001. Hydrology and dissolved organic carbon biogeochemistry in an ombrotrophic bog. Hydrological Processes 15 (16), 3151–3166. 10.1002/hyp.322.

Frei, S., Fleckenstein, J.H., Kollet, S.J., Maxwell, R.M., 2009. Patterns and dynamics of river-aquifer exchange with variably-saturated flow using a fully-coupled model. Journal of Hydrology 375 (3-4), 383–393.

Germann, P., Anderson, M.G., Burt, T.P., 1990. Macropores and hydrologic hillslope processes. Process Studies in Hillslope Hydrology, 327–363.

Gerstberger, P. (Ed.), 2001. Waldökosystemforschung in Nordbayern: Die BITÖK-Untersuchungsflächen im Fichtelgebirge und Steigerwald. Bayreuther Forum Ökologie.

Gillham, R.W., 1984. The capillary fringe and its effect on water-table response. Journal of Hydrology 67 (1-4), 307–324.

Godwin, H., Conway, V., 1939. The ecology of a raised bog near Tregaron, Cardiganshire. The Journal of Ecology, 313–359.

Hauck, A., 1999. Hydrological Charakterization of the Lehstenbach Catchment. unpuplished Diploma Thesis, University of Bayreuth, Bayreuth.

Heliotis, F., DeWitt, C., 1987. Rapid Water Table Responses to Rainfall in a Northern Peatland Ecosystem. JAWRA Journal of the American Water Resources Association 23 (6), 1011–1016.

Hill, A., 1993. Nitrogen dynamics of storm runoff in the riparian zone of a forested watershed. Biogeochemistry 20 (1), 19–44.

Hill, A., Devito, K., Campagnolo, S., Sanmugadas, K., 2000. Subsurface denitrification in a forest riparianzone: Interactions between hydrology and supplies ofnitrate and organic carbon. Biogeochemistry 51 (2), 193–223.

Holden, J., Burt, T.P., 2003. Hydraulic conductivity in upland blanket peat: measurement and variability. Hydrological Processes 17 (6), 1227–1237.

Hood, E., Gooseff, M., Johnson, S., 2006. Changes in the character of stream water dissolved organic carbon during flushing in three small watersheds, Oregon.

Hopp, L., McDonnell, J.J., 2009. Connectivity at the hillslope scale: Identifying interactions between storm size, bedrock permeability, slope angle and soil depth. Journal of Hydrology 376 (3), 378–391.

Hunter, K.S., Wang, Y., van Cappellen, P., 1998. Kinetic modeling of microbially-driven redox chemistry of subsurface environments: coupling transport, microbial metabolism and geochemistry. Journal of Hydrology(Amsterdam) 209 (1), 53–80.

Hyvönen, R., Ågren, G., Linder, S., Persson, T., Cotrufo, M., Ekblad, A., Freeman, M., Grelle, A., Janssens, I., Jarvis, P., 2007. The likely impact of elevated [CO2], nitrogen deposition, increased temperature and management on carbon sequestration in temperate and boreal forest ecosystems: a literature review. New Phytologist 173 (3), 463–480.

Jacks, G., Norrström, A.C., 2004. Hydrochemistry and hydrology of forest riparian wetlands. Forest ecology and Management 196 (2-3), 187–197.

Johnston, C.A., 1991. Sediment and nutrient retention by freshwater wetlands: effects on surface water quality. Critical Reviews in Environmental Science and Technology 21 (5), 491–565.

Jones Jr, J., Fisher, S., Grimm, N., 1995. Vertical hydrologic exchange and ecosystem metabolism in a Sonoran Desert stream. Ecology, 942–952.

Jones, J., Holmes, R., Fisher, S., Grimm, N., Greene, D., 1995. Methanogenesis in Arizona, USA dryland streams. Biogeochemistry 31 (3), 155–173.

Jones, J.P., Sudicky, E.A., Brookfield, A.E., Park, Y.J., 2006. An assessment of the tracer-based approach to quantifying groundwater contributions to streamflow. Water Resources Research 42, W02407. doi:10.1029/2005WR004130.

Jones, J.P., Sudicky, E.A., McLaren, R.G., 2008. Application of a fully-integrated surface-subsurface flow model at the watershed-scale: A case study. Water Resources Research 44, W03407. doi:10.1029/WR005603.

Kalbitz, K., Solinger, S., Park, J., Michalzik, B., Matzner, E., 2000. Controls on the dynamics of dissolved organic matter in soils: a review. Soil Science 165 (4), 277.

Kettunen, A., Kaitala, V., Lehtinen, A., Lohila, A., Alm, J., Silvola, J., Martikainen, P., 1999. Methane production and oxidation potentials in relation to water table fluctuations in two boreal mires. Soil Biology and Biochemistry 31 (12), 1741–1749.

Kinzelbach, W., Rausch, R., 1995. Grundwassermodellierung: Eine Einführung mit Übungen; mit 15 Tabellen. Borntraeger.

Knorr, K., Blodau, C., 2009. Impact of experimental drought and rewetting on redox transformations and methanogenesis in mesocosms of a northern fen soil. Soil Biology and Biochemistry 41 (6), 1187–1198.

Knorr, K., Oosterwoud, M., Blodau, C., 2008. Experimental drought alters rates of soil respiration and methanogenesis but not carbon exchange in soil of a temperate fen. Soil Biology and Biochemistry 40 (7), 1781–1791.

Knorr, K.-H., 2012. DOC-dynamics in a small headwater catchment as driven by redox fluctuations and hydrological flow paths - are DOC exports mediated by iron reduction/oxidation cycles? Biogeosciences Discussions 9, 1–34.

Knorr, K.H., Lischeid, G., Blodau, C., 2009. Dynamics of redox processes in a minerotrophic fen exposed to a water table manipulation. Geoderma 153 (3-4), 379–392.

Koehler, A., Murphy, K., Kiely, G., Sottocornola, M., 2009. Seasonal variation of DOC concentration and annual loss of DOC from an Atlantic blanket bog in South Western Ireland. Biogeochemistry 95 (2), 231–242.

Kristensen, K., Jensen, S., 1975. A model for estimating actual evapotranspiration from potential evapotranspiration. Nordic Hydrology 6 (3), 170–188.

Kruse, J., Lennartz, B., Leinweber, P., 2008. A modified method for measuring saturated hydraulic conductivity and anisotropy of fen peat samples. Wetlands 28 (2), 527–531.

Kværner, J., Kløve, B., 2008. Generation and regulation of summer runoff in a boreal flat fen. Journal of Hydrology (360), 15–30. doi:10.1016/j.jhydrol.2008.07.009.

Lee, S.-Y., Carle, S., Fogg, G., 2007. Geologic heterogeneity and a comparison of two geostatistical models: Sequential Gaussian and transition probability-based geostatistical simulation. Advances in Water Resources 30 (9), 1914–1932.

Lemieux, J., Sudicky, E.A., Peltier, W.R., Tarasov, L., 2008a. Simulating the impact of glaciations on continental groundwater flow systems: 1. Relevant processes and model formulation. Journal of Geophysical Research 113 (F3), F03017.

Lemieux, J., Sudicky, E.A., Peltier, W.R., Tarasov, L., 2008b. Simulating the impact of glaciations on continental groundwater flow systems: 2. Model application to the Wisconsinian glaciation over the Canadian landscape. Journal of Geophysical Research 113 (F3), F03018.

Lemieux, J.M., Sudicky, E.A., Peltier, W.R., Tarasov, L., 2008c. Dynamics of groundwater recharge and seepage over the Canadian landscape during the Wisconsinian glaciation. Journal of Geophysical Research 113 (F1), F01011.

Li, Q., Unger, A.J., Sudicky, E.A., Kassenaar, D., Wexler, E.J., Shikaze, S., 2008. Simulating the multi-seasonal response of a large-scale watershed with a 3D physically-based hydrologic model. Journal of Hydrology (357), 317–336. doi:10.1016/j.jhydrol.2008.05.024.

Lischeid, G., 2008. Combining Hydrometric and Hydrochemical Data Sets for Investigating Runoff Generation Processes: Tautologies, Inconsistencies and Possible Explanations. Geography Compass 2 (1), 255–280. 10.1111/j.1749-8198.2007.00082.x.

Lischeid, G., Kolb, A., Alewell, C., 2002. Apparent translatory flow in groundwater recharge and runoff generation. Journal of Hydrology 265 (1-4), 195–211.

Lischeid, G., Kolb, A., Alewell, C., Paul, S., 2007. Impact of redox and transport processes in a riparian wetland on stream water quality in the Fichtelgebirge region, southern Germany. Hydrological Processes 21 (1), 123–132. 10.1002/hyp.6227.

Lohse, K., Brooks, P., McIntosh, J., Meixner, T., Huxman, T., 2009. Interactions between biogeochemistry and hydrologic systems. Annual Review of Environment and Resources 34, 65–96.

McCarty, J.J., Canziani, O.F., Leary, N.A., Dikken, D.J., White, K.S., 2001. IPCC Climate Change 2001: Impacts, Adaptation and Vulnerability. The Third Assessment Report of Working Group

II of the Intergovernmental Panel on Climate Change (IPCC). Cambridge University Press, Cambridge UK. Accessed.

McMahon, P., 2001. Aquifer/aquitard interfaces: mixing zones that enhance biogeochemical reactions. Hydrogeology Journal 9 (1), 34–43.

McMahon, P.B., Böhlke, J.K., Bruce, B.W., 1999. Denitrification in marine shales in northeastern Colorado. Water Resources Research 35 (5), 1629–1642.

Meixner, T., Huth, A.K., Brooks, P.D., Conklin, M.H., Grimm, N.B., Bales, R.C., Haas, P.A., Petti, JR, 2007. Influence of shifting flow paths on nitrogen concentrations during monsoon floods, San Pedro River, Arizona. J. Geophys. Res 112, G03S03.

Minshall, G., Cummins, K., Petersen, R., Cushing, C., Bruns, D., Sedell, J., Vannote, R., 1985. Developments in stream ecosystem theory. Canadian Journal of Fisheries and Aquatic Sciences 42 (5), 1045–1055.

Molenat, J., Gascuel-Odoux, C., 2002. Modelling flow and nitrate transport in groundwater for the prediction of water travel times and of consequences of land use evolution on water quality. Hydrological Processes 16 (2), 479–492. 10.1002/hyp.328.

Monod, J., 1949. The growth of bacterial cultures. Annual Reviews in Microbiology 3 (1), 371–394.

Murdoch, P., Stoddard, J., 1992. The role of nitrate in the acidification of streams in the Catskill Mountains of New York. Water Resources Research 28 (10), 2707–2720.

Nakayama, T., Watanabe, M., 2006. Simulation of spring snowmelt runoff by considering micro-topography and phase changes in soil layer. Hydrology and Earth System Sciences Discussions 3 (4), 2101–2144.

Nash, J., Sutcliffe, J.V., 1970. River flow forecasting through conceptual models part I—A discussion of principles. Journal of Hydrology 10 (3), 282–290.

National Research Council . Committee on Grand Challenges in Environmental Sciences, 2001. Grand challenges in environmental sciences. National Academies Press.

Nungesser, M., 2003. Modelling microtopography in boreal peatlands: hummocks and hollows. Ecological Modelling 165 (2), 175–207.

Parkhurst, D., 1995. User's guide to PHREEQC: A computer program for speciation, reaction-path, advective-transport, and inverse geochemical calculations. U.S. GEOLOGICAL SURVEY WAter-Resources Investigations Report 95-4227.

Parry, M., 2007. Climate Change 2007: impacts, adaptation and vulnerability: contribution of Working Group II to the fourth assessment report of the Intergovernmental Panel on Climate Change. Cambridge Univ Pr.

Partington, D., Brunner, P., Simmons, C.T., Therrien, R., Werner, A.D., Dandy, G.C., Maier, H.R., 2011. A hydraulic mixing-cell method to quantify the groundwater component of streamflow within spatially distributed fully integrated surface water-groundwater flow models. Environmental Modelling & Software.

Partington, D., Brunner, P., Simmons, C.T., Werner, A.D., Therrien, R., Maier, H.R., Dandy, G.C., 2012. Evaluation of outputs from automated baseflow separation methods against simulated baseflow from a physically-based, surface water-groundwater flow model. Journal of Hydrology.

Paul, S., Küsel, K., Alewell, C., 2006. Reduction processes in forest wetlands: tracking down heterogeneity of source/sink functions with a combination of methods. Soil Biology and Biochemistry 38 (5), 1028–1039.

Porporato, A., Daly, E., Rodriguez-Iturbe, I., 2004. Soil water balance and ecosystem response to climate change. The American Naturalist 164 (5), 625–632.

Price, J., McLaren, R., Rudolph, D., 2010. Landscape restoration after oil sands mining: Conceptual design and hydrological modelling for fen reconstruction. International Journal of Mining, Reclamation and Environment 24 (2), 109–123.

Raymond, P., Saiers, J., 2010. Event controlled DOC export from forested watersheds. Biogeochemistry 100 (1), 197–209.

Reeve, A.S., Di Siegel, Glaser, P.H., 2001. Simulating dispersive mixing in large peatlands. Journal of Hydrology 242 (1-2), 103–114.

Reich, P., Hungate, B., Luo, Y., 2006. Carbon-nitrogen interactions in terrestrial ecosystems in response to rising atmospheric carbon dioxide. Annu. Rev. Ecol. Evol. Syst 37, 611–636.

Richardson, M.C., Branfireun, B.A., Robinson, V.B., Graniero, P.A., 2007a. Towards simulating biogeochemical hot spots in the landscape: A geographic object-based approach. Journal of Hydrology 342 (1-2), 97–109.

Richardson, M.C., Branfireun, B.A., Robinson, V.B., Graniero, P.A., 2007b. Towards simulating biogeochemical hot spots in the landscape: A geographic object-based approach. Journal of Hydrology 342 (1-2), 97–109.

Rodriguez-Iturbe, I., 2003. Hydrologic dynamics and ecosystem structure. Water science and technology, 18–24.

Schimel, D., Braswell, B.H., Parton, W.J., 1997. Equilibration of the terrestrial water, nitrogen, and carbon cycles. Proceedings of the National Academy of Sciences 94 (16), 8280.

Schlotzhauer, S.M., Price, J.S., 1999. Soil water flow dynamics in a managed cutover peat field, Quebec: Field and laboratory investigations. Water Resources Research 35 (12), 3675–3683.

Schulze, K., Borken, W., Matzner, E., 2011. Dynamics of dissolved organic 14 C in throughfall and soil solution of a Norway spruce forest. Biogeochemistry, 1–13.

Seibert, J., Bishop, K., Rodhe, A., McDonnell, J.J., 2003. Groundwater dynamics along a hillslope: A test of the steady state hypothesis. Water Resour. Res 39 (1), 1014. doi:10.1029/2002WR001404, 2003.

Seibert, J., Grabs, T., Köhler, S., Laudon, H., Winterdahl, M., Bishop, K., 2009. Linking soil-and stream-water chemistry based on a Riparian Flow-Concentration Integration Model. Hydrology and Earth System Sciences 13 (12), 2287–2297.

Sharratt, B., Benoit, G., Daniel, J., Staricka, J., 1999. Snow cover, frost depth, and soil water across a prairie pothole landscape. Soil Science 164 (7), 483.

Shaw, M., Zavaleta, E., Chiariello, N., Cleland, E., Mooney, H., Field, C., 2002. Grassland responses to global environmental changes suppressed by elevated CO2. Science 298 (5600), 1987–1990.

Shen, H.W., Julien, P.Y., 1993. Erosion and sediment transport. Handbook of Hydrology, 12.1-12.61.

Solé-Benet, A., Calvo, A., Laīzaro, R., Pini, R., Barbero, J., 1997. Influences of micro-relief patterns and plant cover on runoff related processes in badlands from Tabernas (SE Spain). Catena 31 (1-2), 23–38.

Stoddard, J., 1994. Long-term changes in watershed retention of nitrogen. Its causes and aquatic consequences. Advances in Chemistry[ADV. CHEM. SER.]. 1994.

Stumm, W., Morgan, J.J., 1996. Aquatic chemistry. 3rd. John Wiley and Sons, New York.

Therrien, R., McLaren, R., Sudicky, E., Panday, S., 2008. HydroGeoSphere A Three-dimensional Numerical Model Describing Fully-integrated Subsurface and Surface Flow and Solute Transport (Manual), University of Waterloo.

Tolonen, K., 1971. On The Rgeneration of Northerneuropean Bogs: I. KLAUKKALAN ISOSUO IN S. FINLAND. ACTA AGRAL FENN. 123 P 143-166. 1971. ILLUS.

Tromp-van Meerveld, H.J., McDonnell, J.J., 2006a. Threshold relations in subsurface stormflow: 1. A 147-storm analysis of the Panola hillslope. Water Resources Research 42 (2), W02410.

Tromp-van Meerveld, H.J., McDonnell, J.J., 2006b. Threshold relations in subsurface stormflow: 2. The fill and spill hypothesis. Water Resources Research 42 (2), W02411.

Updegraff, K., Bridgham, S., Pastor, J., Weishampel, P., Harth, C., 2001. Response of CO2 and CH4 emissions from peatlands to warming and water table manipulation. Ecological Applications 11 (2), 311–326.

Van Genuchten, M., 1980a. A closed-form equation for predicting the hydraulic conductivity of unsaturated soils. Soil Science Society of America Journal 44 (5), 892–898.

Van Genuchten, M., 1980b. A closed-form equation for predicting the hydraulic conductivity of unsaturated soils. Soil Science Society of America Journal 44, 892–898.

Vidon, P., Hill, A., 2004. Landscape controls on nitrate removal in stream riparian zones. Water Resources Research 40 (3), W03201.

Waddington, J.M., Roulet, N.T., Hill, A.R., 1993. Runoff mechanisms in a forested groundwater discharge wetland. Journal of Hydrology 147 (1), 37–60.

Walling, D., 1983. The sediment delivery problem. Journal of Hydrology 65 (1), 209–237.

Weiler, M., McDonnell, J., 2004. Virtual experiments: a new approach for improving process conceptualization in hillslope hydrology. Journal of Hydrology 285 (1-4), 3–18.

Weissmann, G., 1999. Toward new models of subsurface heterogeneity: An alluvial fan sequence stratigraphic framework with transition probability geostatistics. unpublished Ph.D. thesis, Universtiy of California, Davis.

Werb, S., 2009. Simulation der hydrologischen Dynamik im Einzugsgebiet des Lehstenbachs mit dem physikalisch begründeten Modell HydroGeoSphere. Diploma Thesis, University of Bayreuth, Bayreuth.

Wigington, P.J., Davies, T.D., Tranter, M., Eshleman, K.N., 1990. Episodic acidification of surface waters due to acidic deposition. US Natl. Acid Precip. Assess. Prog. State of Science Report 12.

Wigmosta, M., Vail, L., Lettenmaier, D., 1994. A distributed hydrology-vegetation model for complex terrain. Water Resources Research 30 (6), 1665–1680.

Worrall, F., Gibson, H.S., Burt, T.P., 2008. Production vs. solubility in controlling runoff of DOC from peat soils–The use of an event analysis. Journal of Hydrology 358 (1), 84–95.

Zehe, E., Becker, R., Bárdossy, A., Plate, E., 2005. Uncertainty of simulated catchment runoff response in the presence of threshold processes: Role of initial soil moisture and precipitation. Journal of Hydrology 315 (1), 183–202.

Zehnder, A., 1988. Biology of anaerobic microorganisms. John Wiley and Sons Inc.

7 Appendix
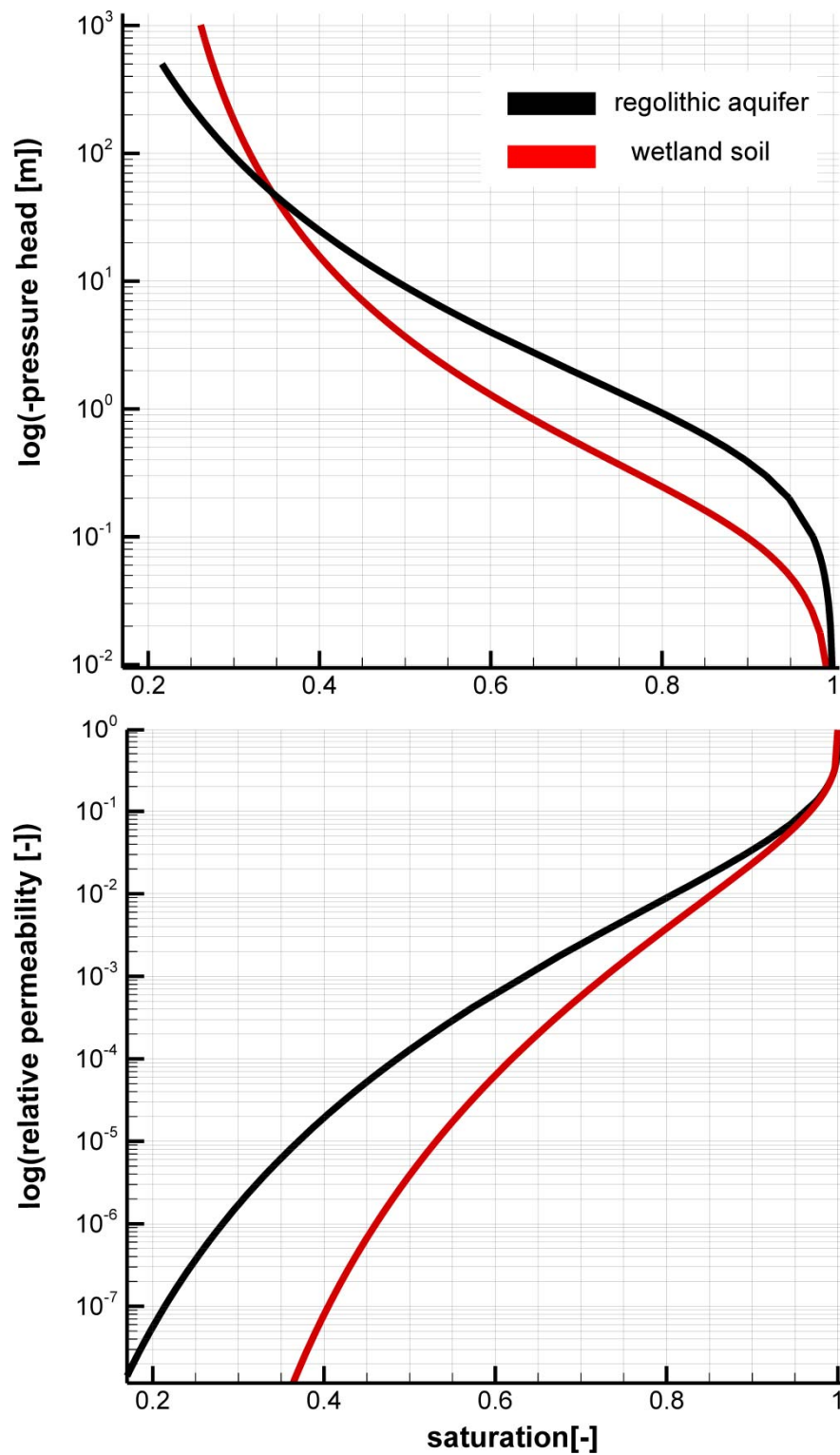
Figure A1: *Soil retention functions used to represent variably saturated flow in the wetland soils and the regolithic aquifer of the catchment scale numerical model and the virtual wetland model. Soil retention functions for the wetland soil are based on the study of Price et al. (2010). Data for the soil retention functions of the regolithic aquifer is based on field measurements performed in the Lehstenbach catchment (unpublished data from Gunnar Lischeid).*
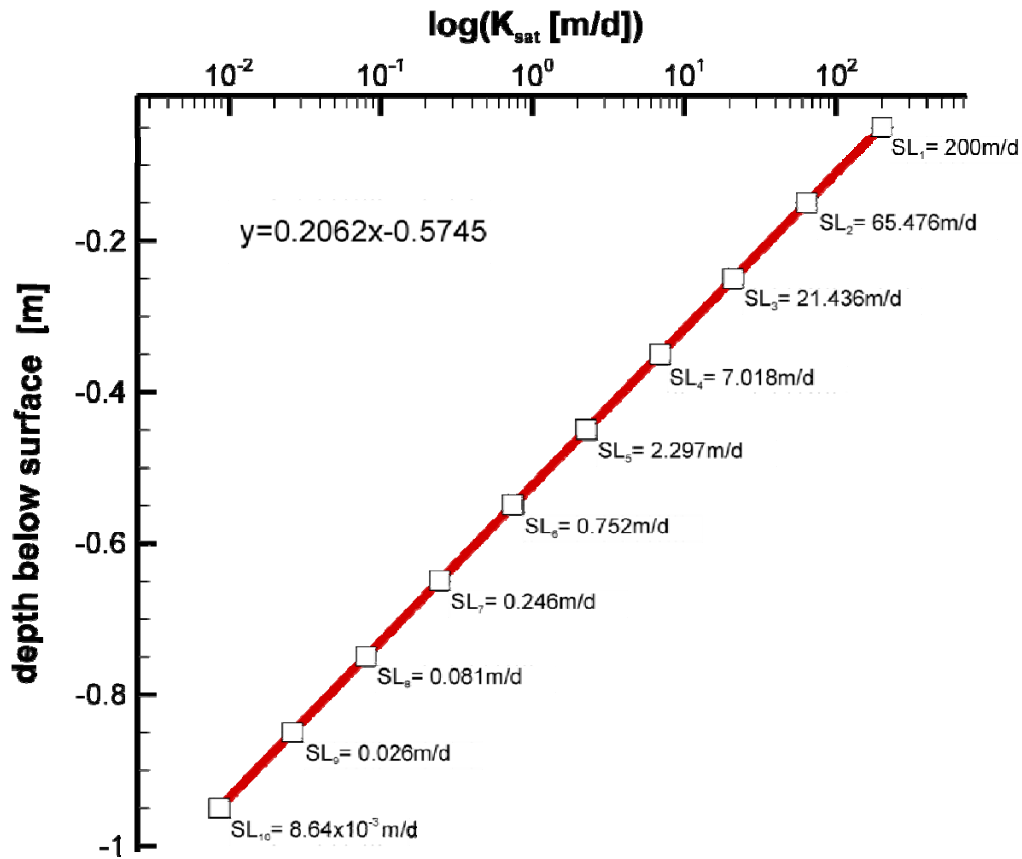
Figure A2: *Saturated hydraulic conductivities K_{sat} assigned to the ten sub-layers SL_1-SL_{10} of the wetland areas for the catchment scale model. K_{sat} values are exponentially decreasing (as indicated by the linear decrease using a logarithmic X-axis) with depth to mimic the transmissivity feedback mechanism. Values for used K_{sat}-values within the wetland areas are based on the study of Jacks and Norrström, (2004).*

Table A1: *Overview of the parameterization of the catchment scale model to represent surface/subsurface flow and interactions for the three different zones (wetlands, upslope areas and stream areas).*

a. Subsurface	Wetlands	Upslope Areas	
saturated hydraulic conductivity [m/d]	variable with depth (see Figure A2)	0.24	
porosity [-]	0.5	0.4	
specific storage [m^{-1}]	0.0001	0.0001	

b. Surface	Wetlands	Upslope Areas	Stream
surface storage [m]	0.1;0.5;1.0	0.01	0.0
coupling length [m]	0.1	0.1	0.0001
friction slopes X and Y [m$^{-1/3}$s]	8.1x10^{-7}	1.9x10^{-6}	4.0x10^{-7}

c. Evapotranspiration	Wetlands	Upslope Areas	
leaf Area Index [-]	3.0	6.5	
root depth [m] (quadratic decay function)	0.8	3.0	
evaporation depth [m] (quadratic decay function)	0.5	0.5	

8 Contributions to the included manuscripts

Study 1

Effects of micro-topography on surface-subsurface exchange and runoff generation in a virtual riparian wetland – a modeling study.

Authors: Sven Frei, Gunnar Lischeid and Jan H. Fleckenstein

Sven Frei:	concepts, modeling, interpretation and discussion of results, manuscript preparation
Gunnar Lischeid:	comments on manuscript, field site coordinator, field data
Jan H. Fleckenstein:	concepts, discussion of result, manuscript preparation

Study 2

Surface micro-topography causes hot spots of biogeochemical activity in wetland systems – a virtual modeling experiment.

Authors: Sven Frei, Klaus-Holger Knorr, Stefan Peiffer and Jan H. Fleckenstein

Sven Frei:	concepts, modeling, interpretation and discussion of results, manuscript preparation
Klaus-Holger Knorr:	field data, concepts, interpretation and discussion of results, manuscript preparation
Stefan Peiffer:	comments on manuscript, discussion of results
Jan H. Fleckenstein:	interpretation and discussion of results, manuscript preparation

Study 3

Representing effects of micro-topography on runoff generation and subsurface flow patterns by using superficial rill storage height variations.

Authors: Sven Frei, and Jan H. Fleckenstein

Sven Frei:	concepts, modeling, interpretation and discussion of results, manuscript preparation
Jan H. Fleckenstein:	concepts, discussion of results, manuscript preparation

[63]

Study 4

Concentrations and fluxes of dissolved organic carbon in runoff from a forested catchment: Insights from high frequency measurements

Authors: Stefan Strohmeier, Klaus-Holger Knorr, Martin Reichert, Sven Frei, Jan H. Fleckenstein, Stefan Peiffer and Egbert Matzner

Stefan Strohmeier:	concepts, interpretation and discussion of results, manuscript preparation, modeling
Klaus-Holger Knorr:	interpretation and discussion of results, laboratory work
Martin Reichert:	field work, laboratory work
Sven Frei:	modeling, interpretation and discussion of results, comments on manuscript
Jan H. Fleckenstein:	comments on manuscript
Stefan Peiffer:	comments on manuscript
Egbert Matzner:	manuscript preparation, concepts, interpretation and discussion of results

Study 5

Interpreting flow generation mechanisms from integrated surface water-groundwater flow models of a riparian wetland and catchment.

Authors: Daniel Partington, Philip A. Brunner, Sven Frei, Craig T. Simmons, Adrian D. Werner, René Therrien, Holger R. Maier, Graeme C. Dandy and Jan H. Fleckenstein

Daniel Partington:	concepts, coding, modeling, interpretation and discussion of results, manuscript preperation
Philip A. Brunner:	concepts, discussion of results, comments on manuscript
Sven Frei:	development of flow models, discussion of results, manuscript preperation
Craig T. Simmons:	discussion of results, comments on manuscript
Adrian D. Werner:	comments on manuscript
René Therrien:	concepts, discussion of results, comments on manuscript
Holger R. Maier:	comments on manuscript
Graeme C. Dandy	comments on manuscript
Jan H. Fleckenstein	comments on manuscript

Study 1

Effects of micro-topography on surface-subsurface exchange and runoff generation in a virtual riparian wetland – a modeling study.

By Sven Frei, Gunnar Lischeid and Jan H. Fleckenstein

Effects of micro-topography on surface-subsurface exchange and runoff generation in a virtual riparian wetland – a modeling study.

Frei[1], S., G. Lischeid[2] and J. H. Fleckenstein[3]

[1] Department of Hydrology, University of Bayreuth, Germany

[2] Leibnitz Centre for Agricultural Landscape Research, (ZALF), Germany

[3] Department Hydrogeology, Helmholtz-Center for Environmental Research – UFZ, Germany

Abstract

In humid upland catchments wetlands are often a prominent feature in the vicinity of streams and have potential implications on runoff generation and nutrient export. Wetland surfaces are often characterized by distinct micro-topography (hollows and hummocks). The effects of such micro-topography on surface-subsurface exchange and runoff generation for a 10 by 20 m synthetic section of a riparian wetland were investigated in a virtual modeling experiment. A reference model with a planar surface was run for comparison. The geostatistically simulated structure of the micro-topography replicates the topography of a peat-forming riparian wetland in a small mountainous catchment in South-East Germany (Lehstenbach). Flow was modeled with the fully integrated surface-subsurface code HydroGeoSphere. Simulation results show that the specific structure of the wetland surface results in distinct shifts between surface and subsurface flow dominance. Surface depressions fill and start to drain via connected channel networks in a threshold-controlled process, when groundwater levels intersect the land surface. These networks expand and shrink in a spill and fill mechanism when the shallow water table fluctuates around the mean surface elevation under variable rainfall inputs. The micro-topography efficiently buffers rainfall inputs and produces a hydrograph that is characterized by subsurface drainage during most of the year and only temporarily shifts to surface flow dominance (> 80% of total discharge) during intense rainstorms. In contrast the hydrograph in the planar reference model is much "flashier" and more controlled by surface runoff. A non-linear, hysteretic relationship between groundwater level and discharge observed at the study site was reproduced with the micro-topography model. Hysteresis was also observed in the relationship between surface water storage and discharge, but over a relatively narrow range of surface water storage values. Therefore it was concluded that surface water storage was a better predictor for the occurrence of surface runoff than groundwater levels.

1   Introduction

Riparian zones contain dynamic interfaces between ground- and surface water flowpaths *[10, 27]*. It is important to understand the mechanisms that govern hydrologic flowpaths and stream flow generation in riparian zones because nutrient transformations and export are integrally related to the hydrologic dynamics *[8, 53, 18, 34]*. However, these dynamics can be quite complex [53, 27] and are generally poorly understood *[49, 28]*.

In humid temperate climates riparian zones are often occupied by wetlands *[34, 36, 27]*. Rapid surface and shallow subsurface flows typically dominate runoff generation in riparian wetlands during rainstorms *[8, 34]*. *Gibson et al. [17]* showed that runoff dynamics highly depend on surface storage and interactions between surface water and shallow groundwater. *Kværner and Kløve [27]* identified distinctly different runoff generation processes with shifts between subsurface and surface flow dominance for low and high flow events. Non-linear relationships between riparian water table depth and stream flow have often been observed *[5, 15, 38, 44]*. For catchments dominated by matrix flow these relationships have been attributed to the transmissivity feedback mechanism *[4, 3, 44]*. Stream flow originating from matrix flow increases exponentially, when the water table rises into soil layers with progressively increasing lateral hydraulic conductivity *[3, 44]*. In systems where shifts between matrix flow and surface flow dominance occur, additional dynamics and non-linearities have been observed (e.g. *[27]*).

Peat-forming wetlands are often characterized by a hummocky topography with sequences of high points (hummocks) and depressions (hollows) at the sub-meter scale, which will affect runoff generation during transitions between surface and subsurface flow dominance. Effects of micro-topography on infiltration and runoff generation processes were first investigated by *Dunne et al. [9]*. They showed that hill slope runoff was controlled by an intricate interplay between rainfall intensity, surface flow depth, vegetation cover and the specific micro-topography of the slope. Micro-topography can attenuate and delay surface flows *[36, 27]*, because surface depressions first need to be filled until a specific surface water storage threshold is exceeded and then surface flow towards the stream channel can be initiated *[2, 12]*. *Tromp-van Meerveld and McDonnell [51]* and *Tromp-van Meerveld and McDonnell [52]* termed similar threshold dynamics in the generation of subsurface stormflows on bedrock surfaces with micro-topography the "fill and spill mechanism". *Qu and Duffy [40]* reported distinct double peaks in hydrographs from single rainfall events, which they ascribed to complex interactions between small scale micro-topography controlled surface runoff in the wetland and subsurface flow.

Several modeling studies have addressed the effects of micro-topography on runoff dynamics. *Dunne et al. [9]* used a conceptual approach to simulate overland flow and infiltration processes for uniform

sinusoidal micro-topography. They demonstrated that micro-topography resulted in significant spatial variability of infiltration and surface flows. *Esteves et al. [11]* and *Fiedler and Ramirez [12]* used finite difference solutions to the two-dimensional depth-averaged dynamic wave equations to simulate overland flow and infiltration processes on small plots with micro-topography. Both studies showed that micro-topography strongly affects flow directions, flow velocities and flow depths and resulted in surface flow along well defined micro-channels. Connectivity indicators for surface flow on plots with micro-topography were systematically investigated with a numerical model by *Antoine et al. [2]*. Each of the aforementioned modeling studies were restricted to surface flows and infiltration and did not account for feedbacks between surface and subsurface flow, an important process in wetlands *[8, 17]*. An exception was the study by *Qu and Duffy [40]*, who used a finite element coupled surface-subsurface flow model to simulate a series of rainfall events for a 0.08 km^2 watershed in Pennsylvania. They demonstrated how small scale topography can control local surface saturation and subsequent connectivity of surface flow paths leading to stream flow generation. However the spatial resolution of the *Qu and Duffy [40]* model was too coarse to account for micro-topography on the sub-meter scale. *Hopp and McDonnell [20]* modeled the effects of bedrock micro-topography on subsurface storm flow generation from hillslopes.

Our work evaluates the complex hydrologic dynamics of a riparian wetland with micro-topography through a virtual modeling experiment. The purpose of the simulations is to examine process dynamics rather than calibration of a model to a specific field site. We argue that to accurately describe these dynamics a numerical model has to account for overland flow, variably saturated subsurface flow and complex interactions between the surface and subsurface domains. A fully-integrated modeling approach simultaneously solves all of the equations that govern the complex interactions between surface and subsurface. Efficient numerical models that use the fully-integrated approach have become available in recent years (e.g. *[25, 50]*). The fully integrated, three-dimensional numerical flow model HydroGeoSphere *[50]* is used here to examine hydrologic dynamics in a virtual riparian wetland with distinct micro-topography (hummocks and hollows). The micro-topographic relief is geostatistically generated for a 10m x 20m area at a resolution of approximately 0.1m based on surveyed micro-topography in a riparian wetland of the small experimental Lehstenbach catchment located in Germany (Figure 1). The wetlands in the catchment, which have a hummocky surface topography, can be classified as fens. The relative elevation differences between hollows and hummocks range between 0.2-0.4 m and the hollows are generally inter-connected. Inflows from deeper groundwater are locally diminished by a basal clay layer. At several locations lateral inflows from adjacent hillslopes are intercepted by small stream channels bounding the wetlands. Most small streams have their headwaters in the wetlands and practically all the water that reaches the streams either originates in or passes through the wetlands.
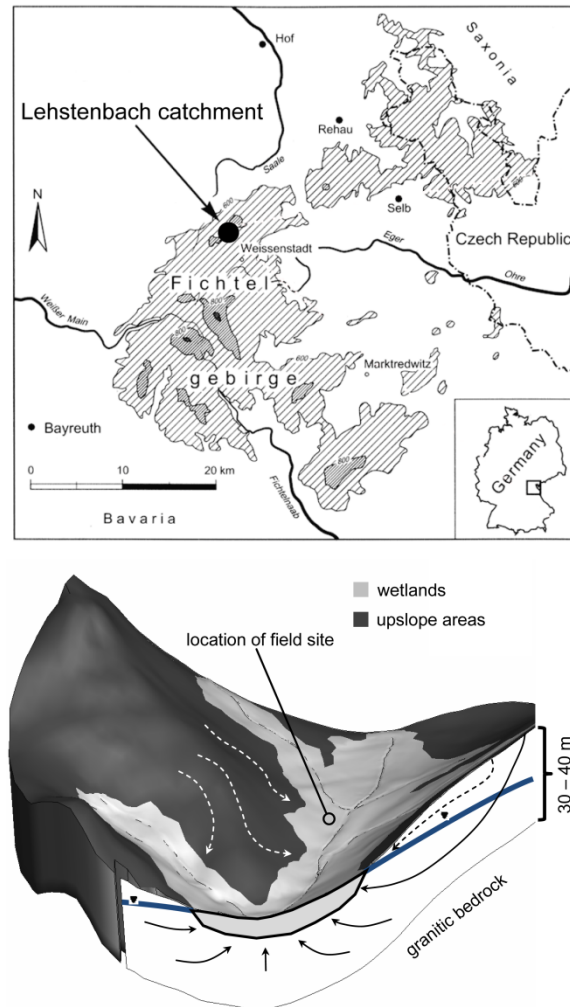
Figure 1: *Location of the Lehstenbach experimental catchment (upper panel). The overall hydrology of the catchment is controlled by the structure of the basin (lower plot). Dark grey areas represent forest and light grey areas wetlands, which occupy almost 1/3 of the 4.2km² catchment area (lower panel). The location of the field site that provided field data is marked with an open circle.*

Previous studies in the Lehstenbach catchment indicated that stream flow generation and solute export are mainly controlled by processes occurring within wetlands *([33, 31, 1, 32])*. The quick response of catchment discharge to intensive rainfall events occurs via surface and shallow subsurface flowpaths *([33, 34])*. Surface runoff within wetland zones is predominantly generated by the saturation excess overland flow mechanism (type Dunne runoff) (*[32]*). Field observations show a distinct non-linear relationship between wetland originating discharge in a first-order stream and the depth to the local groundwater table (Figure 2). This non-linear relationship suggests that runoff generation in the wetland is controlled by a complex threshold response between the formation of shallow subsurface flows and saturation excess overland flow draining into the channel network. We hypothesize that the interplay between water table depth and surface micro-topography (typical pattern of hollows and hummocks) in the wetland results in distinct shifts between surface and subsurface flow dominance that can explain the observed stream discharge behavior.
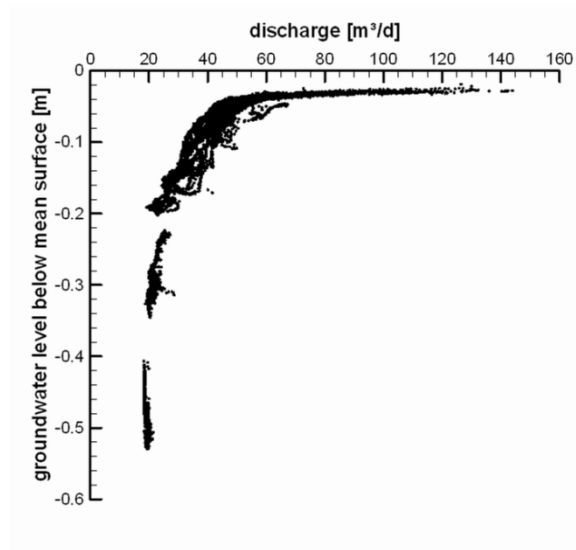
Figure 2: Observed nonlinear relationship between stream discharge at the fen field site (from a first order stream that has its entire headwater in the fen) and groundwater level (measured in a monitoring well in the peat located about 15 m away from the stream). Data was measured in 10 minute intervals from Dec. 15, 1999 to Aug. 15, 2000. Groundwater levels are scaled to the areas mean surface elevation.

The main objective of this study is to improve our understanding of the effects of micro-topography on the complex hydrological process dynamics and interactions that govern surface-subsurface exchange and runoff generation in a riparian wetland. Process dynamics are examined in a virtual test case using an integrated surface-subsurface numerical flow model. In particular the following questions are addressed: 1) What effect does micro-topography in riparian wetlands have on stream discharge generation? 2) Can micro-topography explain the observed non-linear relationship between surface water discharge and the water table depth?

2 Methods

The objectives of this study are addressed through a virtual modeling experiment. Geostatistical indicator simulations based on surveyed elevation data are used to represent the micro-topographic structure for a synthetic riparian wetland section typical for the Lehstenbach catchment. Hydrological dynamics in the synthetic wetland are evaluated with the physically-based surface-subsurface numerical model HydroGeoSphere *[50]*. The conceptual idea behind the modeling is similar to the virtual experiments proposed by *Weiler and McDonnell [58]*. The numerical model is used as a virtual landscape, in which perfect process knowledge is assumed (see e.g. *Zehe et al. [57]*).

2.1 Representation of Micro-topography

The spatial structure of the micro-topography for a typical fen in the Lehstenbach catchment was derived from several surveyed transects. A 2D spatial distribution of elevation classes was generated using geostatistical indicator simulations based on Markov Chain models of transition probabilities between categorical data (**T**ransition **Pro**bability **G**eostatistical **S**oftware, *[7]*). The method was originally developed to realistically represent aquifer heterogeneity with discrete transitions between different hydrofacies *[7]* and it has been widely used for groundwater flow and transport problems (e.g. *[56, 14, 29, 16]*). This approach provides more options to condition the simulation with field data than traditional geostatistical simulation methods for continuous variables based on variogram analysis. The use of geostatistical simulations provided equally probable generation of different spatial structures of micro-topography and several realizations of each individual structure. The following main steps were used in developing the geostatistical model of micro-topography:

First, the elevation classes representing topographical structures like local depressions (hollows), local maxima (hummocks) or transition zones were defined as indicators. The relative elevations (scaled by the mean value: $z - \bar{z}$) were subdivided into five different discrete elevation classes. The upper and lower class bounds and relative frequencies are listed in Table 1. A Markov Chain model of spatial correlation was developed from the relative frequencies of the different elevation classes, the transition probabilities between them and the mean length of topographical structures. Estimates of mean structure length and transition frequencies for the micro-topography were obtained from the existing surveyed elevation profiles for the fen area. All profiles were surveyed within a 30 x 30 m plot.

Table 1: Elevation classes and relative frequencies for defining micro-topography in TPROGS, based on surveyed elevation data from the field site.

	lower limit [m]	upper limit [m]	relative frequency [-]	topographical structure
class 1	-0.1	0.1	0.128	transition zone
class 2	-0.3	-0.1	0.224	hollow
class 3	<-0.3	-	0.224	hollow
class 4	0.1	0.3	0.231	hummock
class 5	>0.3	-	0.192	hummock

Table 2 shows the embedded transition probability matrices in the horizontal directions used to generate the 2D Markov-Chain model within TPROGS *[7]*. The off-diagonal entries represent transition probabilities from one elevation class to another. All transition probabilities were estimated based on the discretized data from the surveyed elevation data. The entries denoted by *b* represent transition probabilities for the background category, which are automatically estimated from the transition probabilities for the other classes based on probability law *[7]*. Diagonal entries represent the mean length of the structures within the corresponding elevation class. Self-transition rates for each class can be directly derived from their respective mean length *[7]*. The same transition probabilities were used in the x- and y-directions as no pronounced anisotropy was observed in the field data. Mean lengths were assigned uniformly ($\overline{L} = 0.5\,\text{m}$) for all five elevation classes based on the measured mean length of hummocks and hollows. This model represents a surface with similarly sized hummocks and hollows of different elevations rather than a binary field where each of the depressions and peaks receive a unique elevation value. This was found to be the most representative simulation of observed field behavior. Using the sequential indicator simulation routine within TPROGS three realizations of the micro-topography for a 10 x 20m grid with a spatial resolution of 0.1m in x- and y–direction were generated. For comparison a spatial model with a mean length of $\overline{L} = 0.25\,\text{m}$ for the structures was generated. This model represents a surface topography with smaller hollows and hummocks.

Table 2: Transition probability matrix for the five elevation classes in the x- and y-directions. $\overline{L}$ denotes mean length of the structures (hollows and hummocks), b refers to the background category (transition probabilities for the background category follow from the other entries in the matrix by probability law).

	x- & y-directions				
class	1	2	3	4	5
1	$\overline{L}$	b	b	b	b
2	b	$\overline{L}$	0.25	0.1	0.05
3	b	0.25	$\overline{L}$	0.1	0.05
4	b	0.1	0.1	$\overline{L}$	0.25
5	b	0.05	0.05	0.25	$\overline{L}$

note: $\overline{L}$= mean length, b=background category/class, s=symmetry

2.2   Surface/Subsurface flow simulation

The numerical code HydroGeoSphere *[50]* is a fully-integrated finite element surface-subsurface flow model. Variably saturated subsurface flow in porous or fractured media is simulated with the Richard's equation in three dimensions (3D). Overland- or stream flow in 2D is represented by the diffusion wave approximation to the depth averaged dynamic wave equations *[50]*. Surface – subsurface coupling is implemented using the conductance concept. The conductance concept assumes that the exchange flux depends on the gradient across a coupling interface, the thickness of the interface (coupling length), its relative permeability, and the vertical saturated hydraulic conductivity *[50]*. The governing equations for surface- and subsurface flow are solved simultaneously via a control volume, finite-element approach *[50]*. HydroGeoSphere has been applied over a range of spatial scales from the plot and river reach scales *[22, 6]* up to entire catchments *[22, 30 and 48]*.

A 3D triangular finite-element grid was set up using HydroGeoSphere and the preprocessing software GRIDBUILDER *[35]*. The grid represents a hypothetical 10 m by 20 m section of a riparian wetland with a surface slope of 0.03m/m that is 2 m thick at the up-stream end (slightly thinner at the downstream end due to the inclined surface) and drains to an adjacent channel segment (Figure 3). The structure and dimensions of the model mimic conditions at a typical fen in the Lehstenbach catchment (with a basal clay layer overlain by a 1.5 to 2 m thick layer of peat). The geostatistically generated micro-topography is superimposed onto the surface plane of the grid. As changes in surface elevation are more gradual than the sharp transitions between different elevation classes in the geostatistical model, elevations in the grid were smoothed in GRIDBUILDER.
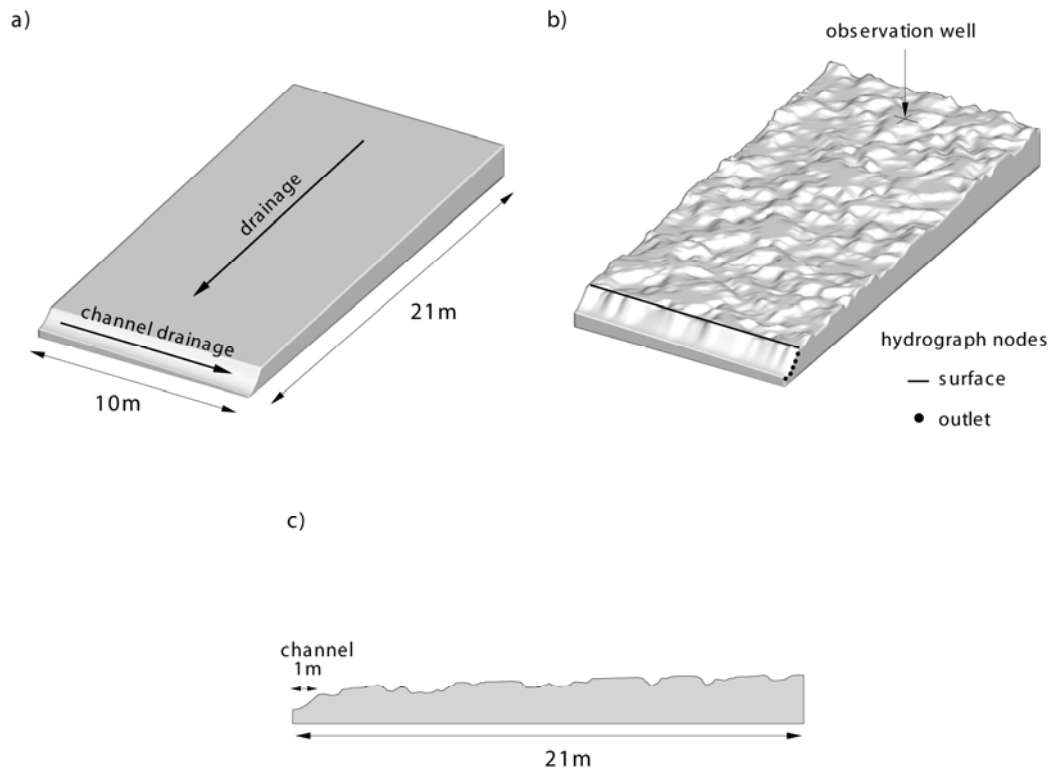
Figure 3: Geometry of the virtual riparian wetland segment: A) planar reference model showing the main drainage direction and channel location; B) smoothed realization of the wetlands micro-topography; C) cross section (Y=5m) of the micro-topography model. Monitoring well location, channel outlet hydrograph nodes (to track total channel discharge) and surface hydrograph nodes (to track surface flow into the channel) are only shown for the micro-topography model, but are also the same in the planar model. The planar model is about 1.35 m thick at the upstream end of the domain, the micro-topography model about 1.95 m (micro-topographic relief is superimposed onto the planar surface).

The smoothing algorithm estimates nodal elevations in the grid based on the average elevation of all connected nodes *[35]*. The final model, subsequently referred to as "micro-topography model", consists of 210,000 grid nodes with a node spacing of about 0.1 m in the X, Y and Z directions. The channel is represented by a parabolically shaped cross section (1m in diameter) draining into the positive Y-direction (see Figure 3) with a constant slope of 0.03 m/m. For comparison, a model with a planar surface is used as a reference model to simulate hydrological dynamics without micro-topographical structures. This model will subsequently be referred to as the "planar model". The peat body was represented as homogenous and isotropic. Heterogeneity was intentionally excluded to clearly separate micro-topographical effects from effects induced by heterogeneity. Isotropic, saturated hydraulic conductivity for the peat estimated as 0.2 m/d, which is in the range of values reported for this site *[19]* and for typical peat soils in general *[42, 26]*. Soil retention characteristics for the simulation of variably saturated flow in peat were taken from *Price et al. [39]*. Boundary conditions for the model were assigned so that water can only leave the model domain at the channel outlet (lower right corner of model in Figure 3). This was realized via a critical-depth boundary

condition at the channel outlet. All other boundaries were set to no-flow boundaries with the exception of the upper model surface where variable rainfall rates are applied. The initial groundwater elevation was prescribed as 0.5 m above the horizontal base of the model with an equilibrium pressure distribution above the water table. Daily precipitation was applied to the model surface based on the rainfall record from the 2000 hydrologic year (November 1999 through October 2000). The surface domain was initialized with a zero depth of ponded water representing dry initial conditions. The friction slope for surface flow calculations is described using Manning's equation. Manning's roughness coefficients for the peat surface were uniformly assigned as 0.03 $m^{-1/3}$s for x and y; a value reported for densely vegetated surfaces *[45]*.

3 Results

3.1 Dynamics of runoff generation for steady rainfall

To investigate the general dynamics of discharge generation under increasing wetness, a simulation with a constant rainfall rate of 0.008 m/d was run until the steady state discharge at the channel outlet was attained. The rainfall rate represented conditions for a moderate to intense rainstorm (exceeded on about 40 days per year for a typical hydrologic year) and ensured that surface flow networks could develop before the final steady state was reached. Figure 4 shows the development of channel discharge and the water table (evaluated at an observation well at the up-stream end of the model domain – see Figure 3) for the planar (upper panel) and the micro-topography model (lower panel) respectively. In the initial stage of both simulations channel discharge gradually increased from subsurface inflows caused by increasing hydraulic gradients towards the channel. The increase was more rapid in the planar model compared to the micro-topography model. The slower and slightly undulating increase in the latter case was caused by the progressive formation of ponds when the water table intersects local surface depressions. At this point the build-up of subsurface gradients towards the channel was slowed. The same input of subsurface heads below the ponds increased less rapidly as if the same amount of water had infiltrated (due to the porosity). Surface flow in the planar model, indicated by a steep increase in channel discharge, occurs after approximately 16 days. Discharge subsequently increased rapidly until the system attained a state of equilibrium with constant discharge around day 24. In the micro-topography model isolated ponds at the surface developed connected channel networks, which eventually spilled into the main channel segment around day 45. The subsequent rapid increase in discharge displayed several kinks, which represented the development and maturation of different surface flow networks. The networks eventually all provided water to the channel when equilibrium was reached around day 50. Groundwater levels at equilibrium (evaluated at the location in the upslope center of the domain – see Figure 3) were about 0.18 m below the land surface for the micro-topography model and at the land surface for the planar model.
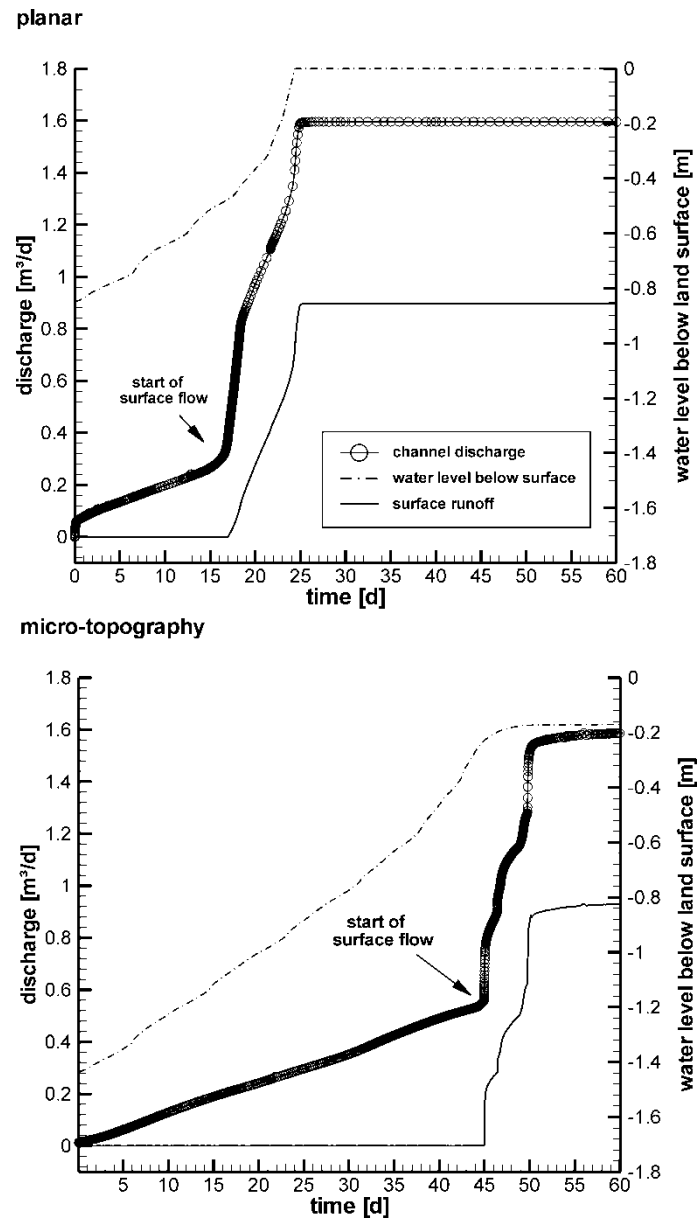
Figure 4: Hydrographs and development of the local groundwater level for a simulation with constant rainfall (0.008 m/d). Results for the planar model are shown at the top and for the micro-topography model on the bottom. Channel discharge and groundwater level are evaluated at the channel outlet and in an observation well (as shown in Figure 3).

3.2 Runoff dynamics and flow components for variable rainfall

Figure 5 shows the simulated discharge hydrograph at the main channel outlet (lower right corner of the domain – see Figure 3) for the micro-topography model. Discharge is separated into a surface and a subsurface flow component. The model-forcing daily precipitation record is depicted on the top axis. The separation of flow components was achieved by placing "hydrograph nodes", which tracked all flow through a node in the grid, along the edged of the channel segment and at the channel outlet (see Figure 3). The surface flow hydrograph nodes tracked surface flow into the channel at each time step of the simulation. The subsurface flow components tracked all flow that exited the model domain (sum of surface and subsurface flows). The difference between the two components represented subsurface flows into the channel segment. Steady rainfall in recharged groundwater, the groundwater levels increased, and the hydraulic gradients to the stream increased, resulting in increased subsurface flows. After initial wetting of the system, surface flow via surface channel networks, was initiated on day 125. Maximum discharge was simulated for day 217 after the most intensive rainfall event in the annual record (48 mm/d). Simulated discharge was generated via subsurface flow during most of the year. Only on 52 of the 365 simulated days was surface flow observed in the model. On these 52 days, surface flow accounted for up to 85% of total channel discharge (see *Fitzgerald et al. [17]* for a field example).

Figure 5: Simulated, yearly hydrograph for the micro-topography model. Precipitation at the field site for the hydrologic year 2000 (10/31/1999 – 11/1/2000) is shown on the top. Surface and subsurface fractions of total channel discharge are shown in green and black respectively.

Figure 6 (panel a) shows a typical situation during periods with low to intermediate rainfall intensities. Water was already ponded in local depressions (hollows) at the surface. However, ponded areas are not all interconnected and surface drainage into the channel segment was inhibited by the micro-topography. Only during high rainfall rates (panel b) did pond areas start to become interconnected and form extended surface flow networks and micro-channels. Under these conditions a large fraction of the wetland surface drained into the adjacent channel. Drainage into the channel occured at two distinct locations (Figure 6). Similar patterns were observed in the fen located at the field site during a rainstorm in the spring of 2009 (Figure 7).
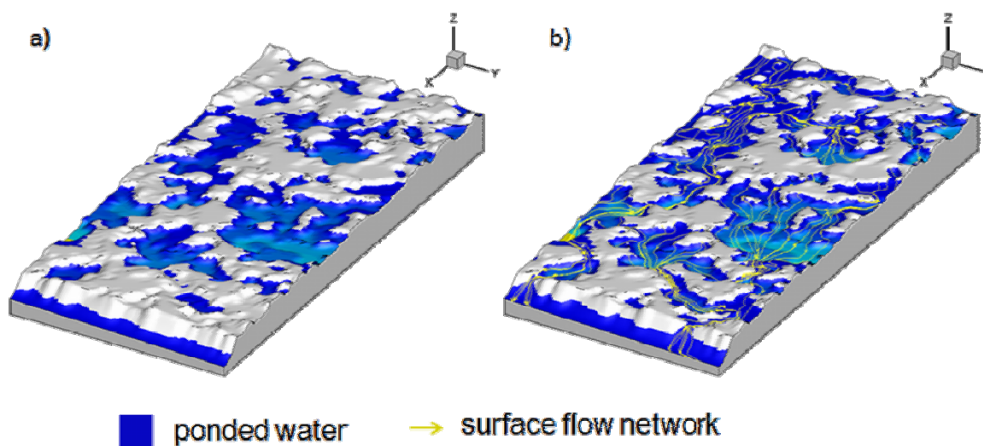
Figure 6: Snapshots of the evolving surface flow networks for a) moderate flow conditions (day 180) and b) during peak flow (day 218). Blue zones indicate ponded surface water and yellow arrows stream traces in the surface flow networks. Snapshots show simulated results.

Figure 7: Picture of the field site taken during a storm-flow event in spring 2009. Channel location is marked by a line.

Figure 8 shows the simulated discharge hydrograph for the planar model. Compared to the micro-topography model, the hydrograph generally showed higher peak discharges. Surface flows were generated much earlier (around day 55) and occured more frequently compared to the micro-topography model (75 of 365 simulated days). During the relatively dry summer period between day 150 and 217, rainfall intensities during the six different events were high enough to generate surface drainage. The micro-topography model, in comparison, did not show any surface drainage during this period. In the planar model surface drainage was not inhibited by micro-topographic structures and could occur as sheet flow as soon as the water table intersected the land surface. In the planar model surface flow contributed up to 95% of the total discharge during individual events.
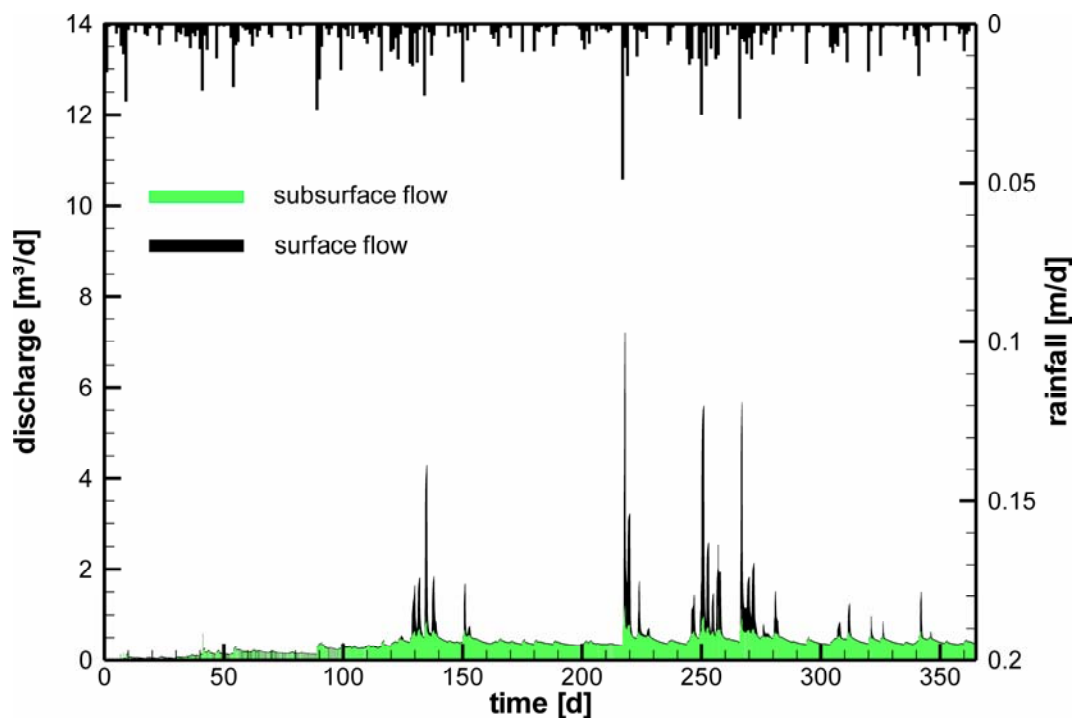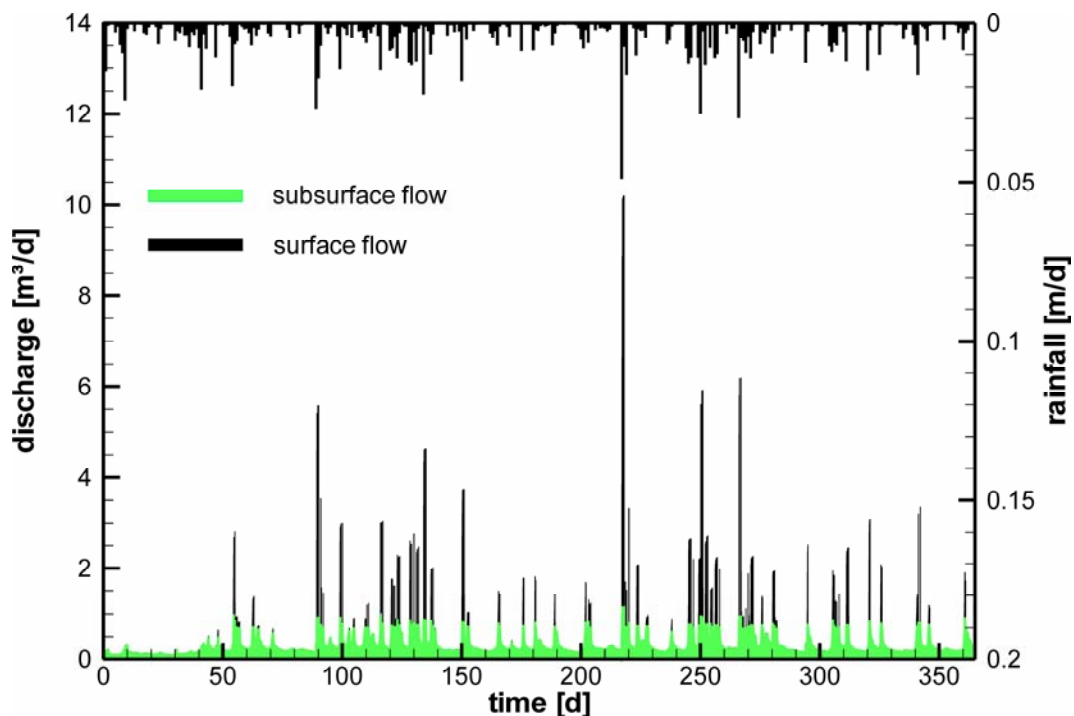

Figure 8: *Simulated, yearly hydrograph for the planar reference model. Precipitation at the field site for the hydrologic year 2000 (10/31/1999 – 11/1/2000) is shown on the top. Surface and subsurface fractions of total channel discharge are shown in green and black respectively.*

3.3 Non-linearities and hysteresis

No unique groundwater level or rainfall rate could be associated with the development of surface flow networks and the onset of surface flows. In contrast the amount of ponded surface water, necessary to initiate flow to the channel via the surface flow networks and micro-channels, was narrowly defined. Figure 9 (upper plot) shows the relationship between surface discharge and surface water storage (total amount of ponded surface water in m³ stored in local depression and flow networks). Figure 9 (upper plot) summarizes results for the 365 day simulation for the micro-topography model. The different loops represent different trajectories for single rainfall events. The trajectory for the most

intense rainstorm of the simulated year is discussed in more detail (marked by a line in Figure 9 upper plot). This precipitation event (48 mm/d) occurred right after an extended drier period (day 150 to 217, see Figure 5) on day 217 followed by only 7.2 mm/d on day 218. In the beginning of the rain storm infiltrating rainwater exclusively recharged groundwater (no surface discharge). With rising groundwater levels, local depressions were filled with water and increasingly more water was stored on the soil surface (increasing surface storage without surface flow in the channel). Later, the filled depressions start to interconnect until a critical surface storage value (~5.6m³) was exceeded. The resulting flow network was subsequently large enough to provide first surface flow to the channel. The surface flow rapidly increased until it reached a stable rate of ~3.8 m³/d. After that surface flow abruptly increased as surface storage exceeded another critical value (~7.2m³). This was caused by a second surface flow network that developed and drained independently from the first one. That is illustrated in Figure 10 by different snapshots, taken for five different time steps.
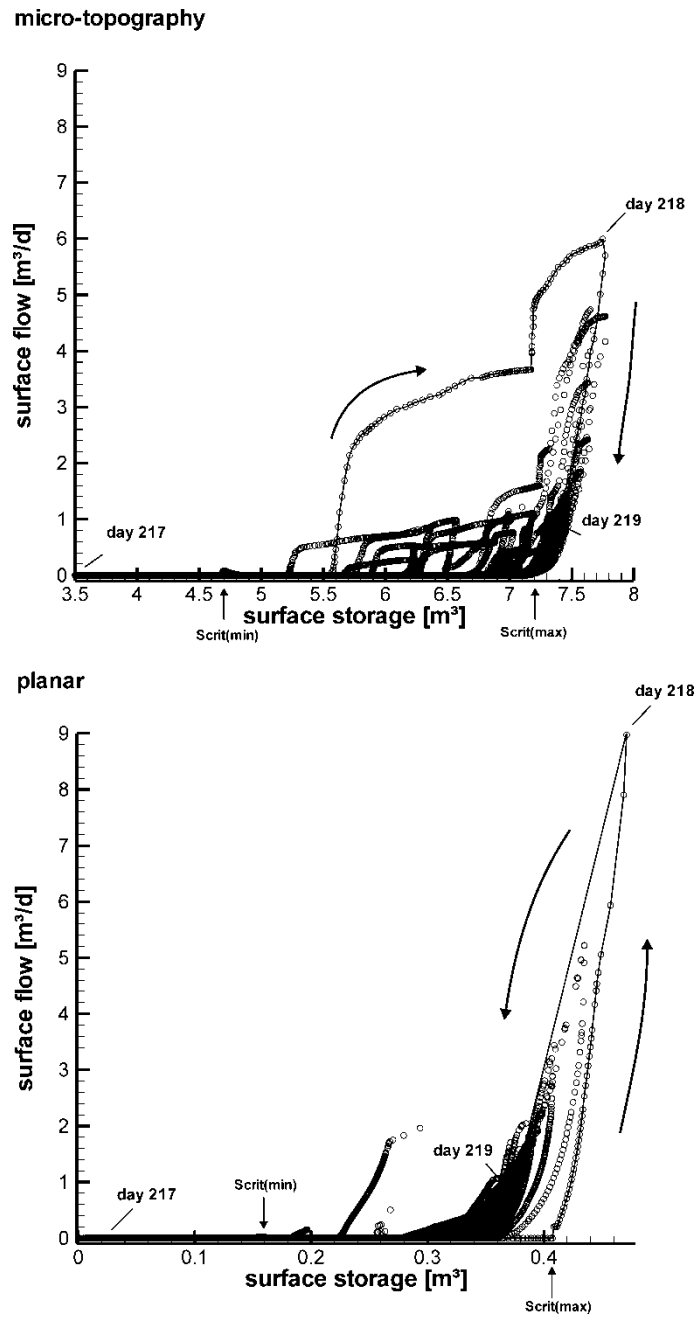
Figure 9: Relationship between surface storage and channel discharge for the micro-topography model (upper panel) and the planar model (lower panel). The black line depicts the peak flow event around day 218. Scrit$_{(max)}$ - Scrit$_{(min)}$ (upper and lower panels) represents the critical range of surface water storage, within which surface flows occur in the yearly simulations.
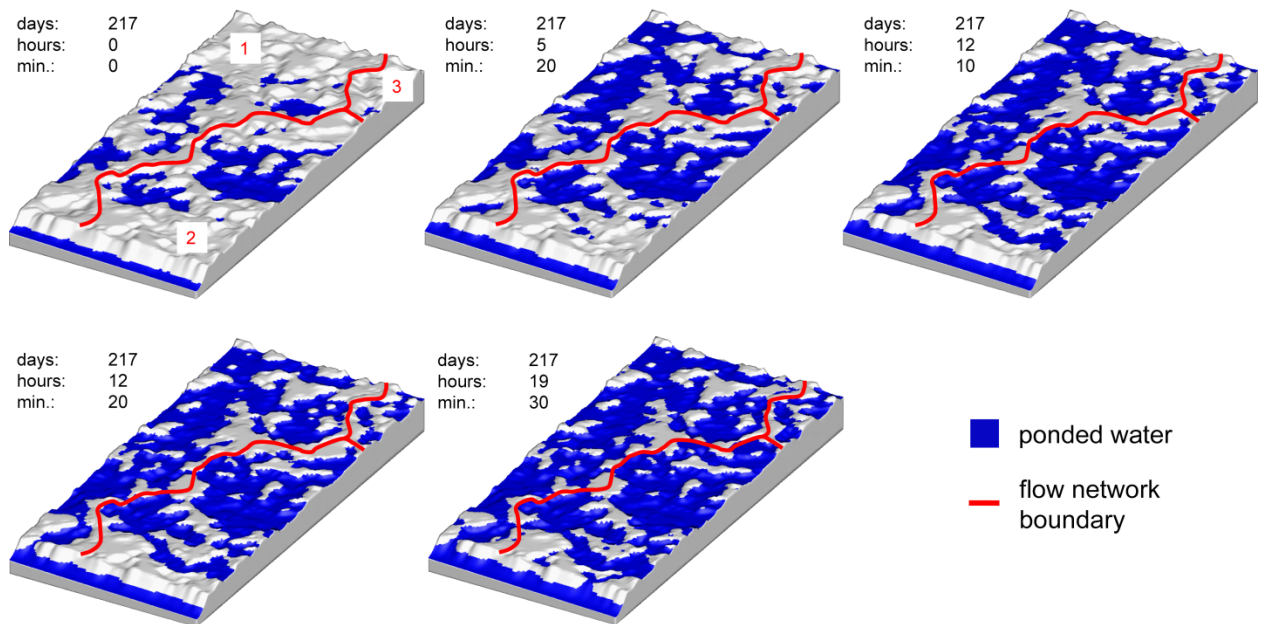
Figure 10: Six consecutive snapshots of the evolving surface flow networks during the largest flow event of the year (day 217 to day 218). The red lines separate different flow networks (1-3) that developed independently from each other.

The lines on the model surface in Figure 10 delineate different surface flow networks, determined by an analysis of overland flow stream traces. The first snapshot shows the situation right at the beginning of the rainstorm on day 217. Due to the preceding drier period only a few, isolated depressions were filled with water. After the onset of rainfall, additional depressions were filled with water and the isolated ponded areas began to interconnect (second snapshot). After 12 hours and 10 minutes (third snapshot) networks 1 and 2 reach their maximum extent, although surface drainage to the channel has not yet been initiated. Although the third snapshot seems to suggest that there were small ponded flow bridges connecting the two networks, an analysis of stream traces showed that there was no surface water exchange. After 12 hours and 20 minutes (fourth snapshot), the first flow network started to drain into the channel causing the first increase in total runoff (Figure 9 upper panel). 7 hours and 10 minutes later (fifth snapshot), the second flow network was activated and starts to spill into the channel resulting in the second rapid increase in discharge (Figure 9 upper panel). Consequently peak discharge (at the end of day 217) occured when both networks were connected to the channel. At that time, the third zone was still not connected to either of the two other networks. This area was characterized by depressions, which remained isolated from the flow networks and where the ponded surface water was immobile during events. The process of growing (during rainfall events) and shrinking networks (during flow recessions) was responsible for the different clockwise loops that can be seen in the relationship shown in Figure 9 (upper panel). In contrast to the wetting process the drying cycle during flow recessions proceeds much more uniformly (Figure 9 upper panel), because it was not characterized by the same stepwise threshold behavior as the wetting

process. This distinctly different behavior of the system during wetting and drying resulted in the observed hysteresis loops. The same behavior was also evident in the development of subsurface and surface flow throughout the event (Figure 12). Subsurface flow showed a gradual increase during wetting of the system, whereas surface flows were initiated at distinct thresholds when specific flow network started to spill into the channel. In contrast recession of surface flow was much more gradual.
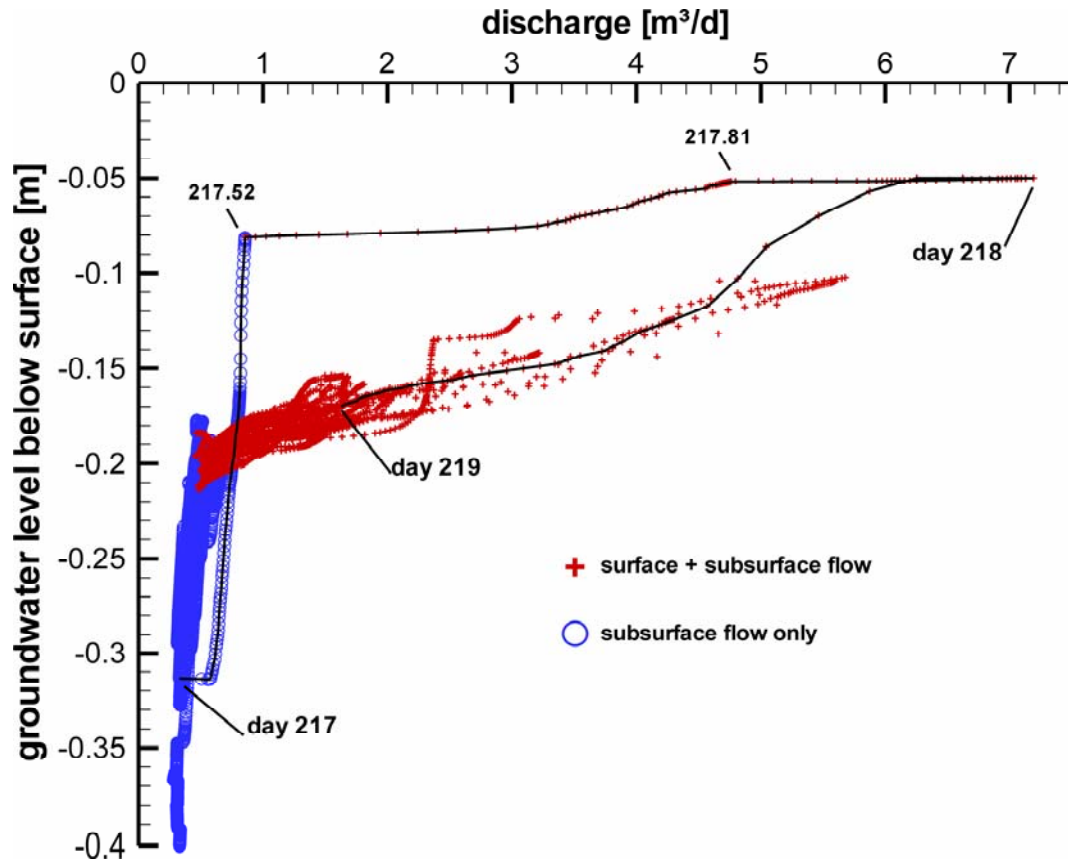
Figure 11: Simulated relationship between groundwater level and channel discharge for the micro-topography model. Blue filled circles represent times when no surface drainage occurs, red open circles represent conditions when surface drainage is being generated, different scales are used on the x-axis for better visibility of hysteretic behavior during low discharges, the sequence of days 217 to 219, representing an intense rain storm, is depicted by a line.
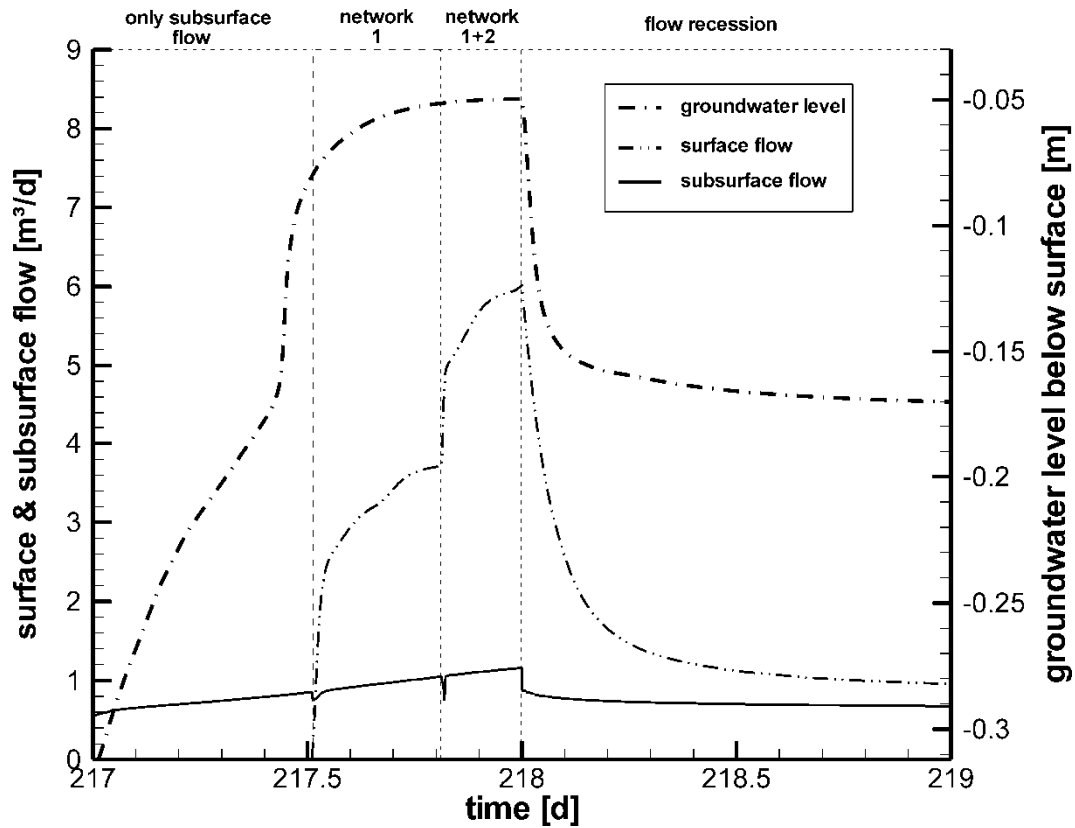
Figure 12: *Simulated development of subsurface, surface flow and groundwater level during the largest rainstorm (day 217-218). Vertical dashed lines mark the different periods when stream flow is characterized by subsurface flow only, subsurface and surface flow with either network 1 or networks 1 + 2 being active and by flow recession.*

Figure 9 (upper panel) also suggests that there is not one critical value of surface storage that, when exceeded, results in surface flow. The figure indicates that there is a range in surface storage that defines when surface flow is likely to occur. This range was much more closely defined than the range of groundwater levels at a specific location that were associated with the presence of surface flow. For the micro-topography model, the minimum ($Scrit_{min}$) and maximum ($Scrit_{max}$) surface storage values for generation of surface flow were 4.7m³ and 7.2m³, respectively. Within this range, every flow event displayed a unique hysteretic trajectory, as seen in Figure 9 (upper panel).

The surface storage-discharge relationship for the planar model is shown in the lower panel of Figure 9. Maximum surface storage ($Scrit_{max}$) before initiation of surface flow is about 0.41 m³, which is almost 20 times smaller than for the micro-topography model. A very mild form of hysteresis (note the different scales on the x-axes in Figure 9) can also be seen in the relationship for the planar model, but in the other direction (counter clockwise) compared to the micro-topography model (clockwise). Hysteretic loops in the planar model only occured over a range of 0.3 m³ of surface storage, whereas the range in the micro-topography model was approximately ten times higher. The mild hysteretic behavior in the planar model was attributed to the curved free water table intersecting the straight planar land surface differently during wetting and drying of the system.

[86]

Figure 11 depicts the simulated relationship between groundwater level (again evaluated at the observation well shown in Figure 3) and channel discharge. It shows a non-linear relationship that is very similar to the one observed at the field site (see Figure 2 – total discharge volumes are different because of different sizes of the contributing areas). When the system was drained by subsurface flow only (indicated by the circles in Figure 11) large groundwater fluctuations were accompanied by relatively small changes in flow to the channel (see also Figure 12). When surface flow was initiated by activation of surface flow networks (indicated by crosses in Figure 11), drastic increases in channel discharge were realized and the system shifted from pure subsurface flow to surface flow dominance. This behavior was best visualized for the most intense rainstorm on day 217 and the subsequent flow recession on day 218 (Figure 12 and solid line in Figure 11). At the beginning of the rain storm, the peat groundwater level in the peat was low (approximatley 0.3 m below surface), due to the dry antecedent conditions. After the onset of rainfall groundwater levels increased to a depth of around 0.08 m below the surface (Figures 11 and 12) with a minimal increase in channel discharge (Figure 11). Then the first surface network started to spill into the channel (at time 217.52 in Figure 11), causing a tripling of channel discharge (from < 1 m^3/d to more than 3 m^3/d) over a very short time period (see Figure 12). The first surface flow network matured and surface and subsurface flow to the channel gradually increased (see Figure 12). At time 217.81 (Figure 11), the next surface storage threshold was reached and the same process was repeated for the second surface flow network. During flow recession (starting on day 218) the relationship shown in Figure 11 takes a different trajectory. The filled surface channel network was rapidly drained into the channel accompanied by a rapid decline in the water table (Figure 12). The difference between the threshold type behavior of the system is shown in Figure 11. A step-wise activation of different surface flow networks occurred during wetting and the more gradual flow recession during drying caused the hysteretic relationship between groundwater level and the channel discharge shown in Figure 11. The same hysteretic loops in this relationship were seen for other rainstorms during wetting and drying of the system (Figure 11). The general form of this pronounced hysteresis was similar to the one seen in the field data (see Figure 2) and the one evident in the surface storage-discharge relationship.

The planar reference model does not show the same consistent hysteretic loops observed as the micro-topography model. The transition between subsurface and surface flow dominance in the planar model was characterized by a very sharp and defined break in the relationship in contrast to the smoother transition in the micro-topography model. The relationship between groundwater level and channel discharge for the flow event on days 217 to 218 in the planar model is shown in Figure 13 (lower right panel) in addition to the same relationship for the micro-topography model (upper left panel). Another geostatistical realization of the micro-topography model (upper right panel) and a model with micro-topographic structures that have half the mean length of the original model (lower left panel) are shown for comparison. The planar model showed no hysteresis in the relationship

between groundwater level and channel discharge. The relationship followed the same trajectory during wetting and drying. The second realization of the original micro-topography model showed a similarly pronounced hysteresis as the first realization. However, in the second model a small surface flow network close to the channel developed more rapidly and started to spill into the channel when the upstream water table was still 0.2 m below the land surface. This identifies the importance of connectivity between the surface depressions, in which the surface flow networks develop, can be different in each realization of one geostatistical model. The micro-topography model, with a reduced mean length showed a less pronounced hysteresis and resembled a shape in the groundwater level-discharge relationship that was somewhere between the planar model and the original micro-topography model.
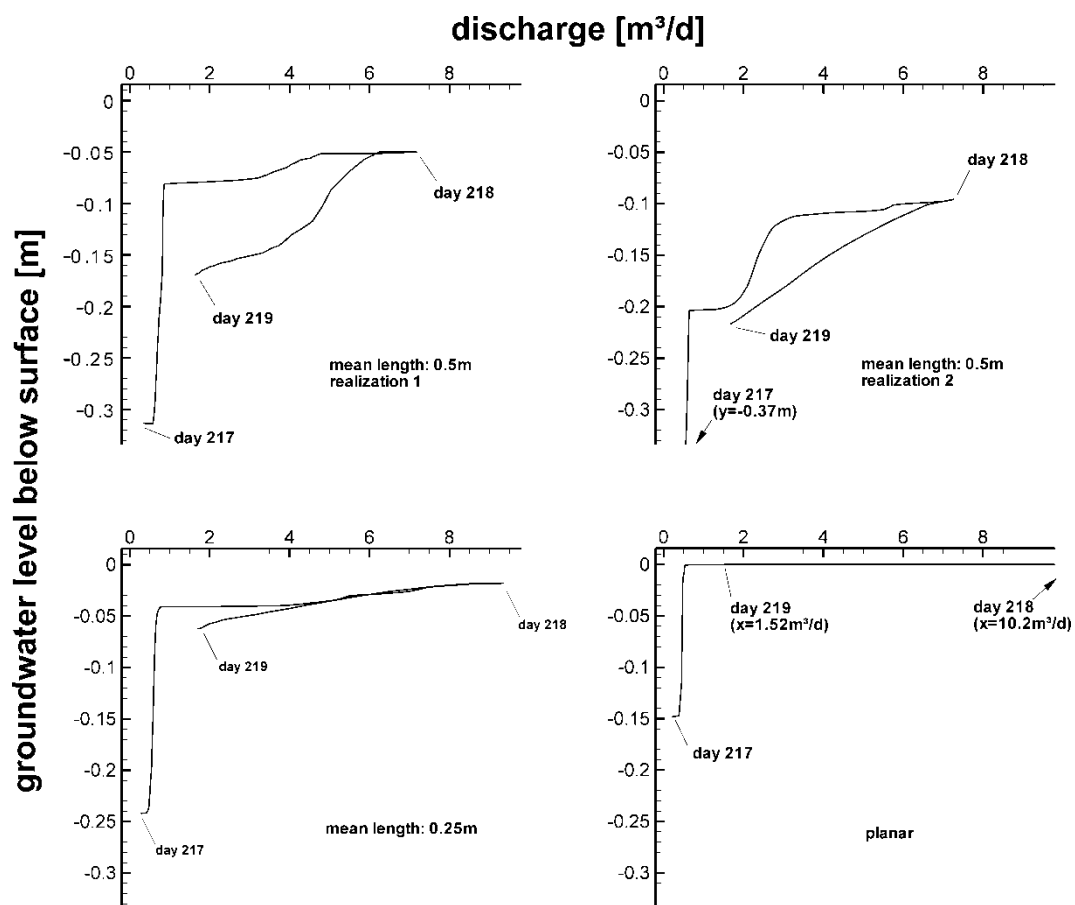
Figure 13: Simulated relationships between channel discharge and groundwater level (evaluated in the observation well) for two different geostatistical realizations of the micro-topography model (upper panels), a micro-topography model with reduced mean length of the structures (1/2 of the original model) (lower left panel), and the planar reference model (lower right panel).

4 Discussion

4.1 Effects of micro-topography on runoff generation

4.1.1 Threshold behavior and flow components

Simulation results showed complex dynamics of runoff generation in riparian wetlands with a distinct micro-topography. For a steady input of rainfall, the stream flow was initially generated from subsurface flow into the stream channel. Generation of surface flow is controlled by a threshold process of surface ponding and the subsequent stepwise formation of different surface flow networks. For variable rainfall input these networks dynamically expand and shrink and the system frequently shifted between subsurface and surface flow dominance. Threshold-controlled dynamics of runoff generation are not uncommon in hydrologic systems *[60]* and have been described for macro-porous soils *[57]*, cracking clay soils *[59, 54]*, complex glaciated landscapes *[47, 46]* and subsurface storm flow on bedrock with micro-topography *[51, 52]*. As in the case presented here, non-linear response of threshold systems to external forcing (e.g. rainfall inputs) is typically controlled by distinct shifts in dominant flow regimes (e.g. *[57]*) and/or a stepwise activation or deactivation of different hydrologic compartments in the system (e.g. *[47]*). *Spence and Woo [47]* described such a system as a spill-and fill runoff system. The same concept was later used by *Tromp-van Meerveld and McDonnell [52]* to describe the generation of subsurface storm flow on slopes with a micro-topographic bedrock structure.

Non-linear response of threshold systems is often difficult to predict, as it depends on the internal microstates of the system at the beginning of an event (e.g. soil moisture, pressure distributions etc.) *[58, 59]*. These microstates are rarely known to a sufficient degree and are usually poorly represented by macrostates of the system (e.g. average soil moisture, average depth to the water table) *[58]*. Hence the specific conditions (e.g. rainfall intensity or depth of groundwater level), under which surface flow is generated in the micro-topography model are difficult to predict. High rainfall intensities, as long as they do not lead to excess infiltration, do not automatically produce surface flow, as long as the groundwater level is deep and surface water storage low. Before surface flow is generated, the groundwater level has to rise up to a certain elevation, so that local pools of water on the surface are able to inter-connect and form the necessary surface flow networks. Consequently a given storm-flow event can lead to instantaneous surface flow for very wet antecedent moisture conditions. The surface flow can be time delayed for moderately wet antecedent conditions and even no surface flow for dry antecedent conditions.

The amount of water stored on the surface was found to be a good indicator for the occurrence of surface flows (Figure 9). A narrow range of surface storage values defined when surface flow was initiated. One possible reason for the absence of a single threshold value could be the dynamics of re-

infiltration in the transition zone between the peat and the channel. Re-infiltration rates were high because of steep gradients between the groundwater and the channel, which varied with the dynamics of the system. Therefore, different amounts of water stored on the surface might be needed to generate sufficient surface flow to exceed re-infiltration rates into this zone.

The simulated stream flow hydrograph in the micro-topography model was significantly moderated compared to the much flashier response in the planar model. Micro-topography functions as a filter that buffers rainfall inputs, facilitates dynamic exchange between surface and subsurface and delays runoff response. Similar moderations of stream flows (e.g. retardation of peak flows due to temporal surface storage of water) have been observed in field settings, e.g. in peat-forming wetlands [27, 13] or in other landscapes with complex surface topography [46]. As a consequence of this flow moderation subsurface flow is the dominant runoff generating process throughout most of the year (during dry to moderately wet conditions). Surface flow only becomes the dominant runoff producing process during intense rainstorms (on 52 out of 365 days in our simulations), when it is responsible for up to 80% of the total discharge generated. In contrast, the planar reference model surface flow contributions occured much more frequently (on 75 days out of 365) and provided up to 95% of total discharge.

4.1.2   *Structure and dynamics of the surface flow networks*

In the simulations with micro-topography several surface flow networks developed that operated independently with no exchange of water between them. Flow depths and velocities in the simulated surface flow networks were found to be highly variable and discontinuous in space and time, and consistent with findings from other field and simulation studies [11, 12]. The specific structure of the micro-topography controlled the timing and magnitude of surface water spills into the channel. These topographic controls and the resulting spill and fill dynamics [51] can cause step-wise increases in channel discharge as seen in the simulations with steady rainfall (Figure 4) or in other studies on runoff generation in systems with micro-topography [2]. Simulation results further showed that the structure of micro-topography resulted in isolated depressions that never were connected to one of the main surface flow networks (Figure 10). Certain flow networks may only be activated during very large rainstorms and remained stagnant during smaller rainfall events. Similar findings were presented by *Antoine et al. [2]*, who performed numerical surface-flow simulations on synthetic micro-topographies with different structures. They concluded that on a larger scale, realistic micro-topographies lead to conditions where connected and unconnected depressions coexist. For variable rainfall inputs the ratio between active and evolving networks and stagnant pools may frequently shift, resulting in a highly non-linear flow response of the system. These results support the conclusion by *Fiedler and Ramirez [12]* that representing complex slopes as planar surfaces and, ignoring small

scale dynamics and interactions between surface and sub-surface, may lead to a false representation of the hydrological system.

4.2   Micro-topography and non linear response

The observed non-linear relationship between groundwater level and discharge (Figure 2) could be adequately represented with the micro-topography model (Figure 11). Similar non-linear relationships have frequently been observed in the field *[41, 37, 23, 15, 38, 43, 13, 28]*. A common explanation for this relationship is the transmissivity feedback effect *[4]*. It is based on an exponential decay of lateral hydraulic conductivity in the soil with depth. As a result transmissivity and consequently the rate of lateral water movement increase exponentially as the groundwater level rises into superficial layers *[4]*. In this study the same non-linear relationship was generated with a uniform distribution of hydraulic conductivities in the subsurface solely by effects of the micro-topography (Figure 11). In contrast, the planar model shows a linear increase of discharge with rising water table and a distinct and much more abrupt shift between subsurface and surface flow dominance (Figure 13). This suggests that additional mechanisms might be at work to generate the non-linear relationships between riparian water table depth and discharge commonly observed in the field. Which mechanism dominantes is dependent on the specific field situation such as magnitude and variability of subsurface hydraulic conductivity, rainfall duration and intensity, initial water table depth and the structure of surface micro-topography.

Similar clockwise hysteresis as seen in the simulated relationship between water table and discharge has also been observed in other field studies in peat-forming wetlands (*[5, 13]*) as well as in riparian zones characterized by mineral soils (*[23]*). A very pronounced hysteresis with very similar characteristics to the ones obtained from our micro-topography simulations was observed by *Fitzgerald et al. [13]* during a rainstorm in a headwater swamp in British Columbia, Canada (Figure 14). Similar to our simulated relationship their study also showed distinctly different hysteresis loops for individual peakflow events. Whereas *Branfireun et al. [5]* and *Kendall et al. [23]* attribute the observed hysteretic behavior to different compartments of the system dominating flow to the channel during rising flows and flow recession *Fitzgerald et al. [13]* provided no specific explanation for the observed relationship. Their study channel flow only increased significantly after extended surface ponding was observed, which suggests similar dynamics as observed in our micro-topography simulations. Hysteresis in our model was caused by a distinct sequence of the threshold-controlled, stepwise increase in surface flow followed by a more gradual draining of the surface flow networks associated with a rapid decline in groundwater levels. In systems that frequently shift between subsurface and surface flow, which is not uncommon in riparian wetlands in humid climates *[13, 27]*, the described micro-topography induced dynamics will superimpose non-linearities caused by transmissivity feedback.
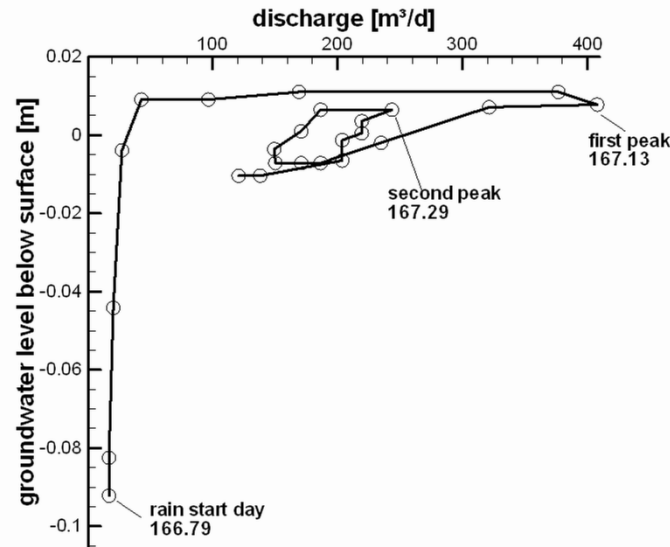
Figure 14: *Relationship between discharge and groundwater level for two peak flow events observed for a small catchment located in British Colombia, Canada (modified after Fitzgerald et al. (2003)).*

4.3 Limitations and constraints

The virtual systems simulated here are a simplification of complex field situations. Peat soils are rarely homogeneous and hydraulic conductivities are usually non-uniform. Retention characteristics of peat soils can be hysteretic. Hence non-linear response of real systems may be caused by several reasons. Furthermore higher effective hydraulic conductivities in some peat soils (e.g. caused by preferential flow) may so efficiently drain a wetland that for a given rainfall rate surface ponding never occurs. Significant inflows from adjacent hillslopes or from deeper groundwater may affect the dynamics of flow in the peat. Most of these aspects were intentionally excluded from this study to highlight the effects of the micro-topography. Although this limits the degree to which the results can be generalized, it provides a new insight into the process dynamics caused by distinct surface micro-topography, which is not uncommon for peat-forming wetlands. The structure of micro-topography, hydraulic conductivities of the peat and rainfall rates were taken from a riparian fen in an experimental watershed in Germany and are believed to be representative for other hummocky riparian wetlands in humid climates. Therefore simulation results can provide new insights into the dynamics of runoff generation in such systems that may help to explain other observed non-linear system responses (e.g. *[13]*).

5 Conclusions

Hydrologic systems typically show complex non-linear stream flow response to rainfall inputs. Deciphering the processes that cause the observed response is usually difficult due to the strongly

non-linear behavior of hydrologic systems *[57]*. Using physically-based numerical models as controlled replicates of natural systems to conduct "virtual experiments" *[55]* can be a useful tool to elucidate individual processes and their interdependencies (see also *Zehe et al. [57]*). This approach was used here to investigate the effects of surface micro-topography on runoff generation in a virtual riparian wetland in a humid climate. Simulation results reveal complex threshold processes with stepwise expansions and contractions of surface flow networks that govern stream flow generation. Distinctly different behavior of the system during wetting and drying results in a pronounced clockwise hysteresis in the non-linear relationship between stream flow and riparian groundwater level that resembles similar relationships observed in the field. Simulations for different micro-topographies and for a planar reference model show clear differences in the shape of the non-linear relationship and demonstrate how stream flow is moderated by the micro-topography. The planar model does not show significant hysteresis in the stream flow-water table relationship. Results from a model with smaller mean length of the micro-topographic structures (1/2 of the original model) suggest that for decreasing size of the structures the response of the system approaches that of the planar model. A comparison of the model results with results presented by *Fitzgerald et al.* (*[13]*) from a field study in a humid riparian wetland in Canada, suggests that the simulated dynamics might provide a consistent explanation for the observed behavior of the system. We hypothesize that the simulated hydrologic dynamics in wetlands with a defined micro-topography can result in a large range of subsurface residence times and dynamic mixing between surface and subsurface water of different age and potentially impact water quality. Preliminary particle tracking simulations, which will be presented in a follow-up paper, support this hypothesis. To what degree the simulated dynamics could provide a new framework to interpret the common variability in stream water chemistry during events that is described in *Kirchner's* double paradox *[24]* remains to be investigated. Future work will also address to what degree simplified conceptual representations of surface structures in numerical models (e.g. by defining a rill storage height for larger model cells) can mimic the effects of the micro-topography on surface flow and surface-subsurface exchange.

Ackonwledgements

References

[1] *Alewell, C.; Paul, S.; Lischeid, G.; Storck, F. R. (*2007), Co-regulation of redox processes in freshwater wetlands as a function of organic matter availability?, Science of the Total Environment 404(2-3):335–342, doi:10.1016/j.scitotenv.2007.11.001.

[2] *Antoine, M.; Javaux, M.; Bielders, C. (*2009), What indicators can capture runoff-relevant connectivity properties of the micro-topography at the plot scale?, Advances in Water Resources 32(8):1297–1310, doi:10.1016/j.advwatres.2009.05.006.

[3] *Bishop, K.; Seibert, J.; Köhler, S.; Laudon, H. (*2004), Resolving the double paradox of rapidly mobilized old water with highly variable responses in runoff chemistry, Hydrol. Process 18185–189.

[4] *Bishop, K.H. ,(*1991) ,Episodic increase in stream acidity, catchment flow pathways and hydrograph seperation, Ph.D. thesis, Cambridge University, Cambridge, UK.

[5] *Branfireun, B. A.; Roulet, N. T. (*1998), The baseflow and storm flow hydrology of a precambrian shield headwater peatland, Hydrological Processes 12(1):57–72.

[6] *Brookfield, A. E.; Sudicky, E. A.; Park, Y. J.; Conant Jr., B. (*2009), Thermal transport modelling in a fully integrated surface/subsurface framework, Hydrological Processes(23):2150–2164, 10.1002/hyp.7282.

[7] *Carle, S.F.; Fogg, G.E. (*1996), Transition Probability-Based Indicator Geostatistics, Mathematical Geology 28(4):453–476.

[8] *Devito, K. J.; Hill, A. R. (*1997), Sulphate dynamics in relation to groundwater-surface water interactions in headwater wetlands of the southern Canadian Shield, Hydrological Processes 11(5):485–500.

[9] *Dunne, T.; Zhang, W.; Aubry, B. F. (*1991), Effects of rainfall, vegetation, and microtopography on infiltration and runoff, Water Resources Research 27(9):2271–2285.

[10] *Duval, T. P.; Hill, A. R. (*2006), Influence of stream bank seepage during low-flow conditions on riparian zone hydrology, Water Resources Research 42(10):10425, doi:10.1029/2006WR004861.

[11] *Esteves, M.; Faucher, X.; Galle, S.; Vauclin, M. (*2000), Overland flow and infiltration modelling for small plots during unsteady rain: numerical results versus observed values, Journal of Hydrology 228(3-4):265–282.

[12] *Fiedler, F. R.; Ramirez, J. A. (*2000), A numerical method for simulating discontinuous shallow flow over an infiltrating surface, International journal for numerical methods in fluids 32(2):219–239.

[13] *Fitzgerald, D. F.; Price, J. S.; Gibson, J. J. (*2003), Hillslope-swamp interactions and flow pathways in a hypermaritime rainforest, British Columbia, Hydrological Processes 17(15):3005–3022, 10.1002/hyp.1279.

[14] *Fleckenstein, J.H.; Niswonger, R.G.; Fogg, G.E. (*2006), River-Aquifer Interactions, Geologic Heterogeneity, and Low-Flow Managment, Groundwater 44(6):837–852.

[15] *Fraser, C. J.D.; Roulet, N. T.; Moore, T. R. (*2001), Hydrology and dissolved organic carbon biogeochemistry in an ombrotrophic bog, Hydrological Processes 15(16):3151–3166, 10.1002/hyp.322.

[16] *Frei, S.; Fleckenstein, J. H.; Kollet, S. J.; Maxwell, R. M. (*2009), Patterns and dynamics of river–aquifer exchange with variably-saturated flow using a fully-coupled model, Journal of Hydrology 375(3-4):383–393.

[17] *Gibson, J. J.; Price, J. S.; Aravena, R.; Fitzgerald, D. F.; Maloney, D. (*2000), Runoff generation in a hypermaritime bog-forest upland, Hydrol. Process 142711–2730, doi: 10.1002/hyp.1279.

[18] *Gilliam, J. W. (*1994), Riparian wetlands and water quality, Journal of Environmental Quality 23(5):896.

[19] *Hauck, Anette ,(*1999) ,Hydrological Charakterization of the Lehstenbach Catchment, unpuplished Diploma Thesis, Department of Ecological Modelling, University of Bayreuth, Bayreuth.

[20] *Hopp, L.; McDonnell, J. J. (*2009), Connectivity at the hillslope scale: Identifying interactions between storm size, bedrock permeability, slope angle and soil depth, <u>Journal of Hydrology,</u> doi:10.1016/j.jhydrol.2009.07.047.

[21] *Jones, J. P.; Sudicky, E. A.; Brookfield, A. E.; Park, Y. J. (*2006), An assessment of the tracer-based approach to quantifying groundwater contributions to streamflow, <u>Water Resources Research</u> 42, W02407, doi:10.1029/2005WR004130.

[22] *Jones, J. P.; Sudicky, E. A.; McLaren, R. G. (*2008), Application of a fully-integrated surface-subsurface flow model at the watershed-scale: A case study, <u>Water Resources Research</u> 44, W03407, doi:10.1029/WR005603.

[23] *Kendall, K. A.; Shanley, J. B.; McDonnell, J. J. (*1999), A hydrometric and geochemical approach to test the transmissivity feedback hypothesis during snowmelt, <u>Journal of Hydrology</u> 219(3-4):188–205, doi:10.1016/S0022-1694(99)00059-1.

[24] *Kirchner, J. W. (*2003), A double paradox in catchment hydrology and geochemistry, <u>Hydrological Processes</u> 17(4):871–874.

[25] *Kollet, J.S.; Maxwell, R.M. (*2006), Integrated surface-groundwater flow modeling: A free-surface overland flow boundary condition in a parallel groundwater flow model, <u>Advances in Water Resources</u> 29(7):945–958.

[26] *Kruse, J.; Lennartz, B.; Leinweber, P. (*2008), A modified method for measuring saturated hydraulic conductivity and anisotropy of fen peat samples, <u>Wetlands</u> 28(2):527–531.

[27] *Kværner, J.; Kløve, B. (*2008), Generation and regulation of summer runoff in a boreal flat fen, <u>Journal of Hydrology</u>(360):15–30, doi:10.1016/j.jhydrol.2008.07.009.

[28] *Laudon, H.; Seibert, J.; Kohler, S.; Bishop, K. (*2004), Hydrological flow paths during snowmelt: congruence between hydrometric measurements and oxygen 18 in meltwater, soil water, and runoff, <u>Water Resources Research</u> 40(3):W03102, doi:10.1029/2003WR002455.

[29] *Lee, S.-Y.; Carle, S.F.; Fogg, G.E. (*2007), Geologic heterogeneity and a comparison of two geostatistical models: Sequential Gaussian and transition probability-based geostatistical simulation, <u>Advances in Water Resources</u> 30(9):1914–1932.

[30] *Li, Q.; Unger, A. J.A.; Sudicky, E. A.; Kassenaar, D.; Wexler, E. J.; Shikaze, S. (*2008), Simulating the multi-seasonal response of a large-scale watershed with a 3D physically-based hydrologic model, <u>Journal of Hydrology</u>(357):317–336, doi:10.1016/j.jhydrol.2008.05.024.

[31] *Lischeid, G.; Lange, H.; Moritz, K.; Büttcher, H. (*2004), Dynamics of runoff and runoff chemistry at the Lehstenbach and Steinkreutz catchment, <u>In: Matzner, E. (ed). Biogeochemistry of Forested Catchments a. Changing Environment: A. German Case Study,</u> Ecological Studies, Vol.172 ,Springer, Heidelberg, pp. 399–436.

[32] *Lischeid, G.; Bittersohl, J. (*2008), Tracing biogeochemical processes in stream water and groundwater using non-linear statistics, <u>Journal of Hydrology</u> 357(1-2):11–28, doi:10.1016/j.jhydrol.2008.03.013.

[33] *Lischeid, G.; Kolb, A.; Alewell, C. (*2002), Apparent translatory flow in groundwater recharge and runoff generation, <u>Journal of Hydrology</u> 265(1-4):195–211.

[34] *Lischeid, G.; Kolb, A.; Alewell, C.; Paul, S. (*2007), Impact of redox and transport processes in a riparian wetland on stream water quality in the Fichtelgebirge region, southern Germany, <u>Hydrological Processes</u> 21(1):123–132, 10.1002/hyp.6227.

[35] *McLaren, R.G. (*2008), GRID BUILDER - A pre-processor for 2D, triangular element, finite-element programs, Groundwater Simulations Group, University of Waterloo, Waterloo.

[36] *Metcalfe, R. A.; Buttle, J. M. (*1999), Semi-distributed water balance dynamics in a small boreal forest basin, <u>Journal of Hydrology</u> 226(1-2):66–87.

[37] *Moldan, F.; Wright, R. F. (*1998), Episodic behaviour of nitrate in runoff during six years of nitrogen addition to the NITREX catchment at Gårdsjön, Sweden, <u>Environmental Pollution</u> 102(1S1):439–444, 10.1016/S0269-7491(98)80066-3.

[38] *Molenat, J.; Gascuel-Odoux, C. (*2002), Modelling flow and nitrate transport in groundwater for the prediction of water travel times and of consequences of land use evolution on water quality, <u>Hydrological Processes</u> 16(2):479–492, 10.1002/hyp.328.

[39] *Price, J. S.; McLaren, R. G.; Rudolph, D. L. (*2009), Landscape restoration after oil sands mining: conceptual design and hydrological modelling for fen reconstruction, International Journal of Mining, Reclamation and Environment 99999(1):1–15.

[40] *Qu, Y.; Duffy, C. J. (*2007), A semidiscrete finite volume formulation for multiprocess watershed simulation, Water Resources Research 43(8):W08419, doi:10.1029/2006WR005752.

[41] *Rice, K. C.; Bricker, O. P. (*1995), Seasonal cycles of dissolved constituents in streamwater in two forested catchments in the mid-Atlantic region of the eastern USA, Journal of Hydrology 170(1-4):137–158, doi:10.1016/0022-1694(95)92713-N.

[42] *Schlotzhauer, S. M.; Price, J. S. (*1999), Soil water flow dynamics in a managed cutover peat field, Quebec: Field and laboratory investigations, Water Resources Research 35(12):3675–3683.

[43] *Seibert, J.; Bishop, K.; Rodhe, A.; McDonnell, J. J. (*2003), Groundwater dynamics along a hillslope: A test of the steady state hypothesis, Water Resour. Res 39(1):1014, doi:10.1029/2002WR001404, 2003.

[44] *Seibert, J.; Grabs, T.; Köhler, S.; Laudon, H.; Winterdahl, M.; Bishop, K. (*2009), Linking soil–and stream-water chemistry based on a iparian flow-concentration integration model, Hydrology and Earth System Sciences, 13:2287-2297.

[45] *Shen, H. W.; Julien, P. Y. (*1993), Erosion and sediment transport, Handbook of Hydrology.12.1-12.61.

[46] *Spence, C. (*2007), On the relation between dynamic storage and runoff: A discussion on thresholds, efficiency, and function, Water Resources Research 43(12):W12416.

[47] *Spence, C.; Woo, M. (*2003), Hydrology of subarctic Canadian shield: soil-filled valleys, Journal of Hydrology 279(1-4):151–166.

[48] *Sudicky, E. A.; Jones, J. P.; Park, Y. J.; Brookfield, A. E.; Colautti, D. (*2008), Simulating complex flow and transport dynamics in an integrated surface-subsurface modeling framework, Geosciences Journal 12(2):107–122.

[49] *Taylor, C. H. (*1997), Runoff processes in temperate headwater wetlands, Ecology of Wetlands and Associated Systems.(SK Majumdar, EW Miller and FJ Brenner, eds.) pp.169–181.

[50] *Therrien, R.; McLaren, R.G.; Sudicky, E.A.; Panday, S.M. (*2008), HydroGeoSphere A Three-dimensional Numerical Model Describing Fully-integrated Subsurface and Surface Flow and Solute Transport (Manual), Groundwater Simulations Group, University of Waterloo.

[51] *Tromp-van Meerveld, H. J.; McDonnell, J. J. (*2006), Threshold relations in subsurface stormflow: 1. A 147-storm analysis of the Panola hillslope, Water Resources Research 42(2):W02410.

[52] *Tromp-van Meerveld, H. J.; McDonnell, J. J. (*2006), Threshold relations in subsurface stormflow: 2. The fill and spill hypothesis, Water Resources Research 42(2):W02411.

[53] *Vidon, P. G.F.; Hill, A. R. (*2004), Landscape controls on nitrate removal in stream riparian zones, Water Resources Research 40(3):W03201, doi:10.1029/2003WR002473.

[54] *Vogel, H. J.; Hoffmann, H.; Roth, K. (*2005), Studies of crack dynamics in clay soil:: I. Experimental methods, results, and morphological quantification, Geoderma 125(3-4):203–211.

[55] *Weiler, M.; McDonnell, J. (*2004), Virtual experiments: a new approach for improving process conceptualization in hillslope hydrology, Journal of Hydrology 285(1-4):3–18.

[56] *Weissmann, G.S. ,(*1999) ,Toward new models of subsurface heterogeneity: An alluvial fan sequence stratigraphic framework with transition probability geostatistics, unpublished Ph.D. thesis, Hydrologic Sciences Graduate Group, Universtiy of California, Davis.

[57] *Zehe, E.; Becker, R.; Bárdossy, A.; Plate, E. (*2005), Uncertainty of simulated catchment runoff response in the presence of threshold processes: Role of initial soil moisture and precipitation, Journal of Hydrology 315(1-4):183–202.

[58] *Zehe, E.; Blöschl, G. (*2004), Predictability of hydrologic response at the plot and catchment scales: Role of initial conditions, Water Resour. Res 40(10):W10202.

[59] *Zehe, E.; Elsenbeer, H.; Lindenmaier, F.; Schulz, K.; Blöschl, G. (*2007), Patterns of predictability in hydrological threshold systems, Water Resour. Res 43(7):W07434.

[60] *Zehe, E.; Sivapalan, M. (*2009), Threshold behaviour in hydrological systems as (human) geo-ecosystems: manifestations, controls, implications, Hydrol. Earth Syst. Sci 131273–1297.

[97]

Study 2

Surface micro-topography causes hot spots of biogeochemical activity in wetland systems – a virtual modeling experiment.

By Sven Frei, Klaus-Holger Knorr, Stefan Peiffer and Jan H. Fleckenstein

Surface micro-topography causes hot spots of biogeochemical activity in wetland systems – a virtual modeling experiment.

Frei[1], S., Knorr[1], K.H., Peiffer[1], S., and Fleckenstein[2]. J.H.

[1] Department of Hydrology, University of Bayreuth, Germany

[2] Department Hydrogeology, Helmholtz-Center for Environmental Research – UFZ, Germany

Abstract

Wetlands provide important ecohydrological services by regulating fluxes of nutrients and pollutants to receiving waters, which can in turn mitigate adverse effects on water quality. Turnover of redox-sensitive solutes in wetlands has been shown to take place in distinct spatial and temporal patterns, commonly referred to as hot spots and hot moments. Despite the importance of such patterns for solute fluxes the mechanistic understanding of their formation is still weak and their existence is often explained by variations in soil properties and diffusive transport only. Here we show that surface micro-topography in wetlands can cause the formation of biogeochemical hot spots solely by the advective redistribution of infiltrating water as a result of complex subsurface flow patterns. Surface and subsurface flows are simulated for an idealized section of a riparian wetland using a fully integrated numerical code for coupled surface-subsurface systems. Biogeochemical processes and transport along advective subsurface flow paths are simulated kinetically using the biogeochemical code PHREEQC. Distinct patterns of biogeochemical activity (expressed as reaction rates) develop in response to micro-topography induced subsurface flow patterns. Simulated vertical pore water profiles for various redox-sensitive species resemble profiles observed in the field. This mechanistic explanation of hot-spot formation complements the more static explanations that relate hot spots solely to spatial variability in soil characteristics and can account for spatial as well as temporal variability of biogeochemical activity, which is needed to assess future changes in the biogeochemical turnover of wetland systems.

1 Introduction

Wetlands provide important ecohydrological services in many mountainous headwater catchments. They store significant amounts of carbon as peat, and act as effective nutrient sinks e.g. for sulfur, phosphorus and nitrogen [*Le Kellogg and Bridgham*, 2003; *Paul et al.*, 2006; *Tauchnitz et al.*, 2010]. Redox conditions and the corresponding biogeochemical processes in these wetlands largely control the source and sink functions of peat-soil dominated catchments [*Bishop et al.*, 2004; *Lischeid et al.*, 2007]. Process activities in such wetlands are spatially nonuniform, though, and have been found to form distinct hot spots [*Jacks and Norrström*, 2004], i. e. areas or patches that show disproportionally high reaction rates relative to the surrounding areas [*McClain et al.*, 2003; *Morris and Waddington*, 2011]. Such hot spots are not easily identified in the scatter of spatiotemporal datasets and hence their relevance for net matter turnover is assumed to be underestimated [*Richardson et al.*, 2007; *McClain et al.*, 2003; *Vidon et al.*, 2010]. Various studies have observed large variations in the spatial distribution of redox-sensitive solutes within wetland soils [*Jacks and Norrström*, 2004; *McMahon and Chapelle*, 2008] on the scale of transects (10-50m) [*Jacks and Norrström*, 2004] as well as in the meter and sub-meter range [*Knorr and Blodau*, 2009; *Mitchell and Branfireun*, 2005; *Wachinger et al.*, 2000]. It seems obvious that complex transport and transformation processes within the subsurface are main drivers for the observed spatial heterogeneity in solute concentrations. Although studies have pointed at potential effects of subsurface flow dynamics in wetlands on solute concentrations, e.g. by enhanced mixing due to hydraulic gradient reversals [*Reeve et al.*, 2006] and the formation of hot spots has conceptually been linked to transport processes [*McClain et al.*, 2003] transport and biogeochemical transformations are rarely combined mechanistically to explain such phenomena. Recent studies in wetlands have mainly attributed the formation of hot spots to lateral variations in local physico-chemical variables such as soil texture, composition, moisture or temperature [*Bruland and Richardson*, 2005; *Morris and Waddington*, 2011] or the local availability of certain reactants such as nitrate or DOC [*Bruland et al.*, 2006]. Differences in these properties may e.g. arise from different degrees of peat decomposition, peat compaction, vegetation or surface micro-topography [*Gafni and Kenneth*, 1990; *Cheng et al.*, 2011; *Bruland and Richardson*, 2005].

This perspective, however, does not consider that microbial processes are dynamic and dependent on variable hydrologic and biogeochemical boundary conditions. The close links between the mechanisms controlling biogeochemical activity in wetlands and the hydrological processes occurring within the wetland have been highlighted in several studies [*Morris and Waddington*, 2011; *Mitchell and Branfireun*, 2005]. Field studies [*Knorr et al.*, 2009; *Knorr and Blodau*, 2009] demonstrated a rapid change of predominant redox processes (i.e. iron(III)-, sulfate reduction and methanogenesis) in a wetland exposed to fluctuations of hydrological boundary conditions during manipulation of the water level. Wetlands in mountainous catchments are often characterized by rapidly fluctuating but

shallow water levels [*Devito and Hill*, 1997; *Lischeid et al.*, 2007]. Such hydrological conditions facilitate fast flow components like saturation excess overland flow and shallow subsurface flows [*Frei et al.*, 2010; *Holden and Burt*, 2003]. The dynamics of these flow components are important controls on mobilization of dissolved solutes (e.g. dissolved organic carbon or nitrate) from wetlands [*Alewell et al.*, 2007; *Lischeid et al.*, 2007; *Hinton et al.*, 1998; *Dosskey and Bertsch*, 1994] but their effect on the biogeochemical processes and distribution of redox-sensitive solutes is still poorly understood and rarely addressed [*Shabaga and Hill*, 2010]. Partly this is because it is nearly impossible to directly investigate and characterize the complex, dynamic subsurface hydrology in the field. Therefore the interpretation of field observations (e.g. depth profiles for redox-sensitive solutes) may be poorly constrained, e.g. if biogeochemical turnover rates are calculated based on the assumption that resupply of dissolved electron acceptors/donors within riparian wetlands is only diffusion limited [*Beer and Blodau*, 2007; *Clymo and Bryant*, 2008]. This simplification may hold true for some sites [*Beer and Blodau*, 2007] and for defined lab incubations [*Knorr and Blodau*, 2009], but it neglects that transport and turnover of redox-sensitive solutes at many natural sites occurs within a complex, three-dimensional (3D) subsurface flow field that is subject to variable boundary conditions. This results in distinct flow paths along which biogeochemical reactions can occur, controlled by the individual kinetics of each process [*Knorr and Blodau*, 2009; *Hill*, 2000; *Brovelli et al.*, 2011]. An improved mechanistic model for the formation and occurrence of biogeochemical hot spots therefore needs to account for flow and transport processes and how they are affected by changes in hydrologic boundary conditions. This is of particular importance if such a model is used to assess the effects of climate change where induced shifts in the frequency of intense rainstorms or extended droughts [*Huntington*, 2006] have the potential to significantly alter the boundary conditions within wetlands.

Virtual experiments [*Weiler and McDonnell*, 2004, 2006] have proven to be a suitable tool to investigate complex hydrologic processes and feedback mechanisms between hydrology and biogeochemistry [*Frei et al.*, 2010; *Boano et al.*, 2010; *Jakobsen*, 2007]. In this study, we use virtual modeling experiments to investigate how complex subsurface flow patterns induced by surface micro-topography affect the subsurface transport of redox-sensitive solutes and the resulting spatial distribution of biogeochemical process activities within a hummocky wetland. We test the hypothesis that the complex subsurface flow-field creates biogeochemical conditions in the subsurface that facilitate the formation of local process hot spots even in soils with uniform soil properties. To address this objective, the numerical simulations of complex surface and subsurface flow processes in the hypothetical section of the riparian wetland with pronounced micro-topography (hollows and hummocks) as described by *Frei et al.*, [2010], is combined with advective particle tracking and multi-species biogeochemical simulations in a sequential stream tube approach. The main redox reactions typically found in peat-forming wetlands are simulated along individual subsurface flow

paths, which are subject to local changes in the biogeochemical boundary conditions, using the geochemical model PHREEQC [*Parkhurst*, 1995]. The simulated wetland reflects the structural and hydrological characteristics of a riparian wetland in the Lehstenbach catchment in Sout-East Germany [*Paul et al.*, 2006] which are not uncommon for peat-forming wetlands elsewhere (e.g. [*Holden and Burt*, 2003; *Inamdar et al.*, 2009]). Hence this study will improve our general understanding of how subsurface hydrology affects redox transformations and turnover rates within riparian wetlands.

2 Material and Methods

2.1 Surface/Subsurface Flow Simulation and Particle Tracking

The numerical flow model presented by *Frei et al.*, [2010] for a small hypothetical section of a wetland with micro-topography (10m by 20m with a maximum thickness of 2m) draining into a channel segment (see Figure 3) was used to simulate riparian runoff generation and subsurface flow patterns. The flow model and its parameterization are only briefly summarized here, as the model is described in more detail in *Frei et al.*, [2010]. The hummocky micro-topography is geostatistically simulated based on a Markov Chain model of transition probabilities, which is derived and conditioned with surveyed elevation data from the Lehstenbach field site [*Frei et al.*, 2010; *Carle and Fogg*, 1996]. Two different models of micro-topography, using a mean length of 0.5m and 0.25m respectively, were generated to represent differently sized hollow and hummock structures. Micro-topography realizations were then superimposed on top of a planar, slightly inclined surface (slope = 0.03) to create a realistic representation of a typical wetland section at the field site as a basis for the flow model (for details see *Frei et al.*, [2010]). Micro-topography models were compared to a model with a planar surface as a reference (hereafter referred to as 'planar reference model'). Transient surface and subsurface flow were simulated using the numerical code Hydrogeosphere (HGS) [*Therrien et al.*, 2008] which provides a fully-integrated 3D solution for variably saturated subsurface flow (Richards equation) and a 2D depth-averaged solution for surface flows based on the diffusive wave approximation to the St. Venant equations [*Therrien et al.*, 2008]. HGS is increasingly used for the simulations of coupled surface-subsurface hydrologic systems (e.g. [*Brookfield et al.*, 2009; *Jones et al.*, 2006]). To drive the flow models observed daily precipitation for the hydrologic year (HY) 2000 (10/31/1999 – 11/1/2000), which represents typical hydrometeorological conditions in the Lehstenbach catchment, were applied as a flux boundary at the model surface. To simplify data handling (each model output file contains velocity data for about 210,000 model nodes) transient model output was only generated in five day intervals (integration time step $\Delta t = 5d$).

Subsurface flow paths for each of the flow models (planar reference + 2 realizations of micro-topography) were derived by applying an advective particle tracking routine, implemented in the Tecplot 360 post-processing software [*Bellevue*, 2003], to a transient flow field that consists of a multi-year (25 years) sequence of the velocity fields simulated for the reference year (HY 2000). 21,000 particles (one per surface node) were placed on the model surface yielding 21,000 individual subsurface flow paths. Particles were tracked from infiltration until the particle leaves the subsurface domain due to exfiltration.

2.2 Multi-species Biogeochemical Simulations

Coupling Hydrology and Biogeochemistry

The basic concept of implementing a biogeochemical model along individual subsurface flow paths is illustrated in Figure 1. Every flow path is split into i_{max} [-] different sub-sections where i_{max} represents how often the integration time step $\Delta t = 5d$ is being repeated until the water particle leaves the subsurface domain due to exfiltration. For a known flow path (as shown in Figure 1) the total subsurface residence time (RT_{total} [T]) for a particle travelling along that path (from the moment of its infiltration until exfiltration) can be approximated by Equation 1:

$$RT_{total} = i_{max} \cdot \Delta t \quad (1)$$

According to Figure 1, each of the different sub-sections *i* has a start (x_{i-1}, y_{i-1}, z_{i-1}) [L,L,L] and end (x_i,y_i,z_i) location [L,L,L], a sub-section's residence time (RT_{sub} [T]) representing the time a water particle spends within a sub-section *i* [-] and a characteristic travel distance (d_i [L]). Each sub-section has a constant sub-section residence time (RT_{sub}) of five days. The flow distance d_i a water particle travels during RT_{sub} depends on the subsurface flow field which varies along the flow path according to the transient solution of the numerical flow model. The characteristic travel distance for a sub-section (d_i) can be linearly approximated via the sub-section's start (x_{i-1},y_{i-1},z_{i-1}) and end locations (x_i,y_i,z_i):

$$d_i = \left\| \begin{pmatrix} x_i \\ y_i \\ z_i \end{pmatrix} - \begin{pmatrix} x_{i-1} \\ y_{i-1} \\ z_{i-1} \end{pmatrix} \right\| \quad (2)$$

The total distance *D* [L] a particle travels from the moment of infiltration until exfiltration can be approximated by summing up the individual travel distances for all sub-sections d_i:

$$D = \sum_{i=1}^{i\,max} d_i \quad (3)$$

For a single subsurface flow path, the corresponding biogeochemical simulation consists of i_{max} individual PHREEQC [*Parkhurst*, 1995] scripts, one script for each sub-section of a subsurface flow path (lower table of Figure 1). Each script uses different boundary conditons which were individually derived from the numerical flow model's solution. During the integration time step ($\Delta t = 5d$), the boundary conditions for a single PHREEQC [*Parkhurst*, 1995] sub-section are kept constant (detailed information on the boundary conditions are given in the following section). A single script simulates all relevant redox reactions, implemented as kinetic formulations (detailed information on the implemented reactions is also given in a subsequent paragraph), that occur within the sub-section

during the integration time step Δt. For all of the 21,000 flow paths and for each of the flow models this approach was used resulting in about 1,450,000 different PHREEQC [*Parkhurst*, 1995] sub-section simulations per flow model.

infiltration
t=0

(x_0,y_0,z_0) i=1

(x_1,y_1,z_1) i=2

$(x_{i-1},y_{i-1},z_{i-1})$ i=3

(x_i,y_i,z_i)

exfiltration
t=$i_{max}\Delta t$

$i=i_{max}$ $(x_{imax},y_{imax},z_{imax})$

$i=i_{max-1}$ $(x_{imax-1},y_{imax-1},z_{imax-1})$

$i=i_{max-2}$ $(x_{imax-2},y_{imax-2},z_{imax-2})$

$(x_{imax-3},y_{imax-3},z_{imax-3})$

$\cdots$ i $\cdots$

d_i

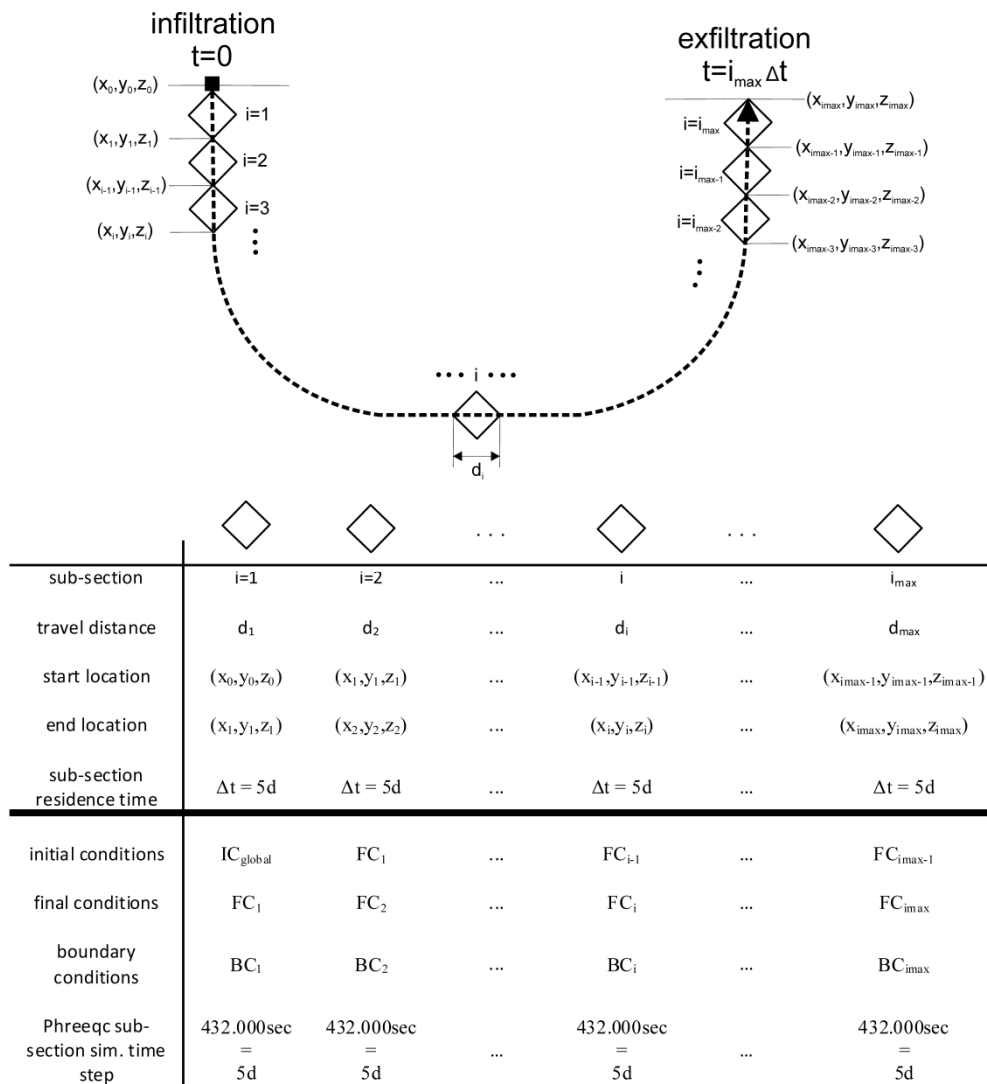| sub-section	i=1	i=2	...	i	...	i_{max}
travel distance	d_1	d_2	...	d_i	...	d_{max}
start location	(x_0,y_0,z_0)	(x_1,y_1,z_1)	...	$(x_{i-1},y_{i-1},z_{i-1})$	...	$(x_{imax-1},y_{imax-1},z_{imax-1})$
end location	(x_1,y_1,z_1)	(x_2,y_2,z_2)	...	(x_i,y_i,z_i)	...	$(x_{imax},y_{imax},z_{imax})$
sub-section residence time	$\Delta t = 5d$	$\Delta t = 5d$	...	$\Delta t = 5d$	...	$\Delta t = 5d$
initial conditions	IC_{global}	FC_1	...	FC_{i-1}	...	FC_{imax-1}
final conditions	FC_1	FC_2	...	FC_i	...	FC_{imax}
boundary conditions	BC_1	BC_2	...	BC_i	...	BC_{imax}
Phreeqc sub-section sim. time step	432.000sec = 5d	432.000sec = 5d	...	432.000sec = 5d	...	432.000sec = 5d

Figure 1. *Schematic plot showing how subsurface hydrology was coupled to the biogeochemical model PHRREQC by using particle tracking techniques. Isolated sub surface flow path lines are split into individual sub-sections for which the redox chemical conditions are simulated depending on the hydrological and biogeochemical boundary conditions.*

Initial and Boundary Conditons

With the exception of the first sub-section of each flow path (representing the first 5 days after infiltration), all PHREEQC [*Parkhurst*, 1995] sub-section simulations i use the final chemical conditions of the previous sub-section (FC_{i-1}) simulation as an initialization for the subsequent sub-section simulation (Figure 1, lower table). The first sub-section simulation of each flow path $i=0$ uses uniformly assigned initial conditions (IC_{global}), which are listed in Table 1.

Table 1: *Initial concentrations IC global for redox-sensitive species. IC global is used to initialize the first PHREEQC sub-section simulation of each flow path. Values are based on field data determined for pore water, near to the surface of a typical wetland in the Lehstenbach catchment [Knorr et al., 2009].*

Species	**IC_{global}**
Ammonium	0 mol/L
Nitrate	1.63×10^{-6} mol/L
Fe(III)	6.76×10^{-5} mol/L
Fe(II)	1.80×10^{-6} mol/L
Sulfate	3.95×10^{-5} mol/L
Sulfide	0 mol/L
pH	4.5

Values for IC_{global} are based on the chemical composition and pH of shallow pore water at the wetland field site in the Lehstenbach catchment [*Knorr et al.*, 2009]. Some redox-reactions within the PHREEQC [*Parkhurst*, 1995] simulations only occur under the presence of oxygen (e.g. aerobic respiration or different oxidation processes). Other processes like denitrification, iron and sulfate reduction are only initiated under conditions where oxygen concentrations are low or zero. Along a flow path, availability of oxygen changes depending on the hydrological conditions (e.g. flow in saturated versus unsaturated media): Within the unsaturated zone, availability of oxygen is assumed to be unlimited because depleted oxygen is continuously supplied by atmospheric diffusion with the rate of resupply ($\tau_{resupply}$) exceeding the rate of oxygen depletion ($\tau_{depletion}$). In the saturated zone, where pores are completely saturated, water acts as an effective diffusion barrier and oxygen becomes increasingly limiting with growing depth below the water table. At a certain depth in the saturated zone $\tau_{resupply}$ becomes equal to $\tau_{depletion}$. Below this point depletion exceeds supply and no more oxygen is available. Availability of oxygen was thus used as the key control for either initiating or suppressing the series of anaerobic redox processes in the biogeochemical simulations. Availability of oxygen, as a boundary condition for the PHREEQC [*Parkhurst*, 1995] sub-section simulations, was coupled to the transient pressure heads ph_{i-1} obtained from the flow model, as these pressure heads describe the relative position with respect to the current local water table (i.e. saturated or unsaturated

zone). Coupling oxygen availability to transient pressure heads was performed as follows: **(1)** For each sub-section's start location (x_{i-1}, y_{i-1}, z_{i-1}) the corresponding time dependent pressure head (ph_{i-1}) was estimated from the solution of the numerical flow model. **(2)** The pressure head (ph_i [L]) was used as an indicator for three different conditions or zones according to Figure 2. Zone 1 (negative pressure head) represents the unsaturated zone where significant fractions of the soil matrix pores are air filled and where oxygen content is constantly high and in equilibrium with the atmosphere. Zone 2 ($0m < ph_i < 0.25m$) represents the transition zone between the zone saturated with oxygen (zone 1) and deeper water-saturated layers where oxygen is completely depleted (zone 3). Within zone 2, atmospheric diffusion becomes less effective, in terms of resupply, with increasing pressure heads (indicative of increasing depths below the water table). If the pressure head ph_i is located within either zone 1 or 2, the oxygen boundary condition (BC_i) is assigned according to the oxygen - pressure head relationship shown in Figure 2, which was derived from observed depth profiles of oxygen sensitive redox species taken at the field site [*Knorr et al.*, 2009]. During the sub-section integration time step Δt, it is assumed that the assigned boundary conditions do not change, which means that the corresponding oxygen concentration during a sub-section simulation remains constant for sub-sections located within zone 1 and 2. For sub-sections where the corresponding pressure head ph_i is located within zone 3 of Figure 2, oxygen is not assigned as a boundary condition instead the PHREEQC [*Parkhurst*, 1995] simulation for these sub-sections is initialized with an oxygen content equal to the residual oxygen content of the preceding sub-section simulation *i-1*. For sub-sections where the corresponding pressure head ph_i lies within zone 3, oxygen can be depleted by oxygen consuming redox reactions.
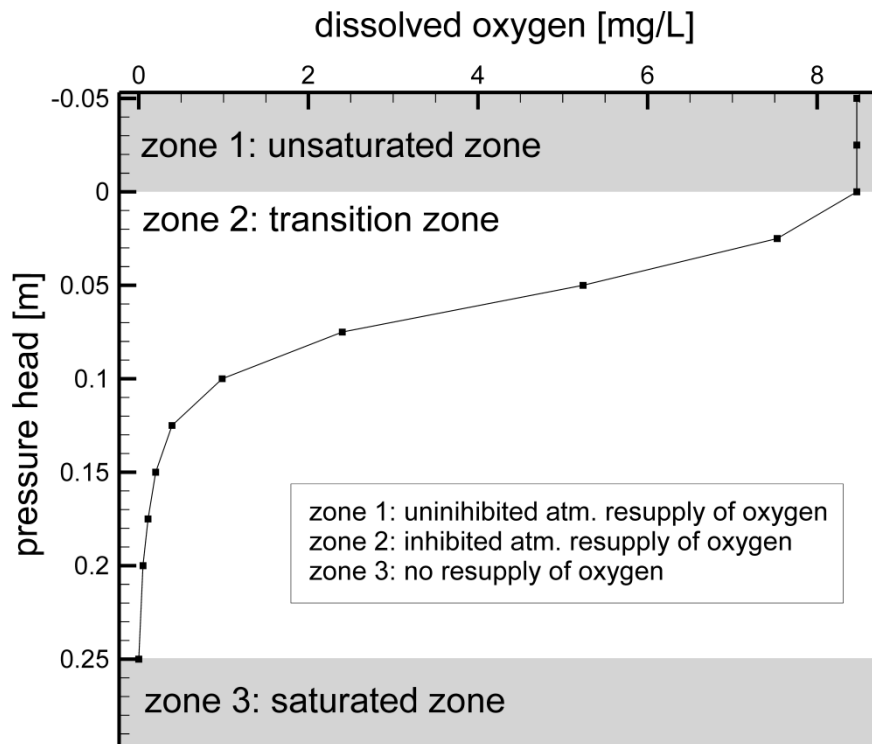
Figure 2: *Typical oxygen depth profile based on observations from a riparian wetland site in the Lehstenbach catchment. Profile was used to assign oxygen boundary conditions to the different PHREEQC sub-section simulations based on transient flow model output.*

All represented reductive processes (detailed information are given in the next paragraph) are treated as reactions catalyzed by microorganisms, comparable to e.g. the process model for methane production in wetlands as shown by *Segers and Kengen* [1998]. These types of reactions depend on the presence of **(a)** an adequate electron acceptor (e.g. oxygen, nitrate, iron(III) or sulfate) and **(b)** a source of labile carbon that is available to microorganisms. As a simplification to reduce model complexity, we considered the electron acceptor as the limiting factor for the presence of the individual catalyzed redox-reactions. We think that this is a reasonable approximation, since the supply of labile carbon (e.g. acetate) may be assumed to be coupled to the organic matter mineralization rate, as usually no intermediates (e.g. from fermentation) accumulate [*Segers and Kengen*, 1998]. The biogeochemical simulations were thus performed based on that concept, implementing an unlimited carbon source as BC for all sub-section simulations and limiting process rates solely by their kinetic parameters. By dynamically assigning the biogeochemical boundary conditions to each individual sub-section the whole sequence of sub-section simulations for one subsurface flow path, can be viewed as a continuous simulation of the redox-chemical evolution of a small water parcel that carries dissolved redox-sensitive solutes and is transported along that specific flow path.

Implemented Reactions and Kinetics

For each sub-section, PHREEQC simulates redox processes as kinetic reactions based on the assigned boundary (BC_i) and initial conditions (IC_{global}/FC_{i-1}). Implemented processes are shown in Table 2. All reduction processes are formulated based on Monod kinetic reactions according to Equation 4:

$$R_k = \frac{dC_k}{dt} = \mu_{max,k} \frac{C_k}{K_{s,k} + C_k} \quad (4)$$

Here R_k [$ML^{-3}\ T^{-1}$] is the kinetic rate of the corresponding reduction reaction k ($k \in [1,2,3,4]$) according to Table 2. $\mu_{max,k}$ [$ML^{-3}T^{-1}$] represents the maximal specific growth rate (for *k=1 aerobic respiration, k=2 de-nitrification, k=3 iron(III)- reduction, k=4: sulfate reduction*) and $K_{s,k}$ [ML^{-3}] represents the substrate saturation constant (i.e. substrate concentration for *k=1 oxygen, k=2 nitrate, k=3 iron(III), k=4 sulfate* at half $\mu_{max,k}$). C_k [ML^{-3}] is the corresponding concentration of the electron acceptor (*for k=1: oxygen, k=2: nitrate, k=3: iron(III); k=4: sulfate*). Monod kinetic coefficients ($\mu_{max,k}$ and $K_{s,k}$) for all reduction processes are based on values reported for biodegradation of organic chemicals in aquifers [*Appelo and Postma*, 2005; *Bekins et al.*, 1998; *Schirmer et al.*, 1999; *MacQuarrie et al.*, 1990; *Eckert and Appelo*, 2002; *Kelly et al.*, 1996; *Goldsmith and Balderson*, 1988] and were later modified and adjusted as part of the calibration process. Simulated depth profiles for redox-sensitive compounds (nitrate, sulfate and iron(II)) were calibrated by systematic variation of the Monod coefficients to best fit observed data taken at the study site [*Knorr and Blodau*, 2009; *Knorr et al.*, 2009]. Calibrated Monod coefficients are listed in Table 2. For all processes where organic carbon is being decomposed, organically bound nitrogen is being released according to the Redfield ratio [*Redfield*, 1934]. Oxidation processes (*k=5 iron(II) oxidation, k=6 nitrification, k=7 aerobic sulfide oxidation and k=8 anaerobic sulfide oxidation*) were formulated using higher order reaction kinetics as listed in Table 2.

Table 2: *Implemented processes and the equivalent reaction specific kinetic rate. Reduction processes are formulated based on Monod type reaction kinetics.*

Process	Rate	Coefficients	Reference
aerobic respiration	according to equation 4	$\mu_{max,1} = $ 1.6 x 10^{-9} mol/Ls $K_{s,1} = 2.9$ x 10^{-6} mol/L	modified and calibrated after [*Appelo and Postma*, 2005; *Bekins et al.*, 1998; *Schirmer et al.*, 1999; *MacQuarrie et al.*, 1990; *Eckert and Appelo*, 2002; *Kelly et al.*, 1996; *Goldsmith and Balderson*, 1988]
denitrification	according to equation 4	$\mu_{max,2} = 1.06$ x 10^{-9} mol/Ls $K_{s,2} = 2.0$ x 10^{-6} mol/L	modified and calibrated after [*Appelo and Postma*, 2005; *Bekins et al.*, 1998; *Schirmer et al.*, 1999; *MacQuarrie et al.*, 1990; *Eckert and Appelo*, 2002; *Kelly et al.*, 1996; *Goldsmith and Balderson*, 1988]
iron(III) reduction	according to equation 4	$\mu_{max,3} = $ 1.5 x 10^{-12} mol/Ls $K_{s,3} = $ 2.94 x 10^{-6} mol/L	modified and calibrated after [*Appelo and Postma*, 2005; *Bekins et al.*, 1998; *Schirmer et al.*, 1999; *MacQuarrie et al.*, 1990; *Eckert and Appelo*, 2002; *Kelly et al.*, 1996; *Goldsmith and Balderson*, 1988]
sulfate reduction	according to equation 4	$\mu_{max,3} = $ 0.5 x 10^{-10} mol/Ls $K_{s,4} = 2.5$ x 10^{-6} mol/L	modified and calibrated after [*Appelo and Postma*, 2005; *Bekins et al.*, 1998; *Schirmer et al.*, 1999; *MacQuarrie et al.*, 1990; *Eckert and Appelo*, 2002; *Kelly et al.*, 1996; *Goldsmith and Balderson*, 1988]
iron(II) oxidation	$R_5 = \dfrac{dC_5}{dt} = A_5 \cdot a(OH^-) \cdot p(O_2) \cdot c(Fe^{2+})$	$A_5 = 8$ x 10^{13} min^{-1}atm^{-1}	[*Appelo and Postma*, 2005; *Stumm and Morgan*, 1995]
ammonium oxidation	$R_6 = \dfrac{dC_6}{dt} = A_6 \cdot c(NH_4^+) \cdot c(O_2)$	$A_6 = 5$ x 10^6 (mol/L)$^{-1}$ a^{-1}	[*Billen*, 1982; *van Cappellen and Wang*, 1996]
aerobic sulfide oxidation	$R_7 = \dfrac{dC_7}{dt} = A_7 \cdot c(HS^-) \cdot c(O_2)$	$A_7 = 1.6$ x 10^5 (mol/L)$^{-1}$ a^{-1}	[*Millero et al.*, 1987; *van Cappellen and Wang*, 1996]
anaerobic sulfide oxidatio oxidation	$R_8 = \dfrac{dC_8}{dt} = A_8 \cdot c(HS^-) \cdot c(Fe^{3+})$	$A_8 = 8$ x 10^3 (mol/L)$^{-1}$ a^{-1}	[*Pyzik and Sommer*, 1981; *van Cappellen and Wang*, 1996]

In redox controlled systems like wetlands, reduction processes can be expected to occur sequentially due to thermodynamic reasons (e.g. [*Achtnich et al.*, 1995]). Oxygen is used as primary electron acceptor, and after depletion nitrate, subsequently iron(III) and finally sulfate are being reduced. Further electron acceptors, such as manganese [*Nealson and Saffarini*, 1994] or organic molecules [*Lovley et al.*, 1996] were not considered in this study. To make sure that the reduction processes proceed sequentially in the biogeochemical simulations, specific redox conditions were defined. These conditions are represented by critical concentrations for redox-sensitive solutes which control whether a redox process can be initiated or not. Critical concentrations C_{crit} [ML^{-3}] for oxygen, nitrate and Iron(III) were derived based on observed depth profiles for redox-sensitive compounds [*Knorr and Blodau*, 2009; *Knorr et al.*, 2009; *Estop-Aragonés and Blodau, 2012*] For example, the critical concentration for oxygen C_{critO2} is the residual concentration of oxygen under which denitrification is being initiated, which was estimated from observed depth profiles and field data. Critical concentrations for oxygen, nitrate and iron(III) are listed in Table 3. The rows of Table 3 represent the conditions under which the different reduction processes are initiated. Entries must be read row-wise, where entries ">0" mean that the corresponding redox-sensitive reactant (column) must be present and "-" means that this process is independent from the presence of this specific compound. For example iron(III) reduction in the biogeochemical simulation is initiated if: **(1)** Dissolved oxygen concentrations fall below C_{critO2}; **(2)** Most of the nitrate is already depleted where concentrations for nitrate fall below $C_{critNO3}$; **(3)** The electron acceptor iron(III) is available. Intervals for the activation of reduction processes are overlapping which means that multiple processes can occur simultaneously in the simulation; this was also observed in laboratory and under field conditions [*Knorr and Blodau*, 2009; *Knorr et al.*, 2009].

Table 3:. *Critical concentrations which are controlling the sequential initialization of the redox sequence. Values were derived from field observations. Table must be read row wise (e.g. denitrification is initiated if 1. oxygen contents drop below Ccrit derived for oxygen and 2. if nitrate is present).*

	Oxygen	Nitrate	iron(III)	sulfate
aerobic respiration	>0	-	-	-
denitrification	$< C_{critO2}$	>0	-	-
iron(III) reduction	$< C_{critO2}$	$< C_{critNO3}$	>0	-
sulfate reduction	$< C_{critO2}$	$< C_{critNO3}$	$< C_{critFe3+}$	>0

C_{critO2}	5.0×10^{-6}	mol/L
$C_{critNO3}$	4.0×10^{-7}	mol/L
$C_{critFe3+}$	5.0×10^{-6}	mol/L

Simplifying Model Assumptions

To reduce the complexity of the represented system and to maintain a tractable model the following simplifying assumptions were made: **(1)** Soil specific parameters (saturated hydraulic conductivity, porosity and retention curves for variably saturated flow) are uniform within the model domain to separate the effects of micro-topography on subsurface flow dynamics from possible impacts of heterogeneity. **(2)** By simulating biogeochemical reactions along isolated subsurface flow paths, it is assumed that there is no interaction between different flow paths where water and/or solutes are exchanged due to hydrodynamic dispersion (mechanic dispersion + diffusion). **(3)** Subsurface flow paths are derived based on a transient flow field resulting from yearly model runs. Particle tracking is performed for a 25 year period by repeating the yearly output of the flow model twenty-five times. This assumes that there are no inter-annual changes in the basic properties of the subsurface flow field (distribution of flow paths and RTs). **(4)** In the biogeochemical simulations availability of DOC, as the primary electron source for microbially catalyzed reactions (aerobic respiration, denitrification, iron(III)- and sulfate reduction) was assumed to be non-limiting. **(5)** Effects of vegetation and its potential influence on subsurface flow and redox processes, i.e. due to root respiration or exudation and evapotranspiration, are not considered. **(6)** Iron(III) species in the biogeochemical simulations are treated as solutes only, which are advectively transported within the subsurface domain and not as immobile solids bound to the peat matrix. **(7)** In the biogeochemical simulations, bioavailability of all involved species is not affected by e.g. complexation with DOC.

3 Results

3.1 Subsurface flow patterns

Subsurface flow paths for the two micro-topography models and the planar reference model are shown in Figure 3 (A-D). For the model with a mean-length of 0.5m (ml-0.5m) flow-paths are shown for the entire 3D model domain (A) as well as for the 2D transect located accross the center of the 3D model domain (dashed line in A). The 2D flow fields for the transects represent projections of the 3D flow paths into a 2D plane (flow components in the y directions are neglected). In contrast to the planar reference model, both micro-topography models showed complex distributed subsurface flow paths where coexisting shallow and deep flow cells developed in 3D. This is a common phenomenon caused by topography and was first described by *Toth*, [1962] for regional groundwater flow systems but can be found for flows in systems with pronounced topography over a range of scales [*Wörman et al.*, 2006; *Stonedahl et al.*, 2010]. Shallow flow cells are most pronounced for the model with a mean length of the surface structures of 0.5m (B) and are associated with the dominant surface structures (largest hummocks). Areas characterized by shallow flow cells are outlined with red dotted lines in Figure 3B. Water infiltrating in these areas relatively quickly returns to the land surface, travels shorter distances and is characterized by short subsurface residence times (Figure 4 A and B). In contrast deeper flow cells, which develop for areas where water infiltrates deep into the subsurface predominately at locations that are located far away from the channel segment, have longer travel distances (often spanning the entire extent of the model domain) and show significantly longer residence times as also reflected in the water ages (residence time in the subsurface since infiltration) plotted for the central 2D transect in Figure 5B. Deeper flow cells are controlled by the general hydraulic gradient across the model domain. The flow field for the micro-topography model with a mean length of 0.25m (ml-0.25m) shows no clear separation between shallow and deep flow cells because the topographic variations are too small to create sufficient variations in subsurface hydraulic potentials that could induce significant shallow flow cells (Figure 3 C). Similarly in the planar reference model (Figure 3 D) flow paths are relatively uniform in space with flow directions almost parallel to the planar land surface.
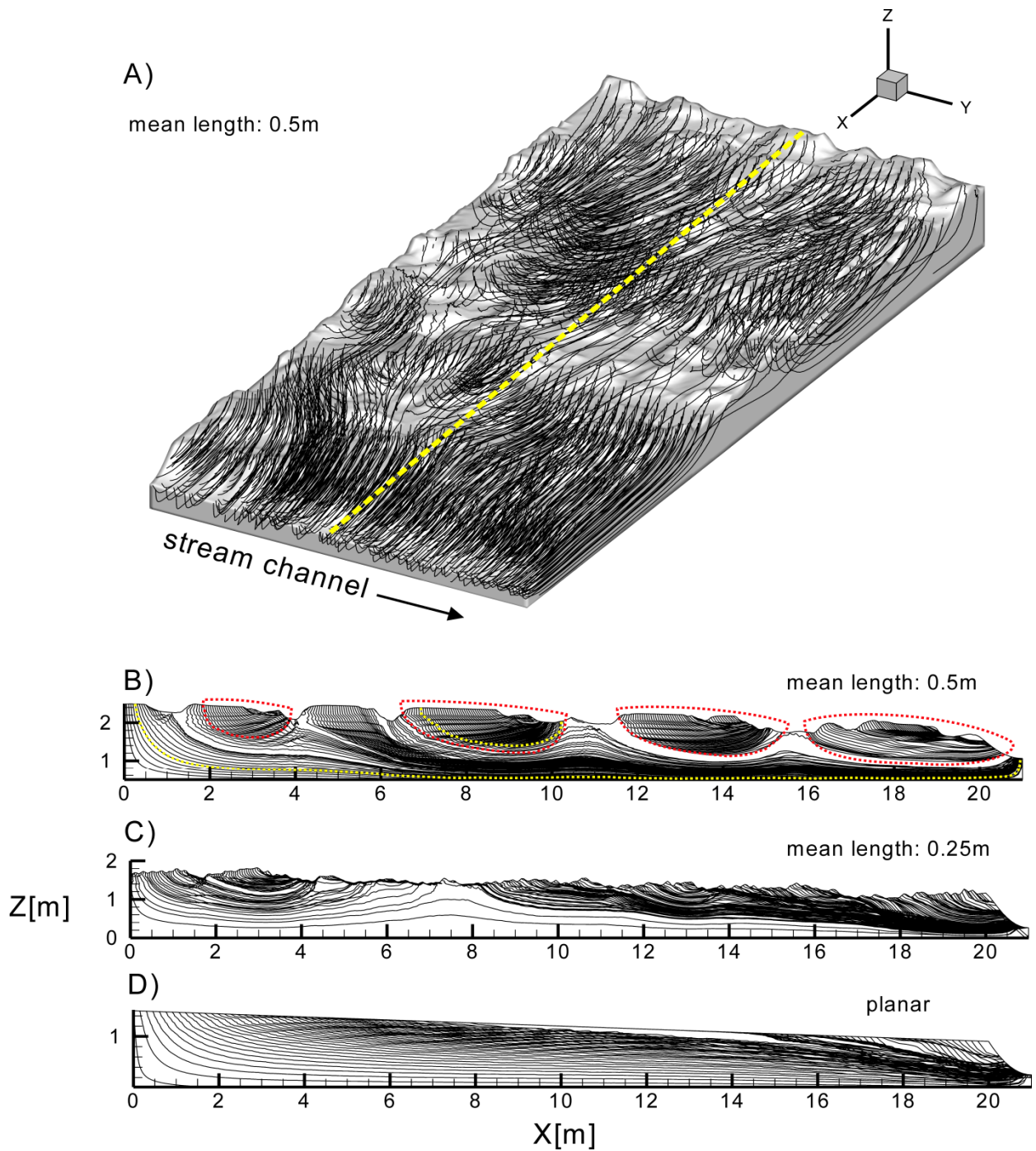
Figure 3: Subsurface flow paths derived from particle tracking. A) Flow paths for the 3D domain of the micro-topography realization with a mean length of 0.5 m. B)-D) Flow paths projected to a cross section at the center of the 3D domain (yellow dashed line in A) for the two micro-topography models and the planar reference model. Outlined areas (red dotted lines) in B) represent the typical down and upwelling movement of the shallow flow system induced by surface micro-topography. Yellow dotted lines represent two flow paths (infiltrating at X = 0.4 m and X = 6.8 m) reflecting long and short subsurface residence times for which the biogeochemical evolution is shown in Figure 4. The model domain is 10 m x 20 m x 2 m.

3.2   Biogeochemical evolution along flow paths

Figure 4 (E-H) depicts exemplarily the results of the biogeochemical simulations, shown for two selected subsurface flow paths of the ml-0.5m micro-topography model. The two flow paths, beginning at location X = 0.4 m and X = 6.8 m (shown as yellow dotted lines in Figure 3B), represent the deep and shallow flow cells respectively. Results for the deep flow path are shown in Figure 4 A, C, E, G and for the shallow one in Figure 4 B, D, F, H. Both flow paths start in the unsaturated zone where pressure heads are negative (C and D). For the unsaturated zone, dissolved oxygen concentrations are constantly high (E and F) due to unlimited diffusive supply of atmospheric oxygen. Aerobic respiration is the dominant process within the unsaturated zone. The high turnover of organic material and the associated release of organically bound nitrogen within the unsaturated zone results in increasing concentrations of ammonium (G and H), which is in turn oxidized to nitrate due to nitrification (E and F). When the flow paths reach the saturated zone (pressure heads become positive), oxygen contents are decreasing and turnover due to aerobic respiration with associated release and oxidation of ammonium are slowed down (E and F). Oxygen contents are initially fluctuating in the saturated zone because of pressure head variations (i.e. water table fluctuations due to rain events), which are coupled to the oxygen boundary condition as shown in Figure 2. Once the flow paths reach a depth below the water table of about 0.25 m (pressure heads >= 0.25 m) oxygen become limiting and is completely depleted after ~90 days for the deep and after ~100 days for the shallow flow path. Under anoxic conditions, increasing concentrations of reduced species (e.g. iron(II) or sulfide) indicates that the system sequentially shifts to de-nitrification, iron(III)- and sulfate reduction (Figure 4 G and H). After 250 days, the deep flow path is in a completely reduced state where all oxidized species are depleted (Figure 4 E and G) and conditions remains reduced until the flow path reemerges at the surface and the water exfiltrates. The shallow flow path reaches completely reduced conditions after 200 days, but shortly before exfiltration oxygen becomes available again and oxidation processes are reactivated (Figure 4 F and H). The reason why re-oxidation only occures at the end of the shallow flow path is related to the corresponding exfiltration location. The shallow flow path ends in a shallow, water filled depression where ponded water heights are low enough (pressure heads < 0.25 m) for atmospheric oxygen to diffuse into the uppermost layers of the peat so that oxygen is in contact with the upwelling reduced water. In contrast, the deep flow path which exfiltrates into the stream channel, where ponded water depths are too large to allow resupply of oxygen by diffusion; no reoxidation of reduced species is observed. Animation 1 and 2 (auxiliary material) show similar results where redox conditions are changing along two isolated subsurface flow paths (deep and shallow) extracted from the 3D model domain.
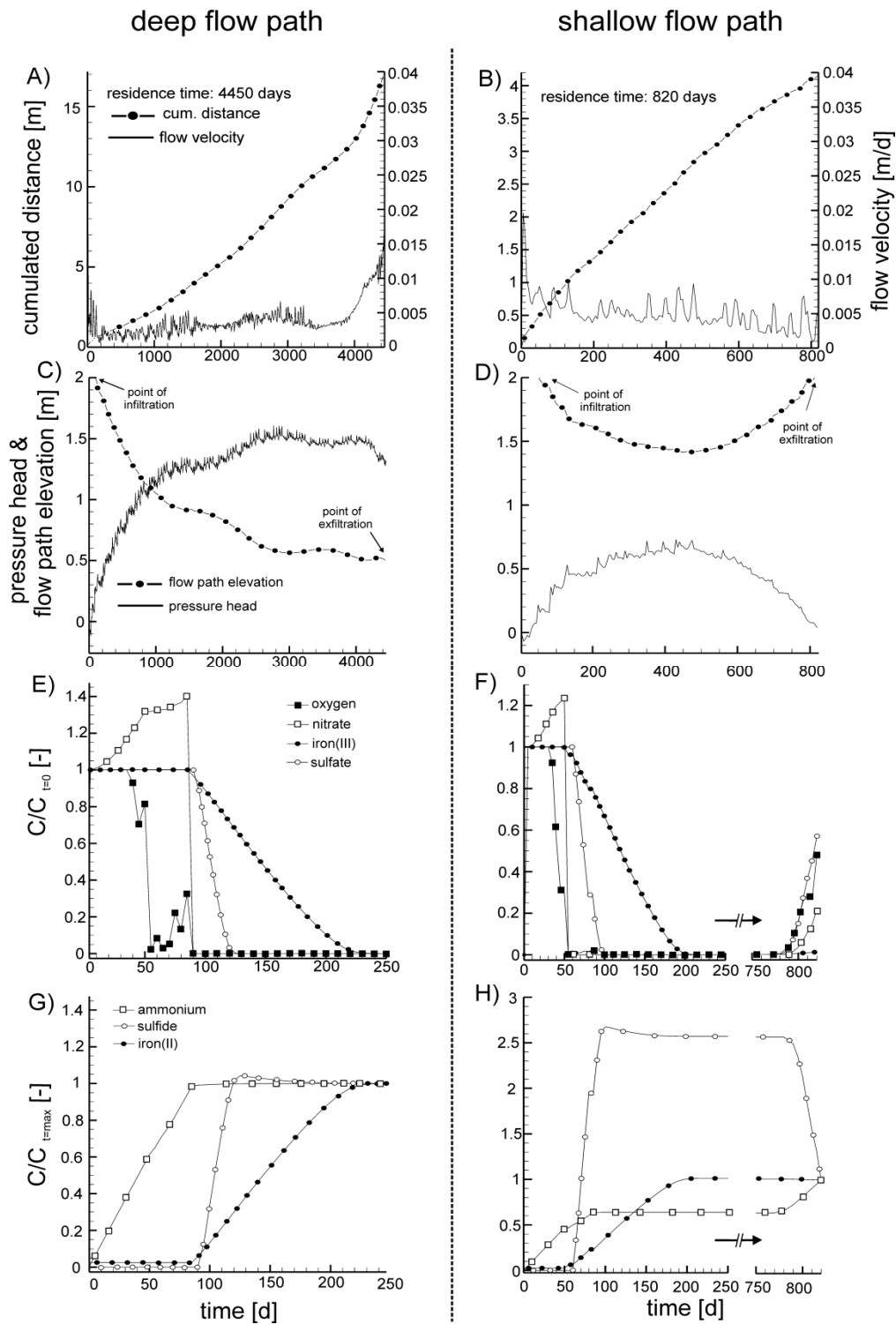
Figure 4: *Results of biogeochemical simulations along two different flow paths. A,C,E,G represent a deep flow path with long subsurface residence time and B,D,E,F a flow path of the shallow flow system. Subsurface flow velocities, pressure heads, flow depths and travel distances as shown in A,B,C,D were derived from numerical flow modeling and were used as hydrologic boundary conditions for the biogeochemical simulations. Additionally, oxygen availability (E, F) was coupled to the pressure head dynamics (C,D), individually for each flow path. E and F show the evolution for oxidized species (nitrate, iron(III) and sulfate) in time normalized to their corresponding initial concentrations $C_{t=0}$ and G and H the evolution of reduced species (ammonium, iron(II) and sulfide) normalized to their final concentrations $C_{t=max}$. How redox condtions are changing in time is also shown in Animation 1 and 2 (auxiliary material).*

3.3 Spatial patterns of hot spots

In the previous paragraph, results of the biogeochemical simulations for two selected subsurface flow paths were presented in the time domain. A representation in space is depicted in Figure 5 and was generated by interpolating local species concentrations and reaction rates from the biogeochemical model for all flow paths into the 3D spatial domain of the flow model. In Figure 5 the results for the process of sulfate reduction in the model with ml $=$ 0.5 m are presented as an example and plotted for the central transect aligned along Y = 5 m (dashed line in Figure 3 A). Panel C and D shows simulated sulfate reduction and sulfide oxidation rates whereas panel E and F show the corresponding concentrations of the reaction product (sulfide) and educt (sulfate). Flow paths are shown in panel A and the age of subsurface water (residence time in the subsurface since infiltration derived from particle tracking) is depicted in panel B. In the cross section, areas of intensive sulfate reduction (hot spots) are visible as well as areas where sulfate reduction is practically inactive (panel C). The latter areas are mainly associated with zones of upwelling subsurface water that is in a reduced state and depleted of sulfate (plot E and F). They are preferentially located below local depressions. For areas of infiltration, preferentially located below local hummocks, hot spots (panel C) for sulfate reduction can develop because the infiltrating water, originating from the oxygenated unsaturated zone, is rich in sulfate which can be reduced when more reducing conditions are encountered at increasing depth (panel E). This general pattern with local reduction hot spots below hummocks and an inhibition or absence of reduction processes below depressions, is also evident for all other redox-sensitive species (e.g. see plots in the supplement Figure A1-A7). In comparison, oxidation processes (*iron(III)- , aerobic sulfide oxidation*) show a reversed pattern, where local hot spots are preferentially generated below depressions where older upwelling water, rich in reduced species, comes in contact with atmospheric oxygen (panel D). In infiltrating areas, oxidation processes are practically inactive as the freshly infiltrated water carries predominantly oxidized species.
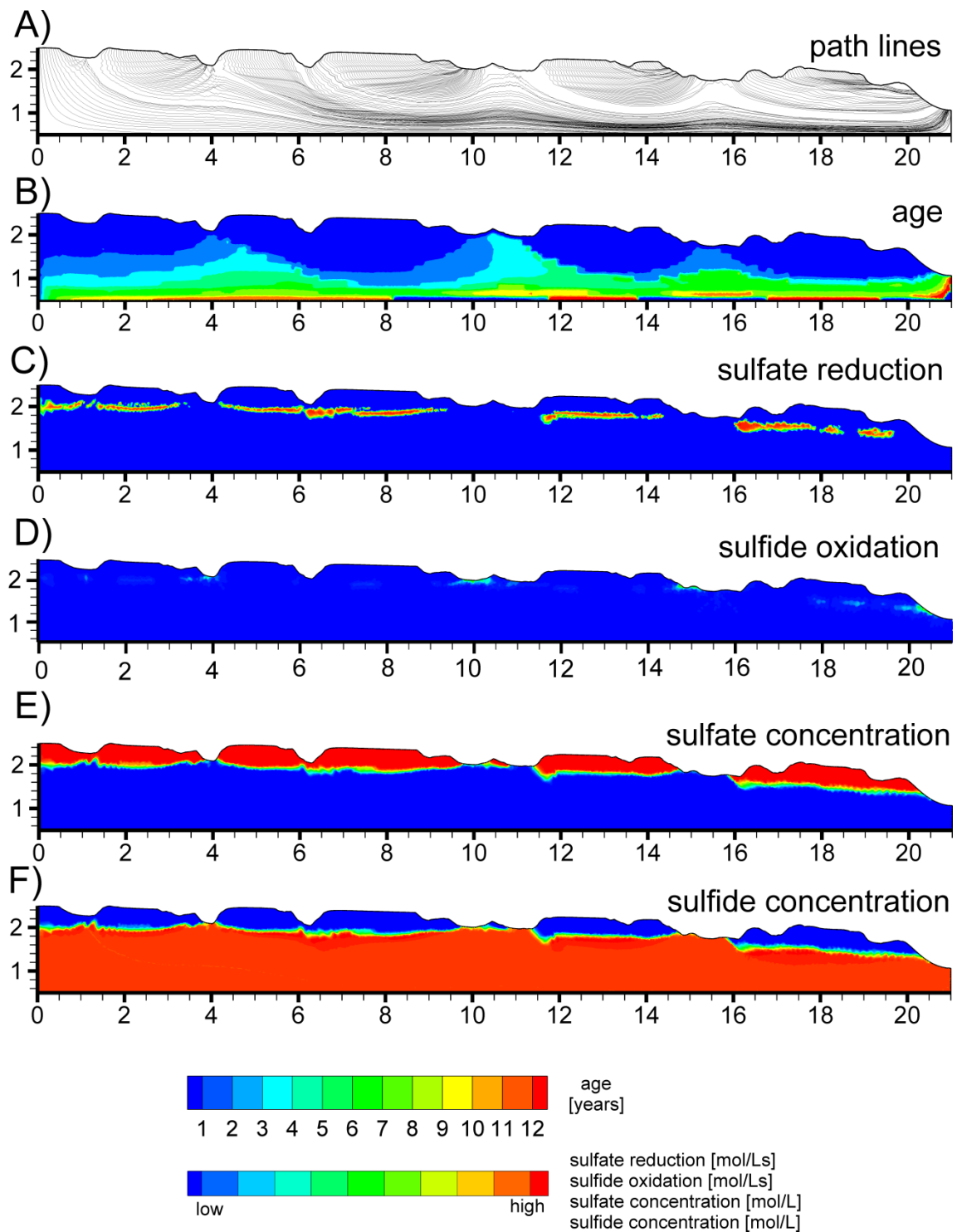
Figure 5: *Results of the biogeochemical simulations shown for the sulfate reduction/oxidation process of the micro-topography scenario with the mean length 0.5m. PHREEQC simulations were performed along the flow paths shown in A. Results were interpolated into the 2D cross sections. B shows the age distribution in years of subsurface flow derived from backward particle tracking. C and D represents process activity of sulfate reduction/oxidation (kinetic rate in mol/Ls). Concentrations in mol/L for sulfate and sulfide are shown in E and F respectively.*

Contrary to other oxidation processes, nitrification also occurs below hummocks (Figure 6), because here ammonium, released during turnover of organic material due to aerobic respiration, reacts with oxygen to form nitrate. Nevertheless, even for nitrification the areas showing the most intensive turnover rates are preferentially located below depressions where upwelling water rich in ammonium gets in contact with atmospheric oxygen. As mentioned before, the location of oxidation and reduction hot spots in the virtual wetland models are strongly correlated with the surface micro-topography as illustrated in Figure 7. For each of the models surface topography is displayed in plan view. A binary classification into areas with higher relative elevation (red areas) and local depressions (blue areas) is used for the micro-topography models, whereas the surface of the planar reference model is displayed in graduated colors. Directly to the right of the plots showing the model surface, plan views of high process activity (hot spots) are shown in black, evaluated based on the maximum process activity across the vertical extent of the model at each location in the 2D horizontal domain (again for sulfate reduction as an example). A strong spatial correlation between hot spots and wetland topography can be seen for the micro-topography models. In close proximity to the stream channel (X > 18 m) also surface depressions can be zones of infiltration because of the steep hydraulic gradients towards the adjacent stream channel. Under these conditions depressions are no longer characterized by upwelling of reduced groundwater, which suppresses oxidation but in turn fosters reduction processes (Plots for the other implemented processes, which are shown in the supplement Figure A8-A12).

Although the formation of hot spots was generally found in both micro-topography models (Figure 8 A and B) it is significantly more pronounced in the model with larger mean length of the structures. The main reason for that are the more pronounced shallow flow cells that develop in the model with coarser micro-topography. In the model with finer micro-topography (ml-0.25m) hot spots are less pronounced (the relative difference in reaction rates between the hot spot and its surrounding area is smaller) and spatially more dispersed. This model represents a transition to the planar reference model (Figure 8 C), where almost the entire surface area of the model shows infiltration and upwelling conditions are restricted to the zone between X = 9 m and 16 m. As a result biogeochemical process patterns are more uniform and less patchy. The characteristic patterns of hot spots are not only visible along the main direction of subsurface flow as shown in the transects but also in 3D, which is shown in Figure 9 (plots for the mean length 0.25 m model and the planar reference are shown in the supplement Figure A13 and A14).
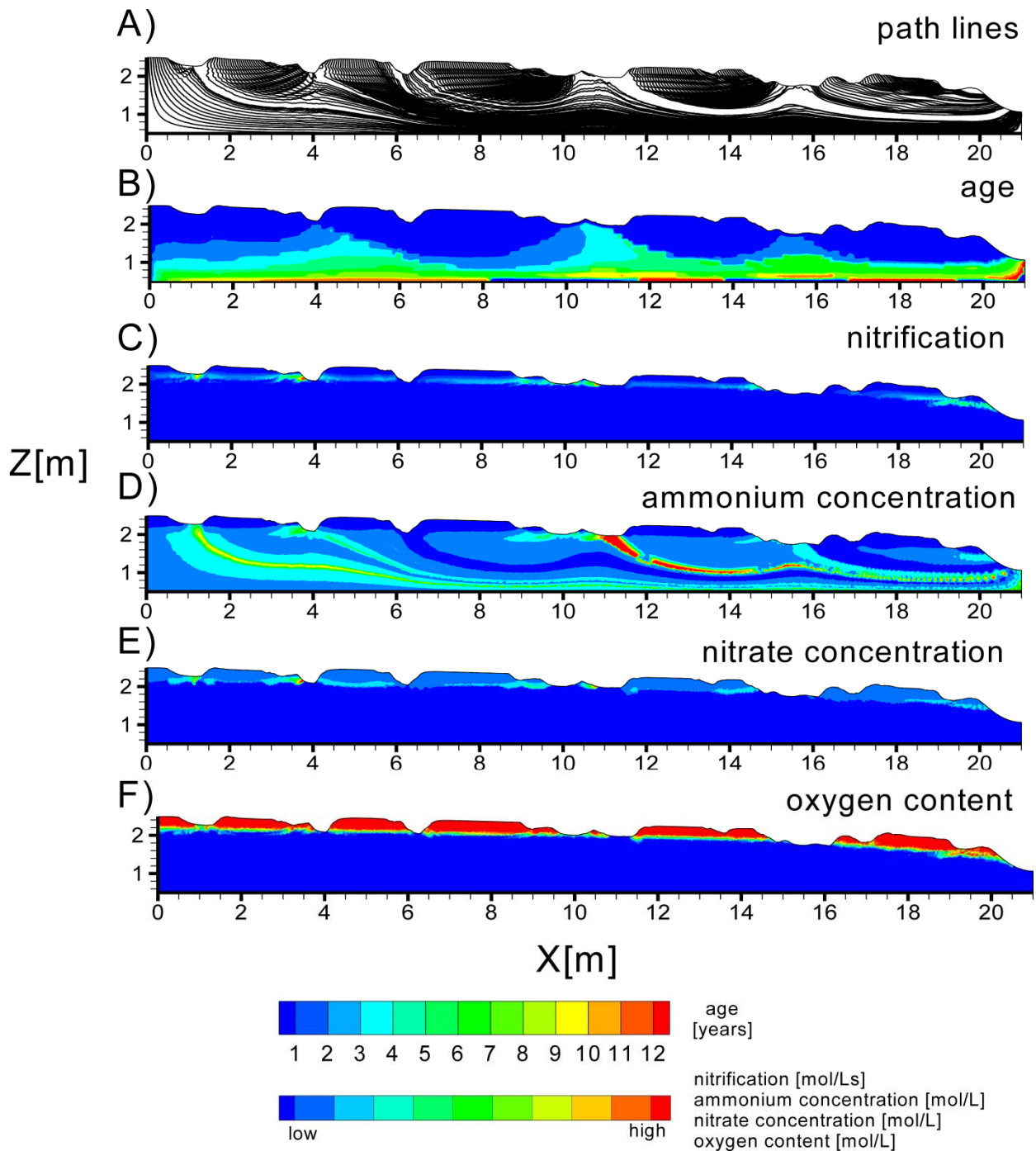
Figure 6: *Results of the biogeochemical simulations exemplarily shown for nitrification of the micro-topography scenario with the mean length 0.5 m. PHREEQC simulations were performed along the flow paths shown in A. Results were interpolated into the 2D cross sections. B shows the age distribution in years of subsurface flow derived from backward particle tracking. C represents process activity of nitrification (kinetic rate in mol/Ls). Concentrations in mol/L for ammonium, nitrate and oxygen are shown in D, E and F respectively.*
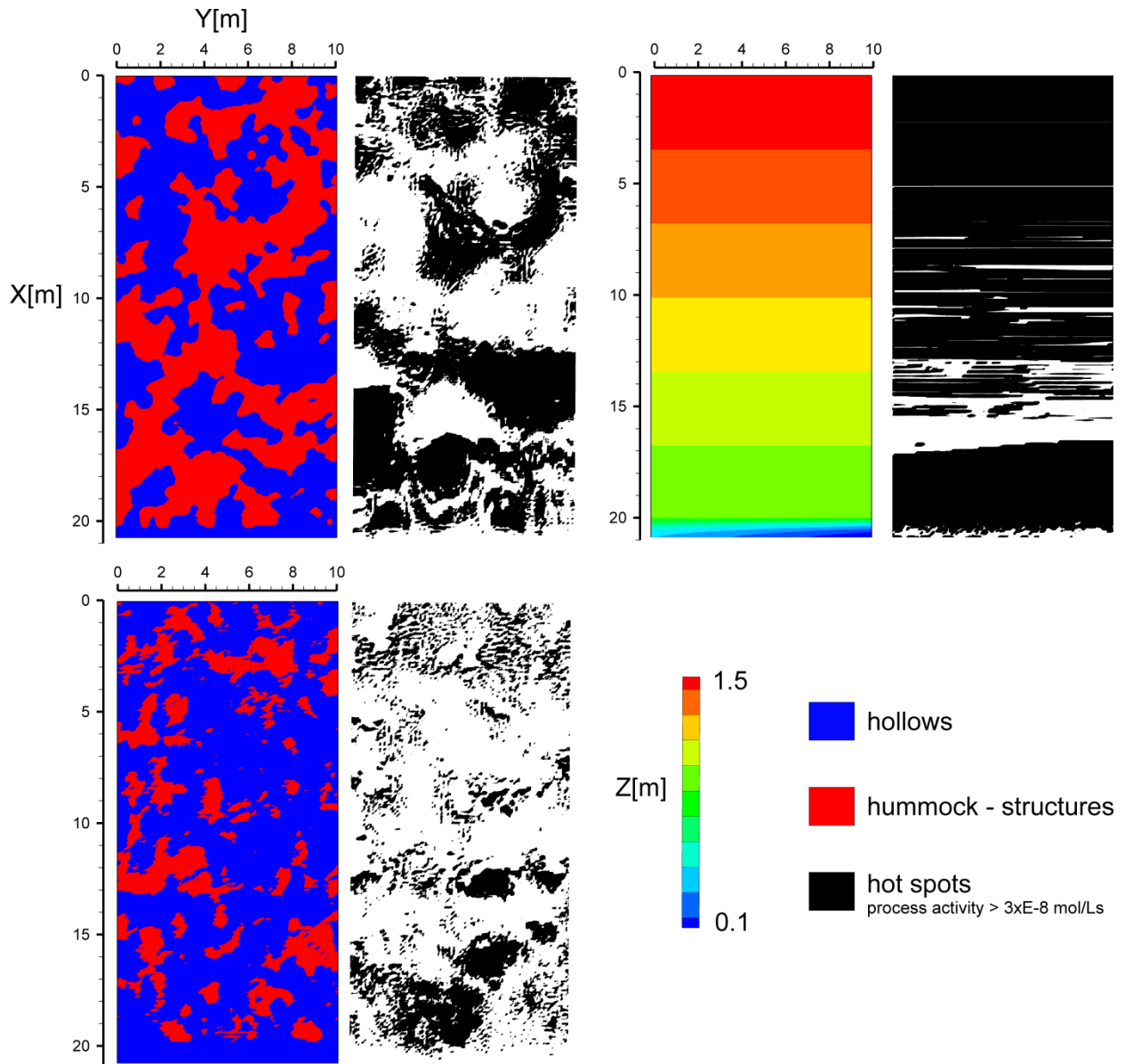
Figure 7: *Plan view of the micro-topography and the planar reference models. Micro-topography is depicted in two categories, red for hummocks and blue for hollows. For the planar reference model elevation classes are shown reflecting the linear slope of the surface. Black areas on the right represent areas of preferential sulfate reduction (hot spots) relative to their surroundings. In general hot spots for reduction processes preferentially form below hummocks and hot spots for oxidation processes below hollows (as shown in the supplement).*

Figure 8: *Comparison of simulated sulfate reduction hot spots for the two different micro-topography scenarios (A and B) and the planar reference (C).*

Figure 9: *Fence plots showing the zones of preferential sulfate reduction for the whole 3D domain of the mean length 0.5 m model (3D plots for the mean length 0.25m and the planar reference case are shown in the supplement).*
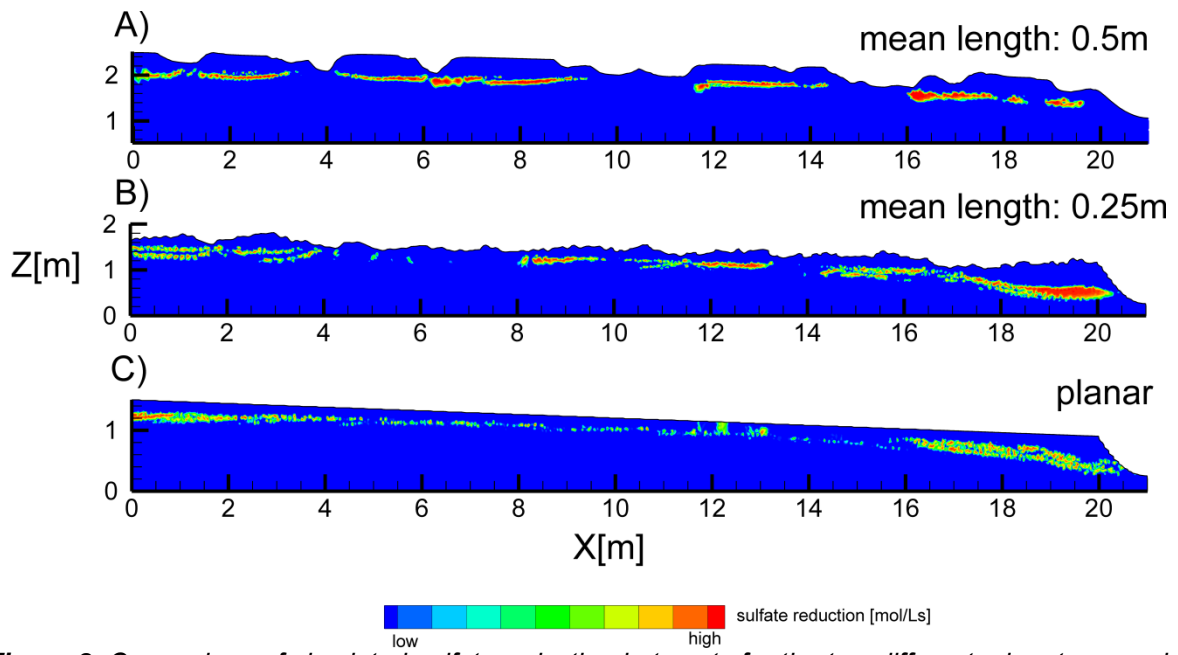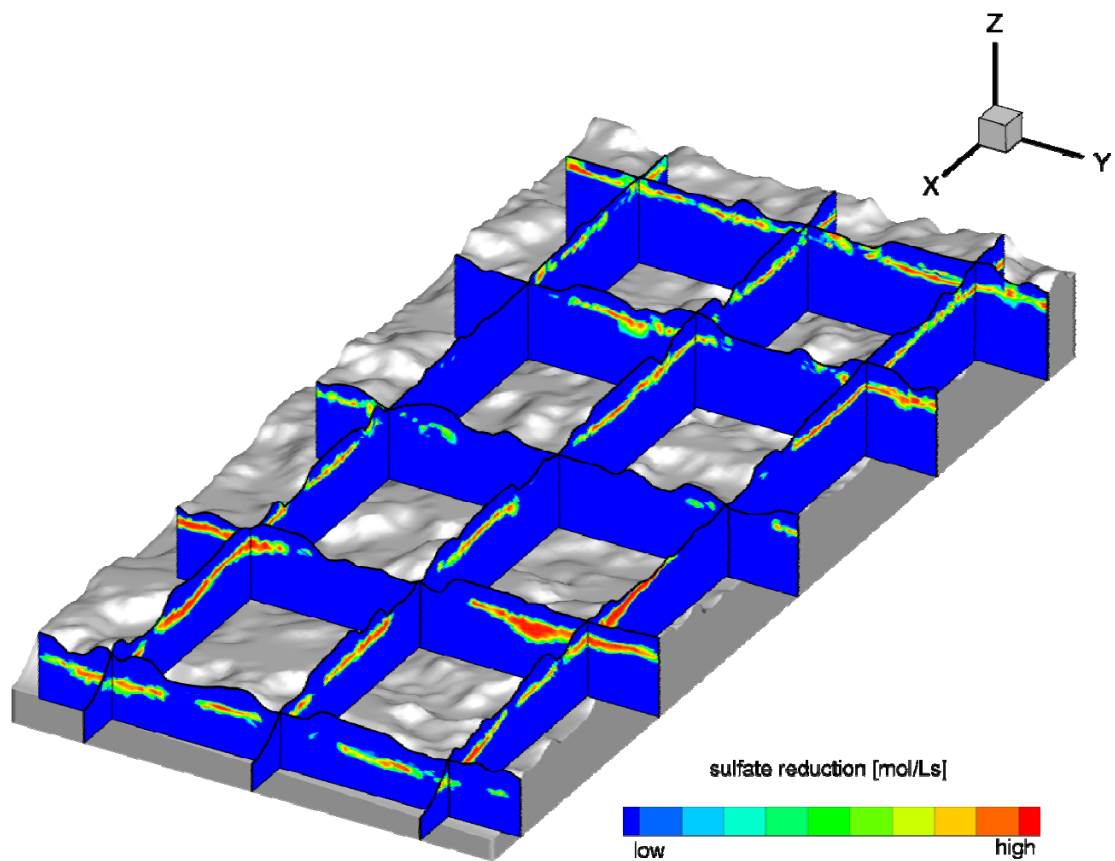
4 Discussion

4.1 Hydrological controls of hot spot formation

Our model scenarios have demonstrated that the basic mechanism of hot spot formation is the same for both micro-topography models. In young, freshly infiltrated subsurface water, electron acceptors are abundant and anaerobic respiration can proceed as soon as the infiltrating water reaches zone 3 where oxygen resupply is assumed to be negligible ($\tau_{resupply} \ll \tau_{depletion}$). After depletion of oxygen, denitrification, iron(III) – and sulfate reduction are sequentially initiated for infiltrating water, triggered by the high availability of electron acceptors. Reductive hot spots are generated below infiltration areas located preferentially underneath hummock structures. Initially, below hummocks, infiltrating water passes the unsaturated zone (zone 1) where resupply of oxygen is assumed to occur instantly ($\tau_{resupply} \gg \tau_{depletion}$), here aerobic respiration is the only active process. As water infiltrates deeper (zone 2), resupply of atmospheric oxygen is assumed to significantly slow down (reduced diffusivity) and anaerobic processes are being initiated. Denitrification, iron(II) and sulfate reduction become dominant in the the part of the saturated zone (zone 3) where the resupply of oxygen is cut off. On the other hand, upwelling zones, where older and already reduced groundwater rises into superficial layers, are characterized by inactivation of reduction processes. Here denitrification, iron(III) and sulfate reduction are inhibited because electron acceptors are not available. Oxidation processes however, are triggered for upwelling areas because here reduced water gets in contact with atmospheric oxygen, which is supplied to zone 2 by diffusion through the saturated pore space. Upwelling of subsurface water preferentially occurs below local depressions. Whether oxidation hot spots can be generated below a depression or not depends on the amount of surface water stored within the superficial depression. If a surface depression is filled with too much water (depth of surface ponding > 0.25 m) diffusive penetration of atmospheric oxygen is inhibited and hence the formation of hot spots for oxidation processes is suppressed. In contrast, very pronounced hot spots for oxidation processes can be found below depressions with upwelling groundwater and low ponding depths. Here the saturated pore space is located within zone 2 where diffusion of atmospheric oxygen still exceeds depletion (as opposed to zone 3) and where oxygen can penetrate into shallow layers where it gets in contact with upwelling water carrying high concentrations of reduced species. How fast turnover of reduced species in oxidation hot spots occurs, depends on the availability of oxygen in zone 2, which is controlled by the amount of surface water being stored in the superficial depression. If surface ponding depths are very low (< 0.05 m) availability of oxygen is assumed to be very high within zone 2 resulting in fast turnover of reduced species and very pronounced local oxidation hot spots. With increasing surface ponding (0.05 m - 0.25 m) oxygen availability drops rapidly resulting in slower turnover rates and less pronounced oxidation hot spots. The availability of oxygen below depressions is therefore mainly controlled by the dynamics of surface water storage, which was found

to be highly variable in space and time in wetlands with a hummocky topography, depending on the climatic boundary conditions [*Frei et al.*, 2010]. During intensive rainfall events, surface storage and runoff generation in wetlands with shallow water table can be controlled by a dynamic fill and spill mechanism [*Frei et al.*, 2010]. Depressions are filled with water due to rising groundwater levels during onset of rainfall. With lasting rainfall, isolated ponded depressions start to interconnect with each other building extended surface flow networks [*Frei et al.*, 2010; *Antoine et al.*, 2009]. These surface flow networks can efficiently drain large fractions of the wetland's surface. At times more than 80% of the generated stream discharge may originate from this type of surface flow [*Frei et al.*, 2010]. During high water table conditions, fast diffusion of atmospheric oxygen into the subsurface system is limited to areas of high elevation (hummocks), which remain unsaturated at the surface. During water table recessions and decreasing surface ponding, diffusion of atmospheric oxygen, below depressions with lower surface ponding, becomes more effective in terms of increasing rates for resupply, which triggers oxidation processes for upwelling conditions. Generally field data on oxygen supply in wetlands, its coupling to water table dynamics and peat properties are scarce [*Aragonès and Blodau.*, 2012], stressing the importance of virtual modeling studies. A special condition can develop during extended dry periods, where depressions become disconnected from the declining water table. Below these disconnected depressions hydraulic gradients may reverse, switching from upwelling to infiltrating conditions. In turn oxidation hot spots will diminish because resupply of reduced species from upwelling groundwater is disrupted. It is reasonable to assume that during droughts hot spot patterns will become less pronounced and may eventually vanish as the system gradually shifts towards a more homogenous distribution of process activities.

In real wetland systems probably more than one mechanism will be responsible for the formation of biogeochemical hot spots [*McClain et al.*, 2003] and a clear separation of the influence of one specific process is almost impossible under field conditions. The simulations presented here, however, demonstrate that heterogeneous process patterns in hummocky wetlands can be explained by the complex re-distribution of redox-sensitive solutes in space as being controlled by micro-topography induced, subsurface transport processes and alternating biogeochemical boundary conditions. Furthermore, the presented concept shows that biogeochemical hot spots can be generated without reference to material heterogeneities which often are hardly observable in horizontally relatively homogenous peat soils [*Morris and Waddington*, 2011; *Holden and Burt*, 2003; *Reeve et al.*, 2001; *Reeve et al.*, 2006; *Clymo*, 1984]. Of course the presented concept neglects important aspects of real field conditions. Effects of the wetlands vegetation like root water uptake and its influence on subsurface flow or the special biogeochemical conditions within the rhizosphere [*Crow and Wieder*, 2005; *Knorr et al.*, 2008; *Wachinger et al.*, 2000] are not considered as well as the potential effects of dispersion the availability of electron acceptors and donors. Hydrodynamic dispersion may cause a smearing effect where the boundaries between hot spots and surrounding areas are not as sharp and

clearly expressed as in an advectively dominated system, because solutes are also re-distributed along concentration gradients (diffusion) and transversally and longitudinally along the advective flow directions (dispersion). The biogeochemical simulations were performed using 5-day time steps, which was necessary because of computational constraints during the flow modeling (e.g. memory overflow, storage limitations). However, it is known that hydrological events at time scales of hours (e.g. single rainstorm events) can influence the biogeochemical processes within wetlands, as e.g. demonstrated for pulses of N_2O emission [*Goldberg et al.*, 2010] or high instantaneous CO_2 production [*Deppe et al.*, 2010] after wetting. Dynamics at these time scales, however, were not the main focus of this work and at this point cannot be fully accounted for in the present modeling approach because of computational limitations. Further it is known that organic carbon in wetlands typically consists of a fraction of labile components that can be easily utilized by micro-organisms (mostly within shallow layers) and more recalcitrant components (more abundant in deeper layers) [*Yavitt and Lang*, 1990; *Reiche et al.*, 2010; *Moore et al.*, 2007]. Labile organic carbon is not uniformly available as is assumed in our approach. However, there are two main reasons why we think that our assumption of unlimited carbon supply is nonetheless reasonable. Firstly, labile organic carbon availability is higher in shallow peat layers, in which most of the modeled processes occur, mostly due to inputs from the vegetation and high fermentation activity in the rhizosphere [*Knorr et al.*, 2008; *Wachinger et al.*, 2000; *Reiche et al.*, 2010]. Secondly, we did not include methanogenesis, for which the supply of electron donors will be the key control, as the ubiquitous CO_2 may serve as electron acceptor [*Achtnich et al.*, 1995]. Field observations suggested that if alternative electron acceptors were present, the respective process proceeded, while under methanogenic conditions, respiratory activity slowed down and partly ceased [*Beer and Blodau*, 2007; *Knorr et al.*, 2009]. Nevertheless, the process rate, constant in this case, depends on the quality of organic matter used and is not universal but substrate specific. The application of the Redfield ratio to simulate release of organic bound nitrogen due to decomposition of organic material in terrestrial ecosystems was probably a weak model assumption. Recent literature reported that C:N:P ratios in terrestrial ecosystems vary depending on vegetation types, but on the global scale average at about 186:13:1 for soil biomass and 60:7:1 for soil microbial biomass [*Cleveland and Liptzin*, 2007]. In our biogeochemical model we assumed that the majority of organic carbon available to microbes originates from vegetation and fermented plant material processed by microorganisms. The Redfield ratio is, however, narrower than the global average observed for soil biomass (106:16:1 compared to 186:13:1) and nitrogen release would be overestimated by our model. That means that the concentrations of ammonia, rates of nitrification and thus also nitrate pools available for denitrification may also be overestimated. Nevertheless, this should translate into slightly longer phases of nitrification or subsequent denitrification only, thus not fundamentally altering spatial patterns of the model output.

4.2 Comparison with field observations

Despite these simplifications, the presented model is capable of reproducing spatial variations in pore water concentrations of redox-sensitive solutes in the field (Figure 10). Vertical concentration profiles were measured in pore water from six different locations at the Lehstenbach field site, for an area, which is comparable in size to the spatial domain of the flow model (10m x 20m) [*Goldberg et al.*, 2010; *Knorr et al.*, 2009]. Simulated maxima in nitrate concentrations are found at a depth of ~0.1m and not directly at the surface, which agrees with measured data. The observed shift of nitrate concentration maxima has been explained as a result of plant uptake from the upper layers, as plant cover often leads to rapid depletion of nitrate concentrations [*Silvan et al.*, 2005]. However our biogeochemical simulations suggest an additional explanation for the increased nitrate concentrations at shallow depth: As shown for the cross sections (Figure 6 C) high nitrification rates are limited to a relatively thin layer where turnover of ammonium to nitrate is highest. This layer of higher reactivity is the result of the vertical transport of water, which is being enriched with ammonium as it passes the unsaturated zone. Because nitrification rates under aerobic conditions depend on the local availability of ammonium, higher ammonium concentrations result in higher nitrification rates, which can be found directly above the de-nitrification zone where anaerobic conditions trigger rapid nitrate reduction. Similar findings were reported for different field studies [*Regina et al.*, 1999; *Goldberg et al.*, 2010]. Measured depth profiles as shown in Figure 10 are often used to calculate biogeochemical turnover rates based on a simplified approach treating wetlands as diffusion limited systems where the resupply of dissolved electron acceptors/donors is solely controlled by diffusion [*Beer and Blodau*, 2007; *Clymo and Bryant*, 2008]. However, model results show that advective transport can be an important component especially for slightly sloping wetlands with micro-topography and can significantly affect the spatial availability and re-distribution of electron acceptors and donors within the subsurface. Vertical concentration profiles simulated in this study suggest that depth variations in the concentrations of redox-sensitive solutes observed in the field are probably the result of a complex interplay between three-dimensional advective transport processes and biogeochemical reactions, which are in turn controlled by micro-topography moderated interactions between surface and subsurface flow processes and do not arise from pure diffusion and reactions alone.

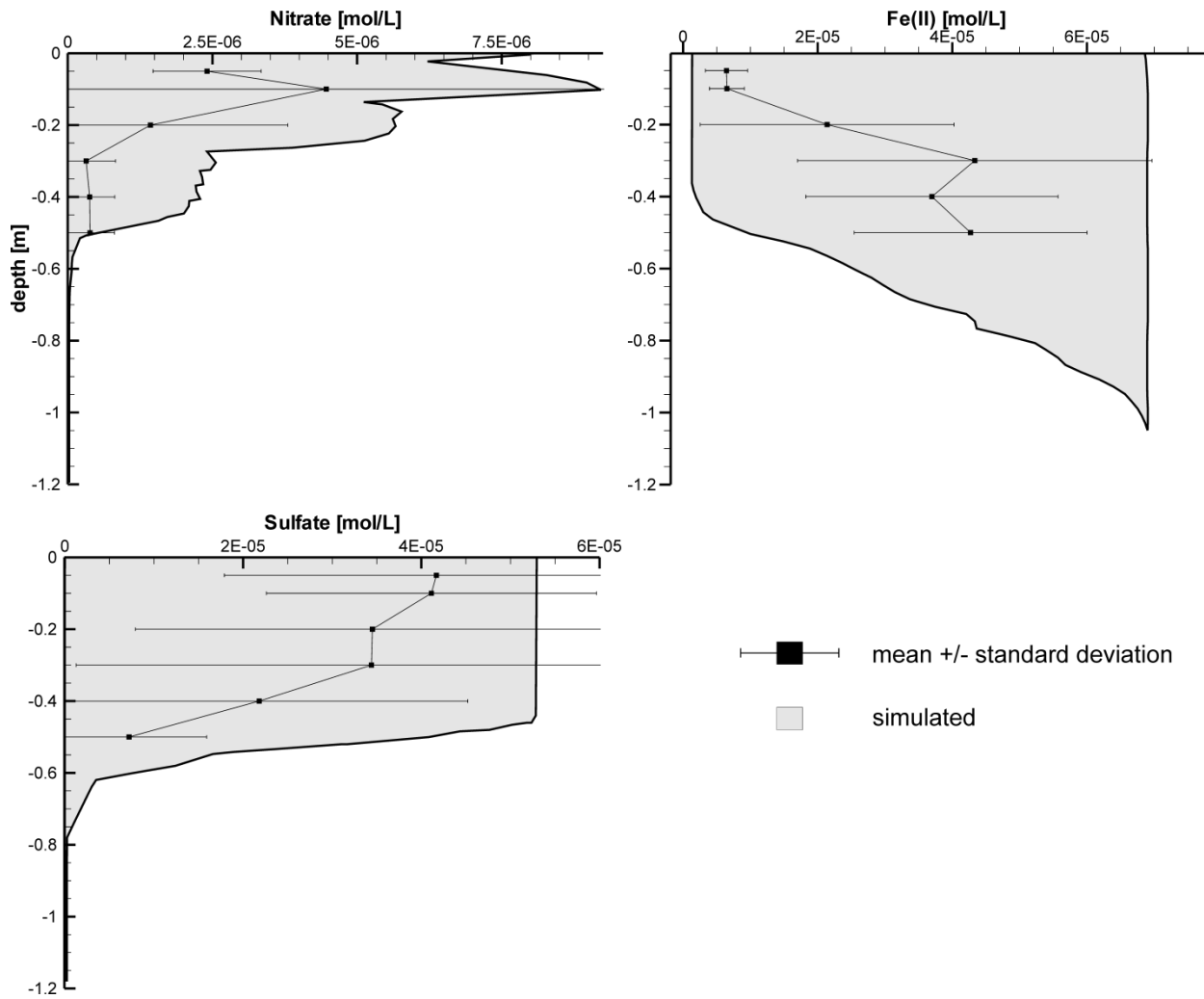**Figure 10:** *Observed and simulated variations of depth profiles for redox-sensitive species (nitrate, iron(II) and sulfate). Grey areas represent envelopes for predicted depth profiles and the black lines (mean +/- standard deviation) actual field observations taken simultaneously at six different locations for an area which is comparable to the model 20 m x 10 m domain at the field site in the Lehstenbach catchment.*

5 Conclusions and Implications

At the landscape scale, riparian wetlands are commonly assumed to be zones of enhanced biogeochemical transformations (e.g. denitrification) due to anaerobic conditions and large carbon supplies [*Johnston*, 1991]. Field studies, however, have shown that biogeochemical conditions within wetlands can be quite diverse where most of the biogeochemical turnover may be accomplished in localized zones of higher reactivity (hot spots) [*Paul et al.*, 2006; *Knorr et al.*, 2009; *Knorr and Blodau*, 2009; *Fenner et al.*, 2011]. Under field conditions, different processes and mechanisms can lead to the formation of hot spots [*McClain et al.*, 2003] depending on the scale of interest. However, explaining such hot spots solely by the heterogeneous distribution of static, physico-chemical properties of the soil [*Reeve et al.*, 2001; *Holden and Burt*, 2003] may be too simplistic. Our simulations indicate that biogeochemical hot spots can form even in homogeneous peat soils as a result of a dynamic subsurface flow system with **(1)** complex surface/subsurface interactions where surface micro-topography induces a subsurface flow field that is characterized by a small-scale zonation of in- and exfiltration and **(2)** hydrological controls of the biogeochemical boundary conditions that either facilitate or suppress redox processes in ex- and infiltration areas. Hence the occurrence of reactivity hot spots does not need to be associated with static heterogeneities in physico-chemical soil properties *a priori*. In fact, the formation of biogeochemical hot spots in wetland systems may have the potential to alter the hydrodynamic properties of the peat and therefore, typically observed material heterogeneity may result from processes described in this study. The precipitation of iron oxides e.g., which preferentially occurs at oxidation hot spots, can lead to a reduction of the effective porosity and a lower hydraulic conductivity, providing a negative feedback on oxygen penetration; or in areas of reduction hot spots e.g. iron sulfides may become enriched that could be reoxidized upon more severe drying. Our results offer a new perspective on biogeochemical transformation processes in riparian wetlands that provides a dynamic framework to explain process heterogeneity in wetland soils and variability in process rates over time and space. Future work will have to address the interplay between different static (e.g. soil properties, vegetation patterns) and dynamic controls (e.g. flow, temperature & vegetation dynamics) of spatial and temporal variations in biogeochemical process activities in wetlands. It is clear that a mechanistic understanding of the links between hydrologic dynamics and biogeochemical transformations will be crucial for an assessment of climate change impacts on wetland functions and associated ecosystems services. The work presented here can serve as starting point for such an assessment by providing an explorative, mechanistic modeling framework to investigate potential shifts in hydrological and biogeochemical processes including changes in feedback mechanisms caused by changes in climatic forcing.

Acknowledgments

References

Achtnich, C., F. Bak and R. Conrad (1995), Competition for electron donors among nitrate reducers, ferric iron reducers, sulfate reducers, and methanogens in anoxic paddy soil, *Biology and Fertility of Soils 19*(1), 65–72.

Alewell, C., S. Paul, G. Lischeid and F. R. Storck (2007), Co-regulation of redox processes in freshwater wetlands as a function of organic matter availability?, *Science of the Total Environment 404*(2-3), 335–342, doi:10.1016/j.scitotenv.2007.11.001.

Antoine, M., M. Javaux and C. Bielders (2009), What indicators can capture runoff-relevant connectivity properties of the micro-topography at the plot scale?, *Advances in Water Resources 32*(8), 1297–1310, doi:10.1016/j.advwatres.2009.05.006.

Appelo, C. A. and D. Postma (2005), *Geochemistry, groundwater and pollution*, Taylor & Francis.

Beer, J. and C. Blodau (2007), Transport and thermodynamics constrain belowground carbon turnover in a northern peatland, *Geochimica et Cosmochimica Acta 71*(12), 2989–3002.

Bekins, B. A., E. Warren and E. M. Godsy (1998), A Comparison of Zero Order, First Order, and Monod Biotransformation Models, *Ground Water 36*(2), 261–268.

Bellevue, W. (2003), Tecplot User's Manual, *Amtec Engineering Inc*.

Billen, G. (1982), An idealized model of nitrogen recycling in marine sediments, *Am. J. Sci 282,* 512–541.

Bishop, K., J. Seibert, S. Köhler and H. Laudon (2004), Resolving the Double Paradox of rapidly mobilized old water with highly variable responses in runoff chemistry, *Hydrol. Process 18*(1), 185–189.

Boano, F., A. Demaria, R. Revelli and L. Ridolfi (2010), Biogeochemical zonation due to intrameander hyporheic flow, *Water Resources Research 46*(2), W02511.

Brookfield, A. E., E. A. Sudicky, Y. J. Park and B. Conant Jr. (2009), Thermal transport modelling in a fully integrated surface/subsurface framework, *Hydrological Processes*(23), 2150–2164, 10.1002/hyp.7282.

Brovelli, A., O. Carranza-Diaz, L. Rossi and D. Barry (2011), Design methodology accounting for the effects of porous medium heterogeneity on hydraulic residence time and biodegradation in horizontal subsurface flow constructed wetlands, *Ecological Engineering*(37), 758–770.

Bruland, G., C. Richardson, and S. Whalen (2006), Spatial variability of denitrification potential and related soil properties in created, restored, and paired natural wetlands, *Wetlands 26*(4), 1042–1056.

Bruland, G. and C. Richardson (2005), Hydrologic, edaphic, and vegetative responses to microtopographic reestablishment in a restored wetland, *Restoration Ecology 13*(3), 515–523.

Carle, S. and G. Fogg (1996), Transition Probability-Based Indicator Geostatistics, *Mathematical Geology 28*(4), 453–476.

Cheng, Y., M. Stieglitz, G. Turk and V. Engel (2011), Effects of anisotropy on pattern formation in wetland ecosystems, *GEOPHYSICAL RESEARCH LETTERS 38*(4), L04402.

Cleveland, C. and D. Liptzin (2007), C:N:P stoichiometry in soil: is there a "Redfield ratio" for the microbial biomass?, *Biogeochemistry 85*(3), 235-252

Clymo, R. S. (1984), The limits to peat bog growth, *Philosophical Transactions of the Royal Society of London. B, Biological Sciences 303*(1117), 605.

Clymo, R. S. and C. L. Bryant (2008), Diffusion and mass flow of dissolved carbon dioxide, methane, and dissolved organic carbon in a 7-m deep raised peat bog, *Geochimica et Cosmochimica Acta 72*(8), 2048–2066.

Crow, S. and R. Wieder (2005), Sources of CO2 emission from a northern peatland: root respiration, exudation, and decomposition, *Ecology 86*(7), 1825–1834.

Deppe, M., Knorr K-H., McKnight D. and Blodau C (2010) Effects of short-term drying and irrigation on CO_2 and CH_4 production and emission from mesocosms of a northern bog and an alpine fen. *Biogeochemistry* 100: 89-103.

Devito, K. J. and A. R. Hill (1997), Sulphate dynamics in relation to groundwater-surface water interactions in headwater wetlands of the southern Canadian Shield, *Hydrological Processes 11*(5), 485–500.

Dosskey, M. and P. Bertsch (1994), Forest sources and pathways of organic matter transport to a blackwater stream: a hydrologic approach, *Biogeochemistry 24*(1), 1–19.

Nealson, K. and D. Saffarini (1994), Iron and manganese in anaerobic respiration: environmental significance, physiology, and regulation, *Annual Reviews in Microbiology 48*(1), 311–343.

Eckert, P. and C. A. Appelo (2002), Hydrogeochemical modeling of enhanced benzene, toluene, ethylbenzene, xylene (BTEX) remediation with nitrate, *Water Resources Research 38*(8), 1130.

Estop-Aragonés, C. and C. Blodau (2012), Controls on in situ oxygen and DIC dynamics in peats of a temperate fen., *Journal of Geophysical Research – Biogeosciences* 117(G2), G02002.

Fenner, N., R. Williams, H. Toberman, S. Hughes, B. Reynolds and C. Freeman (2011), Decomposition hotspots in a rewetted peatland: implications for water quality and carbon cycling, *Hydrobiologia,* 1–16.

Frei, S., G. Lischeid and J. H. Fleckenstein (2010), Effects of micro-topography on surface-subsurface exchange and runoff generation in a virtual riparian wetland-a modeling study, *Advances in Water Resources 33*(11), 1388–1401.

Gafni, A. and N. Kenneth (1990), Hydraulic characteristics of four peatlands in Minnesota, *Canadian Journal of Soil Science 70*(2), 239–253.

Goldberg, S., K. Knorr, C. Blodau, G. Lischeid and G. Gebauer (2010), Impact of altering the water table height of an acidic fen on N2O and NO fluxes and soil concentrations, *Global Change Biology 16*(1), 220–233.

Goldsmith, C. D. and R. K. Balderson (1988), Biodegradation and growth kinetics of enrichment isolates on benzene, toluene, and xylene, *Water Science and Technology WSTED 4 20*(11/12).

Hill, A. R. (2000), Stream chemistry and riparian zones, *Streams and ground waters,* 83–110.

Hinton, M. J., S. L. Schiff and M. C. English (1998), Sources and flowpaths of dissolved organic carbon during storms in two forested watersheds of the Precambrian Shield, *Biogeochemistry 41*(2), 175–197.

Holden, J. and T. P. Burt (2003), Hydraulic conductivity in upland blanket peat: measurement and variability, *Hydrological Processes 17*(6), 1227–1237.

Huntington, T. G. (2006), Evidence for intensification of the global water cycle: Review and synthesis, *Journal of Hydrology 319*(1-4), 83–95.

Inamdar, S., J. Rupp and M. Mitchell (2009), Groundwater flushing of solutes at wetland and hillslope positions during storm events in a small glaciated catchment in western New York, USA, *Hydrological Processes 23*(13), 1912–1926.

Jacks, G. and A. C. Norrström (2004), Hydrochemistry and hydrology of forest riparian wetlands, *Forest ecology and Management 196*(2-3), 187–197.

Jakobsen, R. (2007), Redox microniches in groundwater: A model study on the geometric and kinetic conditions required for concomitant Fe oxide reduction, sulfate reduction, and methanogenesis, *Water Resources Research 43*(12), W12S12.

Johnston, C. A. (1991), Sediment and nutrient retention by freshwater wetlands: effects on surface water quality, *Critical Reviews in Environmental Science and Technology 21*(5), 491–565.

Jones, J. P., E. A. Sudicky, A. E. Brookfield and Y. J. Park (2006), An assessment of the tracer-based approach to quantifying groundwater contributions to streamflow, *Water Resources Research 42, W02407,* doi:10.1029/2005WR004130.

Kelly, W. R., G. M. Hornberger, J. S. Herman and A. L. Mills (1996), Kinetics of BTX biodegradation and mineralization in batch and column systems, *Journal of contaminant hydrology 23*(1-2), 113–132.

Knorr, K. H., B. Glaser and C. Blodau (2008), Fluxes and 13C isotopic composition of dissolved carbon and pathways of methanogenesis in a fen soil exposed to experimental drought, *Biogeosciences* 5: 1457–1473.

Knorr, K. H., G. Lischeid and C. Blodau (2009), Dynamics of redox processes in a minerotrophic fen exposed to a water table manipulation, *Geoderma 153*(3-4), 379–392.

Knorr, K. and C. Blodau (2009), Impact of experimental drought and rewetting on redox transformations and methanogenesis in mesocosms of a northern fen soil, *Soil Biology and Biochemistry 41*(6), 1187–1198.

Le Kellogg and S. D. Bridgham (2003), Phosphorus retention and movement across an ombrotrophic-minerotrophic peatland gradient, *Biogeochemistry 63*(3), 299–315.

Lischeid, G., A. Kolb, C. Alewell and S. Paul (2007), Impact of redox and transport processes in a riparian wetland on stream water quality in the Fichtelgebirge region, southern Germany, *Hydrological Processes 21*(1), 123–132, 10.1002/hyp.6227.

Lovley, D., J. Coates, E. Blunt-Harris, E. Phillips and J. Woodward (1996), Humic substances as electron acceptors for microbial respiration, *Nature 382*(6590), 445–448.

MacQuarrie, K. T., E. A. Sudicky and E. O. Frind (1990), Simulation of biodegradable organic contaminants in groundwater: 1. Numerical formulation in principal directions, *Water Resources Research 26*(2), 207–222.

McClain, M., E. Boyer, C. Dent, S. Gergel, N. Grimm, P. Groffman, S. Hart, J. Harvey, C. Johnston and E. Mayorga (2003), Biogeochemical hot spots and hot moments at the interface of terrestrial and aquatic ecosystems, *Ecosystems 6*(4), 301–312.

McMahon, P. B., and F. H. Chapelle (2008), Redox processes and water quality of selected principal aquifer systems, *Ground Water 46*(2), 259–271.

Millero, F. J., S. Hubinger, M. Fernandez and S. Garnett (1987), Oxidation of H2S in seawater as a function of temperature, pH, and ionic strength, *Environmental Science & Technology 21*(5), 439–443.

Mitchell, C. and B. Branfireun (2005), Hydrogeomorphic controls on reduction-oxidation conditions across Boreal upland Peatland interfaces, *Ecosystems 8*(7), 731–747.

Moore, T., J. Bubier and L. Bledzki (2007), Litter decomposition in temperate peatland ecosystems: the effect of substrate and site, *Ecosystems 10*(6), 949–963.

Morris, P. J. and J. M. Waddington (2011), Groundwater residence time distributions in peatlands: Implications for peat decomposition and accumulation, *Water Resources Research 47*(2), W02511.

Parkhurst, D. (1995), User's guide to PHREEQC: A computer program for speciation, reaction-path, advective-transport, and inverse geochemical calculations, *U.S. GEOLOGICAL SURVEY WAter-Resources Investigations Report 95-4227*.

Paul, S., K. Küsel and C. Alewell (2006), Reduction processes in forest wetlands: tracking down heterogeneity of source/sink functions with a combination of methods, *Soil Biology and Biochemistry 38*(5), 1028–1039.

Pyzik, A. J. and S. E. Sommer (1981), Sedimentary iron monosulfides: kinetics and mechanism of formation, *Geochimica et Cosmochimica Acta 45*(5), 687–698.

Redfield, A. (1934), On the proportions of organic derivatives in sea water and their relation to the composition of plankton, *James Johnstone memorial volume 176,* 92.

Reeve, A. S., Di Siegel and P. H. Glaser (2001), Simulating dispersive mixing in large peatlands, *Journal of Hydrology 242*(1-2), 103–114.

Reeve, A., R. Evensen, P. Glaser, D. Siegel and D. Rosenberry (2006), Flow path oscillations in transient ground-water simulations of large peatland systems, *Journal of Hydrology 316*(1-4), 313–324.

Regina, K., J. Silvola and P. Martikainen (1999), Short-term effects of changing water table on N2O fluxes from peat monoliths from natural and drained boreal peatlands, *Global Change Biology 5*(2), 183–189.

Reiche, M., G. Gleixner and K. Küsel (2010), Effect of peat quality on microbial greenhouse gas formation in an acidic fen, *Biogeosciences 7*(1), 187–198.

Richardson, M. C., B. A. Branfireun, V. B. Robinson and P. A. Graniero (2007), Towards simulating biogeochemical hot spots in the landscape: A geographic object-based approach, *Journal of Hydrology 342*(1-2), 97–109.

Schirmer, M., B. J. Butler, J. W. Roy, E. O. Frind and J. F. Barker (1999), A relative-least-squares technique to determine unique Monod kinetic parameters of BTEX compounds using batch experiments, *Journal of contaminant hydrology 37*(1-2), 69–86.

Segers, R. and S. W. Kengen (1998), Methane production as a function of anaerobic carbon mineralization: a process model, *Soil Biology and Biochemistry 30*(8-9), 1107–1117.

Shabaga, J. and A. Hill (2010), Groundwater-fed surface flow path hydrodynamics and nitrate removal in three riparian zones in southern Ontario, Canada, *Journal of Hydrology 388*(1), 52–64.

Silvan, N., E. Tuittila, V. Kitunen, H. Vasander and J. Laine (2005), Nitrate uptake by Eriophorum vaginatum controls N2O production in a restored peatland, *Soil Biology and Biochemistry 37*(8), 1519–1526.

Stonedahl, S., J. Harvey, A. Wörman, M. Salehin and A. Packman (2010), A multiscale model for integrating hyporheic exchange from ripples to meanders, *Water Resources Research 46*(12), W12539.

Stumm, W. and J. J. Morgan (1995), Aquatic chemistry: chemical equilibria and rates in natural waters, *JOHN WILEY & SONS, NEW YORK, NY 10158(USA). 1995*.

Tauchnitz, N., R. Meissner, S. Bernsdorf and U. Wegener (2010), Nitrogen Fluxes of a Slope Mire in the German Harz Mountains, *Water, Air, & Soil Pollution 205*(1), 107–112.

Therrien, R., R. McLaren, E. Sudicky and S. Panday (2008), HydroGeoSphere A Three-dimensional Numerical Model Describing Fully-integrated Subsurface and Surface Flow and Solute Transport *(Manual)*, University of Waterloo.

Toth, J. (1962), A theory of groundwater motion in small drainage basins in central Alberta, Canada, *Journal of Geophysical Research 67*(11), 4375–4387.

Van Cappellen, P. and Y. Wang (1996), Cycling of iron and manganese in surface sediments: a general theory for the coupled transport and reaction of carbon, oxygen, nitrogen, sulfur, iron, and manganese, *American-Journal ok Science 296,* 197–243.

Vidon, P., C. Allan, D. Burns, T. P. Duval, N. Gurwick, S. Inamdar, R. Lowrance, J. Okay, D. Scott and S. Sebestyen (2010), Hot Spots and Hot Moments in Riparian Zones: Potential for Improved Water Quality Management1, *JAWRA Journal of the American Water Resources Association 46*(2), 278–298.

Wachinger, G., S. Fiedler, K. Zepp, A. Gattinger, M. Sommer and K. Roth (2000), Variability of soil methane production on the micro-scale: spatial association with hot spots of organic material and Archaeal populations, *Soil Biology and Biochemistry 32*(8-9), 1121–1130.

Weiler, M., and J. McDonnell (2006), Testing nutrient flushing hypotheses at the hillslope scale: a virtual experiment approach, *Journal of Hydrology 319*(1-4), 339–356.

Weiler, M. and J. McDonnell (2004), Virtual experiments: a new approach for improving process conceptualization in hillslope hydrology, *Journal of Hydrology 285*(1-4), 3–18.

Wörman, A., A. I. Packman, L. Marklund, J. W. Harvey and S. H. Stone (2006), Exact three-dimensional spectral solution to surface-groundwater interactions with arbitrary surface topography, *Geophys. Res. Lett 33*(L07402), 1–4, doi:10.1029/2006GL025747.

Yavitt, J. and G. Lang (1990), Methane production in contrasting wetland sites: Response to organic-chemical components of peat and to sulfate reduction, *Geomicrobiology Journal 8*(1), 27–46.

Electronic supplementary material to the article published in

Journal of Geophysical Research Letters – Biogeosiences (in press)

Surface micro-topography causes hot spots of biogeochemical activity in wetland systems – a virtual modeling experiment.

Electronic supplementary material

Frei[1], S., Knorr[1], K.H., Peiffer[1], S., and Fleckenstein[2]. J.H.

[1] Department of Hydrology, University of Bayreuth, Germany

[2] Department Hydrogeology, Helmholtz-Center for Environmental Research – UFZ, Germany

No. of pages: 14

No. of figures: 14

Figure A1:. *Results of the biogeochemical simulations shown for the aerobic respiration of the micro-topography scenario with the mean length 0.5 m. PHREEQC simulations were performed along the flow paths shown in A. Results were interpolated into the 2D cross sections. B shows the age distribution in years of subsurface flow derived from backward particle tracking. C represents process activity of aerobic respiration. Dissolved oxygen contents in mol/L are shown in D.*
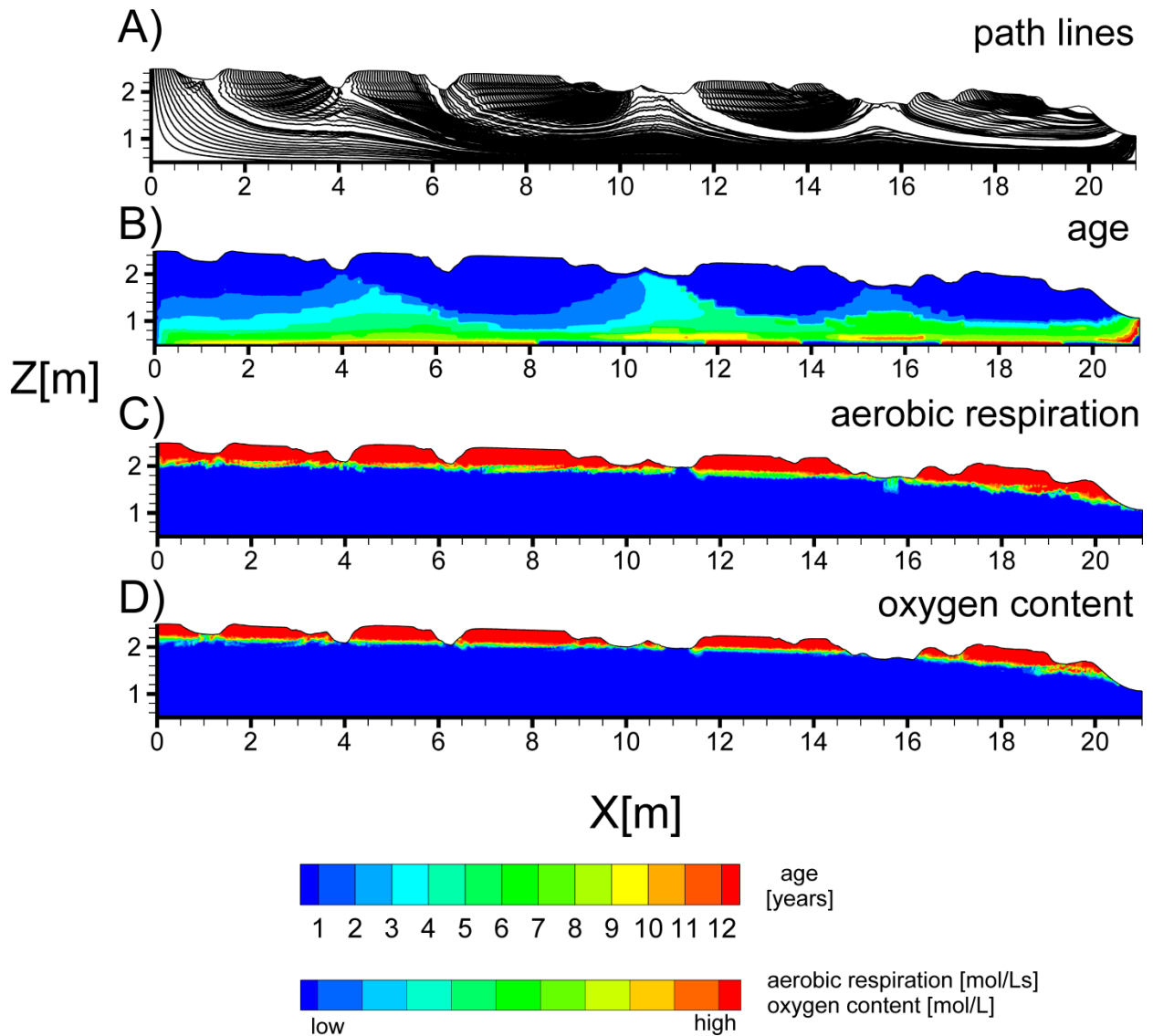
Figure A2:. *Results of the biogeochemical simulations shown for the denitrification of the micro-topography scenario with the mean length 0.5 m. PHREEQC simulations were performed along the flow paths shown in A. Results were interpolated into the 2D cross sections. B shows the age distribution in years of subsurface flow derived from backward particle tracking. Nitrate concentrations in mol/L are shown in C. For denitrification the process activity could not be plotted because turnover of nitrate occurs very fast (below five days). Denitrification, actually is simulated within PHREEQC but visualization of process activity is only possible if the complete turnover of a species last longer than five days.*
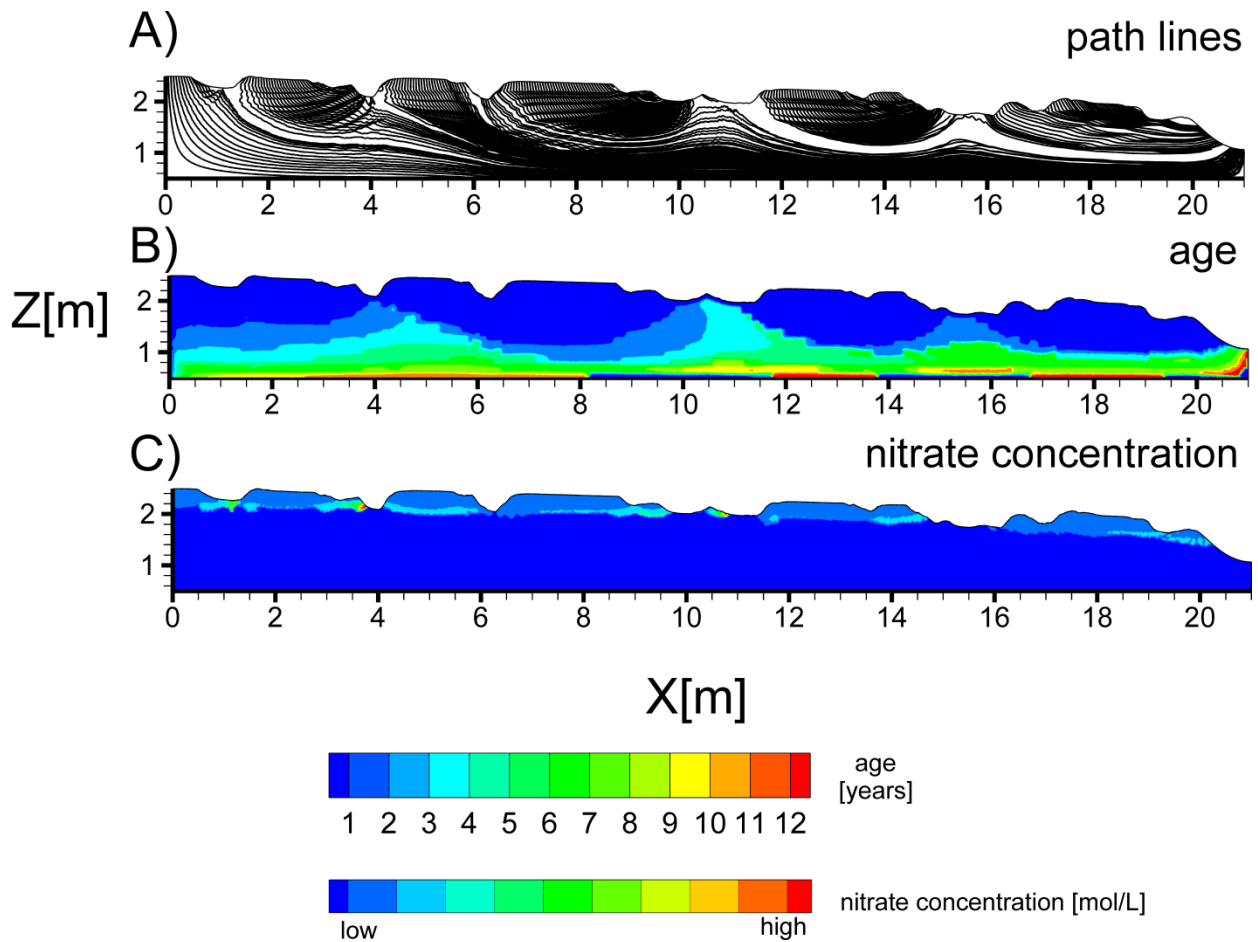
Figure A3: *Results of the biogeochemical simulations shown for the iron(III) reduction of the micro-topography scenario with the mean length 0.5 m. PHREEQC simulations were performed along the flow paths shown in A. Results were interpolated into the 2D cross sections. B shows the age distribution in years of subsurface flow derived from backward particle tracking. Iron(III) reduction rates in mol/Ls are shown in C. Iron(III) and iron(II) concentrations in mol/L are shown in D and E respectively.*

Figure A4: *Results of the biogeochemical simulations shown for the iron(II) oxidation of the micro-topography scenario with the mean length 0.5 m. PHREEQC simulations were performed along the flow paths shown in A. Results were interpolated into the 2D cross sections. B shows the age distribution in years of subsurface flow derived from backward particle tracking. Iron(II) oxidation rates in mol/Ls are shown in C. Iron(III) and iron(II) concentrations in mol/L are shown in D and E respectively. Dissolved oxygen concentrations in mol/L are shown in F*
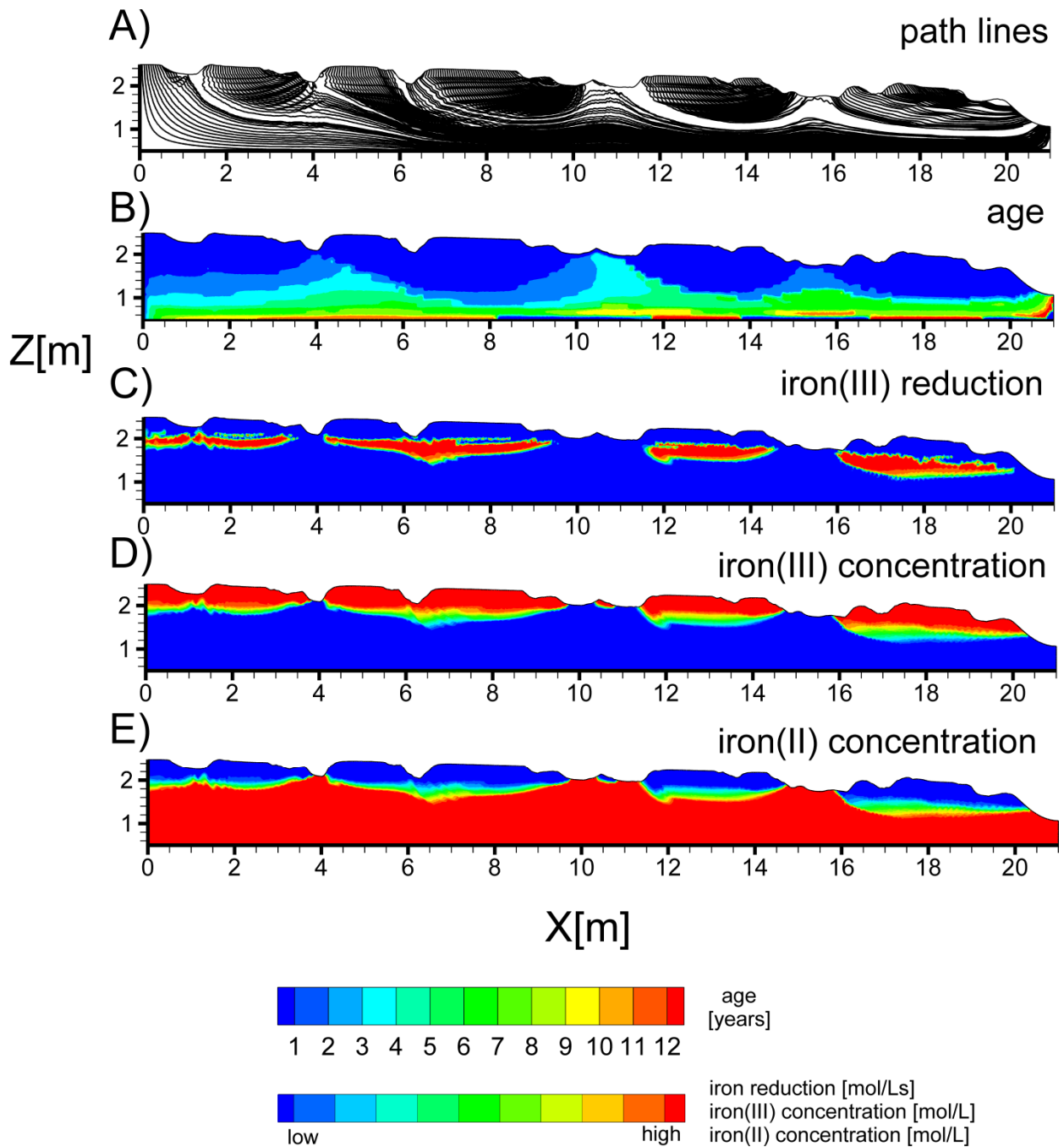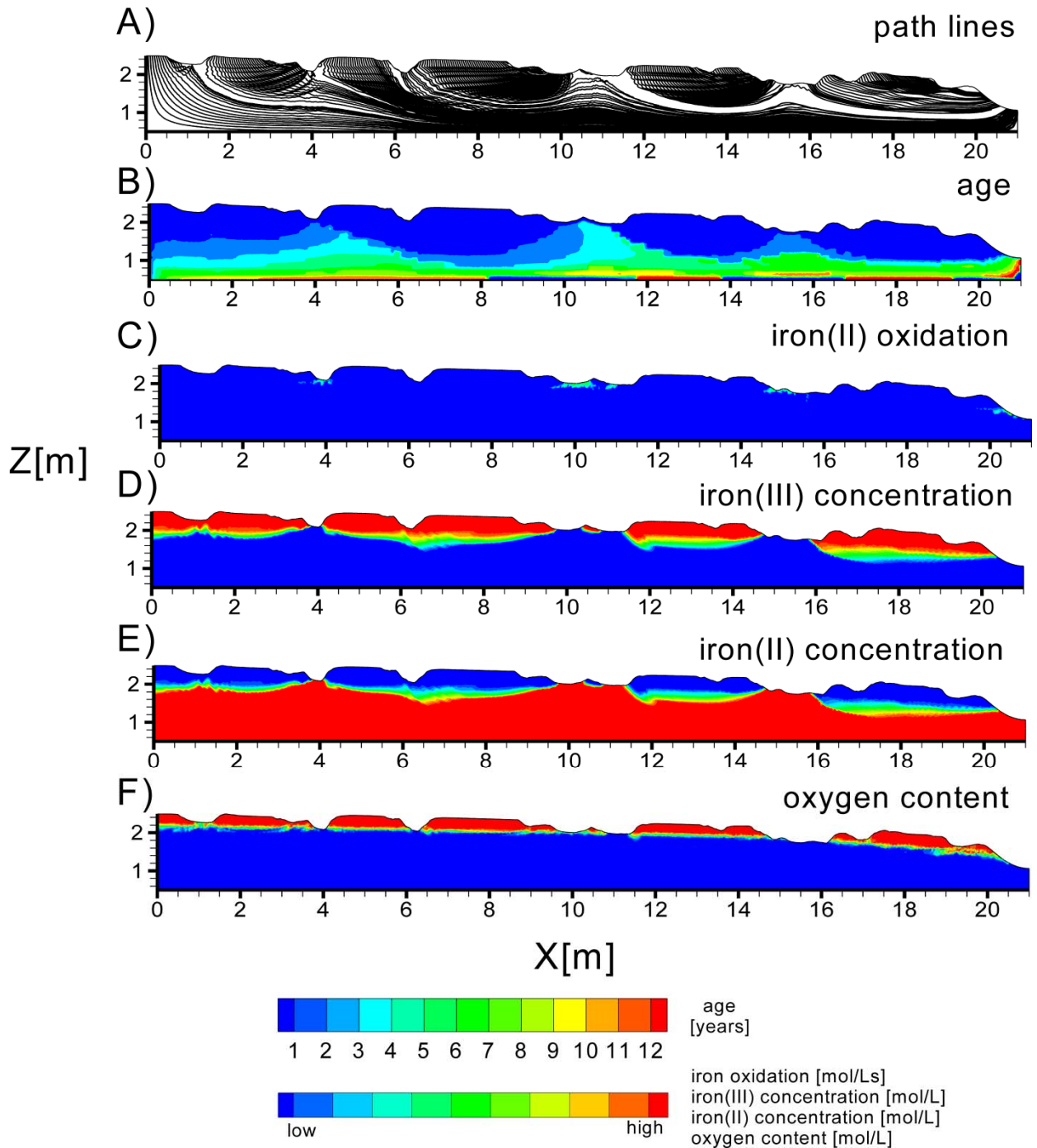
Figure A5: *Results of the biogeochemical simulations shown for the nitrification of the micro-topography scenario with the mean length 0.5 m. PHREEQC simulations were performed along the flow paths shown in A. Results were interpolated into the 2D cross sections. B shows the age distribution in years of subsurface flow derived from backward particle tracking. Nitrification rates in mol/Ls are shown in C. Ammonium concentrations and nitrate concentrations in mol/L are shown in D and E respectively. Dissolved oxygen concentrations in mol/L are shown in F.*
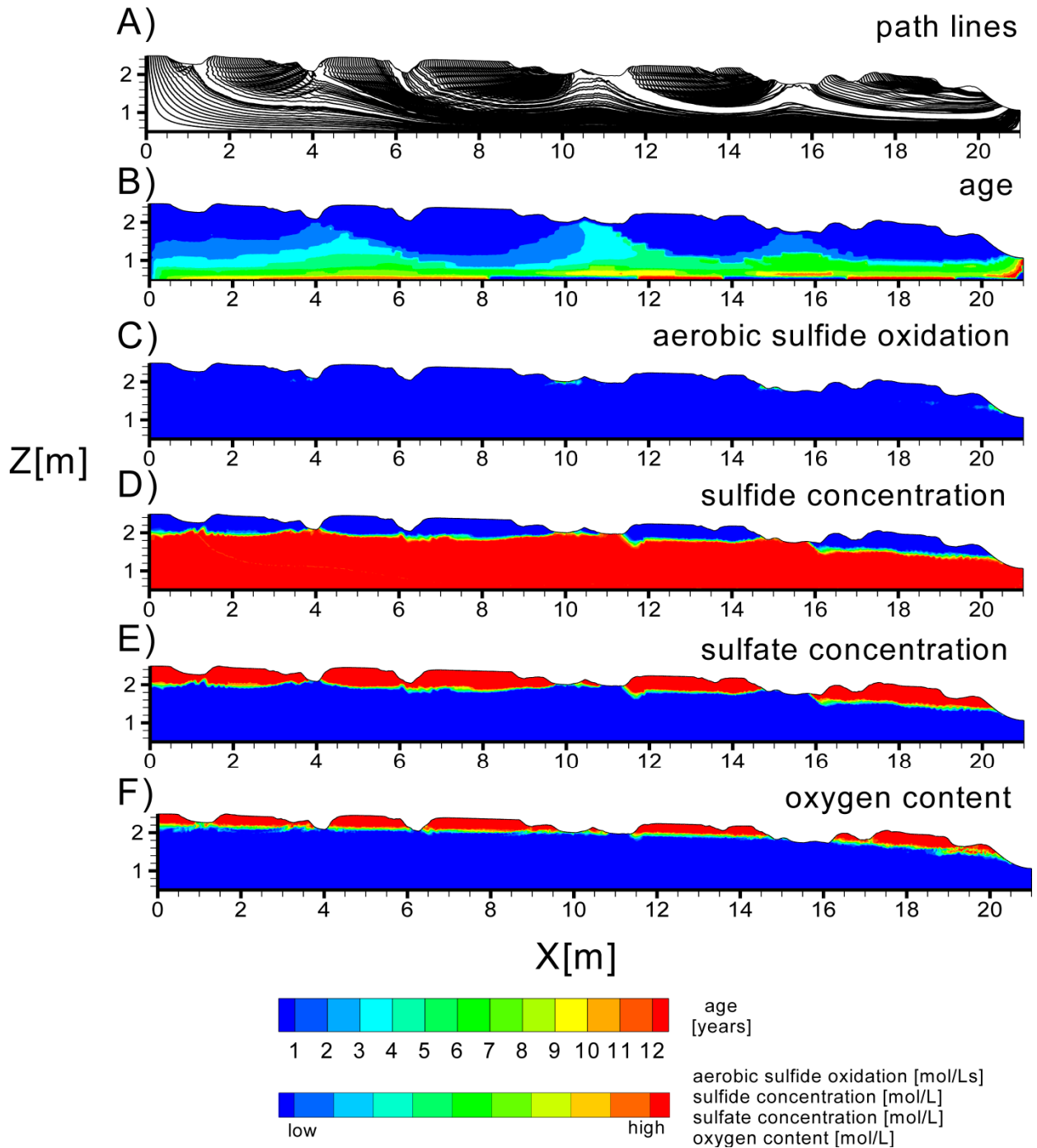
Figure A6: *Results of the biogeochemical simulations shown for the aerobic sulfide oxidation of the micro-topography scenario with the mean length 0.5 m. PHREEQC simulations were performed along the flow paths shown in A. Results were interpolated into the 2D cross sections. B shows the age distribution in years of subsurface flow derived from backward particle tracking. Aerobic sulfide oxidation rates in mol/Ls are shown in C. Sulfide concentrations and sulfate concentrations in mol/L are shown in D and E respectively. Dissolved oxygen concentrations in mol/L are shown in F.*
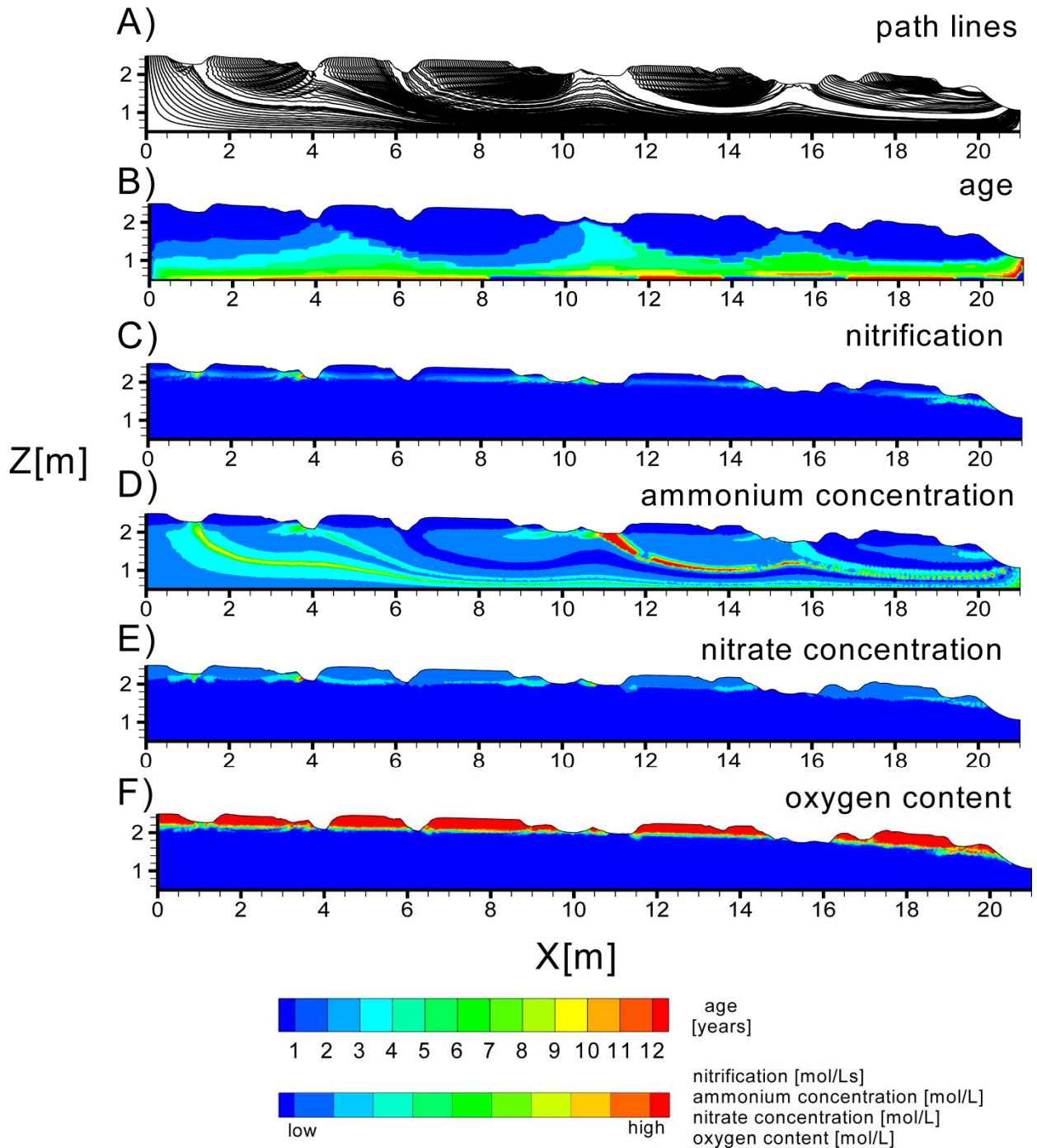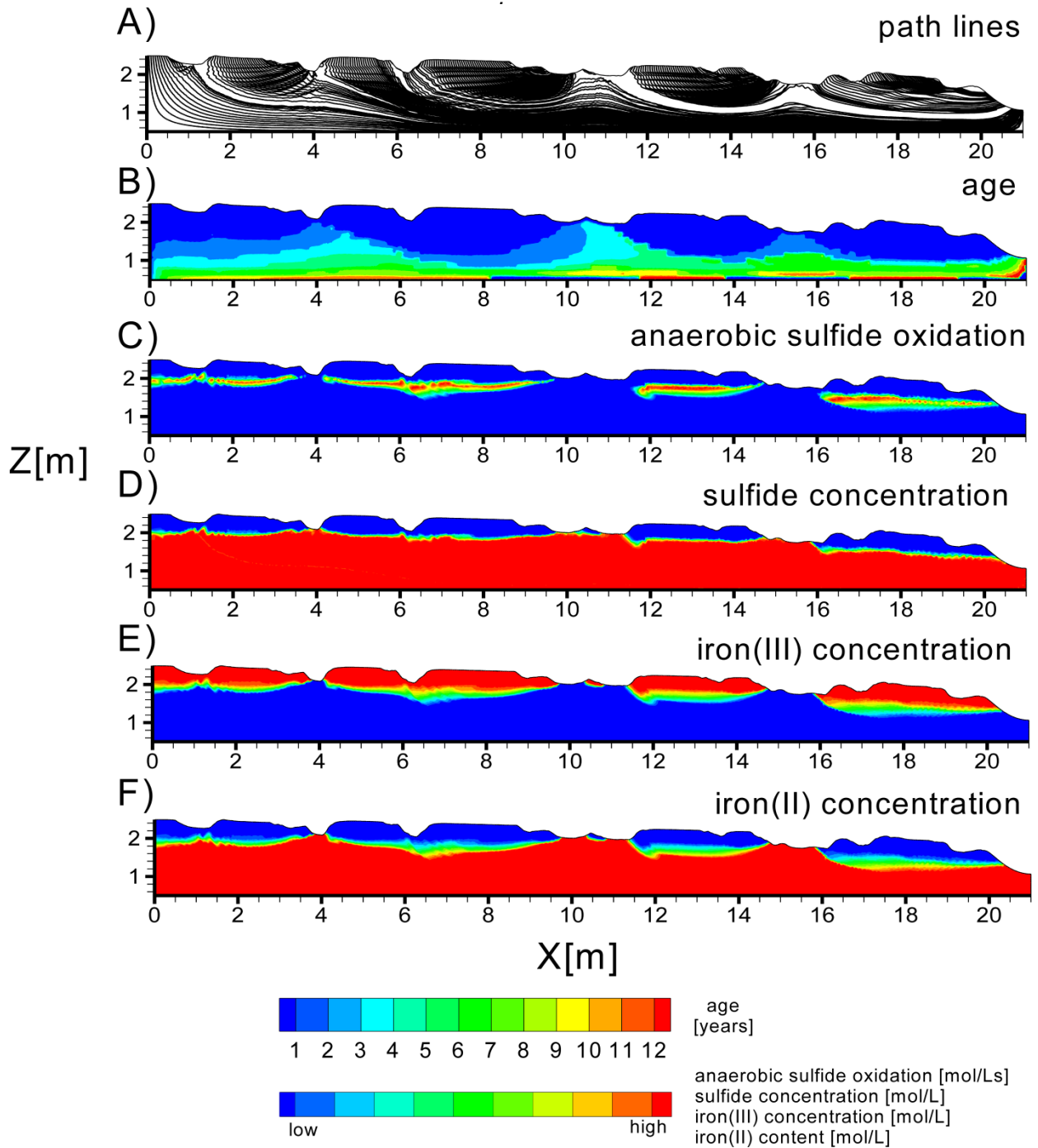
Figure A7: *Results of the biogeochemical simulations shown for the anaerobic sulfide oxidation of the micro-topography scenario with the mean length 0.5 m. PHREEQC simulations were performed along the flow paths shown in A. Results were interpolated into the 2D cross sections. B shows the age distribution in years of subsurface flow derived from backward particle tracking. Anaerobic sulfide oxidation rates in mol/Ls are shown in C. Sulfide concentrations, iron(III) and iron(II) concentrations in mol/L are shown in D-F respectively.*

Figure A8: *Top view for the micro-topography scenarios and the planar reference. Micro-topography is shown in categories, red for hummock and blue for hollow structures. Additionally, for the planar reference the linear slope is shown. Black areas to the ride sides represent areas of aerobic respiration hot spots relative to their surroundings. Aerobic respiration can only occur if oxygen is present. Below hummocks a variably saturated zone with high oxygen contents is stable where preferential aerobic respiration occurs. Zones below hollows usually are water saturated where no oxygen is available for aerobic respiration.*

Figure A9: *Top view for the micro-topography scenarios and the planar reference. Micro-topography is shown in categories, red for hummock and blue for hollow structures. Additionally, for the planar reference the linear slope is shown. Black areas to the ride sides represent areas of preferential iron(III) reduction (hot spots) relative to their surroundings. The patchy pattern develops because Iroon(III) reduction preferentially occurs below hummock structures because of higher iron(III) abundance. Below hollows upwelling water is rich in reduced iron species (Iron(II)).*
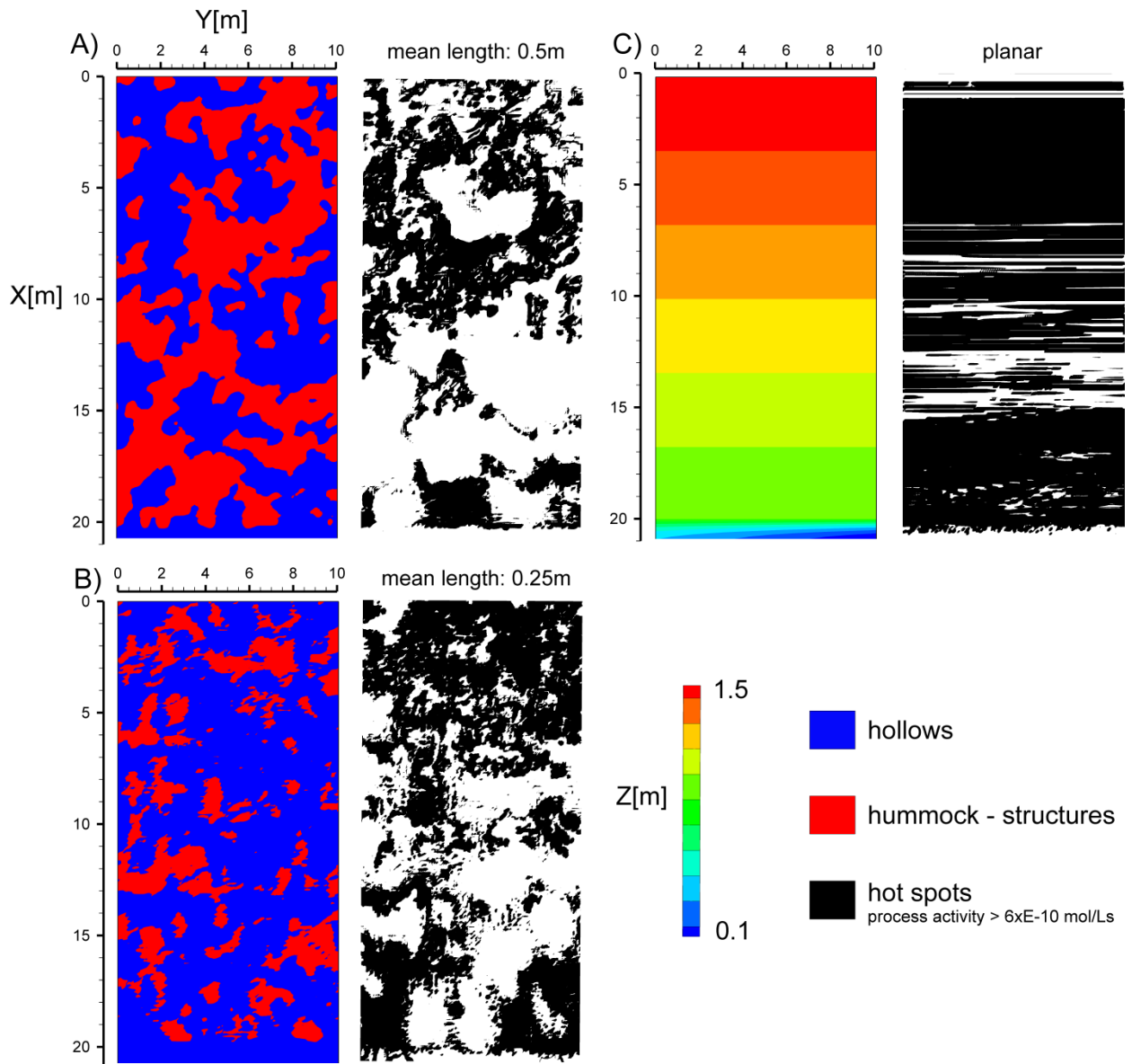
Figure A10: *Top view for the micro-topography scenarios and the planar reference. Micro-topography is shown in categories, red for hummock and blue for hollow structures. Additionally, for the planar reference the linear slope is shown. Black areas to the ride sides represent areas of preferential ammonium oxidation (hot spots) relative to their surroundings.*
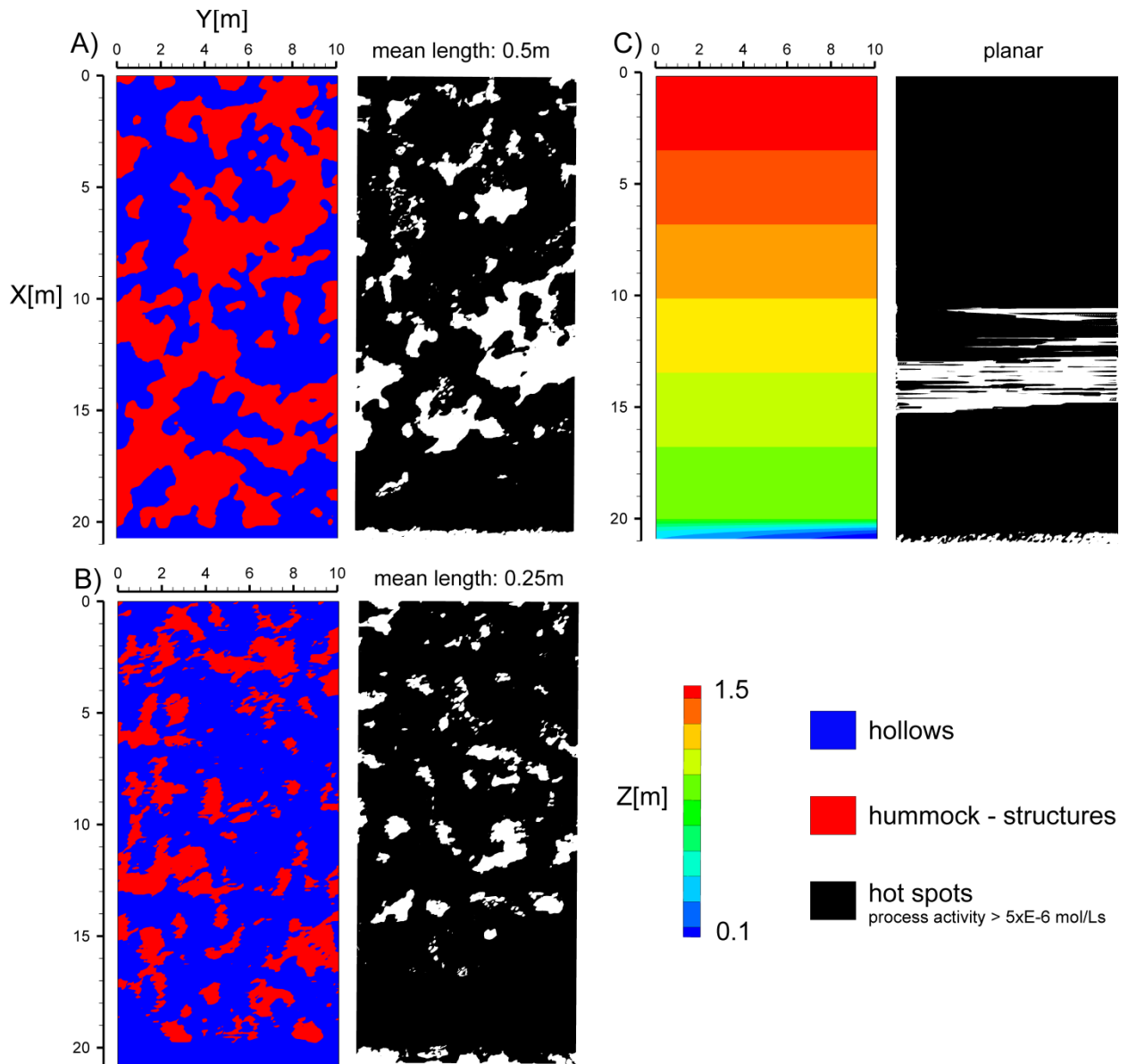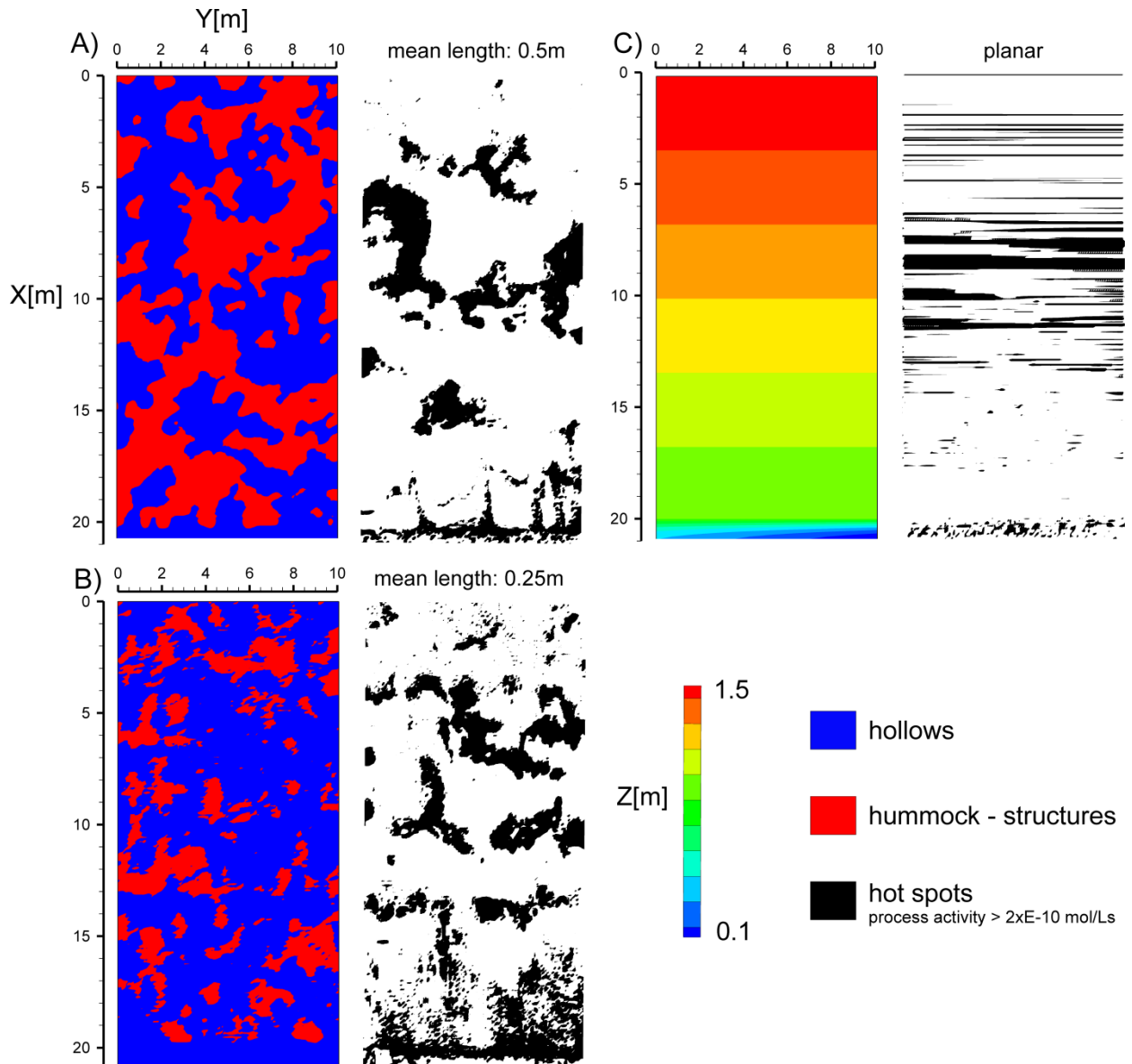
Figure A11: *Top view for the micro-topography scenarios and the planar reference. Micro-topography is shown in categories, red for hummock and blue for hollow structures. Additionally, for the planar reference the linear slope is shown. Black areas to the ride sides represent areas of preferential iron(II) oxidation (hot spots) relative to their surroundings.*
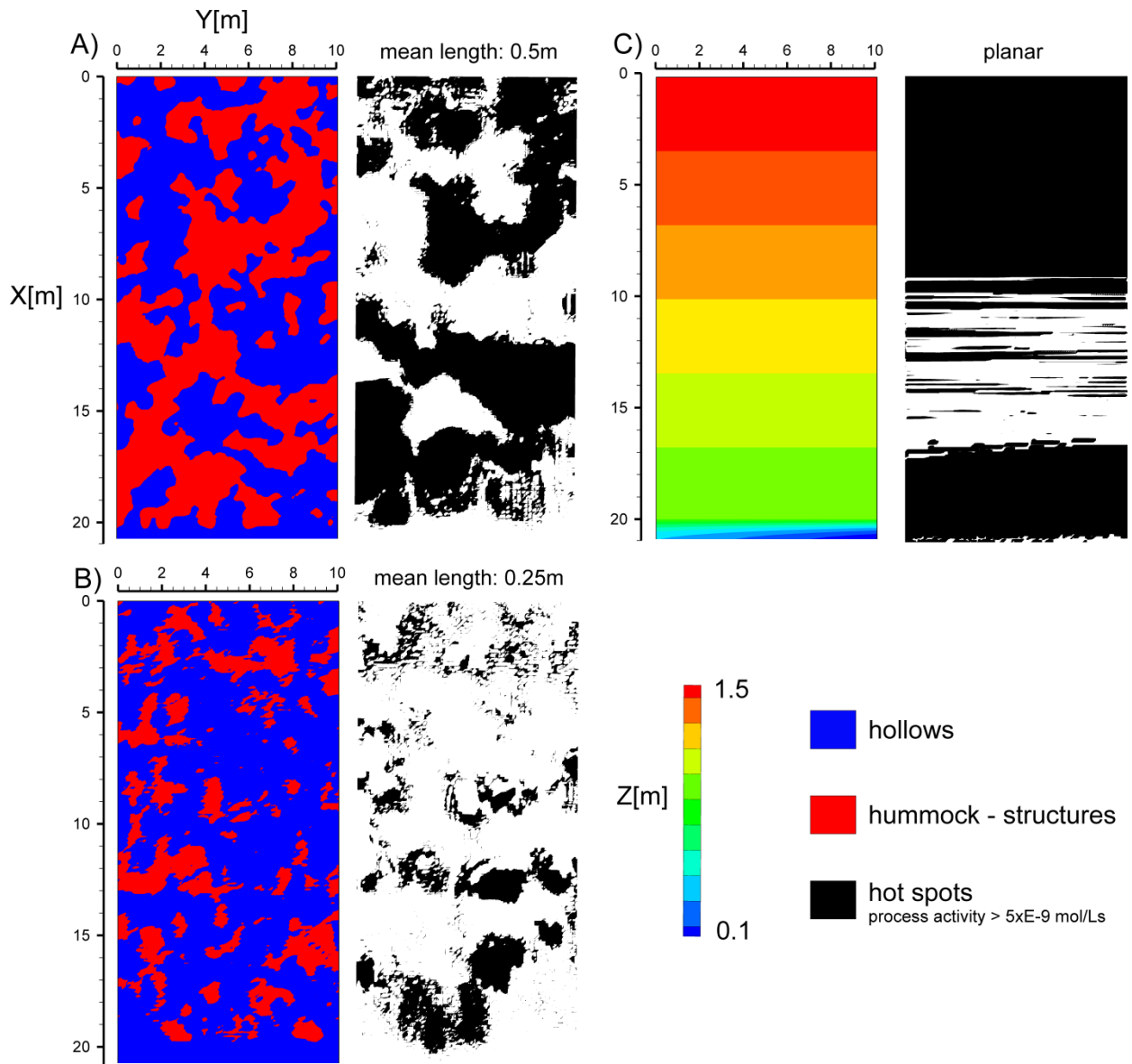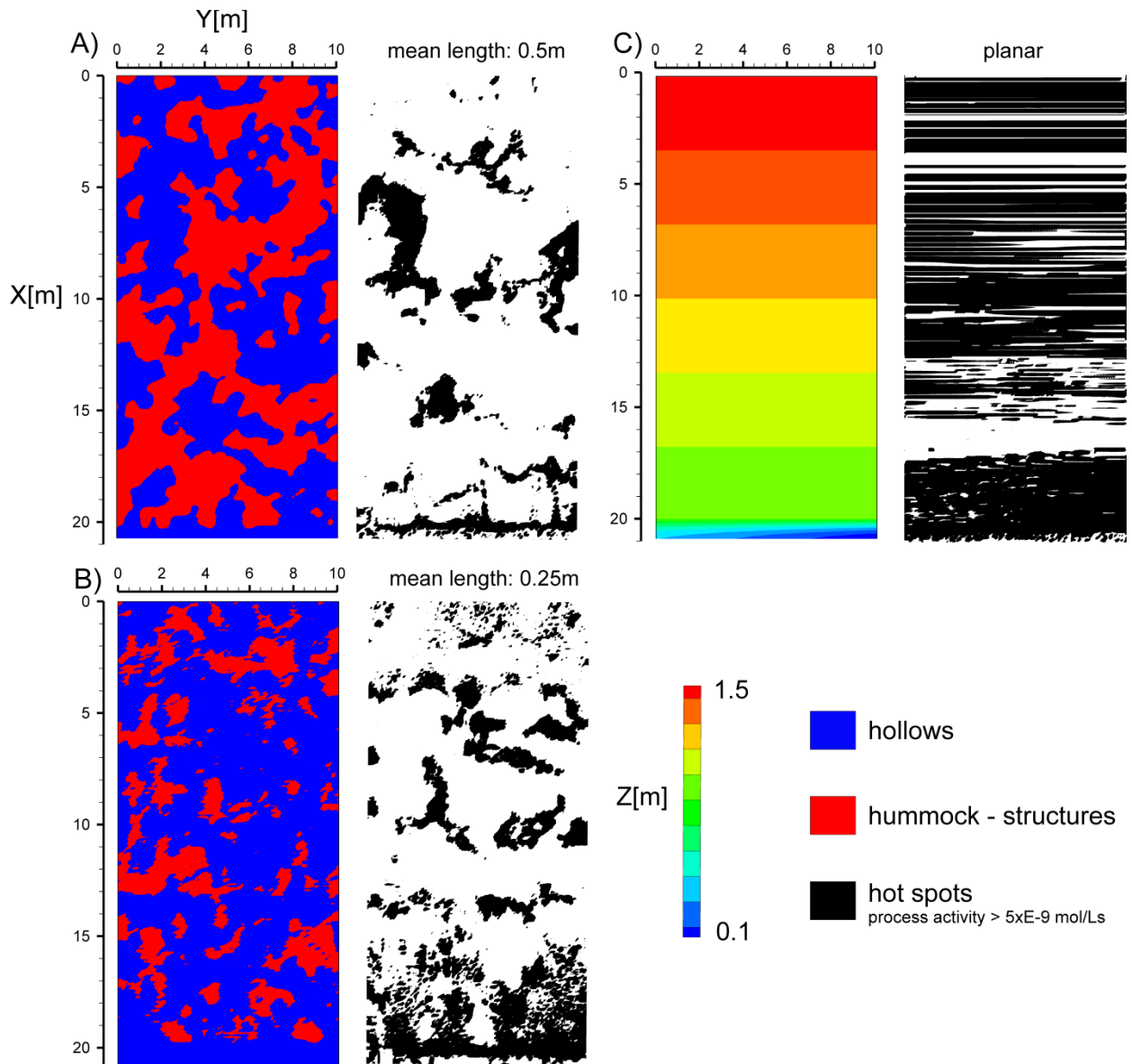
Figure A12: *Top view for the micro-topography scenarios and the planar reference. Micro-topography is shown in categories, red for hummock and blue for hollow structures. Additionally, for the planar reference the linear slope is shown. Black areas to the ride sides represent areas of preferential sulfide oxidation (hot spots) relative to their surroundings.*
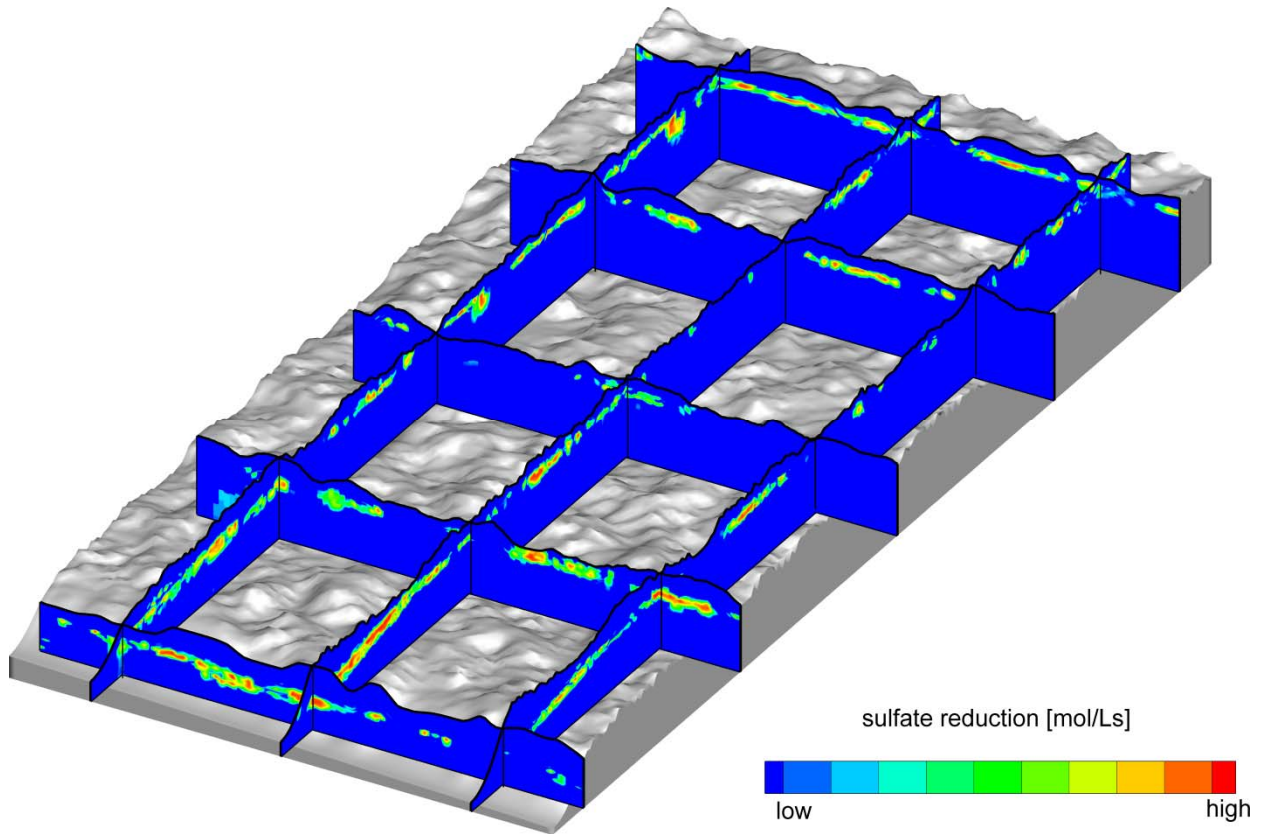
Figure A13:*. Fence plots showing the zones of preferential sulfate reduction for the whole 3D domain of the mean length 0.25 m model.*
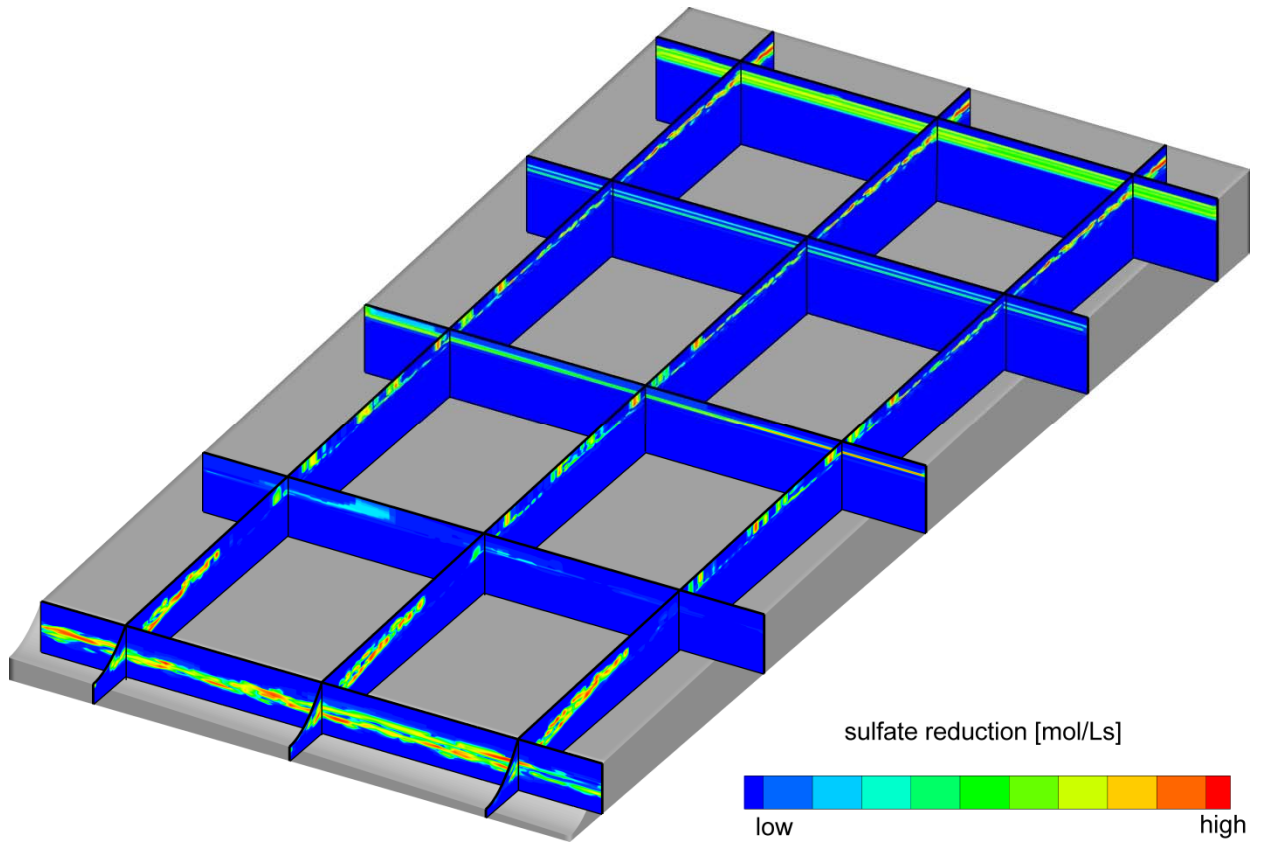
Figure A14: *Fence plots showing the zones of preferential sulfate reduction for the whole 3D domain of the planar reference model*

Study 3

Representing effects of micro-topography on runoff generation and subsurface flow patterns by using superficial rill storage height variations.

By Sven Frei and Jan H. Fleckenstein

Ready for submission to Environmental Modelling & Software

Ready for submission to Environmental Modelling & Software

Representing effects of micro-topography on runoff generation and subsurface flow patterns by using superficial rill storage height variations.

Frei[1], S. and Fleckenstein[2]. J.H.

[1] Department of Hydrology, University of Bayreuth, Germany

[2] Department Hydrogeology, Helmholtz-Center for Environmental Research – UFZ, Germany

Abstract

An adequate representation of micro-topography in spatially-explicit, physically-based models can be crucial in modeling runoff generation, surface/subsurface flow interactions or subsurface flow patterns in hydrological systems with pronounced micro-topography. However, representation of micro-topography in numerical models usually requires high grid resolutions to capture relevant small scale variations in topography at the range of centimeters to meters. High grid resolutions usually result in longer simulation times, especially if fully integrated model approaches are being used, where the governing partial differential equations for surface and subsurface flow are solved simultaneously. This often restricts the implementation of micro-topography to plot scale models where the overall model domain is small to minimize computational cost resulting from a high grid resolution. In this study an approach is presented where a highly resolved digital elevation model (DEM) for a hummocky topography in a plot scale wetland model (10m x 21m x 2m), is represented by spatially distributed rill storage zones in a numerical model with a planar surface. By replacing the micro-topographic DEM with spatially distributed rill storage zones, important effects of micro-topography on surface flow generation and subsurface transport characteristics (e.g. residence time distributions) are being preserved, while at the same time the number of computational nodes is reduced significantly. Results indicate that the rill storage concept may be an appropriate tool to represent micro-topography in plot scale models more efficiently because model runtimes drop significantly. Because important aspects of micro-topography induced surface and subsurface flow processes, principally can be mimicked by applying the rill storage concept on a coarser grid, it may also be a useful tool to represent micro-topography in numerical flow models beyond the plot scale.

1 Introduction

Surface topography significantly controls surface and subsurface flow processes at various scales. Topography was identified to influence residence times and transport processes in catchments (Kirchner et al., 2001, Haggerty et al., 2002, McGuire et al., 2005, Wörman et al., 2006, Cardenas and Wilson, 2007), which in turn are important controls for retention and degradation of contaminants in groundwater. A strong topographic relationship between the mean residence times and topographic flow path gradients was described by McGuire et al. (2005), where residence times in general decrease with increasing topographic gradients. On the very small scale, surface properties with the dimensions of centimeters to meters like for example in-channel bedforms such as ripples or dunes were identified to be important controls for hyporehic exchange in stream ecosystems (Salehin et al., 2004, Cardenas, 2008). Experimental, as well as modeling studies, which investigated how system specific properties like the extend of the vadose zone (Kollet and Maxwell, 2008b), subsurface heterogeneity (Haggerty et al., 2000) or topography (Wörman et al., 2006, Kollet and Maxwell, 2008b, Kirchner et al., 2001) influence subsurface flow patterns, residence times and transport processes at different scales, describe a common characteristic in the behavior of the system that is independent of the scale of observations. This characteristic, which was described by Kirchner et al. (2000), is called fractal behavior or fractal scaling and is related to the long term memory of hydrologic systems due to extremely slow groundwater transport mechanisms. Hydrologic systems, showing fractal behavior, usually show typical power law distributed subsurface residence times (Kirchner et al., 2001, Cardenas, 2008, Kollet and Maxwell, 2008b). Across the different spatial scales, time scales of subsurface transport of course do vary, however the statistical distribution of subsurface residence times in systems showing fractal behavior, does not. Power law distributed residence times were reported for hyporehic exchange processes, induced by small scale (10 cm) in-channel bed forms (Cardenas, 2008), for transport through channel bend deposits (10m) (Cardenas, 2008) as well as for transport processes at the watershed-scale (Cardenas, 2008, Kollet and Maxwell, 2008b). Cardenas and Wilson (2007) and Kollet and Maxwell (2008b) have shown that surface topography has the potential to induce groundwater flow with fractal behavior and power law distributed subsurface residence times, even if the subsurface is homogenous. Cardenas and Wilson (2007) explained the fractal behavior by the presence of persistent stagnation points in the subsurface flow field where flow velocities are extremely low or even zero. Such stagnation points can be induced by surface topography and are responsible for subsurface velocity distributions that span a wide range of time scales, which will finally lead to fractal scaling and power law distributed residence times (Cardenas and Wilson, 2007).

The impact of small scale, topographical structures with dimensions of centimeters to meters (commonly referred to as micro-topography or micro-relief) on surface/subsurface flow processes and interactions, in years have become the focus of several studies. One of the first studies, that

investigated effects of micro-topography on infiltration and runoff generation, was Dunne et al. (1991). They showed how infiltration and hill slope runoff generation was controlled by an intricate interplay between rainfall intensity, surface flow depth, vegetation cover and the specific micro-topography. Devito and Hill (1999) showed that micro-topography in wetlands can be responsible for small scale variations of the water table elevation and peat saturation, which in turn can control the generation and mobilization of sulfate during summer droughts. Micro-topography also seems to play a significant regulating role in the generation of surface runoff (Dunne et al., 1991, Hairsine et al., 1992, Feyen et al., 1999, Govers et al., 2000, Kværner and Kløve, 2008) by buffering incoming precipitation and attenuating and delaying surface flows which modifies shape and volume of catchment surface runoff response (Abedini et al., 2006). Micro-topography induced surface runoff generation was identified to be a threshold-controlled process, where local depressions first need to be filled before any surface flow towards the stream channel is being initiated (Fiedler and Ramirez, 2000, Antoine et al., 2009, Frei et al., 2010). The dynamics of surface flow generation for micro-topographic surfaces under fluctuating climatic boundary conditions were found to be highly complex. Frei et al. (2010) found a highly non-linear and hysteretic relationship between micro-topographically controlled surface flow generation and the depression storage (water volume stored in local depressions) of the micro-relief. In their modeling study, Frei et al. (2010) investigated, under which boundary conditions (rainfall intensity and depth of the riparian groundwater table) surface runoff is being generated for a hummocky topography of a riparian wetland. Surface runoff, in their simulations, was generated mostly under wet initial conditions or during very intensive rainstorm events which are capable of exceeding a critical amount of depression storage at which surface runoff is initiated. Soleī-Benet et al. (1997), Antoine et al. (2009) and Frei et al. (2010) reported that surface runoff for micro-topographies occurs in defined micro-channels and extended surface flow networks (build by interconnected ponded depressions), which dynamically expand and shrink in a spill and fill mechanism. Micro-channeling effects were reported for infiltration excess (Soleī-Benet et al., 1997) as well as for saturation excess (Frei et al., 2010) surface flow generation. Further, micro-topography and its influence on surface/subsurface flow interactions can be responsible for complex head distributions in the subsurface resulting in complex subsurface flow patterns as it has been reported for streambed topographies (Salehin et al., 2004, Cardenas and Wilson, 2007, Wörman et al., 2006) and below hollow and hummock structures of in riparian wetlands (Frei et al., in press). For riparian wetlands, with their complex biogeochemistry, such distinct subsurface flow patterns, induced by the small scale elevation variations of the superficial micro-topography, can have a very profound impact on internal nutrient cycling and biogeochemical transformation of redox-sensitive solutes like sulfate, nitrate or dissolved organic carbon (DOC) (Frei et al., in press).

Although, effects of micro-topography like attenuation of surface flow, buffering of rainfall or the induced subsurface flow patterns take place at limited spatial extend, their significance for the overall

hydrology of catchments should not be neglected. Bronstert and Plate (1997), Nakayama and Watanabe (2006) and Sharratt et al. (1999) stated that an accurate forecast of runoff production, both qualitatively and quantitatively, of catchments or hillslopes can only be achieved, if the specific influence of micro-topography in hydrological models is being accounted for.

So far, several modeling studies have addressed the effects of micro-topography on hydrological processes. More conceptual modeling approaches were used in Dunne et al. (1991) to simulate overland flow and infiltration processes for a uniform sinusoidal micro-topography. Spatially-explicit, physically-based approaches focusing on representing overland flow by solving the two dimensional depth-averaged dynamic wave equations were used in Esteves et al. (2000), Fiedler and Ramirez (2000) and Antoine et al. (2009). Spatially-explicit, physically-based and integrated models, which are capable of simultaneously representing surface and subsurface flow processes were used in Qu and Duffy (2007) and Frei et al. (2010). Each of the aforementioned studies represented micro-topography at the plot scale using different geostistical approaches to represent micro-topography like Kriging interpolation (Weiler and Naef, 2003), Gaussian methods (Antoine et al., 2009), a combination of fractal and Markov-Gaussian processes (Abedini et al., 2006) or Markov Chain models of transitions probabilities (Frei et al., 2010). Especially the representation of micro-topographical effects in fully integrated models, were the governing partial differential equations (PDEs) for the overland and subsurface flow domains are solved simultaneously, has proven to be computationally extremely demanding. Frei et al. (2010) for example reported excessively long simulation runtimes of almost two month for solving a yearly modeling scenario. The high effort, necessary to represent micro-topography in spatially-explicit hydrological models, restricts the application to small scales. However, to reduce the computational and numerical complexity and in order to account for micro-topography beyond the plot scale in regional or watershed models, which is necessary for an accurate prediction of runoff production (Bronstert and Plate, 1997, Nakayama and Watanabe, 2006, Sharratt et al., 1999), a new approach in representing micro-topography in numerical flow models is required.

In this study, we want to introduce an approach were micro-topography and its influence on surface and subsurface flow, in numerical flow models, can be represented more efficiently. For that purpose, the study exemplarily uses the synthetic hydrological/biogeochemical wetland model established in Frei et al. (2010) and Frei et al. (in press) as a test case scenario. Frei et al. (2010) investigated surface runoff generation during rainfall events of variable intensity for a small synthetic wetland section with hummocky topography using a fully integrated surface/subsurface flow model. In a second study, Frei et al. (in press) used a coupled hydrological/biogeochemical model to show, that the micro-topographic controlled interactions between fast surface flow and slower matrix flow, can result in quite complex subsurface flow patterns which are responsible for the formation of local biogeochemical hot spots and a heterogeneous spatial distribution of redox-sensitive solutes. By

applying this new approach to models presented in Frei et al. (2010) and Frei et al. (in press), we want to show that important hydrological controls, induced by surface micro-topography, principally can be mimicked by using a, planar model with a lower grid resolution and superimposed, spatially distributed rill storage height variations. Rill storage is a commonly used concept in numerical flow models to account for retention of surface flow due to vegetation or small scale surface properties (Therrien et al., 2008). As part of this study, two plot scale (10m x 20m) flow models with different spatial resolutions, simulating surface and subsurface flow interactions for a common hydrological year, were set up using the rill storage concept to represent micro-topography. The models with planar surfaces and superimposed rill storage height variations are compared to a model, which uses a highly resolved three-dimensional DEM for representation of micro-topography and a planar reference case without rill storage height variations. Specifically we want to show that the introduced rill-storage concept is basically able to (1) mimic the dynamics and spatial patterns of surface flow generation (micro-channeling effects); (2) accurately represent typical subsurface flow patterns and residence time distributions; (3) represent important biogeochemical patterns that are induced by micro-topography (hot spot formation). Findings from this study may help modelers to better account for micro-topography in numerical flow models because the rill storage concept offers possibilities where high model grid resolutions can be circumvented which results in significantly reduced computation times.

2 Materials and Methods

This study combines numerical flow modeling for integrated simulation of surface and sub-surface flow processes with geostatisitcal indicator simulations to define zones of variable rill storage height to represent surface micro-topography. For the characterization of sub-surface flow patterns, particle tracking was used. Results of the numerical flow model were coupled to a biogeochemical model based on the sequential stream tube approach described in Frei et al. (in press). Detailed information about the numerical flow code, the applied geostatistical approaches and the concept of coupling subsurface hydrology and biogeochemistry are given in Frei et al. (2010) and Frei et al. (in press) and are only briefly summarized in this section.

2.1 Surface/Subsurface Flow Simulations

Surface and subsurface hydrology was simulated for a hypothetical section of a riparian wetland representing a field site in the Lehstenbach experimental catchment in south eastern Germany (Gerstberger, 2001). The numerical code HydroGeoSphere (Therrien et al., 2008), subsequently referred to as HGS, was used to simulate surface and subsurface hydrology. HGS is a fully integrated numerical surface-subsurface flow model, which is increasingly used within the hydrologic/hydrogeologic community. Variably saturated flow in porous media is simulated by solving the Richards Equation in three dimensions. Overland, flow in two dimensions, is implemented using the diffusion wave approximation to the depth averaged dynamic wave equations (Therrien et al., 2008). Coupling of the surface and sub-surface domains is implemented via the conductance concept assuming that the exchange flux depends on the gradient across a coupling interface, the thickness of the interface (coupling length), its relative permeability and the vertical saturated hydraulic conductivity (Therrien et al., 2008). Governing equations for variably saturated subsurface and surface flow are solved simultaneously via a control volume, finite element approach (Therrien et al., 2008). As part of this study, four different flow models were set up using HGS (a summary is given in Table 1):

(1) The micro-topography model, as presented in Frei et al. (2010), uses a geostatisitcally generated DEM representing highly resolved micro-topographical structures (hollow and hummocks). The model was generated for a 10m x 20m domain using a regular finite element grid with an uniform grid spacing of 0.1m in X, Y and Z. The micro-topography model was used as a reference to test the rill storage concept against a model with a highly resolved DEM.

(2) A planar reference model was set up using an identical grid resolution compared to the micro-topography model, but here the model was set up using a planar, inclined surface to represent runoff generation and flow conditions without micro-topographical structures and rill storage height variations. The planar reference was used as a reference to compare results for a plain surface.

[158]

(3) The highly resolved, planar model with superficial rill storage height variations (p-rs-high) uses a planar, inclined surface with superimposed, spatially distributed rill storage height variations. This model uses the same grid resolution as the micro-topography model.

(4) The low grid resolution planar model with rill storage height variations (p-rs-low) has a much coarser numerical grid and in contrast to the other models uses irregular finite elements. Average grid spacing was reduced from 0.1 m to 0.4 m leading to a ten fold reduced number of computational nodes (210,000 compared to 20,878).

Table 1: *Characteristics of the different flow models used in this study. All models expect for the p-rs-low model use a regular finite element mesh (regular) with 210,000 computational nodes and constant grid spacing of 0.1 m. The p-rs-low model uses an irregular finite element mesh (irregular) with an average grid spacing of 0.4 m and 20,878 computational nodes.*

	surface type	spatial resolution	grid spacing	nodes (surface nodes)
micro-topography	geostatistically derived DEM representing a hummocky topography of a riprain wetland section	21m x 10m x 2m	0.1m (regular)	210,000 (21,000)
planar reference	planar, inclined surface	21m x 10m x 2m	0.1m (regular)	210,000 (21,000)
planar + rill storage, high resolution (p-rs-high)	planar, inclined surface with superficial rill storage height variations derived from a geostatistical indicator field.	21m x 10m x 2m	0.1m (regular)	210,000 (21,000)
planar + rill storage, low resolution (p-rs-low)	planar, inclined surface with superficial rill storage height variations representing spatial distribution of pronounced hollow and hummock structures	21m x 10m x 2m	0.4m (average) (irregular)	20,878 (1,898)

All flow models use identical boundary and initial conditions: Boundary conditions for the models were assigned so that water can only leave the domain at the channel's outlet (Figure 4). All other boundaries were set to no-flow with the exception of the upper model surface where variable rainfall rates are applied (daily rainfall rates recorded for the hydrological year 2000 in the Lehstenbach catchment Frei et al., 2010). As an initialization for the subsurface flow domain the groundwater level was set to 0.5 m above the horizontal base of the model with an equilibrium pressure distribution above the water table. The whole surface flow domain was initialized with a zero depth of ponded water representing dry initial conditions. The friction slope for surface flow calculations is described using Manning's equation. Manning's roughness coefficients for the peat surface was uniformly assigned as 0.03 m$^{-1/3}$ for x and y; a value reported for densely vegetated surfaces (Shen and Julien, 1993). The peat body in all flow models was represented as homogenous and isotropic using a uniform saturated hydraulic conductivity of 0.2 m/d which is in range of values reported for this site and for typical peat soils in general (Hauck, 1999). Soil retention characteristics for the simulation of variably saturated flow in peat were taken from Price et al. (2010).

2.2   Rill Storage Height Variations

According to its definition, rill storage, which is also known as depression storage represents an amount of surface storage that must be filled first before any lateral surface flow is generated (Therrien et al., 2008). HGS uses a modified equation for surface flow in which rill storage can be accounted for. Surface runoff in HGS is represented by the diffusive wave approximation, subsequently written in vectorial notation (Equation 1). In Equation 1 d_0 represents the water depth of surface flow [L]; q_0 the surface flux [L T^{-1}]; Γ_0 the fluid exchange rate with the subsurface domain [T^{-1}]; Q_0 volumetric flow rate per unit area representing external sinks and sources [L T^{-1}]; ϕ_0 surface porosity [-] and h_0 the water surface elevation [L].

$$-\nabla(d_o q_o) - d_o \Gamma_o + Q_o = \frac{\partial \phi_o h_o}{\partial t} \qquad (1)$$

The surface flux q_0 is given by Equation 2 where K_o is the surface (overland) flow conductance tensor in [L T^{-1}].

$$q_0 = -K_o \nabla(d h_o) \qquad (2)$$

In Equation 1 and 2, h_o can be replaced by Equation 3 where z_o is the elevation of the land surface [L].

$$h_o = z_o + d_o \qquad (3)$$

If the rill storage feature of HGS is being used, d_o in the first term of Equation 1 is estimated by equation 4 where H_d represents the user defined rill storage height [L] according to Figure 1. Equation 4 only affects the first term in equation 1 which means that lateral surface flow only occurs above

elevations $z_o + H_d$ (Figure 1). The terms for in-/exfiltration ($d_o\Gamma_o$), for sinks and sources Q_o are not affected by Equation 4.

$$h_o \leq (z_o + H_d) \qquad \rightarrow \qquad d_o = 0$$

$$\tag{4}$$

$$h_o > (z_o + H_d) \qquad \rightarrow \quad d_o = h_o - (H_d + z_o)$$
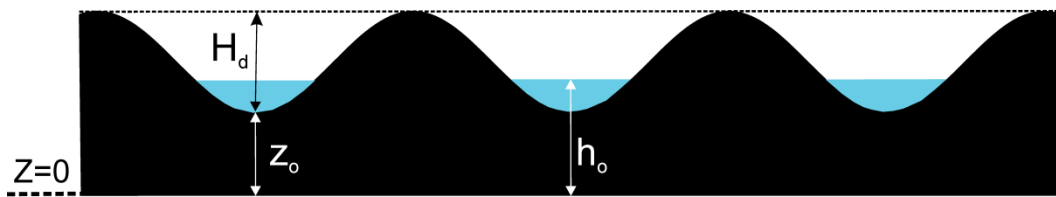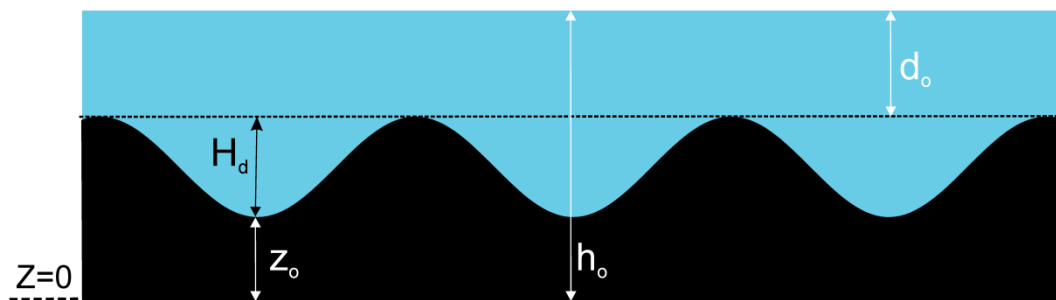
Figure 1: *Rill storage feature as it is implemented in HGS (Equations 1 – 4). Surface flow in models with a defined rill storage height is generated if ponding depths h_0 exceed the rill assigned rill storage height H_d plus the local elevation z_o. Relevant depths of surface flow d_0 are calculated according to equation 4.*

In HGS, it is possible to spatially distribute rill storage heights H_d, which means that different rill storage heights can be assigned to individual finite elements of the surface grid. For the models p-rs-high and p-rs-low rill storage heights are spatially distributed according to Figure 2. For the p-rs-high model geostatistical indicator simulations, originally used in Frei et al. (2010) for generation of the micro-topography DEM, were used to spatially distribute different zones of rill storage heights. For the p-rs-high model, finite elements belonging to the channel segment (blue areas in Figure 2) and to areas with lower relative elevations like deep depressions are assigned a zero rill storage height ($H_d =$ 0 m). For these areas, surface flow can be generated as soon as surface ponding occurs. For transition zones between local depressions and hummocks and shallower depressions, a rill storage height of 0.02 m and 0.01 m (Figure 2) was used respectively. For hummock structures, finite elements were assigned to a rill storage height of 0.1 m (lower) and 0.2 m (higher). For the p-rs-low model only two

different rill storage zones were used to represent micro-topography. Here, the model's surface is separated into elements belonging to depressions including the channel segment (blue areas in Figure 2) and hummocks (red areas in Figure 2). Elements belonging to depression areas and the channel segment were given a zero rill storage height and hummocks a rill storage height of 0.15m.
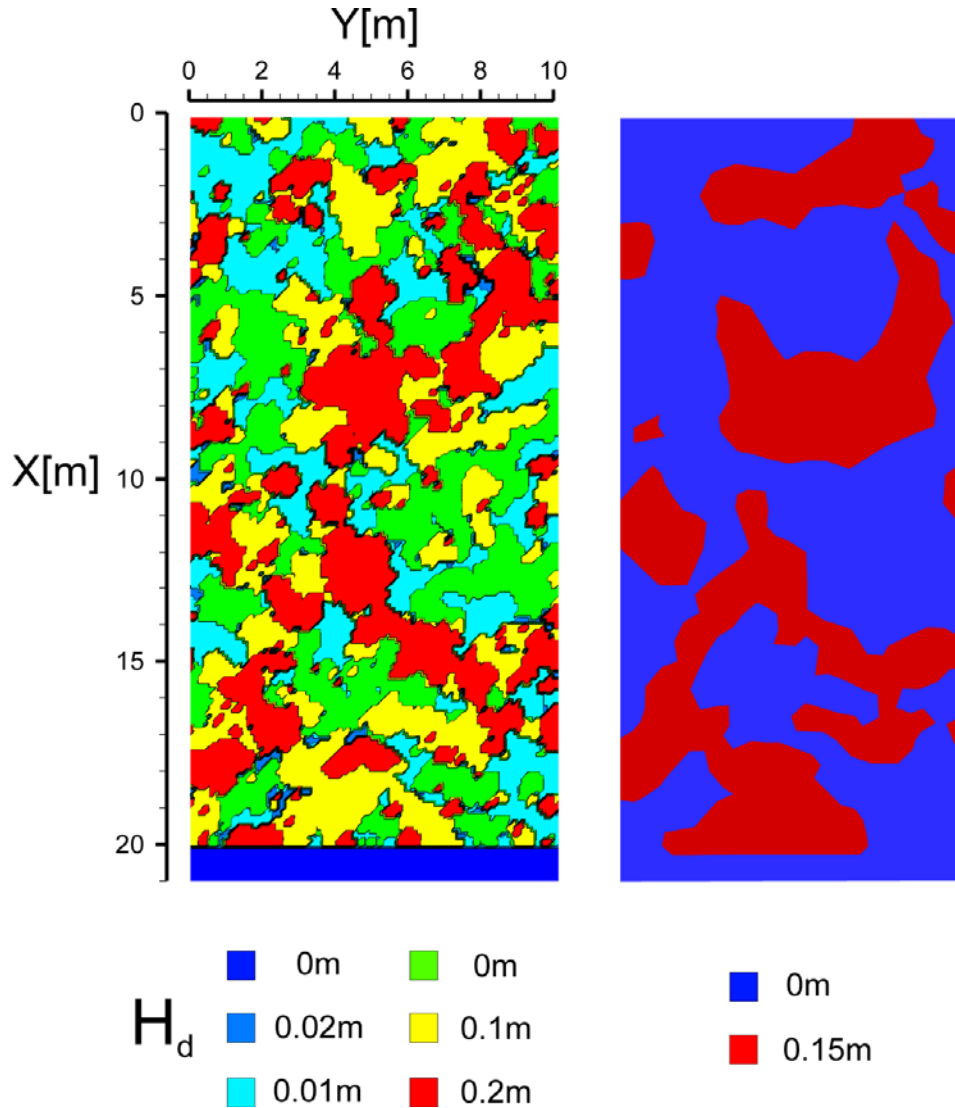
Figure 2: Spatial distribution of rill storage heights, superimposed on top of a planar model for the p-rs-high (left side) and the p-rs-low (right side) model. Rill storage height zones for the p-rs-high model are spatially distributed by using a geostatistical indicator simulation with four different rill storage height values. Zero rill storage height areas represent deep depressions (green) and the stream channel (dark blue). Small rill storage heights are assigned to areas with shallow depressions (turquoise) and to transition zones between depressions and hummocks (bright blue). High rill storage height values are used to define small (yellow) and high (red) hummock structures. Rill storage height zones in the p-rs-low model are distributed to represent the spatially most pronounced hollow (blue) and hummock (red) areas.

2.3   Coupled Hydrological/Biogeochemical Simulations

In Frei et al. (in press) an approach was introduced were a transient subsurface flow field derived from numerical simulations and particle tracking was coupled to the geochemical model PhreeqC (Parkhurst, 1995). In this sequential stream tube approach, redox reactions typically occurring in wetlands (aerobic respiration, denitrification, iron(III)-, sulfate reduction and diverse oxidation reactions) were simulated along isolated subsurface flow path lines, for a set of hydrological and biogeochemical boundary conditions. The same approach was used as part of this study to investigate whether superficially distributed rill storage zones can reproduce the same effects on the spatial re-distribution of redox-sensitive solutes and biogeochemical process in the subsurface as the complex micro-topography reference model.

3   Results and Discussion

According to Frei et al. (2010) and Frei et al. (in press) micro-topography is directly or indirectly responsible for: (1) Complex runoff generation processes during events where saturated overland flow occurs in defined surface flow networks and micro-channels. (2) Characteristic subsurface flow patterns as a result of micro-topography moderated surface/subsurface flow interactions. (3) Formation of biogeochemical hot spots as a result of the interactions between micro-topography moderated surface/subsurface flow and biogeochemical processes in the subsurface. To assess how good micro-topographical induced effects can be represented by using a planar surface with superficial rill storage height variations, criteria for a successful representation were formulated based on the findings described in Frei et al. (2010) and Frei et al. (in press): (1) During intensive rainstorm events surface runoff, for the planar models with superficial rill storage height variations, occurs in discrete micro-channels forming extended surface flow networks. Surface flow is not generated as sheet flow, the surface flow process typically assumed for planar surfaces. (2) Micro-topography induced subsurface flow patterns and characteristics, as identified in Frei et al. (in press), can be successfully represented for a planar surface model by applying the rill storage concept. (3) Interactions between surface/subsurface flow and biogeochemistry for simulations with a planar surface and superficial rill storage height variations lead to similar patterns of biogeochemical hot spots as the ones observed for the micro-topography model (Frei et al., in press). (4) The distribution of subsurface residence times is being preserved for a planar model using superficial rill storage height variations compared to the micro-topography model.

3.1   Surface Flow Generation

Figure 3 shows the simulated hydrographs estimated at the channel outlet for the four different simulations. Total discharge is indicated by the circled line and the fraction originating from surface flow by the grey line. Simulations were performed by applying a constant rainfall rate of 0.008 m/d until a steady state discharge at the channel outlet was reached. The rainfall rate represents conditions for a moderate to intense rainstorm event and ensured that in the end of the simulations, the surface flow networks are fully developed. The characteristic kinks in the flow hydrograph of the micro-topography model are related to the dynamic development and maturation of the surface flow networks (Antoine et al., 2009; Frei et al., 2010,) were depressions, after onset of rainfall, are being filled with water before they start to interconnect with each other building surface flow networks that finally spill into the channel segment. The hydrograph of the planar reference model doesn't show the characteristic kinks because here, surface runoff is generated as sheet flow were the whole surface equally contributes to surface runoff. In contrast the planar surface with superficial rill storage height variations creates a flow hydrograph with the same kinks as in the reference model. This indicates that

surface runoff in these simulations is not generated as sheet flow but rather due to dynamically developing surface flow networks, similar to those observed for the micro-topography model.
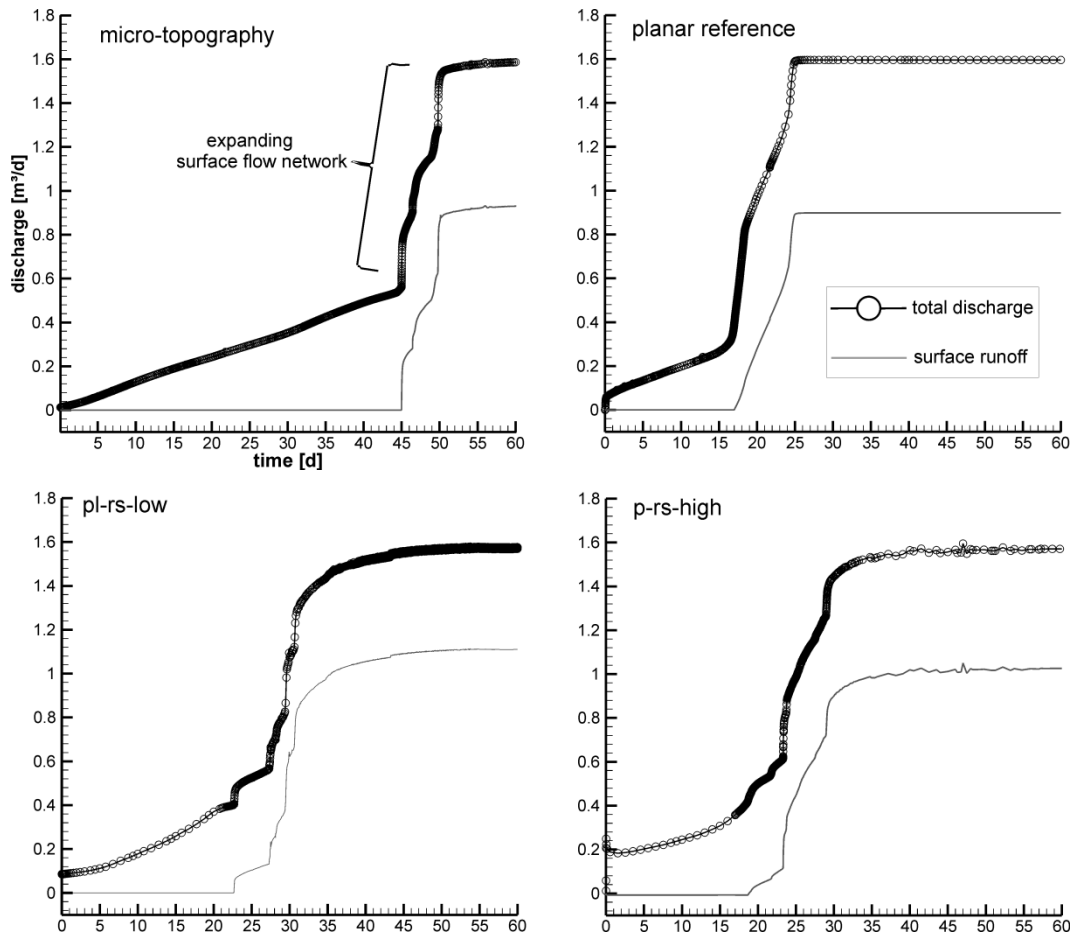
Figure 3: *Flow hydrographs for the steady rainfall simulations. Total discharge, estimated at the channel's outlet (X = 20 m – 21 m / Y = 10 m in Figure 2) is shown as a circled line and the surface flow component which flows superficially into the channel segment is shown as a bright grey line. The kinks in the hydrographs of the micro-topography and the rill storage height models are related to the maturing of surface flow networks and activation of surface flow bridges inter-connecting different ponded depression areas (Figure 4).*

The spatial patterns of the surface flow networks are shown in Figure 4. Snap shots were taken at the end of the uniform rainfall simulations, after reaching steady state conditions where the surface flow networks are spatially fully developed and connected to the channel segment. Yellow lines represent individual surface flow path lines and were used to visualize the spatial extent and direction of the flow networks. Red areas represent spatially extended hummock structures (high rill storage heights) and blue areas depressions (low rill storage heights). At certain locations, labeled "flow bridges" and indicated by the white dashed lines in Figure 4, surface flow lines in the rill storage and micro-topography models cut across hummock areas. In the simulations isolated, water filled depressions become interconnected by the formation of these distinct flow bridges. During the maturing process of the surface flow networks, individual flow bridges are being activated due to rising groundwater levels and increasing surface ponding. As shown in Figure 4, surface flow networks are fully

developed when all flow bridges are active. The kinks in the hydrographs shown in Figure 3 represent the consequtive activation of different flow bridges resulting in a stepwise increase in discharge due to the expanding drainage area. In contrast to surface flow network drainage, surface runoff for the planar reference is generated as sheet flow where the whole surface is equally affected (Figure 4).
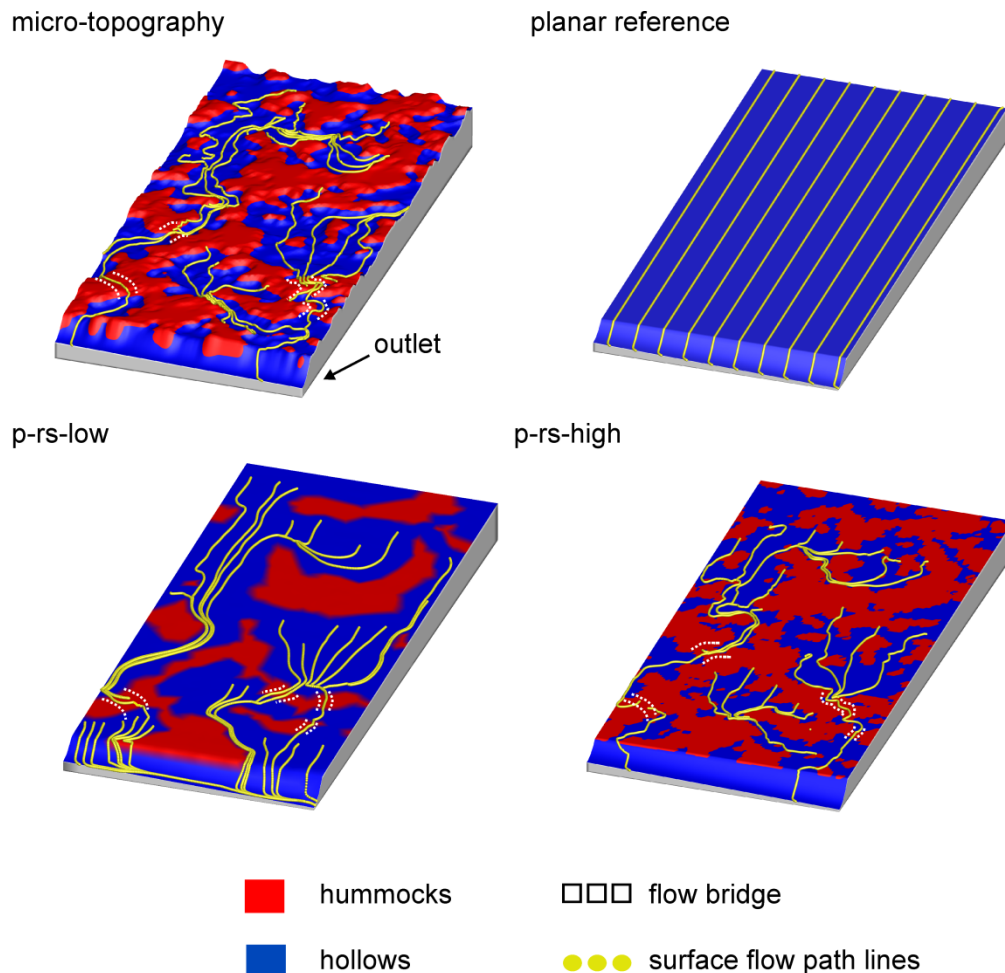
Figure 4: Snap shots taken at the end of the steady rainfall simulations showing the fully developed surface flow networks (yellow) which are generated in the micro-topography model as well as in the models with rill storage height variations but not for the planar reference case. Surface flow networks dynamically develop out of inter-connected, ponded depression areas. Flow bridges (white squares) belong to hummock zones were the inter-connection between ponded depressions occurs by over spilling.

Simulations show, that surface runoff generation for the simulations with superficial rill storage height variations follow the same fill and spill mechanism as demonstrated for surfaces with micro-topography (Antoine et al., 2009; Frei et al., 2010). For the fill and spill mechanism, isolated depressions fill with water before they start to interconnect, building extended surface flow networks which finally spill into the adjacent stream channel. The distinct kinks in the flow hydrograph, caused by the expansion of the surface flow networks (Frei et al., 2010) can be adequately reproduced with a planar model with superficial rill storage height variations. However, results also show that surface runoff is generated much earlier in the simulations (Figure 3) with a planar surface and rill storage

height variations (day 19 and 23) compared to the micro-topography model (day 45). This is due to the fact that attenuation of surface flow and buffering of rainfall inputs is not captured correctly in the simulations with rill storage height variations. This is related to two different aspects: First, hummocks in the micro-topography model are represented as three-dimensional structures where, compared to a flat surface, additional pore space for subsurface water storage is available. This additional pore space is not equally accounted for in the simulations with rill storage height variations. Secondly, the surface storage threshold (depression storage) for water, which must be filled before any surface runoff can be generated is higher for the micro-topography model. Higher storage capacities in the subsurface and surface, both lead to a higher delay of surface runoff in the micro-topography model compared to the rill storage models. Differences in the flow hydrographs among both rill storage models, e.g. a delayed generation of surface flow or differently pronounced kinks in the hydrograph, are the result of the different grid resolutions and the differently assigned rill storage heights used for representation of micro-topography. However, the mechanism of surface runoff generation where surface flow networks are dynamically expanding can be successfully represented for both planar models with rill storage height variations, even if the model's resolution is significantly reduced.

3.2   Subsurface Flow Patterns

For characterization and visualization of subsurface flow patterns, particle tracking was performed based on the transient flow field of the numerical simulations. As described in Frei et al. (in press), particle tracking simulations were carried out for a twenty-five year period, based on a yearly repetitions of the annual simulation with variable rainfall inputs. Results of particle tracking are shown in Figure 5 where subsurface path lines are shown for cross sections taken at the middle of the 3D domain. As described in Frei et al. (in press), superficial micro-topographical structures in wetland systems can be responsible for a spatially very heterogeneous and complex subsurface flow path distribution (shown for the micro-topography plot). During the yearly simulations with variable rainfall inputs, surface near water level fluctuates for the upper 10-30 cm. Simulated water level never rises above the elevation of hummock structures because of the prior generation of surface flow which efficiently drains the wetland stabilizing the groundwater level. This means that hummocks constantly remain unsaturated, even during periods with intensive rainfall rates (Frei et al., 2010). Head gradients below hummock structures are always directed downwards (as shown in Figure 5) which indicates that these areas constantly contribute to infiltration even during very wet conditions. Surface ponding in local depressions, on the other hand, is affected by dynamic fluctuations of the groundwater level, where groundwater even during moderate rainfall events often rises above the elevation of local depressions. During the yearly simulation, most depressions are constantly ponded because of the shallow water table fluctuations. Only during very dry periods in summer, a significant amount of depressions are getting disconnected from the dropping groundwater level. Head gradients below

ponded depressions generally point upwards indicating upwelling conditions. The spatial distribution of preferential in- and exfiltration areas below hummocks and hollows results in the observed subsurface flow patterns, as shown for the micro-topography model in Figure 5. In general, subsurface flow for the micro-topography model can be separated into a shallow and a deep flow system (Frei et al., in press). The subsurface flow paths in the shallow flow system are characterized by short sequences of down- and subsequent upwelling (small and shallow flow cells). Subsurface residence times in the shallow flow system are relatively short as indicated by the groundwater age distribution in Figure 5. At specifc locations water infiltrates deep into the wetland and stays within deeper layers for a relatively long period before exfiltration occurs (long and deep flow cells), predominately into the channel segment at location x > 20m. These deep subsurface flow paths are characterized by subsurface residence times that are generally orders of magnitudes higher than in the shallow flow system. In Frei et al. (in press), the coexistence of deep and shallow flow systems was identified as an effect of the superficial micro-topographical structures. Such subsurface flow patterns cannot be reproduced in models using a planar surface only (planar reference Figure 5). However, by using spatially distributed rill storage heights superimposed onto a planar surface the characteristic subsurface flow patterns induced by micro-topography can be reproduced (p-rs-high/p-rs-low models in Figure 5). In the rill storage models the spatially distributed rill storage heights result in a spatially variable head distribution at the planar model surface, which has a very similar effects on subsurface flow as the micro-topography. As stated earlier, hummocks in the rill storage models are represented by finite elements with higher and local depressions by finite elements with lower rill storage heights. During the intensive rainfall events, groundwater levels in the rill storage models uniformly rise above the model surface, but in contrast to the planar reference, initial overland flow is only generated in zones with low rill storage height. In the zones representing hummocks, ponded surface water is retained because the assigned rill storage height is not exceeded by the ponded water depth so that the water cannot run off. The resulting head gradients between areas with higher (hummocks) and lower (hollows) ponding depths results in re-infiltration of the immobile, retained surface water at hummock locations. This mechanism mimics the down and upwelling movement of the shallow flow system observed for the micro-topography model. Even if the grid resolution is significantly reduced (p-rs-low in Figure 5), rill storage height variations are able to represent the characteristic micro-topographical sub-surface flow patterns, including the in- and exfiltration behavior of the shallow flow system, for a planar surface.
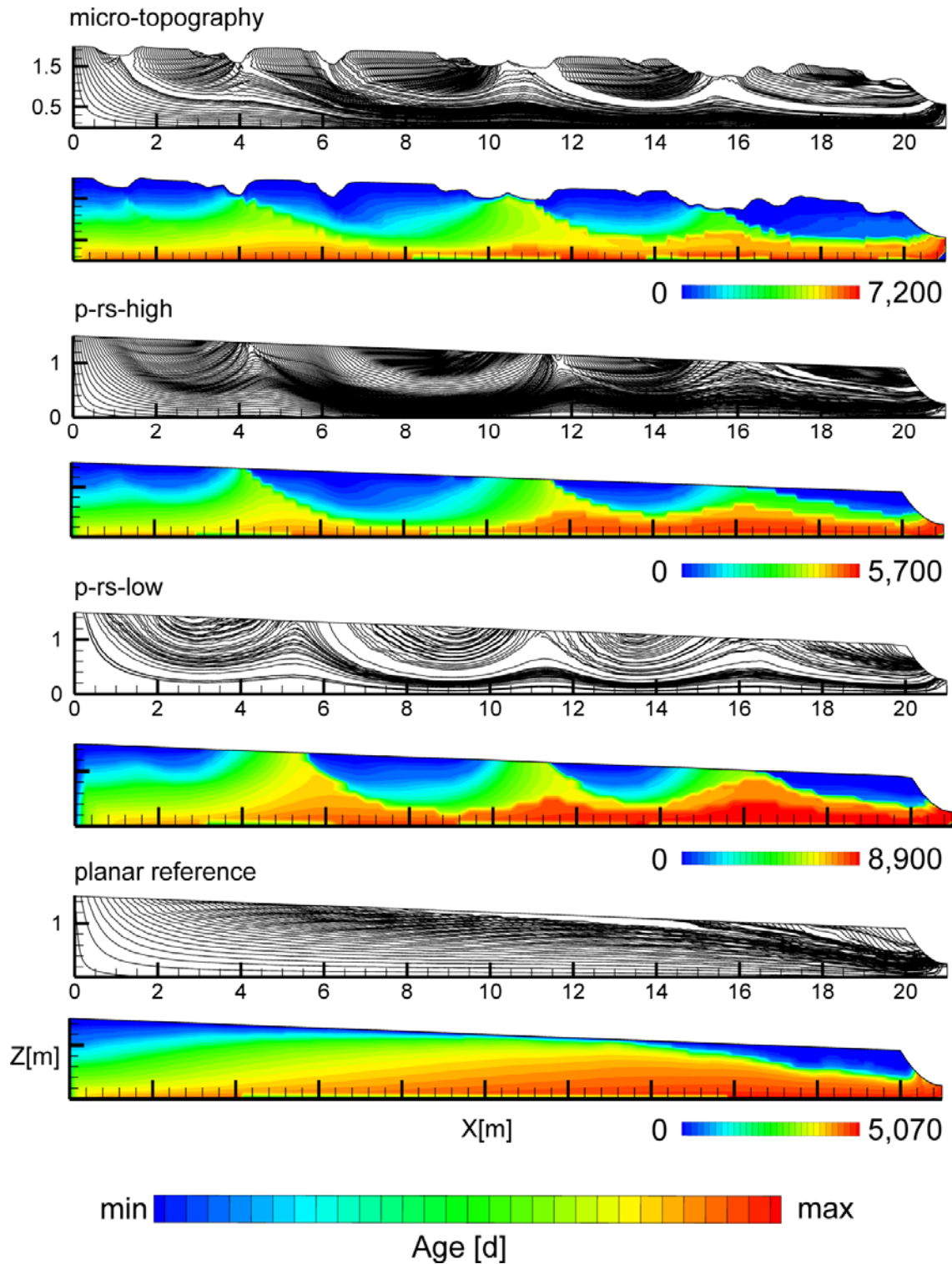
Figure 5: *Cross sections extracted at Y=5m out of the 3D model domain. The upper cross section of each model shows a projection of the subsurface flow field estimated form particle tracking based on a repeating early simulation scenario as described in Frei et al. (2010) and Frei et al. (in press). The micro-topography model and the models with rill storage height variations show characteristic down and upwelling flow patterns (shallow flow systems) and a deeper flow system. Contrary, the planar reference shows a very homogenous subsurface flow field because micro-topographical structures and/or rill storge height variations are missing. Lower cross sections shows the estimated groundwater age since infiltration derived from backward particle tracking.*

3.3   Subsurface Residence Times Distribution

Fractal scaling and power law distributed residence times have been shown to be a common characteristic of many hydrologic systems, which is partly caused by the effects of topography at various scales. Power law distributed residence times were reported for subsurface flow processes over a wide range of scales, from streambeds (10^0m) up to the continental scale (10^6 m) (Kollet and Maxwell, 2008b). Compared to other common distribution models for residence times, like exponential or advection/dispersion models, the power law distribution has a long tail reflecting very long sub-surface residence times. Figure 6 shows the estimated subsurface residence times for the four different flow models. The subsurface residence times, estimated for the micro-topography model, can be well approximated with a power law distribution (R^2=0.9188). Subsurface residence times for the planar reference model apparently follow a different kind of distribution as indicated by the worse approximation with the power law distribution (R^2=0.6377). Similar as observed for small scale in-channel bedforms (Cardenas, 2008), the hummocky topography of riparian wetlands and its effect on subsurface flow processes, leads to power law scaling of residence times. By replacing the three-dimensional micro-topography with distributed rill storage height zones, subsurface residence times remain power law distributed as indicated by the good fit of the p-rs-high model (R^2=0.9002). Slopes of the fitted distributions for the micro-topography and the p-rs-high model (A=-1.1849 and -1.1729) lie within the range of reported values (between -1.088 and 1.28) for hydrological systems showing fractal behaviour (Haggerty et al., 2002, Cardenas, 2008). However, compared to the micro-topography model, smallest subsurface residence times (0-20 days) are underrepresented in the distribution of the p-rs-high model and maximum observed subsurface residence times are higher (5,700 days compared to 7,200 days). For the p-rs-low model, residence times still show a very good fit to a power law distribution (R^2=0.87) but seem to be shifted towards higher residence times as indicated by the slightly flatter linear slope (A=-0.8671), which might be explained by the reduced grid resolution where only 1,898 individual subsurface flow path lines were evaluated (one path line per surface node) compared to 21,000 path lines for the p-rs-high model.
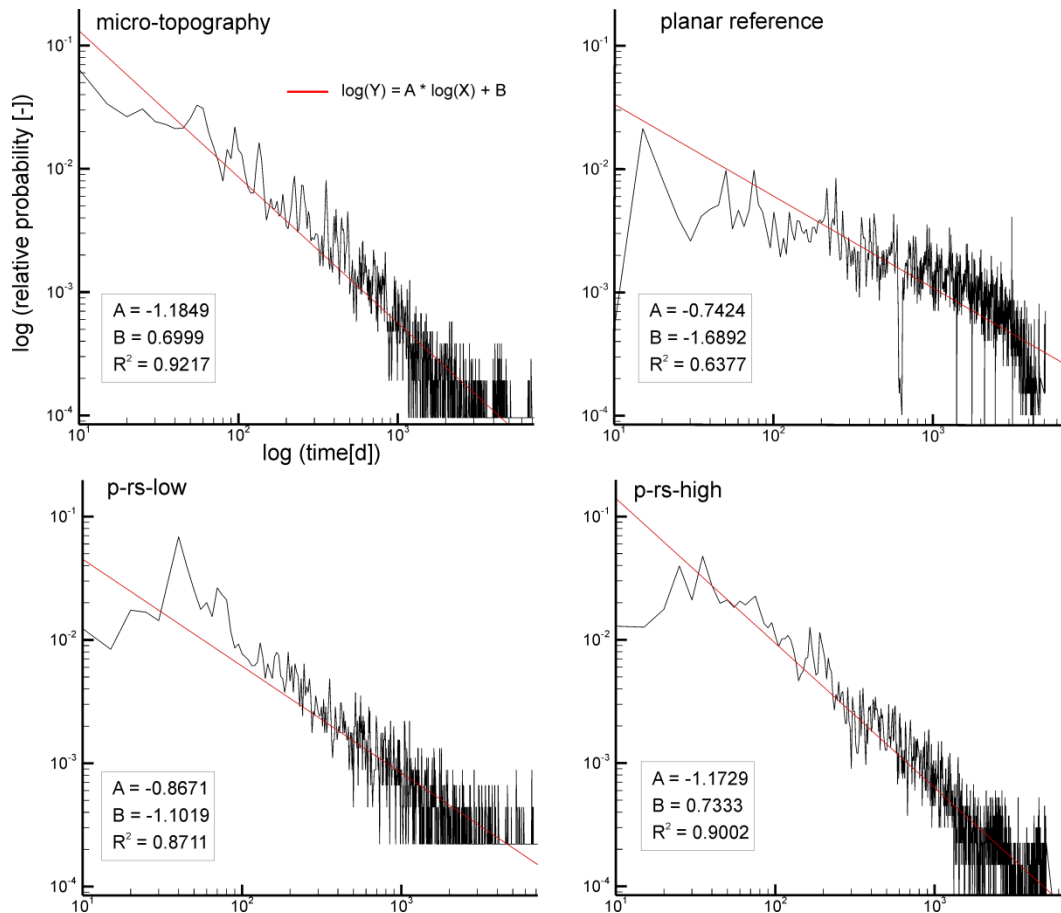
Figure 6: *Estimated subsurface residence time distributions for the different flow models. Residence times estimated for the micro-topography model and the rill storage height models show a good fit (R^2) to a power law distribution (red line as shown using a double logarithmic scale). The fitting parameters represent the linear slope (A) and the center distance to the x-axis (B). Residence time distribution estimated for the planar reference do not follow a power law distribution as indicated by the bad fit.*

3.4 Biogeochemical Process Patterns

For a hummocky wetland, Frei et al. (in press) showed that local biogeochemical hot spots, for specific redox-sensitive processes, are generated because of the complex subsurface flow patterns and the non-uniform exposure to different hydrological and biogeochemical boundary conditions. Formation of local hot spots formation for the micro-topography model is shown in Figure 7. Hot spots for reduction processes (e.g. de-nitrification, sulfate or iron reduction) are preferentially generated below hummock structures because here, infiltrating water is rich in oxidized species (e.g. nitrate, sulfate or iron(III)) which are being depleted under anaerobic conditions (Frei et al., in press). Below depressions, reduction processes are inactive because the upwelling water is already in a reduced condition which means that no oxidized species are available for reduction processes. However, upwelling water is rich in reduced species like sulfide or iron(II) and below depressions, these reduced species may get in contact with atmospheric oxygen. This is the reason why local hot

spots for oxidation processes are generated below depressions (Frei et al., in press). Small scale variations of activation and inactivation of redox-sensitive processes in Frei et al. (in press) are directly related to the superficial micro-topography.
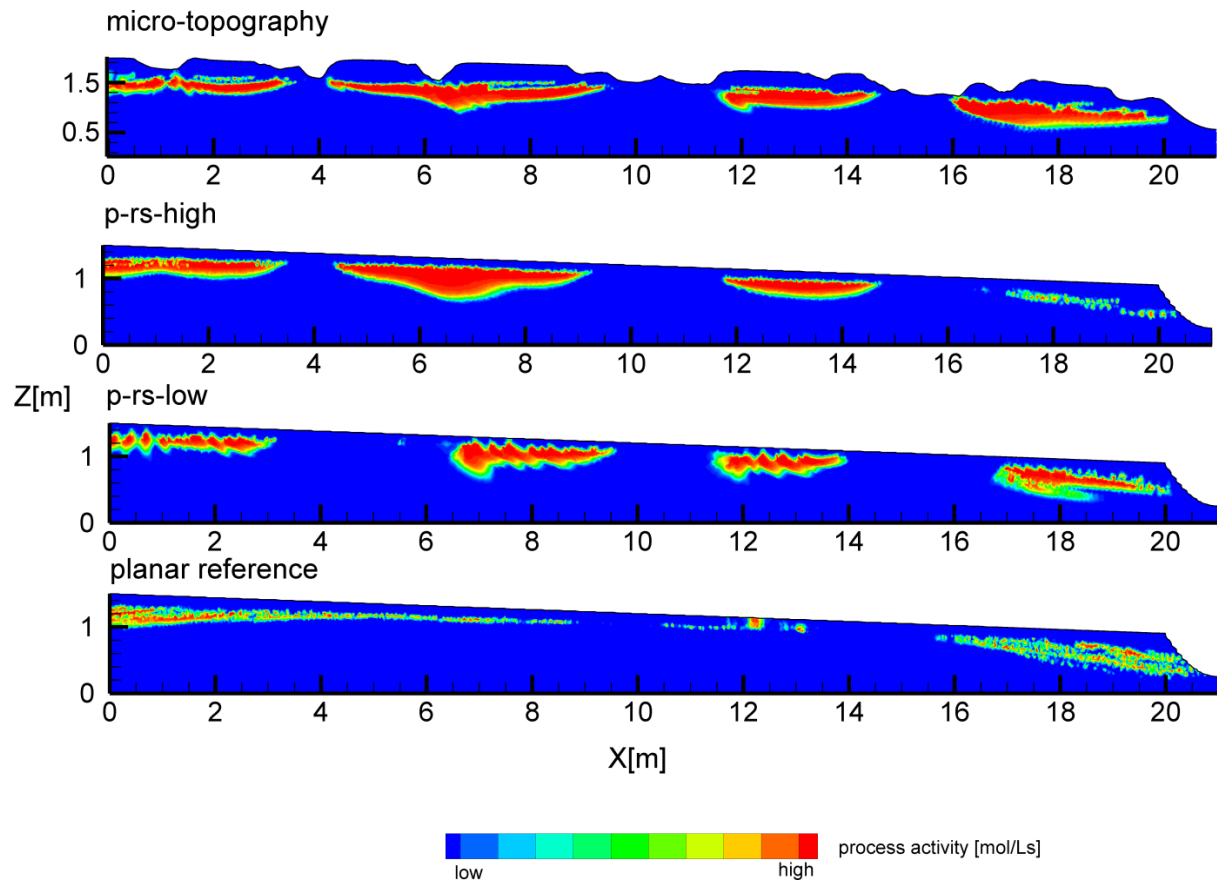
Figure 7: *Cross sections showing the formation of biogeochemical hot spots as a result of the complex flow path distribution and the non-uniform exposure to different hydrological and biogeochemical boundary conditions. Results exemplarily show the results of the coupled hydrological/biogeochemical simulations described in Frei et al. (in press) for iron reduction. The micro-topography model and the rill storage height models show spatially pronounced hot spots in the subsurface, where the planar reference shows a more homogenous distribution of biogeochemical activity.*

As shown before, if spatially distributed rill storage zones are superimposed on top of a planar surface, subsurface flow patterns can be generated, which are very similar to those observed for the micro-topography model. By applying the same streamtube approach as presented in Frei et al. (in press) to represent biogeochemistry, results show that for a planar surface with rill-storage height variations similar biogeochemical patterns can be generated (Figure 7) compared to the micro-topography model. For the p-rs-high model, hot spots for sulfate reduction are correctly generated below infiltration areas (hummocks) hot spots for oxidation processes (not shown) below upwelling areas (depressions). By reducing the grid resolution, it is still possible to generate typical hot spot patterns for in- and exfiltration areas. Resulting hot spots, however, are spatially not as clearly defined

in the p-rs-low model compared to the micro-topography or the p-rs-high models. For the p-rs-low model particle tracking simulations are only based on 1,898 individual flow paths (one particle per surface node) instead of 21,000 flow paths for the more highly resolved p-rs-high and micro-topography models, which will results in more diffuse hot spots in these model as compared to the models using a higher grid resolution.

3.5   Simulation Runtimes

All simulations were performed using the non-parallel version of HGS, running on a modern multi-core workstation. Due to the high grid resolution and the integrated simulation of surface and subsurface flow, the computational efficiency for the original micro-topography model is very low. Especially for stress periods where surface flow is generated, converging time steps become extremely small, which clearly affects the overall model performance. For a yearly scenario with variable rainfall inputs, the micro-topography model needs up to 48 days to be solved (Table 2 according to Frei et al., 2010). By using the same grid resolution while replacing the three-dimensional micro-topography with superficial rill storage height variations (p-rs-high), computation time can be reduced by a factor of almost two (Table 2). If superficial rill storage height variations are used together with a ten times reduced grid resolution (p-rs-low), computation time for solving the yearly scenario drop below one day.

Table 2: Computation times to solve a yearly scenario with variable rainfall inputs for the different models with micro-topography, spatially distributed rill storage height variations (p-rs-high/p-rs-low) and the planar reference.

	simulation period [days]	computation time (real time) [days]
micro-topography	365	48
planar reference	365	23
p-rs-high	365	25
p-rs-low	365	0.63

4   Summary and Conclusions

A representation of micro-topography in numerical flow models can be crucial if the mechanisms of runoff generation, interactions between surface and subsurface flow, the distribution of heads and flow paths in the subsurface or feedback mechanisms between hydrology and biogeochemistry are to be simulated mechanistically. Geostatistical techniques offer an efficient way to generate specific structures of micro-topography that can be implemented in hydrological flow models without the need for a highly resolved DEM, obtained from field survey methods like laser scanning. However, even if a geostatistically generated DEM is used its explicit representation in a physically-based flow models will still require a high grid resolution. The consequence is a large number of computational nodes, which is computationally expensive. Computational costs are even higher when integrated numerical flow models are being used where governing equations for the overland and subsurface flow domain are solved simultaneously. Use of the rill storage concept, as presented in this study, provides a viable alternative to models high grid resolution that allows to reproduce relevant effects of surface micro-topography with much coarser numerical grids.

Results of this study show that by applying the rill storage concept to represent typical effects of a hummocky topography on the plot scale, grid resolutions can be significantly reduced without neglecting important small scale process mechanisms and flow patterns. Hummock and hollow structures in the rill storage models were represented by areas using lower (hollows) and higher rill storage heights (hummocks). Micro-channeling effects and surface flow networks, which were reported to be characteristic for surface flow generation in systems with micro-topography (Frei et al., 2010, Antoine et al., 2009), were successfully simulated by applying the rill storage concept in combination with planar flow models. However, the exact timing of surface flow generation as a response to rainfall could not be simulated correctly by applying the rill storage concept mainly because of the insufficient representation of the surface and subsurface storage capacities. Furthermore, the rill storage concept was tested for its ability to correctly capture subsurface flow patterns and subsurface residence time distributions, which are affected and controlled by micro-topography. The complex interactions between surface and subsurface flow processes, which have been shown to be controlled by micro-topography (Frei et al., 2010) could adequately be represented by applying the rill storage concept. Results from particle tracking showed that subsurface residence times for a hummocky topography follow a power law distribution, which indicates fractal behavior, similar to other hydrologic systems described in the literature (Kirchner et al., 2000, Cardenas, 2008, Kollet and Maxwell, 2008b) and that this behavior can be adequately reproduced by simpler computationally more efficient models that use the rill storage concept to represent micro-topography. Surface-, subsurface flow patterns and residence time distributions are also generally preserved in models with rill storage height variations, even with significantly reduced grid resolutions. Formation of local biogeochemical hot spots for redox-reactions has been suggested by Frei et al., (in press) to be

[174]

a possible response of wetland biogeochemistry to the complex subsurface flow patterns and the dynamic shifts in hydrological and biogeochemical boundary conditions induced by the hummocky topographies typical for wetland systems. These processes and the resulting heterogeneous distribution of redox- sensitive solutes including the formation of local hot spots can be simulated using the rill storage concept.

On the plot scale, the rill storage concept can be an efficient way to represent the impact of micro-topography on hydrological processes. As shown for the synthetic wetland model, grid resolution can be significantly reduced by using spatially distributed rill storage zones resulting in increased computational efficiencies and significantly reduced simulation times while important aspects of micro-topography induced surface and subsurface flow processes are being preserved. However, surface runoff in our test case model is generated predominantly because of saturation excess where the local groundwater level rises above the land surface. Whether the rill storage concept can also be applied to systems with micro-topography where surface runoff is generated due to infiltration excess, like for example in arid system as described by Solé-Benet et al. (1997), remains to be tested. In larger scale models (e.g for entire watersheds) where it is impossible to explicitly account for micro-topography because of the coarser grid resolutions, the rill storage concept may provide a viable means to account for micro-topography. First results along those lines look promising. However further work is needed to more rigorously test, which aspects of micro-topography driven surface and subsurface flow processes can be adequately mimicked at larger scales by applying the rill storage concept and which ones not.

Acknowledgments

References

Abedini, M.J., Dickinson, W.T., Rudra, R.P., 2006. On depressional storages: The effect of DEM spatial resolution. Journal of Hydrology 318 (1), 138–150.

Antoine, M., Javaux, M., Bielders, C., 2009. What indicators can capture runoff-relevant connectivity properties of the micro-topography at the plot scale? Advances in Water Resources 32 (8), 1297–1310. doi:10.1016/j.advwatres.2009.05.006.

Bronstert, A., Plate, E., 1997. Modelling of runoff generation and soil moisture dynamics for hillslopes and micro-catchments. Journal of Hydrology 198 (1-4), 177–195.

Cardenas, M., 2008. Surface water-groundwater interface geomorphology leads to scaling of residence times. GEOPHYSICAL RESEARCH LETTERS 35 (8), L08402.

Cardenas, M., Wilson, J., 2007. Dunes, turbulent eddies, and interfacial exchange with permeable sediments. Water Resour. Res 43 (8), W08412.

Devito, K., Hill, A., 1999. Sulphate mobilization and pore water chemistry in relation to groundwater hydrology and summer drought in two conifer swamps on the Canadian Shield. Water, Air, & Soil Pollution 113 (1), 97–114.

Dunne, T., Zhang, W., Aubry, B.F., 1991. Effects of rainfall, vegetation, and microtopography on infiltration and runoff. Water Resources Research 27 (9), 2271–2285.

Esteves, M., Faucher, X., Galle, S., Vauclin, M., 2000. Overland flow and infiltration modelling for small plots during unsteady rain: numerical results versus observed values. Journal of Hydrology 228 (3-4), 265–282.

Feyen, H., Wunderli, H., Wydler, H., Papritz, A., 1999. A tracer experiment to study flow paths of water in a forest soil. Journal of Hydrology 225 (3), 155–167.

Fiedler, F.R., Ramirez, J.A., 2000. A numerical method for simulating discontinuous shallow flow over an infiltrating surface. International journal for numerical methods in fluids 32 (2), 219–239.

Frei, S., Knorr, K., Peiffer, S., Fleckenstein, J., in press. Surface micro-topography can cause hot spots of biogeochemical activity in wetland systems. Journal of Geophysical Research - Biogeosciences.

Frei, S., Lischeid, G., Fleckenstein, J.H., 2010. Effects of micro-topography on surface-subsurface exchange and runoff generation in a virtual riparian wetland-a modeling study. Advances in Water Resources 33 (11), 1388–1401.

Gerstberger, P. (Ed.), 2001. Waldökosystemforschung in Nordbayern: Die BITÖK-Untersuchungsflächen im Fichtelgebirge und Steigerwald. Bayreuther Forum Ökologie.

Govers, G., Takken, I., Helming, K., 2000. Soil roughness and overland flow. Agronomie 20 (2), 131–146.

Haggerty, R., McKenna, S., Meigs, L., 2000. On the late-time behavior of tracer test breakthrough curves. Water Resources Research 36 (12), 3467–3479.

Haggerty, R., Wondzell, S.M., Johnson, M.A., 2002. Power-law residence time distribution in the hyporheic zone of a 2nd-order mountain stream. GEOPHYSICAL RESEARCH LETTERS 29 (13), 1640.

Hairsine, P.B., Moran, C.J., Rose, C.W., 1992. Recent developments regarding the influence of soil surface characteristics on overland flow and erosion. Soil Research 30 (3), 249–264.

Hauck, A., 1999. Hydrological Charakterization of the Lehstenbach Catchment. unpuplished Diploma Thesis, University of Bayreuth, Bayreuth.

Kirchner, J.W., Feng, X., Neal, C., 2000. Fractal stream chemistry and its implications for contaminant transport in catchments. Nature 403 (6769), 524–527.

Kirchner, J.W., Feng, X., Neal, C., 2001. Catchment-scale advection and dispersion as a mechanism for fractal scaling in stream tracer concentrations. Journal of Hydrology 254 (1-4), 82–101.

Kollet, S.J., Maxwell, R.M., 2008b. Demonstrating fractal scaling of baseflow residence time distributions using a fully-coupled groundwater and land surface model. GEOPHYSICAL RESEARCH LETTERS 35 (7), 7402.

Kværner, J., Kløve, B., 2008. Generation and regulation of summer runoff in a boreal flat fen. Journal of Hydrology (360), 15–30. doi:10.1016/j.jhydrol.2008.07.009.

McGuire, K.J., McDonnell, J.J., Weiler, M., Kendall, C., McGlynn, B.L., Welker, J.M., Seibert, J., 2005. The role of topography on catchment-scale water residence time. Water Resources Research 41 (5), W05002.

Nakayama, T., Watanabe, M., 2006. Simulation of spring snowmelt runoff by considering micro-topography and phase changes in soil layer. Hydrology and Earth System Sciences Discussions 3 (4), 2101–2144.

Parkhurst, D., 1995. User's guide to PHREEQC: A computer program for speciation, reaction-path, advective-transport, and inverse geochemical calculations. U.S. GEOLOGICAL SURVEY WAter-Resources Investigations Report 95-4227.

Price, J., McLaren, R., Rudolph, D., 2010. Landscape restoration after oil sands mining: Conceptual design and hydrological modelling for fen reconstruction. International Journal of Mining, Reclamation and Environment 24 (2), 109–123.

Qu, Y., Duffy, C.J., 2007. A semidiscrete finite volume formulation for multiprocess watershed simulation. Water Resources Research 43 (8), W08419. doi:10.1029/2006WR005752.

Salehin, M., Packman, A., Paradis, M., 2004. Hyporheic exchange with heterogeneous streambeds: Laboratory experiments and modeling. Water Resour. Res 40 (11), W11.

Sharratt, B., Benoit, G., Daniel, J., Staricka, J., 1999. Snow cover, frost depth, and soil water across a prairie pothole landscape. Soil Science 164 (7), 483.

Shen, H.W., Julien, P.Y., 1993. Erosion and sediment transport. Handbook of Hydrology, 12.1-12.61.

Solé-Benet, A., Calvo, A., Laĩzaro, R., Pini, R., Barbero, J., 1997. Influences of micro-relief patterns and plant cover on runoff related processes in badlands from Tabernas (SE Spain). Catena 31 (1-2), 23–38.

Soleĩ-Benet, A., Calvo, A., Laĩzaro, R., Pini, R., Barbero, J., 1997. Influences of micro-relief patterns and plant cover on runoff related processes in badlands from Tabernas (SE Spain). Catena 31 (1-2), 23–38.

Therrien, R., McLaren, R., Sudicky, E., Panday, S., 2008. HydroGeoSphere A Three-dimensional Numerical Model Describing Fully-integrated Subsurface and Surface Flow and Solute Transport (Manual), University of Waterloo.

Weiler, M., Naef, F., 2003. Simulating surface and subsurface initiation of macropore flow. Journal of Hydrology 273 (1), 139–154.

Wörman, A., Packman, A.I., Marklund, L., Harvey, J.W., Stone, S.H., 2006. Exact three-dimensional spectral solution to surface-groundwater interactions with arbitrary surface topography. Geophys. Res. Lett 33.

Study 4

Concentrations and fluxes of dissolved organic carbon in runoff from a forested catchment: Insights from high frequency measurements

By Stefan Strohmeier, Klaus-Holger Knorr, Martin Reichert, Sven Frei, Jan H. Fleckenstein, Stefan Peiffer and Egbert Matzner

Concentrations and fluxes of dissolved organic carbon in runoff from a forested catchment: Insights from high frequency measurements

S. Strohmeier[1], K.-H. Knorr[2], M. Reichert[2], S. Frei[2], J.H. Fleckenstein[3], S. Peiffer[2]

and E. Matzner[1]

[1]Department of Soil Ecology, Bayreuth Center of Ecology and Environmental Research (BayCEER), University of Bayreuth, 95448 Bayreuth, Germany

[2]Department of Hydrology, Bayreuth Center of Ecology and Environmental Research (BayCEER), University of Bayreuth, 95440 Bayreuth, Germany

[3]Department of Hydrogeology, Helmholtz Center for Environmental Research (UFZ), 04318 Leipzig, Germany

Abstract

Concentrations of dissolved organic carbon (DOC) in runoff from catchments are often subject to substantial short term variations. The aim of this study was to identify the spatial sources of DOC and the causes for short term variations in runoff from a forested catchment. Furthermore, we investigated the implication of short term variations for the calculation of annual runoff fluxes. High frequency measurements (30 minute intervals) of DOC in runoff, of discharge and groundwater table were conducted for one year in the 4.2 km^2 forested Lehstenbach catchment, Germany. Riparian wetland soils represent about 30% of the catchment area. The quality of DOC was investigated by three-dimensional fluorescence excitation-emission matrices in samples taken from runoff, deep groundwater and shallow groundwater from the riparian wetland soils. The concentrations of DOC in runoff were highly variable at an hourly to daily time scale, ranging from 2.6 mg l^{-1} to 34 mg l^{-1} with an annual average of 9.2 mg l^{-1}. The concentrations were positively related to discharge, with a pronounced, counter clockwise hysteresis. Relations of DOC to discharge were steeper in the summer/fall than in the winter/spring season. Dynamics of groundwater table, discharge, DOC concentrations and DOC quality parameters indicated that DOC in runoff originated mainly from the riparian wetland soils, both under low and high flow conditions. The annual export of DOC from the catchment was 84 kg C ha^{-1} yr^{-1} when calculated from the high frequency measurements. If the annual export was calculated by simulated random fortnightly samplings, the range was 47 to 124 kg C ha^{-1} yr^{-1}. Calculations of DOC export fluxes might result in significant errors when based on infrequent (e.g. fortnightly) sampling intervals. Future changes in the precipitation and discharge patterns will influence the DOC dynamics in this catchment, with largest effects in the summer season.

1   Introduction

The importance of dissolved organic carbon (DOC) for the functioning of terrestrial and aquatic ecosystems is widely known. DOC plays an important role in the C cycle, in the acid-base chemistry of soils and surface waters, it influences nutrient cycling, and affects the mobility and availability of metals and contaminants (Bolan et al. (2011[5]), Kalbitz et al. (2000)[23]). Although numerous studies on DOC in soils and catchments have been published in the last decade, sources and sinks of DOC in soils and the transition of DOC from terrestrial to the aquatic ecosystems are still poorly understood in their quantitative response to driving factors, like climatic conditions, flow paths, vegetation and soil conditions. DOC in runoff from forested catchments originates mostly from soil organic matter (Degens et al. (1991)[11]). Depending on precipitation, flow paths and catchment characteristics, different soil types and soil horizons from different parts of the catchment may feed the runoff with DOC, resulting in temporal variations of DOC quality and quantity in runoff. In general, the DOC export from forested catchments in Skandinavia was found to be positively related to the area of wetland soils (Laudon et al. (2011)[29]). To identify the spatial sources of DOC in runoff, quality parameters of DOC can be used, like fluorescence spectroscopy (Ishii and Boyer (2012)[20], Fellman et al. (2009)[13], Austnes et al. (2010)[3]). This is a highly sensitive method to determine changes in DOC quality and can be applied to a large number of samples. DOC concentrations in runoff from forested catchments are often subjected to temporal variations of one order of magnitude at time scales ranging from hours to seasons. This can be attributed to the large differences in DOC concentrations in the two dominant flow components contributing to individual discharge events, i.e. groundwater (baseflow) versus shallow groundwater and surface runoff from riparian wetland soils (high flow) (McGLynn and McDonnell 2003[36], Hood et al. 2006[18]). Ludwig et al. (1996)[33] related the DOC fluxes to drainage intensity, basin slope, and the amount of carbon stored in soils. Interestingly, they found a negative relationship between basin slope and DOC concentrations as steeper slopes may cause a restricted contact between soil and water, and thus lead to lower DOC concentrations in runoff.

Hysteretic relationships between discharge and solute concentrations have been observed by *inter alia* Hornberger et al. (1994)[19], Evans and Davies (1998)[12], Butturini et al. (2006)[7], Raymond and Saiers (2010)[43], Pellerin et al. (2012)[41], and Jeong et al. [22]. Evans and Davies (1998)[12] proposed the hysteretic concentration/discharge relationship for the analysis of episode hydrochemistry. Using a three component model, they categorized the concentration/discharge relationships into clockwise and counter-clockwise hysteresis with a positive, negative or no trend. This categorization allows the distinction of flow components that are drained during the rising or falling limbs of the hydrograph. Generally, high concentrations during the rising limb of the hydrograph lead to clockwise hysteresis, while high concentrations during the falling limb imply counter-clockwise hysteresis. Clockwise hysteretic patterns have been attributed to early flushing and

depletion effects as well as changes in the connectivity of riparian or hillslope flowpaths (Hornberger et al. 1994[19], Boyer et al. 2000[6], Âgren et al. 2008[1], Pacific et al. 2010[40], McGlynn and McDonnell 2003[36]).

Only recently, field-deployable automated devices became available to analyze physico-chemical parameters of runoff in high temporal resolution. From such measurements, new insights in the hydrological, chemical and biological controls of runoff chemistry might emerge (Kirchner et al 2004)[25]. Using high frequency measurements of DOC quality parameters, Spencer et al. (2007[47]) found diurnal patterns, which would not have been revealed by discrete sampling strategies, whereas Jeong et al. (2012)[22]), for a catchment in monsoonal climate, showed up to 23% of the annual exports of DOC and 48% of POC being realized in only a few discrete events. The DOC export fluxes with runoff might represent a substantial contribution to the net C budget of ecosystems (Kindler et al. (2011)[24]). If the DOC concentration varies with discharge, the flux calculation is subjected to potential errors since discharge is in most cases recorded permanently, while DOC concentrations are often measured infrequently in larger time intervals (like fortnightly) with interpolation procedures needed for the calculation of annual fluxes (e.g. Method 5, Walling and Webb (1985)[49]). It is a matter of debate whether the period-weighted interpolation method leads to an underestimation of annual DOC fluxes as the majority of DOC is exported during storm events in a rather short time period which are likely missed by the interpolation method (Clark et al. (2007)[9]). The risk of miscalculation depends on catchment properties and the discharge/concentrations relations. Koehler et al. (2009[26]) reported the annual DOC flux with runoff from 30 min measurements to be similar to calculations based on infrequent samplings once a day, once a week and once a month. In case of mineral elements (sulfate, nitrate, chloride), that typically show more of a chemostatic behavior, fortnightly sampling of runoff will be adequate to capture annual fluxes (Alewell (2004)[2]). Overall, the state on knowledge indicates that concentrations and fluxes of DOC in runoff from forested catchments are largely driven by hydrological conditions and that catchment properties, like the occurrence of riparian wetland soils have a major impact. The objectives of this study were thus (1) to quantify the effect of hydrological conditions on DOC variations in runoff from a forested watershed, (2) to identify the spatial origin of DOC in runoff, and (3) to investigate the implications of the short term variations for the calculation of DOC export fluxes at the annual scale.To these ends we have studied the relationship between DOC, discharge and groundwater level in a forested headwater catchment based on high temporal resolution techniques.

2 Material & Methods

2.1 Study site

The Lehstenbach catchment is located in the Fichtelgebirge region (50°8'35'' N, 11°52'8'' E) in southeastern Germany (Frei et al. (2010)[14]). The catchment area is 4.2 km^2 with elevations ranging from 695 to 877 m above sea level. Mean annual precipitation is 1150 mm (1971-2000). The annual temperature averages at 5.3°C (1971-2000). During winter a substantial snow cover develops regularly. The bedrock is variscan granite. Most abundant soil types are Dystric Cambisols, Haplic Podsols and Histosols (WRB (2007)[52]). About one third of the catchment area is covered by Histosols, mostly by minerotrophic fens with some bogs in between (in the following referred to as wetland soils). The wetland soils have been drained by ditches established probably in the 19th century and some active ditches still exist. Norway spruce (*Picea abies* (L.) KARST.) covers approx. 90% of the catchment area. The wetland soils are covered partly by Norway spruce, but also by *Sphagnum* mosses with patches of *Vaccinium myrtillus*, *Juncus effusus*, *Carex nigra*, *Carex rostrata*, *Carex canescens*, *Molinia caerulea*, and *Eriophorum vaginatum* (Matzner (2004[35])). In the upland areas of the catchment the mean groundwater depth is more than 10 m. Inclination of the catchment averages at 3° and surface runoff is of minor importance (Lischeid et al. (2002)[31]). However, based on a modeling approach, Frei et al. (2010)[14] suggested some surface runoff from the wetland soils. Concerning both discharge and solute concentrations, the catchment runoff usually reacts within hours to rain storm events (Lischeid et al. (2004)[32]). The groundwater level was measured in the riparian wetland soils about 2 m away from the stream using a piezometer with an immersed pressure sensor (Solinst Canada Ltd., Georgetown, Ontario, Canada). Discharge of the Lehstenbach stream was measured using a pressure sensor (Solinst Canada Ltd., Georgetown, Ontario, Canada), which was immersed at a discharge flume and weir at the catchment outlet. Precipitation was continuously recorded in the upper part of the catchment by a tipping bucket rain gauge. DOC concentrations were measured in different compartments of the catchment (Table 1). Concentrations were largest in the wetland soils and in the Oa horizon of the forest floor percolates. Lowest concentrations were observed in the deeper layers of the upland forest soils and in the deeper groundwater.

Table 2: *Range of DOC concentration in different compartments of the Lehstenbach catchment*

compartment	range (mg l^{-1})	reference
soil solution beneath Oa horizon (upland forest soil)	30 - 80	Schulze et al. 2011
soil solution in 90 cm depth (upland forest soil)	3 - 5	Schulze et al. 2011
soil solution in 0-30 cm depth (riparian wetland soil)	10 - 150	this study
soil solution in > 30 cm depth (riparian wetland soil)	10 – 80	this study
shallow groundwater in 50-100cm depth (riparian wetland soil)	4 - 40	this study
deeper groundwater (3-15 m depth)	0.8 - 3	this study
Catchment runoff	3 – 34	this study

2.2   Measurements of DOC concentrations in runoff in high temporal resolution

DOC concentrations in runoff were measured in 30 min intervals from the 6th of August 2010 to the 5th of August 2011 by a spectrometric device (spectro::lyser, s::can Messtechnik GmbH, Vienna, Austria) which was permanently immersed in the stream at the weir at the catchment outlet. A UV-VIS spectrum with a range from 200 to 732 nm was recorded every 2.5 nm. DOC concentrations were calculated by the specto::lyser software based on the inclusion of about 80 wavelengths under correction for turbidity. The spectro::lyser device was calibrated by measured DOC concentrations in runoff from the Lehstenbach. Hence, we used a customized calibration instead of a general setting. Although the spectro::lyzer could potentially also measure nitrate from absorption in the UV-range, we found that this is not possible in presence of high and variable concentrations of DOC. For quality control, the spectro::lyser measurements were regularly cross-checked with direct DOC measurements by thermo-catalytic oxidation (TOC-VCPN-Analyzer, Shimadzu, Kyoto, Japan). To do so, runoff samples were obtained by an automated sampling system (ISCO portable sampler, Teledyne Isco, Inc., Lincoln, Nebraska, USA). These cross-checks were done in August, September, and November 2010 and in March, April and June 2011. The R^2 of the linear correlation between the two methods ranged from 0.95 and 0.98 (data not shown). As there was no drift of the DOC concentration due to environmental conditions, we decided against installing an automated cleansing system. The measuring cell was manually cleaned fortnightly.

[185]

Due to instrumental failure no measurements of DOC concentrations were available from the 25th of August 2010 to the 2nd of September 2010, from the 8th to the 23rd of December 2010, and from the 13th to the 14th of January 2011. The missing concentration data (7 % of all measurements) were interpolated by means of an Artificial Neural Network (software SPSS 19, Modeler 14.1, IBM, Armonk, New York, United States) using the high resolution measurements (30 minutes) that were aggregated to daily mean values and then processed. A multilayer perceptron model with a Feed-Forward algorithm, one hidden layer and five neurons was used to model the daily values of DOC concentration. The model was trained with a back propagation algorithm using 70 % of the data. Validation of the model was done with the remaining 30 % of the data. This resulted in a model efficiency of $R^2 = 0.89$ and a RMSE of 1.63 mg l^{-1}. The best prediction for the daily average DOC concentrations was achieved with four input parameters in the order of 1) the precipitation sum of the 6 days before the gauging, 2) mean discharge on the day of measurement, 3) mean temperature of the 170 days before the measurement and 4) the precipitation at the day of measurement. A detailed analysis of 24 storm events > 5 mm was done, relating discharge dynamics to dynamics of DOC concentrations and fluxes in runoff. The 24 events represented 61 % of the annual DOC export flux with runoff, and 60 % of the annual rainfall sum.

2.3   DOC fluxes with runoff

Annual fluxes of DOC with runoff were calculated by multiplying the 30 minute discharge with the corresponding 30 minute DOC concentrations, and then cumulated to the annual flux for the period 08/2010 – 08/2011. Due to instrumental failure no data were available for 27 days. For these days the fluxes were calculated based on daily average values of concentrations and discharge, with concentrations derived from the artificial neural network interpolation (see above). The interpolated data accounted for 7% of the annual flux. To simulate the effect of infrequent sampling strategies on the calculation of annual runoff fluxes, the daily 12.00 h values of the 30-minute records of concentrations and discharge were taken for a simulated fortnightly sampling strategy with shifting starting dates from the 6th of August 2010 to the 19th of August 2010. The data from these artificially created fortnightly observations were inserted into the Method 5-equation of Walling and Webb (1985[49]) (Equation 1) to calculate the annual flux.

$$F = K * Q_r * \left(\frac{\sum_{i=1}^{n} C_i Q_i}{\sum_{i=1}^{n} Q_i} \right) \quad \text{(Equation 1)}$$

F stands for the annual DOC flux; K stands for the conversion factor (here number of seconds in the corresponding period of time); Q_r stands for the daily mean discharge of the year; Q_i stands for the discharge at the sampling day; C_i stands for the DOC concentration at the sampling day; and n is the number of sampling events.

2.4   DOC quality

To identify the spatial origin of DOC in runoff, the quality of DOC in the potential source areas was compared to the quality of DOC in runoff. Samples from shallow groundwater in the wetland soils (28 samples), from deeper (oxic) groundwater (4 wells, depth 3-15 m, 12 samples), from upstream runoff without riparian wetlands (4 samples), and from downstream runoff (26 samples) were taken on 4 occasions in summer 2011 (27.04., 18.05., 2.06., 16.06.). Shallow groundwater from the riparian wetland soils was sampled using a plastic syringe and silicon tube, deep groundwater was sampled from a well located in the upland forest area using an electric pump (Eijkelkamp, Giesbeek, the Netherlands), and surface water from the wetlands was taken as a grab sample. For time resolved sampling of runoff, we used an ISCO bottle sampler (ISCO 6712, Teledyne Isco, Inc., Lincoln, Nebraska, USA) programmed in a 2 h time interval. We chose samples according to DOC concentration and discharge measurements, trying to represent the rising limb of the hydrograph, DOC concentration peak and the falling limb with 5-10 samples per event. Samples were stored in 100 ml PE bottles at 2°C until analysis. In total, 116 runoff samples were analyzed for DOC quality (26 on same dates as groundwater samples, 90 on other occasions). Three-dimensional fluorescence excitation-emission matrices (EEMs) with subsequent evaluation by parallel factor analysis (PARAFAC, Stedmon et al. (2003)[48]) were used to characterize DOC quality. DOC samples were filtered (0.45 μm nylon, WICOM, Heppenheim, Germany) and diluted if necessary to an absorption at 254 nm < 0.3 to minimize inner filter effects (ultrapure water, Barnstead Nanopure, Dubuque, Iowa, USA). Inner filter correction was performed following McKnight et al. (2001)[37], as implemented in the MATLAB toolbox by Cory and McKnight (2005)[10]. To this end, UV-VIS absorption scans were recorded on a Varian Cary 1E spectrophotometer (range 200-800 nm, 0.5 nm resolution, Varian Inc., purchased by Agilent Technologies, Santa Clara, California, United States). Sample correction according to the toolbox of Cory and McKnight (2005)[10] further includes blank subtraction and normalization of fluorescence intensities to the Raman peak intensity at an Excitation of 350 nm. Raman scans, EEMs for blanks, and sample EEMs were recorded on a Perkin Elmer LS 55 fluorescence spectrometer (Waltham, Massachusetts, USA) at a resolution of 0.5 nm for emission (300-600 nm) and 5 nm for excitation (240-450 nm). All data evaluation and PARAFAC modeling was done using MATLAB 2008a (MathWorks, Natick, Massachusetts, USA) and following the toolbox by Cory and McKnight (2005)[10]. Therefore, EEMs were reshaped to the appropriate resolution and range (excitation 250-400 nm, 5 nm steps; emission 350-440 nm, 2 nm steps). The PARAFAC Model from Cory and McKnight (2005)[10] uses 13 fixed, previously identified components to describe each sample EEM. These components were found to sufficiently explain quality differences in our samples with only small residuals remaining unexplained. As a chemical molecular interpretation of the PARAFAC components identified by Cory and McKnight (2005) has become a matter of discussion (Macalady and Walton-Day 2009), we used the 13 PARAFAC

[187]

components to derive statistical fingerprints mainly, omitting a distinct discussion about chemical quality of the DOC of the respective sources

2.5 Statistical Analysis

Statistical data analysis, data processing, and plotting were done in R-project version 2.13.0 [42] if not otherwise stated. To aggregate the 30 minute data to daily values we used the functions *daily* from the R project package *Animal* [17] and the function *ddply* from the package *plyr* [50].

3   Results

3.1   Discharge, groundwater and precipitation

Precipitation from 08/2010 – 08/2011 occurred at 232 days and summed up to 1057 mm (Figure 1). Highest rainfall intensity was observed on the 5th of June 2011 with a rainfall of 15 mm within 30 minutes. Maximum discharge was 0.89 m^{-3} s^{-1}, observed on the 14th of January 2011 (snow melt event), minimum discharge was 0.018 m^{-3} s^{-1} on the 29th of June 2011. Discharge averaged at 0.087 m^{-3} s^{-1}. The discharge responded within minutes to hours to rain fall events, indicating the flashiness of the catchment (Figure 1). The groundwater table in the riparian wetland soils showed rapid changes in response to precipitation events (Figure 1). Groundwater was near surface in August 2010, and in the winter months 2010/2011. Lowest levels were observed on the 31st of May 2011 at 0.62 m below surface.
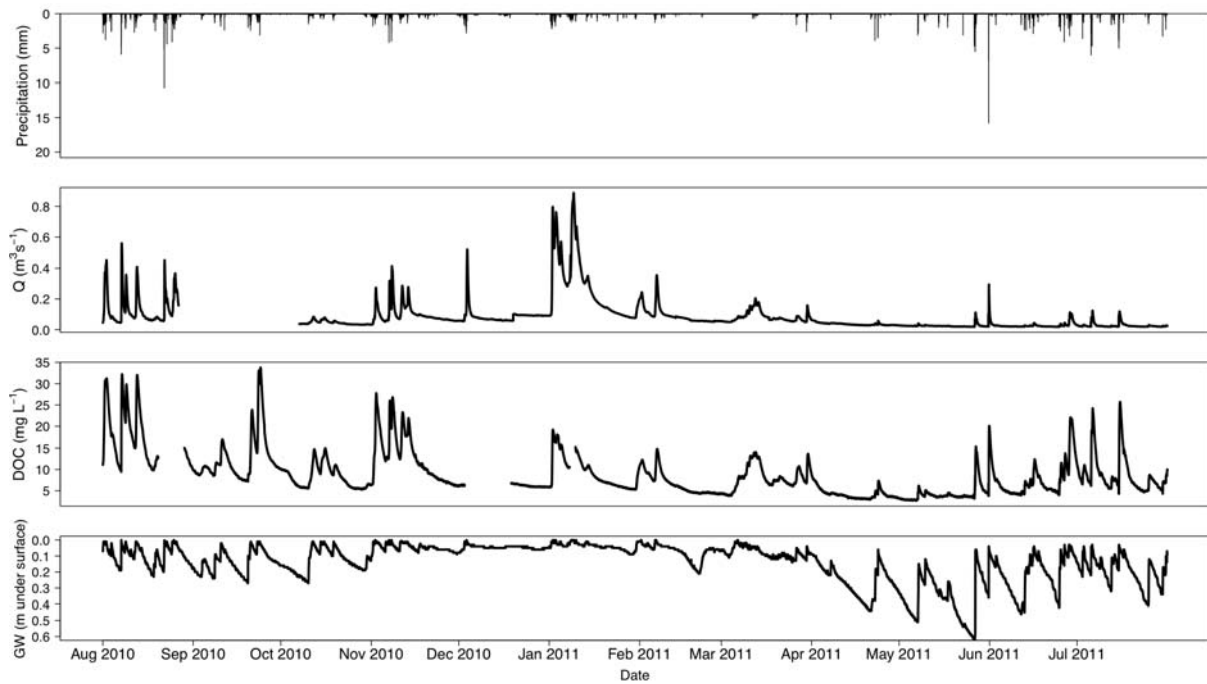

Figure 1: *Precipitation, discharge (Q), DOC concentration and riparian groundwater level in the Lehstenbach catchment*

3.2   DOC concentrations

During the one-year period, DOC concentrations in runoff averaged at 9.2 mg l^{-1}. The minimum was 2.6 mg l^{-1} in May 2011, and the maximum was 33.8 mg l^{-1} in September 2010 (Figure 1). The concentrations of DOC changed rapidly within hours and corresponded generally to the dynamics of the groundwater table and discharge with highest concentrations observed at shallow groundwater table and high discharge. The maxima of the DOC concentrations in runoff had a time delay of a few hours in relation to the maxima of the groundwater table and discharge (Figure 2, Table 2). The average time delay of the DOC maxima was 160 minutes after the discharge peak and the range of delays was from 30 to 390 minutes (Table 2). No significant correlation between DOC delay and the single co-variables of Table 2 was found. The response of DOC to discharge followed counter-clockwise hysteretic loops and was seasonally different (Figure 3). The hysteretic loops for the whole gauging period can be divided into an upper and a lower branch. The branch with shallower slopes in the concentration-discharge relationship represents the winter to spring events whereas the upper branch displays summer and fall events. To compare the hysteretic relationship between different seasons in more detail, we selected one rainfall event in the winter/spring season and one in the summer/fall season both with a similar amount of discharge of 0.35 to 0.40 m^3/s (Figure 4). The loop of February 2011 had lower DOC concentrations than the loop of November 2010. Also, the hysteresis was more pronounced in November with a larger distance between the rising and falling limb. The larger hysteresis in the summer/fall season than in winter/spring was also found for other events (Figure 3).

Table 2: *Detailed analysis of 24 events with rainfall > 5 mm.*

| Event	Start	End	Duration	Rain	Q sum	DOC delay	DOCmax	DOC flux
			[hours]	[mm]	[m3]	[min]	[mg l-1]	[kg ha-1 event-1]
1	2010-08-06 00:00	2010-08-07 06:00	30.0	45	24800	120	31.2	3.0
2	2010-08-12 06:00	2010-08-12 19:30	13.5	26	14226	150	32.2	1.8
3	2010-08-13 19:00	2010-08-13 23:30	4.5	10	14453	120	29.8	1.6
4	2010-08-16 19:00	2010-08-18 05:30	34.5	28	19881	90	32.0	2.3
5	2010-08-26 20:30	2010-08-27 23:30	27.0	35	14879	n.d.	21.1	1.3
6	2010-08-29 14:00	2010-08-31 13:00	47.0	33	27327	n.d.	25.1	2.8
7	2010-09-27 16:30	2010-09-29 00:30	32.0	35	57490	n.d.	33.8	6.6
8	2010-11-05 20:00	2010-11-08 08:30	60.5	30	23660	120	27.8	1.9
9	2010-11-11 20:00	2010-11-13 06:30	34.5	35	29567	360	26.8	2.9
10	2010-11-15 16:30	2010-11-17 07:00	38.5	33	15220	90	23.3	1.3
11	2010-11-18 06:30	2010-11-18 14:30	8.0	7	18251	150	21.9	1.5
12	2010-12-07 11:00	2010-12-08 20:30	33.5	44	27084	150	22.3	2.3
13	2011-01-06 10:30	2011-01-09 23:00	84.5	67	128631	60	19.2	8.5
14	2011-01-12 15:30	2011-01-15 12:00	68.5	38	120430	n.d.	15.3	7.1
15	2011-02-04 10:00	2011-02-04 22:30	12.5	9	30773	270	12.3	1.3
16	2011-02-11 00:00	2011-02-12 12:00	36.0	10	25846	180	14.8	1.3
17	2011-03-16 19:00	2011-03-18 19:00	48.0	9	35501	120	14.1	1.8
18	2011-04-04 06:00	2011-04-04 15:00	9.0	11	7962	390	13.7	0.4
19	2011-05-31 19:00	2011-06-01 16:30	21.5	41	7645	150	15.4	0.3
20	2011-06-05 16:30	2011-06-06 02:30	10.0	26	4790	150	20.1	0.3
21	2011-06-20 17:30	2011-06-21 10:30	17.0	10	2203	120	12.4	0.1
22	2011-07-07 22:00	2011-07-08 07:30	9.5	6	1464	150	11.1	0.1
23	2011-07-10 16:00	2011-07-11 05:00	13.0	19	4755	30	24.2	0.4
24	2011-07-20 06:30	2011-07-20 19:30	13.0	23	4874	240	25.7	0.4
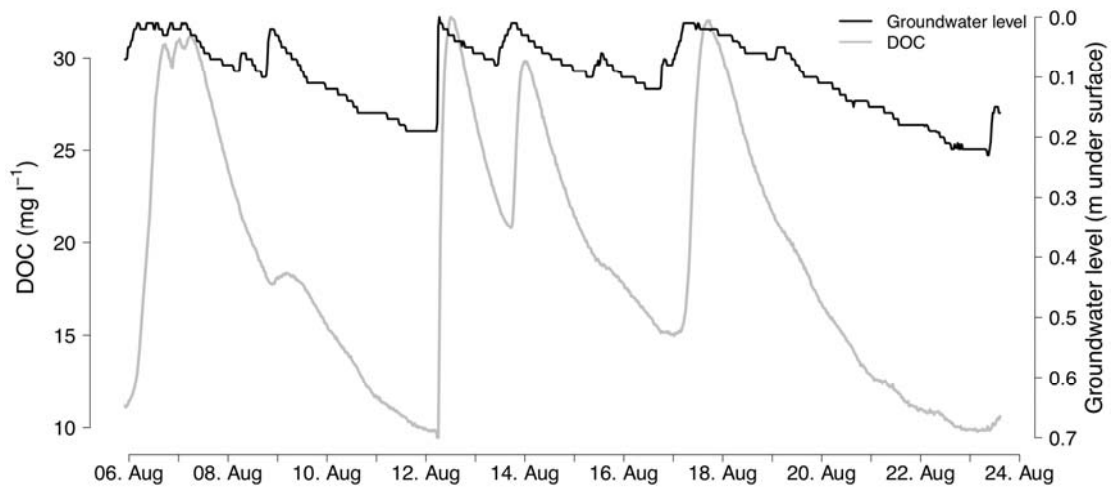
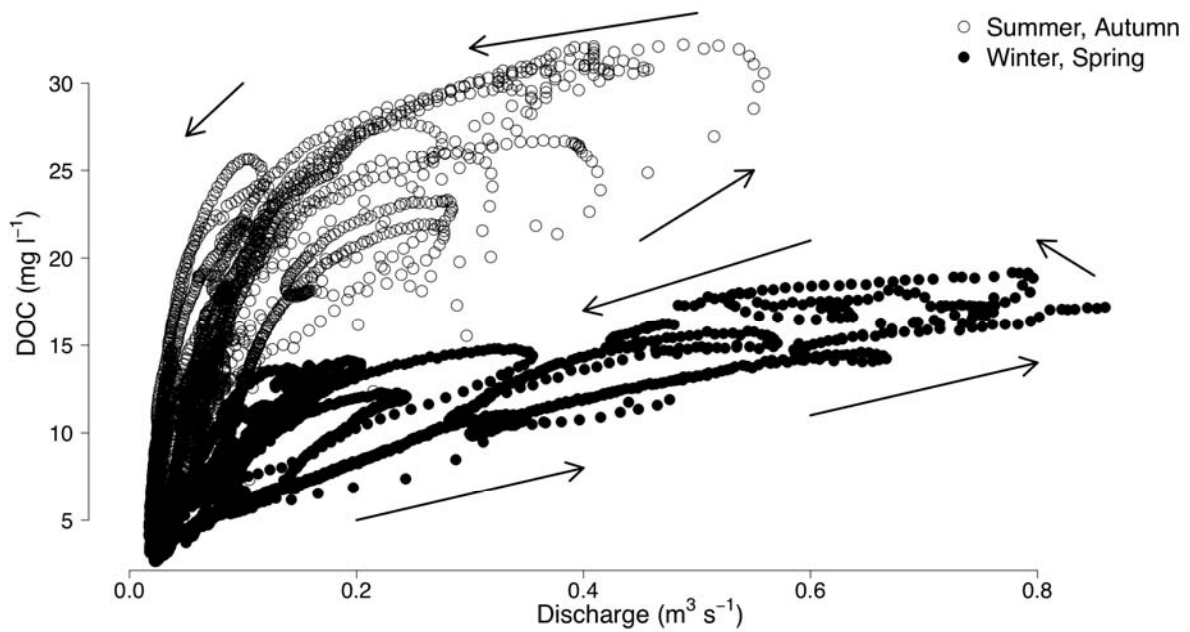**Figure 2**: *Cumulative discharge and cumulative DOC export with runoff*

Figure 3: *Dynamics of DOC concentration in runoff and of the riparian groundwater level in August 2010.*
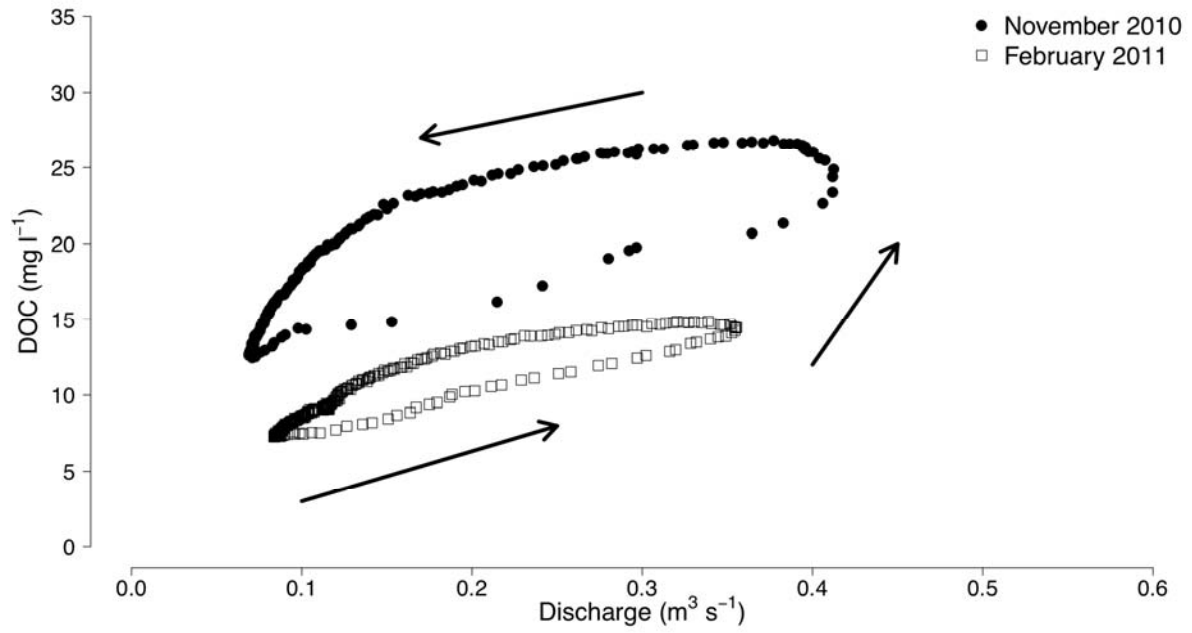
Figure 4: *Hysteretic loops of DOC concentrations in response to discharge*

3.3 DOC quality

The DOC fingerprinting by fluorescence excitation-emission matrices with subsequent PARAFAC analysis clearly separated DOC originating from deep groundwater, shallow groundwater from riparian wetland soils and from runoff (Figure 5). From the 13 fluorescence components of the applied PARAFAC Model (nomenclature according to Cory and McKnight 2005 is given in brackets), components 1 (C1), 5 (SQ1), and 6 (unidentified) were more prominent in wetland samples; components 3 (unidentified), 8 (Tryptophan-like), and 12 (Q3) were more prominent in groundwater samples. Exemplarily, we used component 1 (C1, Cory and McKnight 2005[10]) indicative of samples from riparian wetland soils, and component 12 (Q3) as indicative of groundwater samples (other components not shown). Contribution of component 1 in DOC-fluorescence of runoff samples lined up between deep groundwater and the shallow wetland groundwater samples, suggesting a mixture of both sources, but clearly dominated by wetland-borne DOC. Using both component 1 and component 12 (Cory and McKnight (2005[10]), a clear separation of samples was possible (Figure 5), yielding 2 groups of either groundwater dominated samples or DOC-rich samples dominated by wetland-borne DOC. While fluorescence of DOC-rich samples from shallow wetland groundwater was characterized by higher relative contribution of component 1, deeper groundwater samples where characterized by higher contribution of component 12. With respect to these two distinctive components, DOC quality in upstream runoff, with negligible influence from riparian wetland water and closer to a groundwater spring, was similar to deep groundwater samples (Figure 5, open diamonds). A rise in DOC concentrations with discharge always coincided with an increasing contribution of component 1 and a decrease in component 12 (Figure 6).
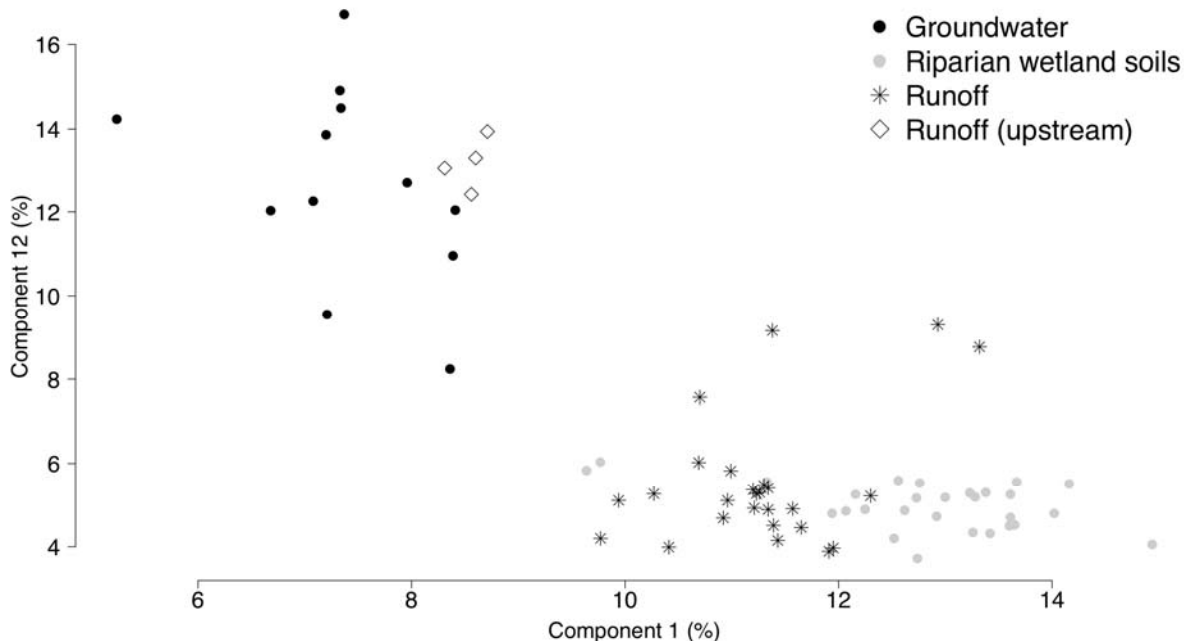

Figure 5: *Hysteretic loops of DOC concentrations in response to discharge for two selected events.*
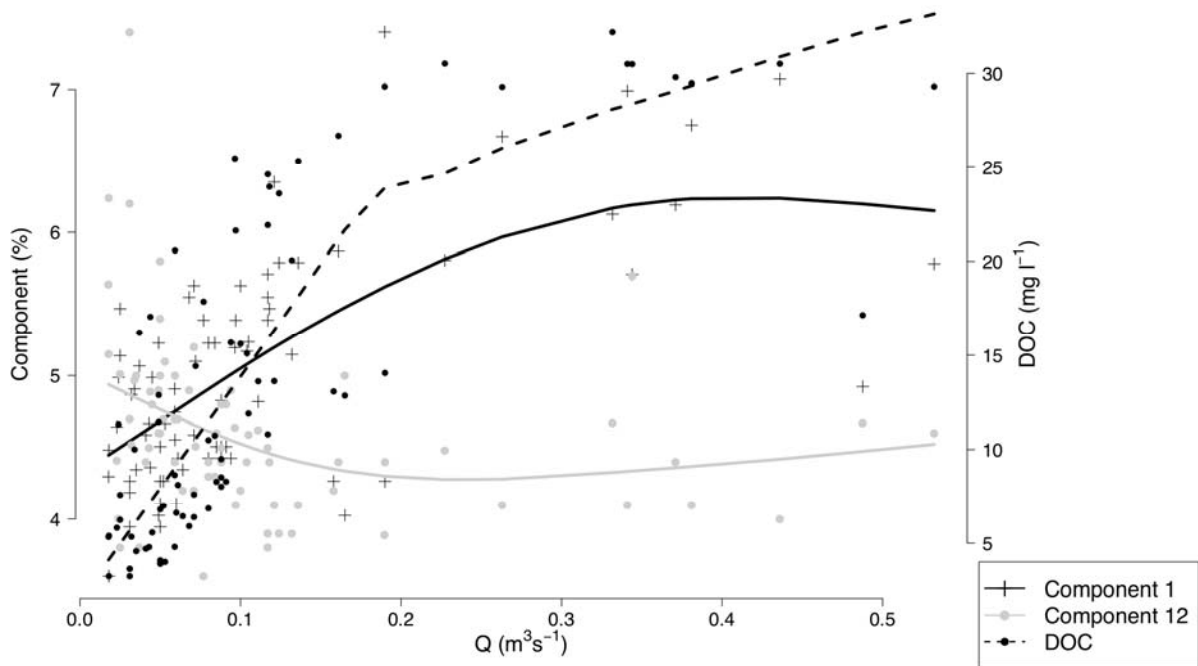
Figure 6: *Quality of DOC from different origins as revealed by fluorescence excitation-emission matrices with subsequent PARAFAC analysis*

3.4   DOC fluxes with runoff

The cumulative DOC fluxes followed generally the cumulative discharge (Figure 7). However, during the discharge events in summer and autumn 2010, the curve for DOC was steeper than for discharge. The snow melt in January 2011 resulted in a huge increase of both cumulative discharge and DOC export. The cumulative fluxes increased only slightly after the snowmelt in 2011 due to generally low discharge rates without major discharge peaks (Figure 1). The DOC flux calculations based on high frequency measurements (30 minutes) yielded an annual export of 84 kg C ha^{-1} yr^{-1} with 51.3 kg C ha^{-1} yr^{-1} during rainfall events > 5 mm (Table 2). 43% of the annual DOC export occurred in the growing season (Mai - October) and 57% in the dormant season (November – April). The calculation of DOC fluxes from the artificially created fortnightly sampling sequences with different starting dates (Table 3) resulted in variations of the annual flux from 47 to 124 kg C ha^{-1} yr^{-1}.
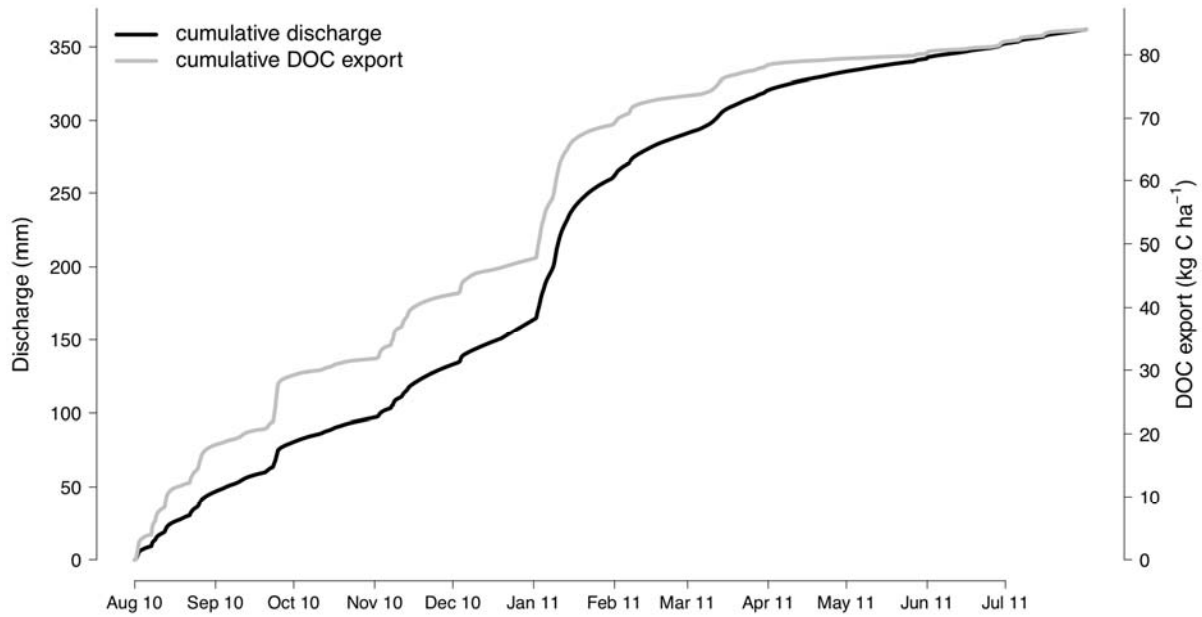
Figure 7: *DOC concentration and quality in response to discharge*

Table 3: *Effect of shifting starting dates on the annual DOC fluxes with runoff.*

Start date	End date	Export (kg ha-1 yr-1)
2010-08-06	2011-08-05	102
2010-08-07	2011-07-23	121
2010-08-08	2011-07-24	70
2010-08-09	2011-07-25	64
2010-08-10	2011-07-26	55
2010-08-11	2011-07-27	47
2010-08-12	2011-07-28	83
2010-08-13	2011-07-29	92
2010-08-14	2011-07-30	84
2010-08-15	2011-07-31	73
2010-08-16	2011-08-01	73
2010-08-17	2011-08-02	112
2010-08-18	2011-08-03	124
2010-08-19	2011-08-04	70

4 Discussion

4.1 Range, origin and mobilization of DOC in runoff

The DOC concentrations in runoff from the Lehstenbach catchment were highly variable at hourly to daily time scales, and ranged from 3 to 34 mg l^{-1}. The DOC concentrations in the lower range occurred at baseflow conditions, whereas concentrations increased with discharge. In comparison to other studies in forested watersheds, temporal variations and average concentrations (9.2 mg l^{-1}) of DOC in runoff in our study are quite high (Jeong et al. (2012)[22], Koehler et al. (2009[26])). However, Roulet et al. (2007)[44] reported even higher average DOC concentrations of 47.5 ± 13 mg l^{-1} in a study on a northern ombrotrophic bog. Short term variations of DOC in runoff have been related to changing water flow paths under high-flow, draining different compartments than under baseflow conditions (Hood et al. (2006[18]). In the Lehstenbach catchment the quality of DOC, concentration range and groundwater dynamics, point to the riparian wetland soils as the main source of DOC in runoff under high-flow conditions. The fluorescence spectroscopy of DOC distinguished between deep groundwater and water samples from shallow groundwater in the riparian wetland soils. The decrease of the groundwater component with rising discharge and the increase of the wetland component strongly suggest the riparian soils as the origin of both the fast runoff components (Frei et al. (2010)[14]) and high DOC concentration.

Although an interpretation in a molecular sense of PARAFAC derived fluorescence components from Cory and McKnight (2005[10]) seems to be limited (Macalady and Walton Day 2009 & 2011[34, 28]), this approach proved to be suitable for distinguishing DOC sources in our study, when interpreting fluorescence compounds as bulk quality indices or fingerprints. Taking the shallow wetland groundwater samples and deeper groundwater samples as possible end members in DOC quality indices, e.g. component 1 was indicative of wetland soil derived, shallow groundwater, while component 12 dominated fluorescence of DOC originating from deeper groundwater with low DOC contents (Figure 5). Correspondingly, under groundwater derived base-flow conditions low in DOC, relative contribution of component 12 increased, while under high discharge conditions rich in DOC, component 1 increased (Figure 6). Following Cory and McKnight (2005), component 1 was correlated to Ketal or Acetal Carbon as analyzed by ^{13}C NMR, and component 12 to % aliphatic carbon content. Due to its refractory character, a higher proportion of aliphatic carbon seems reasonable in groundwater with longer residence times. Fellmann et al. (2009[13]) attributed an increase in riparian wetland-borne DOC to increases in tryptophan-like fluorescence, with tryptophan being a rather labile amino acid. However, according to the PARAFAC Model of Cory and McKnight (2005[10]), who assigned component 8 to tryptophane-like fluorescence, in our dataset tryptophane-like fluorescence was higher in deeper groundwater than in shallow riparian wetland groundwater. This indicates that the interpretation of PARAFAC modeling, even if not on a molecular level, is

probably not unique and needs to be done with caution. The conclusion that the primary source for DOC in runoff is located in the wetland soils is also supported by the observed low DOC concentrations in deeper soil layers and groundwater (Table 1). Forested upland soils as a potential source of peaking DOC concentrations can practically be ruled out since direct surface runoff that could rapidly connect the upper soil layers with the streams is not observed in the Lehstenbach catchment, and response times of respective flow paths are too long to explain short term variations. The water percolating the forest floor layers enters deeper groundwater after DOC being removed largely by sorption or decomposition in the soil (Schulze et al. 2011[45]), resulting in DOC concentrations in the groundwater of only about 1-3 mg l^{-1} in our study. Lastly, increasing DOC in runoff always coincided with shallow groundwater levels in the riparian wetland soils, as also observed by Morel et al. (2009[39]) for a catchment in France.

An explanation for the observed short term variations of DOC in runoff is the non-linear increase in catchment discharge with rising riparian groundwater levels. This increase is probably the combined effect of efficient surface flow networks that develop when groundwater levels reach surface depressions (Frei et al. 2010)[14] and a general non-linear decrease of lateral hydraulic conductivity with depth (e.g. Seibert et al. 2009)[46]. Both mechanisms result in a rapid, non-linear increase of drainage efficiency of the system when riparian groundwater levels are rising. The latter mechanism has been termed *Transmissivity Feedback* (Bishop et al. 2004)[4] and was shown to control the transfer of solutes from the riparian zone to the streams (Seibert et al. 2009)[46]). The lateral hydraulic conductivity is typically lower in the deeper layers of wetland soils due to the compacted and more decomposed organic matter than in the porous and less decomposed shallow layers. The differences in hydraulic conductivities between deeper layers and shallow layers of wetland soils can be several orders of magnitude (Jacks und Norrström 2004[21]), causing shallow layers to drain much more effectively than deep soil layers. The shallow layers of the riparian wetland soils typically contain more DOC than deeper soil layers (Table 1). Rising groundwater levels in the riparian soils progressively engage soil layers with higher hydraulic conductivity and increasing DOC concentrations in the runoff generation process causing the strong response of DOC in runoff. The DOC pool available for mobilization in the riparian wetland soils seems to be large (Worrall et al. (2008)[51]) as also in our study there was no decrease in maximum DOC concentrations during subsequent rain events.

4.2   Temporal dynamics of DOC in runoff

The high temporal resolution of the DOC concentrations enabled a number of observations that would have been missed by typically infrequent samplings. The response of the DOC concentrations in runoff to discharge was characterized by counterclockwise hysteretic loops with lower concentrations on the rising limb compared to the falling limb. No flush of DOC at the beginning of the event was

observed and the peak of DOC occurred a few hours (160 min on average) after the discharge peak. Furthermore, the hysteretic loops were more pronounced and had a steeper slope in the summer/fall season than in the winter/spring season. The majority of hysteretic loops described in the literature are clockwise (e.g., Hornberger et al. (1994)[19], Butturini et al. (2006)[7], Jeong et al. (2012)[22]. This was also reported in studies where DOC was found to originate mainly from riparian wetland soils (McGlynn and McDonnell 2003[36], Hood et al. 2006[18]). Minding the proposed *Transmissivity Feedback* (Bishop et al. (2004)[4]) for DOC exports and highest DOC concentrations in the riparian wetland soils, this would also be expected for our catchment. However, although we could clearly identify the wetlands as DOC source areas based on DOC quality, we found counter-clockwise hysteretic loops, indicating that the peak of DOC concentration occurred on the falling limb of the hydrograph. The relation of DOC to discharge on the falling limb was steady and uniform, whereas the relation during the rising limb seems to depend on the preceding groundwater level in the wetland soils.

Evans and Davies (1998)[12] used hysteretic loops to analyze episode hydrochemistry and hydrologic characteristics of catchments. According to their classification Lehstenbach catchment fall into the category A2: Counter-clockwise and positive. The A2 type requires a near surface hydrological component with lower DOC concentrations than in the shallow groundwater of the wetland riparian soils. Hence, the counterclockwise hysteretic loops in our study are likely caused by a small, short term, but still significant water flux with less DOC than in the shallow groundwater of the wetland soils. Such a bypass in the Lehstenbach catchment might be caused by the still existing ditches in the wetland soils. According to this model, the restricted contact between this runoff component and the DOC-rich soil layers during initial runoff will result in lower DOC concentrations in the rising limb as compared to the falling limb. A possible bypass effect by a surface or surface-near flow component was further suggested by occasional, small peaks in nitrate concentrations at the begin of rain events after longer drought (data not shown), minding that in the riparian wetlands there is usually no nitrate present due to anoxic conditions (Goldberg et al. (2010)[16]). The effect of the bypass seems short term as indicated by the few hours delay of the DOC peaks in relation to the discharge peaks.

The mobilization of DOC from soil organic matter often follows seasonal patterns with increasing concentrations during the summer season. This has been shown for forest floors in field (Michalzik & Matzner 1999[38]) and in laboratory studies (Gödde et al. 1996[15]) as well as for wetland soils (Koehler et al. (2011[27]), Clair et al. (2002)[8]). The mobilization of DOC from soil organic matter is partly driven by microbial (enzymatic) processes and partly by physicochemical processes (Bolan et al. (2011)[5]), both being temperature dependent. Hence, the steeper slope of the hysteretic loops and the more pronounced hysteresis in the summer/fall season than in the winter/spring season seems largely due to a temperature effect on DOC mobilization. In addition, the flow paths of water in the winter season might be different from the summer/autumn season, since the top layers of the riparian

wetland soils – in summer responsible for high DOC concentrations in runoff– might not be drained due to freezing.

4.3 DOC fluxes

The annual export of DOC from the Lehstenbach catchment amounted to 84 kg ha^{-1} a^{-1}. The annual export is rather high in comparison to other forested watersheds. Kindler et al. (2011)[24] calculated average DOC losses for 5 Northern European forested catchments to be 35 kg C ha^{-1} yr^{-1}. The carbon export rates at the Lehstenbach catchment might be relatively high because a substantial part of the catchment is covered by riparian wetland soils. Laudon et al. (2011[29]) defined the ratio of wetlands to upland soils in boreal forested catchments as a driving variable for the DOC export with runoff. However, they suggest that the proportion of DOC in runoff from wetlands decrease with rising discharge as the contribution of water from upland zones increases. In our study we observed the opposite, since the proportion of DOC from wetlands increased with discharge.If we assume that the majority of DOC export from the Lehstenbach catchment results from the riparian wetland soils, representing 30% of the area, the solute C export from these soils is in the range of 240 kg C ha^{-1} yr^{-1}. This equals the average C accumulation rates of northern peatlands (Lavoie et al. (2005)[30]), emphasizing the huge contribution of DOC to net C exchange in these ecosystems.

Annual DOC exports were calculated both from high frequency measurements and by simulated infrequent sampling intervals with subsequent interpolation (Method 5, Walling and Webb 1985[49]). The 30 minute data yielded a DOC export of 84 kg C ha^{-1} yr^{-1}, which is taken here as the "true" reference flux. When the data were aggregated to daily values, the resulting flux was similar (82.4 kg C ha^{-1} yr^{-1}). However, applying the widely used interpolation equation from Walling and Webb (1985[49]) on the fortnightly shifted date sequences, a range of 47 and 124 kg C ha^{-1} yr^{-1} resulted, equal to 56 and 148 % of the "true" flux. Hence, massive errors in calculating DOC export by e.g. fortnightly samplings are possible. Our results contradict Koehler et al. (2009[26]) who suggested a weekly or monthly sampling frequency as adequate to calculate the yearly DOC flux with runoff from an Atlantic blanket bog catchment.

5 Conclusions

In the Lehstenbach catchment, DOC concentrations in runoff are subjected to substantial short term variations at an hourly to daily time scale driven by dynamics of the hydrological regime. Concentrations increased with increasing discharge, with strongest response in the summer/fall season. Quality parameters as well as the dynamics of groundwater table in the riparian zone document that the DOC in runoff originates from the riparian wetland soils. The DOC export represents a major contribution to the net C budget of the wetland soils. Future changes in the hydrological regime, e.g. by changing distribution and intensities of precipitation, will influence the

DOC dynamics in this catchment, with largest effects in the summer/fall season. The high frequency measurements documented that calculations of DOC export fluxes based on infrequent samplings might be subject to significant errors if steep concentration/discharge relations exist.

6 Acknowledgments

References

[1]   Anneli Agren, Ishi Buffam, Martin Berggren, Kevin Bishop, Mats Jansson, and Hjalmar Laudon. Dissolved organic carbon characteristics in boreal streams in a forest-wetland gradient during the transition between winter and summer. *JOURNAL OF GEOPHYSICAL RESEARCH-BIOGEOSCIENCES*, 113(G3), SEP 3 2008.

[2]   C. Alewell, G. Lischeid, U. Hell, and B. Manderscheid. High temporal resolution of ion fluxes in semi-natural ecosystems - gain of information or waste of resources? *Biogeochemistry*, 69:19–35, 2004. 10.1023/B:BIOG.0000031029.46798.7f.

[3]   Kari Austnes, Christopher D. Evans, Caroline Eliot-Laize, Pamela S. Naden, and Gareth H. Old. Effects of storm events on mobilisation and in-stream processing of dissolved organic matter (DOM) in a Welsh peatland catchment. *BIOGEOCHEMISTRY*, 99(1-3):157–173, JUL 2010.

[4]   K Bishop, J Seibert, S Koher, and H Laudon. Resolving the Double Paradox of rapidly mobilized old water with highly variable responses in runoff chemistry. *HYDROLOGICAL PROCESSES*, 18(1):185–189, JAN 2004.

[5]   Nanthi S Bolan, Domy C Adriano, Anitha Kunhikrishnan, Trevor James, Richard McDowell, and Nicola Senesi. Chapter one - dissolved organic matter: Biogeochemistry, dynamics, and environmental significance in soils. In *Advances in Agronomy*, volume 110, pages 1 – 75. 2011.

[6]   EW Boyer, GM Hornberger, KE Bencala, and DM McKnight. Effects of asynchronous snowmelt on flushing of dissolved organic carbon: a mixing model approach. *HYDROLOGICAL PROCESSES*, 14(18, SI):3291–3308, DEC 30 2000. 57th US/Canadian Annual Eastern Snow Conference, SYRACUSE, NEW YORK, MAY 17-19, 2000.

[7]   A Butturini, F Gallart, J Latron, E Vazquez, and F Sabater. Cross-site comparison of variability of DOC and nitrate c-q hysteresis during the autumn-winter period in three Mediterranean headwater streams: A synthetic approach. *BIOGEOCHEMISTRY*, 77(3):327–349, FEB 2006.

[8]   TA Clair, P Arp, TR Moore, M Dalva, and FR Meng. Gaseous carbon dioxide and methane, as well as dissolved organic carbon losses from a small temperate wetland under a changing climate. *ENVIRONMENTAL POLLUTION*, 116(1):S143–S148, 2002. Advances in Terrestrial Ecosystem: Carbon Inventory Measurements and Monitoring Conference, RALEIGH, NORTH CAROLINA, OCT 03-05, 2000.

[9]   Joanna M Clark, Stuart N Lane, Pippa J Chapman, and John K Adamson. Export of dissolved organic carbon from an upland peatland during storm events: Implications for flux estimates. *J Hydrol*, 347(3-4):438–447, Jan 2007.

[10]   RM Cory and DM McKnight. Fluorescence spectroscopy reveals ubiquitous presence of oxidized and reduced quinones in dissolved organic matter. *Environ Sci Technol*, 39(21):8142–8149, Jan 2005.

[11]   E. T. Degens, S. Kempe, and J. Richey. Biogeochemistry of major world rivers : Summary. In *"Biogeochemistry of Major World Rivers" (eds. E.T. Degens, S. Kempe & J. Richey), SCOPE Report 42, Chichester, New York, Brisbane, Toronto, Singapore, J. Wiley & Sons: 323-347.* Wiley, 1991.

[12]   C Evans and T.D Davies. Causes of concentration/discharge hysteresis and its potential as a tool for analysis of episode hydrochemistry. *Water Resources Research*, 34(1):129–137, 1998.

[13] Jason B. Fellman, Eran Hood, Richard T. Edwards, and David V. D'Amore. Changes in the concentration, biodegradability, and fluorescent properties of dissolved organic matter during stormflows in coastal temperate watersheds. *JOURNAL OF GEOPHYSICAL RESEARCH-BIOGEOSCIENCES*, 114, MAR 20 2009.

[14] S. Frei, G. Lischeid, and J. H. Fleckenstein. Effects of micro-topography on surface-subsurface exchange and runoff generation in a virtual riparian wetland - A modeling study. *ADVANCES IN WATER RESOURCES*, 33(11, SI):1388–1401, NOV 2010.

[15] Monika Gödde, Mark B. David, Martin J. Christ, Martin Kaupenjohann, and George F. Vance. Carbon mobilization from the forest floor under red spruce in the northeastern u.s.a. *Soil Biology and Biochemistry*, 28(9):1181 – 1189, 1996.

[16] Stefanie Daniela Goldberg, Klaus-Holger Knorr, Christian Blodau, Gunnar Lischeid, and Gerhard Gebauer. Impact of altering the water table height of an acidic fen on N2O and NO fluxes and soil concentrations. *GLOBAL CHANGE BIOLOGY*, 16(1):220–233, JAN 2010.

[17] L. Hanninen and M. Pastell. Cowlog: Open source software for coding behaviors from digital video. *Behavior Research Methods*, 41(2):472–476, 2009.

[18] Eran Hood, Michael N. Gooseff, and Sherri L. Johnson. Changes in the character of stream water dissolved organic carbon during flushing in three small watersheds, Oregon. *JOURNAL OF GEOPHYSICAL RESEARCH-BIOGEOSCIENCES*, 111(G1), FEB 3 2006.

[19] GM Hornberger, KE Bencala, and DM McKnight. Hydrological controls on dissolved organic carbon during snowmelt in the snake river near montezuma, colorado. *Biogeochemistry*, 25(3):147–165, 1994.

[20] Stephanie K. L. Ishii and Treavor H. Boyer. Behavior of reoccurring parafac components in fluorescent dissolved organic matter in natural and engineered systems: A critical review. *Environmental Science & Technology*, Online:A–L, 2012.

[21] G Jacks and AC Norrstrom. Hydrochemistry and hydrology of forest riparian wetlands. *FOREST ECOLOGY AND MANAGEMENT*, 196(2-3):187–197, JUL 26 2004.

[22] J.-J. Jeong, S. Bartsch, J. Fleckenstein, E. Matzner, J. D. Tenhunen, S. D. Lee, S. K. Park, and J.-H. Park. Differential storm responses of dissolved and particulate organic carbon in a mountainous headwater stream, investigated by high-frequency in-situ optical measurements. *J. Geophys. Res.*, 2012 (in press).

[23] K Kalbitz, S Solinger, JH Park, B Michalzik, and E Matzner. Controls on the dynamics of dissolved organic matter in soils: A review. *SOIL SCIENCE*, 165(4):277–304, APR 2000.

[24] Reimo Kindler, Jan Siemens, Klaus Kaiser, David C Walmsley, Christian Bernhofer, Nina Buchmann, Pierre Cellier, Werner Eugster, Gerd Gleixner, Thomas Grunwald, Alexander Heim, Andreas Ibrom, Stephanie K Jones, Mike Jones, Katja Klumpp, Werner Kutsch, Klaus Steenberg Larsen, Simon Lehuger, Benjamin Loubet, Rebecca McKenzie, Eddy Moors, Bruce Osborne, Kim Pilegaard, Corinna Rebmann, Matthew Saunders, Michael W. I Schmidt, Marion Schrumpf, Janine Seyfferth, Ute Skiba, Jean-Francois Soussana, Mark A Sutton, Cindy Tefs, Bernhard Vowinckel, Matthias J Zeeman, and Martin Kaupenjohann. Dissolved carbon leaching from soil is a crucial component of the net ecosystem carbon balance. *Global Change Biol*, 17(2):1167–1185, Jan 2011.

[25] JW Kirchner, XH Feng, C Neal, and AJ Robson. The fine structure of water-quality dynamics: the (high-frequency) wave of the future. *HYDROLOGICAL PROCESSES*, 18(7):1353–1359, MAY 2004.

[26] Ann-Kristin Koehler, Kilian Murphy, Gerard Kiely, and Matteo Sottocornola. Seasonal variation of doc concentration and annual loss of doc from an atlantic blanket bog in south western ireland. *Biogeochemistry*, 95(2-3):231–242, Jan 2009.

[27] Ann-Kristin Koehler, Matteo Sottocornola, and Gerard Kiely. How strong is the current carbon sequestration of an Atlantic blanket bog? *GLOBAL CHANGE BIOLOGY*, 17(1):309–319, JAN 2011.

[28] Macalady Donald L. and Walton-Day Katherine. *Redox Chemistry and Natural Organic Matter (NOM): Geochemists' Dream, Analytical Chemists' Nightmare*, chapter 6, pages 85–111. Aquatic Redox Chemistry 2011.

[29] Hjalmar Laudon, Martin Berggren, Anneli Agren, Ishi Buffam, Kevin Bishop, Thomas Grabs, Mats Jansson, and Stephan Köhler. Patterns and dynamics of dissolved organic carbon (DOC) in boreal streams: The role of processes, connectivity, and scaling. *Ecosystems*, 14:880–893, 2011. 10.1007/s10021-011-9452-8.

[30] Martin Lavoie, David Pare, and Yves Bergeron. Impact of global change and forest management on carbon sequestration in northern forested peatlands. *Environmental Reviews*, 13(4):199–240, 2005.

[31] G Lischeid, A Kolb, and C Alewell. Apparent translatory flow in groundwater recharge and runoff generation. *J Hydrol*, 265(1-4):195–211, Jan 2002.

[32] G Lischeid, H Lange, K Moritz, and H Büttcher. Dynamics of runoff and runoff chemistry at the Lehstenbach and Steinkreuz catchment. Ecological Studies(172):399–436, 2004.

[33] W Ludwig, JL Probst, and S Kempe. Predicting the oceanic input of organic carbon by continental erosion. *GLOBAL BIOGEOCHEMICAL CYCLES*, 10(1):23–41, MAR 1996.

[34] Donald L. Macalady and Katherine Walton-Day. New light on a dark subject: On the use of fluorescence data to deduce redox states of natural organic matter (NOM). *AQUATIC SCIENCES*, 71(2):135–143, JUN 2009.

[35] Egbert Matzner. *Biogeochemistry of Forested Catchments in a Changing Environment: A German Case Study*, volume 172 of *Ecological Studies*. Springer, 2004.

[36] BL McGlynn and JJ McDonnell. Role of discrete landscape units in controlling catchment dissolved organic carbon dynamics. *WATER RESOURCES RESEARCH*, 39(4), APR 11 2003.

[37] DM McKnight, EW Boyer, PK Westerhoff, PT Doran, T Kulbe, and DT Andersen. Spectrofluorometric characterization of dissolved organic matter for indication of precursor organic material and aromaticity. *LIMNOLOGY AND OCEANOGRAPHY*, 46(1):38–48, JAN 2001.

[38] B Michalzik and E Matzner. Dynamics of dissolved organic nitrogen and carbon in a Central European Norway spruce ecosystem. *EUROPEAN JOURNAL OF SOIL SCIENCE*, 50(4):579–590, DEC 1999.

[39] B. Morel, P. Durand, A. Jaffrezic, G. Gruau, and J. Molenat. Sources of dissolved organic carbon during stormflow in a headwater agricultural catchment. *HYDROLOGICAL PROCESSES*, 23(20):2888–2901, SEP 30 2009.

[40] Vincent J. Pacific, Kelsey G. Jencso, and Brian L. McGlynn. Variable flushing mechanisms and landscape structure control stream DOC export during snowmelt in a set of nested catchments. *BIOGEOCHEMISTRY*, 99(1-3):193–211, JUL 2010.

[41] Brian A. Pellerin, John Franco Saraceno, James B. Shanley, Stephen D. Sebestyen, George R. Aiken, Wilfred M. Wollheim, and Brian A. Bergamaschi. Taking the pulse of snowmelt: in situ sensors reveal seasonal, event and diurnal patterns of nitrate and dissolved organic matter variability in an upland forest stream. *BIOGEOCHEMISTRY*, 108(1-3):183–198, APR 2012.

[42] R Development Core Team. *R: A Language and Environment for Statistical Computing*. R Foundation for Statistical Computing, Vienna, Austria, 2011. ISBN 3-900051-07-0.

[43] Peter A. Raymond and James E. Saiers. Event controlled DOC export from forested watersheds. *BIOGEOCHEMISTRY*, 100(1-3):197–209, SEP 2010.

[44] Nigel T Roulet, Peter M Lafleur, Pierre J. H Richard, Tim R Moore, Elyn R Humphreys, and Jill Bubier. Contemporary carbon balance and late holocene carbon accumulation in a northern peatland. *Global Change Biol*, 13(2):397–411, Jan 2007.

[45] Kerstin Schulze, Werner Borken, and Egbert Matzner. Dynamics of dissolved organic C-14 in throughfall and soil solution of a Norway spruce forest. *BIOGEOCHEMISTRY*, 106(3):461–473, NOV 2011.

[46] J. Seibert, T. Grabs, S. Kohler, H. Laudon, M. Winterdahl, and K. Bishop. Linking soil- and stream-water chemistry based on a Riparian Flow-Concentration Integration Model. *HYDROLOGY AND EARTH SYSTEM SCIENCES*, 13(12):2287–2297, 2009.

[47] Robert G. M. Spencer, Brian A. Pellerin, Brian A. Bergamaschi, Bryan D. Downing, Tamara E. C. Kraus, David R. Smart, Randy A. Dahgren, and Peter J. Hernes. Diurnal variability in riverine dissolved organic matter composition determined by in situ optical measurement in the San Joaquin River (California, USA). *HYDROLOGICAL PROCESSES*, 21(23):3181–3189, NOV 1 2007.

[48] Colin A Stedmon, Stiig Markager, and Rasmus Bro. Tracing dissolved organic matter in aquatic environments using a new approach to fluorescence spectroscopy. *Marine Chemistry*, 82(3–4):239 – 254, 2003.

[49] DE Walling and BW Webb. Estimating the discharge of contaminants to coastal waters by rivers: Some cautionary comments. *Marine Pollution Bulletin*, 16(12):488 – 492, 1985.

[50] Hadley Wickham. The split-apply-combine strategy for data analysis. *Journal of Statistical Software*, 40(1):1–29, 2011.

[51] F. Worrall, H. S. Gibson, and T. P. Burt. Production vs. solubility in controlling runoff of DOC from peat soils - The use of an event analysis. *JOURNAL OF HYDROLOGY*, 358(1-2):84–95, AUG 30 2008.

[52] IUSS Working Group WRB. *World Reference Base for Soil Resources 2006, first update 2007*. Number 103. FAO, Rome, 2007.

Study 5

Interpreting flow generation mechanisms from integrated surface water-groundwater flow models of a riparian wetland and catchment.

By Daniel Partington, Philip Brunner, Sven Frei, Craig T. Simmons, Adrian D. Werner, René Therrien., Graeme C. Dandy, Holger R. Maier and Jan H. Fleckenstein

Ready for Submission

Ready for Submission

Interpreting flow generation mechanisms from integrated surface water-groundwater flow models of a riparian wetland and catchment.

D. Partington[1], P. Brunner[2].,S. Frei[3], C.T. Simmons[4], A.D. Werner[4], R. Therrien[5], G.C. Dandy[1], H.R. Maier[1] and J.H. Fleckenstein[6].

[1]School of Civil, Environmental and Mining Engineering, The University of Adelaide, Adelaide, South Australia 5005, Australia

[2]Centre of Hydrogeology and Geothermics (CHYN), Rue Emile-Argand 11, CP 158, CH-2009 Neuchâtel, Switzerland

[3]Department of Hydrology, Bayreuth Center of Ecology and Environmental Research (BayCEER), University of Bayreuth, 95440 Bayreuth, Germany

[4]School of the Environment and National Centre for Groundwater Research and Training, Flinders University, GPO Box 2100, Adelaide, South Australia 5001, Australia

[5]Department of Geology and Geological Engineering, Université Laval, Quebec, Canada G1K 7P4

[6]Department of Hydrogeology, Helmholtz Center for Environmental Research (UFZ), 04318 Leipzig, Germany

Abstract

A prerequisite for meaningful separation of a streamflow hydrograph is that stream-water derived from all stream and overland flow generation mechanisms is followed on its journey through the catchment, to the point at which the hydrograph is being measured. However, tracking of these mechanisms is not straight forward. In this study, a Hydraulic Mixing-Cell (HMC) methodology is presented that allows tracking of stream and overland flow generation mechanisms to attain meaningful separations of streamflow hydrographs within physically-based, distributed models. Application of the HMC methodology is demonstrated using two models of: (1) a virtual riparian wetland, and (2) a catchment of area 4.2 km^2. Simulation of surface and subsurface flow within these two systems was carried out under the hydrological driving forces of rainfall and evapotranspiration. Analysis of flow simulation results for a large storm event showed complex spatiotemporal transience in streamflow generation and surface water-groundwater interaction. Further analyses of both model results using the HMC method elucidated this complexity in the spatiotemporal distribution of the fraction of flow derived from different stream and overland flow generation mechanisms. The catchment scale model's year long stream and overland flow generation contributions to the outlet showed similarity with upstream model observation points, highlighting uniformity in flow generation

processes across this catchment, although this was not apparent over the period of the large storm event. This study showed within a modelling framework, that the HMC method can aid investigation into quantifying stream and overland flow generation processes. Use of this methodology is encouraged in physically distributed modelling studies for spatiotemporal assessment of catchment functioning and to provide meaningful separation of streamflow hydrographs.

1 Introduction

Understanding streamflow generation and surface water-groundwater (SW-GW) interaction is of great importance for the advancement of hydrology as highlighted in multiple reviews (Winter (1999), Sophocleous (2002), and more recently Fleckenstein *et al.* (2010)). Fleckenstein *et al.* (2010) highlighted advances in measurement of SW-GW interaction with improved spatiotemporal scales, but noted that there are difficulties in the ability to conduct such measurements, or to scale up such measurements to the catchment scale. High resolution spatiotemporal measurement of SW-GW interaction at the catchment scale is still almost impossible, and as a result, such data are limited. A precocious candidate for exploring data poor areas is through the analysis of detailed spatiotemporal model data obtained through numerical experimentation.

Studies in streamflow generation and SW-GW interaction using numerical experimentation are becoming increasingly widespread and are often carried out using an integrated, surface-subsurface hydrological model (ISSHM). The term "ISSHM" (Sebben *et al.*, 2012) referred to herein describes physically-based ISSHMs developed in the essence of the Freeze and Harlan (1969) blueprint – examples of such models are HydroGeoSphere (Therrien *et al.*, 2009), InHM (Vanderkwaak, 1999), ParFLOW (Kollet and Maxwell, 2006), CATHY (Camporese *et al.*, 2010) and MODHMS (HydroGeoLogic Inc., 2006). ISSHMs are not surrogates for real world observation; however, numerical experimentation using these types of models can assist in analysing and interpreting hydrological processes conceptually, even if the simulation is ill-posed (Ebel and Loague, 2006). Numerical experimentation in SW-GW studies has been utilised to examine a range of issues relating to streamflow generation and SW-GW interaction. For example, there have been studies (using ISSHMs) of micro-topographical influences on rainfall-runoff (Frei *et al.*, 2010), Hortonian rainfall-runoff processes (Kollet and Maxwell, 2008), controls on runoff generation (Vivoni *et al.*, 2007), quantification of the origins of stream water (Jones *et al.*, 2006; Park *et al.*, 2011), and stream-aquifer connection and disconnection (Brunner *et al.,* 2009). A common thread of these numerical studies is the need to identify the controls on how water reaches a stream (e.g. via overland flow, groundwater discharge), or where water is lost from a stream (e.g. via streambed losses).

The outlet streamflow hydrograph is usually one of the main model outputs analysed in ISSHM studies (e.g. Loague and Vanderkwaak, 2002; Ebel *et al.*, 2008; Li *et al.*, 2008; Shen and Phumikar, 2010; Mirus *et al.*, 2011; Park *et al.*, 2011). The focus on the outlet streamflow hydrograph results from the availability of flow data and the notion of streamflow hydrographs as integrated catchment descriptors. As a consequence of this notion, there have been many attempts to deconvolute and/or extract information from the streamflow hydrograph with respect to flow paths, sources and streamflow generation mechanisms. Unfortunately, accurate separation of the streamflow hydrograph into sources and streamflow generation mechanisms is still not possible, despite the advent of tracers

as integrated catchment descriptors to inform the separation (Jones *et al*., 2006; Park *et al*., 2011). ISSHMs can be used to determine conceptually the processes leading to streamflow generation (e.g. Loague *et al*., 2010; Vivoni *et al*., 2007); however, an underexploited advantage of ISSHMs is the use of this process information to determine the streamflow hydrograph makeup, i.e. which flow generation processes are driving streamflow at points of interest.

Numerical experimentation using ISSHMs results in a plethora of model outputs. These outputs describe surface flow discretely and the surface-subsurface exchanges spatiotemporally. With all of these outputs, it is still difficult to separate the streamflow hydrograph into different streamflow generation mechanisms (Partington *et al.*, 2011). For example, during a rainfall event, overland flow may occur on one part of a catchment, then infiltrate into the subsurface, percolate to a shallow aquifer and finally discharge to the stream months after the rainfall event. In this case, the area where that overland flow was generated during the rainfall event (i.e. the 'active' process) bears no relation to any overland flow contributions to streamflow (i.e. 'contributing' process) at the outlet during the same rainfall event. More generally, understanding the complexity of this problem is helped by considering the surface flow path of any parcel of water as it first enters the surface to the point where the streamflow hydrograph is measured. Firstly, upon entry the travel time for particular surface flow paths varies. Secondly, for some points of entry at particular points in time it does not always reach the outlet because of losses across an overland area and/or along a stream. The summation of flow generation processes across a catchment at a point in time represents the 'active' flow generation processes; however, it is not clear how these 'active' processes relate to the 'contributing' flow generation processes that make up a streamflow hydrograph at some point within a catchment. This idea of 'active' vs. 'contributing' processes is adapted from a paper by Ambroise (2004), which highlighted a need for the distinction between 'active' and 'contributing' areas or periods.

Capturing and summarising streamflow generation with respect to streamflow hydrographs necessitates accounting for the travel time and losses of water along a stream. Partington *et al.* (2011 and 2012) carried out this accounting using a Hydraulic Mixing-Cell (HMC) method, which provided the groundwater contribution to streamflow at any point along the stream. Their studies focused on the contribution of groundwater to streamflow in a synthetic catchment that exhibited both gaining and losing reaches, and furthermore that displayed time lags for flow from upstream areas. However, Partington *et al.* (2011 and 2012) did not consider the mechanisms driving overland flow (and eventually streamflow). Also, their implementation of the HMC method was only applicable on regular grids. Partington *et al.* (2011) highlighted that their formulation and coding of their HMC method suffered from some shortcomings (e.g. fixed flow direction and fixed river width), limiting its applicability to a broader range of hydrological settings. Another issue highlighted was that the HMC method was only stable if the ratio of outflow to storage was less than 1, and the fluid mass balance error was very small (Partington *et al.*, 2011). However, Partington *et al.* (2011) had no provision for

dealing with these stability issues, therefore requiring very high accuracy in the fluid mass balance at each HMC, as well as small time steps. Overcoming these limitations would enable the use of the HMC method in more complex systems than the idealised catchment of Partington *et al.* (2011), and would allow for better assessment of simulations within ISSHMs by extracting stream and overland generation mechanisms. In order to overcome these limitations, the HMC method is improved within this paper by: (1) integrating the HMC method within an ISSHM, (2) accounting for overland flow generation mechanisms in the HMC method, (3) developing a sub-timed HMC scheme, and (4) implementing HMC stability constraints.

Demonstration of these improvements is carried out in a case study of the Lehstenbach catchment in South-eastern Germany. The Lehstenbach catchment is chosen due to the complex nature of rainfall-runoff arising from the pronounced micro-topography in the wetlands adjacent to the stream (see Frei *et al*. 2010). Two models based on the Lehstenbach catchment are used for demonstrating the improved HMC analysis. The first model is of a virtual riparian wetland-typical of wetlands within the Lehstenbach catchment, and the second model is of the entire Lehstenbach catchment. In the context of numerical simulation, the improvements to the HMC method allow the following questions to be explored within the Lehstenbach catchment:

Q1.   What are the stream and overland flow generation mechanisms driving surface flow?

Q2.   What is the spatiotemporal variability at different scales in stream and overland flow generation mechanisms?

Q3.   Do the 'active' and 'contributing' processes differ significantly within the catchment?

Answering these questions will provide a new insight into the functioning of the catchment, as interpreted from the models (e.g. the controls on surface-runoff). This insight, obtained from model simulation, will hopefully provide improved knowledge of the catchment processes.

2   Improved HMC method

2.1   Integrating the HMC method in HGS.

The HMC analysis applied in Partington *et al.* (2011 and 2012) was done so as a post-processor outside of the numerical simulator HydroGeoSphere (HGS) (further details of HGS are detailed in section 4.1). Whilst suitable for those studies, this external post-processing required output of a large number of data files from HGS, to provide the nodal fluid mass balance at each HMC. Additionally, this post-processing implementation only accommodated a regular grid structure, fixed flow direction, and simple stream definition. These restrictions preclude it from application to models with a large number of nodes, irregular grids, variable flow direction, and complex streams.

To address these shortcomings, the HMC method is implemented within the HydroGeoSphere (HGS) code to seamlessly integrate it into simulations (avoiding outputting large datasets from HGS). Integrating into the HGS code allows the HMC method to be applied for all the options within the code, accommodating for both regular and irregular grids, irrespective of flow direction and stream definition. In particular, this implementation provides improved ease of use and allows other users of the HGS code to utilise the HMC method.

2.2   Capturing stream and overland flow generation mechanisms.

Overland flow generation mechanisms were overlooked in the studies of Partington *et al.*(2011 and 2012) due to the focus on the groundwater contribution to streamflow. The HMC method is expanded here to include overland flow generation and to also allow further control on which surface nodes are tracked.

Each flow generation mechanism is denoted by a unique fraction *f*, in the HMC fluid mass balance. Over each time step of the model simulation, inflowing water from either the subsurface (e.g. groundwater discharge) or surface boundary conditions (e.g. rainfall) is assigned the corresponding fraction (e.g. groundwater discharge to the stream, rainfall to the stream etc.) equal to 1. Inflow from adjacent HMCs is assigned the fractions from the upstream HMC. The calculation of fraction *f* for each stream or overland flow generation mechanism *k* at time *N* in HMC *i* is described by:

$$f_{i(k)}^{N} = \left(\frac{V_i^{N-1}}{V_i^N} - \frac{\sum_{j=1}^{m} V_{ij}\big|_{N-1}^{N}}{V_i^N} \right) f_{i(k)}^{N-1} + \frac{\sum_{j=1}^{n} V_{ji}\big|_{N-1}^{N} f_{j(k)}^{N-1}}{V_i^N} \quad (1)$$

Where there are *n* sources and *m* sinks for cell *i*; $f_{j(k)}^{N-1}$ denotes fraction *k* at time *N-1* in the neighbouring cell *j*, *V* denotes the volume with the superscript denoting time state and subscript *i*

denoting the cell, *ij* denoting volume into *j* from *i* over the time step from *N*-1 to *N* and *ji* denoting volume from neighbour *j* into *i*.

Streamflow generation mechanisms are determined based on surface node definition: e.g. stream or overland or 'other' nodes. 'Other' nodes could be lakes, reservoirs, upstream inflow boundaries that may not be of interest in HMC analysis. Flow generation at 'other' nodes is not captured explicitly. Any water flowing from 'other' nodes to an 'interest' node, (e.g. stream node) is assigned an 'other' fraction of unity (i.e. $f_{other} = 1$). Initial conditions for surface water in each HMC at the beginning of model simulations default to having the fraction 'initial' (i.e. $f_{initial} = 1$) unless defined otherwise.

2.3   Sub-timed HMC algorithm.

The stability of the HMC method is dependent on the ratio of outflow to storage. This is because the volume of water leaving from an HMC over a given time step cannot be greater than the volume in storage. The volume leaving an HMC is calculated using the fluid mass balance, accounting for imperfect fractions (i.e. $\sum f_{i(k)}{}^N \neq 1$) within each HMC (for outflow and storage). The HMC ratio for each HMC *i* is defined as:

$$HMC\ ratio\,(i) = \frac{\sum\limits_{j=1}^{m} V_{ij}\Big|_{N-1}^{N} f_{i(k)}^{N-1}}{V_i^{N-1} \sum\limits_{\forall k} f_{i(k)}^{N-1}} \quad (2)$$

Instability in the HMC method results when the HMC ratio is greater than 1 in any HMC. For small HMCs, the storage volume may be quite small relative to the flow out. Maintaining the HMC ratio below 1 can necessitate very small time steps when the HMC's storage is small relative to the flow. This is problematic for long term transient simulations requiring large time steps in the flow solution. As part of the improved HMC method a sub-timed HMC algorithm is implemented to prevent the necessity of a large number of relatively small time steps (i.e. computationally restrictive). This implementation removes the stability restrictions imposed by the HMC on the maximum time-step for the flow solution. The sub-timed HMC algorithm is applied when the maximum HMC ratio at any of the HMCs is greater than 1. It works by subdividing the time step into smaller time steps, and in turn subdividing the volume of water flowing into and out of each HMC into smaller volumes, as well as the changes in water storage over each time step.

The sub-timed scheme is reliant on the ability to reconstruct temporal in/out flow functions for each HMC. As all flows are fixed over each time step (i.e. step function), changes in storage are linear over time. Breaking up the time step (if the maximum HMC ratio is greater than 1) ensures the HMC ratio across all HMCs is less than or equal to 1. After each time step of the flow solution is completed, the sub-timed scheme is applied as follows:

[215]

(a) Calculate the number of sub-time steps required to ensure *HMC ratio max* ≤ 1:

$$Sub\text{-}steps = [HMC\ ratio\ max] + 1 \quad (3)$$

(b) Calculate the ratio for adjusting inflows, outflows and storage for all but the last sub-time step:

$$dt\ ratio = 1/(Sub\text{-}steps - 1) \quad (4)$$

(c) Calculate the ratio for adjusting inflows, outflows and storage for last sub-time step:

$$dt\ ratio\ end = 1 - dt\ ratio * (Sub\text{-}steps - 1) \quad (5)$$

(d) Calculate change in storage for the HMC over the last time step:

$$dS = V_i^N - V_i^{N-1} \quad (6)$$

(e) Calculate the sub-timed HMC fractions as follows:

When *sub-time step* $= 1$:

$$V_i^{SUB} = V_i^{N-1} + sub\ time\ step * dt\ ratio * dS \quad (7)$$

$$f_{i(k)}^{N(sub\ time\ step)} = \left(\frac{V_i^{N-1}}{V_i^{SUB}} - \frac{\sum_{j=1}^{m} V_{ij}\Big|_{N-1}^{N} * dt\ ratio}{V_i^{SUB}} \right) f_{i(k)}^{N-1} + \frac{\sum_{j=1}^{n} V_{ji}\Big|_{N-1}^{N} f_{j(k)}^{N-1} * dt\ ratio}{V_i^{SUB}} \quad (8)$$

When *sub-time step* $<$ *Sub-steps*:

$$V_i^{SUB-1} = V_i^{N-1} + (sub\ time\ step - 1) * dt\ ratio * dS \quad (9)$$

$$V_i^{SUB} = V_i^{N-1} + sub\ time\ step * dt\ ratio * dS \quad (10)$$

$$f_{i(k)}^{N(sub\ time\ step)} = \left(\frac{V_i^{SUB-1}}{V_i^{SUB}} - \frac{\sum_{j=1}^{m} V_{ij}\Big|_{N-1}^{N} * dt\ ratio}{V_i^{SUB}} \right) f_{i(k)}^{N(sub\ time\ step-1)} + \frac{\sum_{j=1}^{n} V_{ji}\Big|_{N-1}^{N} f_{j(k)}^{N(sub\ time\ step-1)} * dt\ ratio}{V_i^{SUB}} \quad (11)$$

When *sub-time step* $=$ *Sub-steps*:

$$V_i^{SUB-1} = V_i^{N-1} + (sub\,time\,step - 1)*dt\,ratio*dS \quad (12)$$

$$f_{i(k)}^N = \left(\frac{V_i^{SUB-1}}{V_i^N} - \frac{\sum_{j=1}^m V_{ij}\Big|_{N-1}^N *dt\,ratio\,end}{V_i^N} \right) f_{i(k)}^{N(sub\,time\,step-1)} + \frac{\sum_{j=1}^n V_{ji}\Big|_{N-1}^N f_{j(k)}^{N(sub\,time\,step-1)} *dt\,ratio\,end}{V_i^N} \quad (13)$$

2.4   Stability constraints for efficient execution of the HMC method.

The sub-timed HMC scheme allows large time steps in the flow solution. The number of sub-steps undertaken is dictated by the *HMC ratio*, which when large (e.g. > 10000), results in a large number of sub-time steps. In terms of computational efficiency, this is not desirable for HMCs that only have very small volumes of water in storage. This is because, for example, when an HMC is near dry, the onset of rainfall, groundwater discharge or overland flow immediately causes the *HMC ratio* to be much greater than 1. This problem tends to occur in simulating ephemeral reaches of streams whereby the stream HMCs become dry. Similarly, this occurs in simulating overland flow whereby the overland HMCs are often dry (due to overland flow only normally occurring in rainfall events).

To address these problems and ensure stability and computational efficiency, the following criteria are embedded in the method and used to determine if each HMC should be evaluated:

a) *Minimum volume criteria*. An HMC that has a very small amount of storage is not considered unless it has a surface flow greater than zero (less than $10^{-10}\,m^3$ in this study).

b) *Ponding only*. If the inflow and outflow are less than the storage (for HMCs where no surface flow occurs), then the HMC is not considered if it is ponding without surface flow, and the inflow or outflow are greater than the ponded water storage.

c) *Maximum HMC ratio*. If the *HMC ratio* (Eq. 2) is considered too large at any HMC, then it is not considered (set to 10000 in this study).

d) *Relative volume error too high*. If the ratio of the absolute volume error to storage is deemed too high, then the HMC is not considered (where the absolute volume error denotes the absolute value of the error in the volumetric HMC balance).

e) *Error in HMC excessive*. If the absolute error in an HMC (due to imperfect nodal fluid mass balance) is greater than a certain amount (e.g. 50%) after updating the fractions in the HMC, the HMC is not considered.

If any of the criteria are not, then these HMC's are 'reset', which means that all fractions f in the reset HMC are set equal to zero, and then the HMC is assigned the reset fraction ($f_{Reset} = 1$). The criteria for a 'reset' HMC are checked at each time step allowing it to become active if the 'reset' criteria are no longer met. This 'Reset' fraction allows the tracking of the fraction of water for which the flow generation is unknown (due to being reset), which quantifies the effect of this 'reset' fraction. The tracking of the 'reset' fraction will highlight if this unknown flow generation is significant. If the 'reset' fraction of flow in the streamflow hydrograph is high (>1%) then each criterion can be modified to bring this to a satisfactory level (<1%).

3   Case study: Lehstenbach catchment

The Lehstenbach catchment is located in South-eastern Germany, shown in Figure1. Elevations for the site vary between 877 m above sea level for upslope areas and 690 m above sea level for the catchment's outlet. Average annual precipitation over the 4.2 km² catchment is approximately 1150 mm with an annual mean temperature of approximately 5°C (Gerstberger, 2001). The main regional aquifer of the Lehstenbach catchment (around 40 m thick) is made of regolithic material originated from the weathering of the granitic bedrock (Lischeid *et al.*, 2002). Nearly one-third of the catchment's total area can be classified as riparian wetlands, which are located around all major streams preferentially at the bottom of the basin-shaped catchment. Within the wetlands, annual groundwater fluctuations are limited to the upper 0.5 m of the organic peat soil. For upslope areas which are mainly forested (*Piceaabies*), the local groundwater level lies relatively deep below the surface (5 m - 10 m). In parts, the groundwater located within the riparian wetlands is disconnected from the deeper regolithic aquifer due to a clogging clay layer of variable thickness. Previous studies performed for the Lehstenbach catchment indicated that important mechanisms of runoff generation (fast flow components e.g. saturated overland flow or shallow subsurface flow) originate within the wetland area. Core zones of these wetlands, mainly located near the catchment's outlet are characterized by a pronounced micro-topography, sequences of hollow and hummock structures, built by the wetland's typical vegetation (Knorr *et al*. 2008).
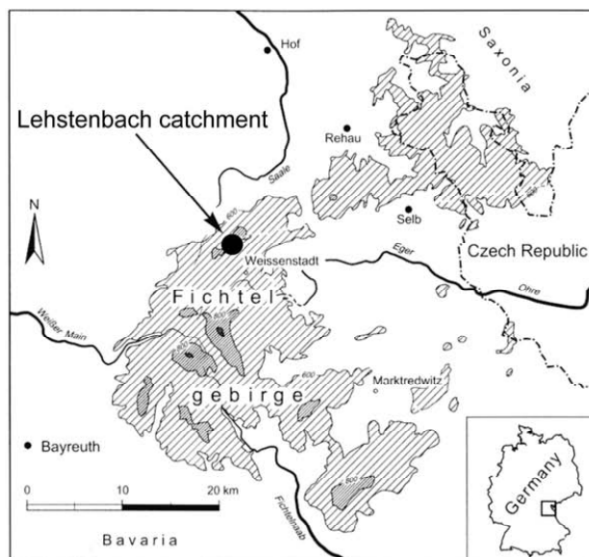

Figure 1: *Location of the Lehstenbach catchment.*

Figure 2 shows a conceptual hill-slope plot depicting the stream and overland flow generation mechanisms in the Lehstenbach catchment.
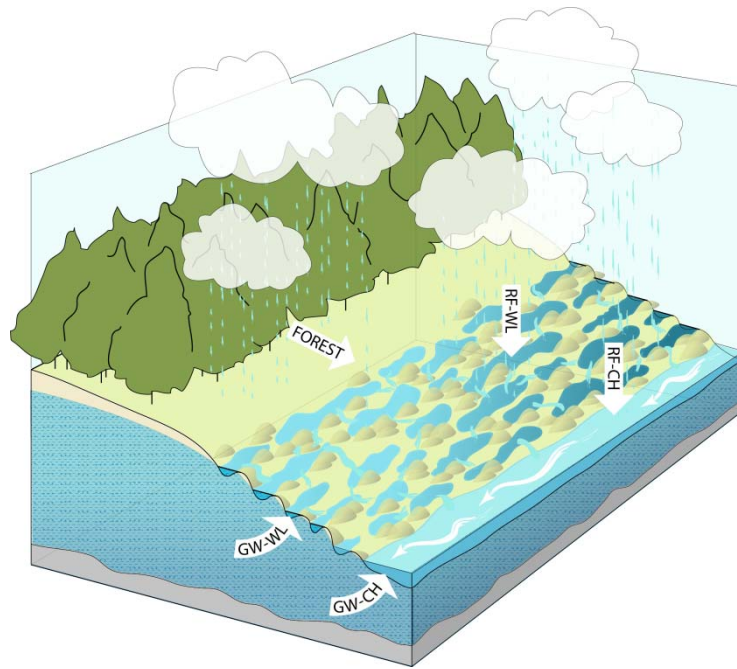
Figure 2: Conceptual diagram of stream and overland flow generation mechanisms typical of the Lehstenbach catchment during storm events. The stream and overland flow generation mechanisms shown are groundwater discharge to the wetlands and channel, direct rainfall to the wetlands and channel, and runoff from the forest.

4 Methodology

The ISSHM HGS is used for hydrological modelling in this study. Stream and overland flow generation is analysed within HGS using the improved HMC method detailed in Section 2. The modelling investigation into stream and overland flow generation is carried out at two different scales. Firstly, an analysis of a virtual wetland model is carried out, followed by the analysis of a catchment model. Then a comparison between these two models is performed to allow assessment of the differences, if any, of controls on streamflow generation. These analyses allow questions Q1-Q3 in the introduction to be addressed.

4.1 The fully integrated modelling platform

This modelling study is carried out using HGS (Therrien *et al.*, 2009). HGS incorporates 3D variably saturated subsurface flow using a modified form of the Richard's equation and 2D surface flow using the diffusion wave approximation to the St Venant equations, further details of which can be found in Therrien *et al.* (2009). The surface and subsurface are coupled using a first order exchange coefficient (Park *et al.*, 2009). An important characteristic of fully integrated models such as HGS is that there is no requirement for *a priori* assumptions of specific streamflow generation mechanisms (Mirus *et al.*, 2011). Consequently, the onus is on the modeller to interpret the model outputs for quantifying streamflow generation mechanisms within the model.

4.2 Development of HGS models

4.2.1 *Virtual wetland model setup*

The model setup for the virtual wetland model is described in Frei *et al.* (2010), and so only a brief description is presented here. The virtual wetland model (Figure 3) is at the plot scale (21 m x 10 m) representing a relatively flat hill-slope (constant slope of 0.03 m/m) made up of a sequence of hummocks and hollows. The spatial structure of the micro-topography is represented using geostatistical indicator simulations based on a Markov Chain model of transition probabilities (Carle and Fogg, 1996). The model domain is made up of 410,832 elements and 210,000 nodes, providing a fine discretisation in the X, Y and Z axes. The subsurface is represented as homogeneous with a saturated hydraulic conductivity of 0.2 m/d which was reported for the field site (Hauck, 1999) and for wetlands in general (Kruse et al., 2008; Schlotzauer and Price, 1999). Variably saturated flow is represented using the Van Genuchten model of the soil retention function (Van Genuchten, 1980) based on field measurements for similar wetlands located in Alberta, Canada (Price *et al.*, 2009).
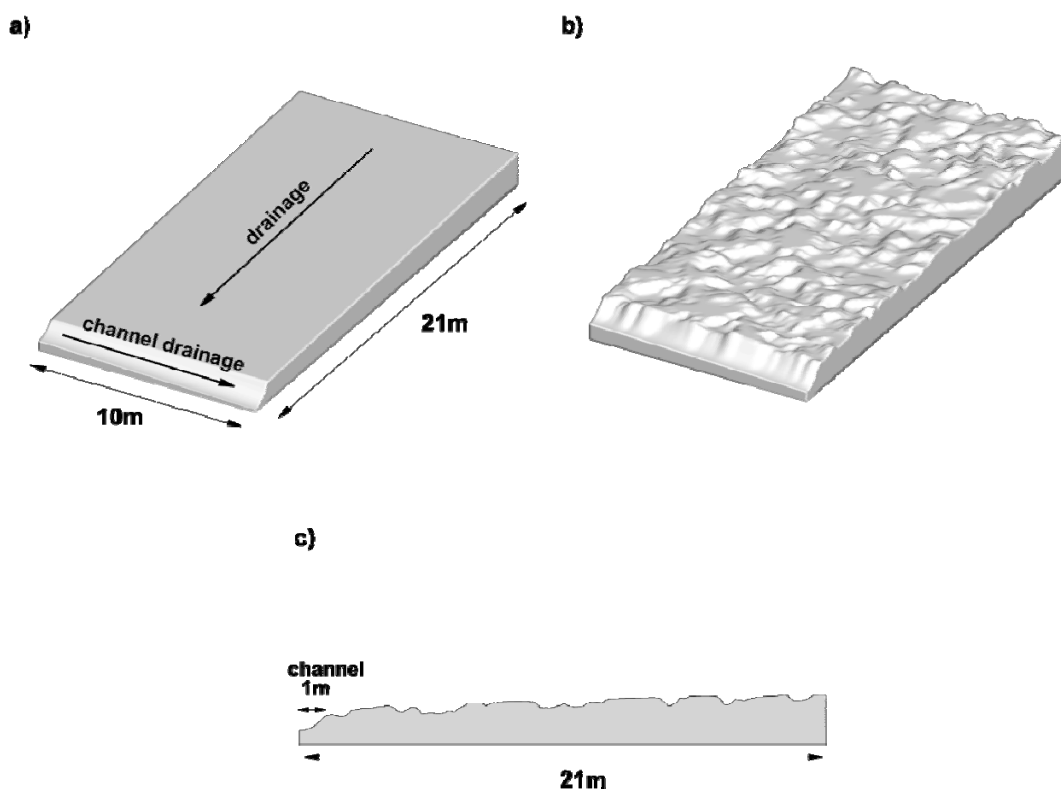
Figure 3: Geometry of the virtual wetland segment: a) planar reference model showing the main drainage direction and channel location; b) smoothed realisation of the wetlands hummocky micro-topography; c) cross section (Y = 5 m) of the micro-topography model.

Frei *et al.* (2010) demonstrated, through numerical simulation, a hysteretic relationship between surface water storage and channel discharge. Frei *et al.* (2010) concluded that enhanced mixing between surface and subsurface water had potential implications for the water quality within the catchment. The study of Frei *et al.* (2010) did not explore mixing of ponded rainfall and ponded groundwater discharge within the wetlands, which would have necessitated adequate understanding of overland flow and ponding generation as well as an understanding of each of these overland flow contributions to the channel flow. The application of the HMC method to the micro-topography model expands on the work of Frei *et al.* (2010), and is used to elucidate the proportion of overland flow that is generated from rainfall running off the wetlands and groundwater discharging to the wetlands.

The simulation period focuses on a large storm event (13th- 21st July, 2001) from the 2000-2001 hydrological year. The simulation starts with a recession period (i.e. no rain) lasting 14 days. After day 14, an extended rainfall event occurs (shown in the hyetograph of Figure 6). The rainfall event persists for 8 days leading to the depressions on the slope filling until they spill to the adjacent down-slope depressions. Details of this fill and spill mechanism and its influence on overland flow are covered in Frei *et al.* (2010).

4.2.2   Catchment model setup

A digital elevation model (DEM) with a spatial resolution of 5 m x 5 m is used to represent the basin shaped topography of the catchment. Vertically, the model is discretised into two main layers of variable thickness to represent the major soil types and subsurface geology of the Lehstenbach catchment. Within the wetland areas, the upper surface layer (1 m thick) represents the organic peat soils. This upper layer is further divided into 10 sub-layers each with a spatial resolution of 0.1 m in the vertical (see Table 1). For the ten sub-layers, the saturated hydraulic conductivities (K_{sat}) vary exponentially with depth to account for effects related to the transmissivity feedback mechanism, which is a common feature for wetlands (Bishop *et al.*, 2004; Jacks and Norrström, 2004). Values for K_{sat} for the different sub-layers ranged between 20 m/d for the uppermost layer (representing fresh and less compacted organic material) and 8.6×10^{-3} m/d for the basal clay layer which disconnects the wetlands from the deeper aquifer (Table 1). The values for K_{sat} for the wetland areas are based on the study of Jacks and Norstöm (2001) who performed slug tests for similar wetlands located in the Luntoma catchment in South-western Sweden. The lower model layer (20-40m thick) is used to represent the main regolithic aquifer of the Lehstenbach catchment. Variably saturated flow is represented using the Van Genuchten model for soil retention functions. Soil retention functions are applied uniformly to the upper wetland layers based on field measurements performed by Price *et al.* (2009) for similar wetlands in Alberta, Canada. For the main regolithic aquifer, a Van Genuchten model is adapted to field measurements performed for the Lehstenbach catchment (Werb, 2009) and applied uniformly to the lower model layer.

Horizontally, the model uses a triangular mesh with variable grid resolutions (Figure 4). Nodal spacing for the model varies between 10 m directly near the streams, 30 m within riparian wetlands and 100 m for upslope areas. Within HGS, the locations of streams develop out of the model's topography. However, the DEM used was too coarse to resolve differences in elevation between stream channels and the surrounding areas. Therefore, the elevation of surface nodes which coincide with stream locations were manually lowered (1 m). For the subsurface flow domain, the model boundaries were set to no flow to represent the impermeable granitic bedrock (lower boundary) and because it can be assumed that there is no exchange of groundwater with areas located outside of the Lehstenbach catchment. For the surface flow domain, the upper boundary condition uses a combination of variable rainfall, interception and simulated evapotranspiration. Interception and comprehensive evapotranspiration (Panday and Huyakon, 2004), within HGS, are simulated as mechanistic processes governed by plant and climatic conditions as noted by Kristensen and Jensen (1975) and Wigmosta *et al.* (1994). The edges of the surface flow domain use a critical depth boundary to allow surface water to flow out of the model. Manning's roughness coefficients for the forested upslope areas were assigned uniformly to 1.9×10^{-6} d/m$^{1/3}$ representing areas of minor ground vegetation (Shen and Julien 1993). Friction slopes for the X and Y in the wetlands were set to 8.1 x

10^{-5} d/m$^{1/3}$, typical for high grass (Shen and Julien 1993). K_{sat} for the lower model layer was modified to better represent the observed discharge measurements for the hydrologic year 2000 (11/1/2000 – 10/31/2001). Optimal results were achieved using an isotropic K_{sat} of 0.24 m/d, assigned uniformly to the lower model layer. The Nash-Sutcliffe efficiency for the catchment model was 0.5 based on the hydrological years 2001-2005 (Figure 5).

Table 1: *Surface and subsurface parameters for the Lehstenbach catchment model. Further details of these parameters can be found in Therrien et al. (2009).*

Parameter	Value	Parameter	Value
Surface		**Evapotranspiration**	
Forest		*Wetlands and Forest*	
Manning's roughness n	1.9×10^{-6} d/m$^{1/3}$	Evaporation depth *	0.5m
Rill storage	0.5 m		
		Transpiration fitting parameter	
Wetlands		c1	0.2
Manning's roughness n	8.1×10^{-5} d/m$^{1/3}$	c2	0.5
Rill storage	0.1, 0.5 and 1 m	c3	1.0
		Wilting point	0.24
Stream		Oxic limit	1.0
Manning's roughness n	4.0×10^{-7} d/m$^{1/3}$	Anoxic limit	1.0
Rill storage	0.0 m	Limiting saturation (min)	0.24
		Limiting saturation (max)	0.4
Surface/Subsurface coupling		Canopy storage parameter	1×10^{-6}m
Coupling Length	0.1 m	Initial interception storage	1×10^{-6}m
Subsurface		*Wetlands*	
Bottom, Middle and Top Layer		Root depth	0.8m
Hydraulic conductivity K_{sat}	0.24 m/d	Leaf area index	3.0
Porosity	0.4	Field capacity	0.35
Van Genuchten α	2.69 m^{-1}		
Van Genuchten β	1.45	*Forest*	
Residual Saturation θ_r	0.1	Root depth	3.0m
		Leaf area index	6.5
Wetland Layers (bottom-top)		Field capacity	0.34
Hydraulic conductivity K_{sat}	0.01, 0.02, 0.05, 0.13, 0.29, 1.59, 3.69, 8.60, 20.00 m/d		
Porosity	0.5		
Van Genuchten α	3.5 m^{-1}		
Van Genuchten β	1.7		
Residual Saturation θ_r	0.1		
Clay Layer			
Hydraulic conductivity K_{sat}	0.86 m/d		
Porosity	0.45		
Van Genuchten α	1.55 m^{-1}		
Van Genuchten β	1.26		
Residual Saturation θ_r	0.1		

* quadratic decay function

The topography and land use for the Lehstenbach catchment are shown in Figure 4. The elemental type distribution shown in Figure 4 is used to delineate the stream, wetlands and forest areas. Even though the detailed micro-topography of the virtual wetland model cannot be included at the catchment scale (due to computational constraints), the threshold behaviour of the runoff from

wetlands should still be apparent due to spatially distributed rill storage height zones which are used to mimic depressional storage characteristics and the typical fill and spill mechanisms of the wetland's micro-topography. However, the behaviour of the wetlands in this model (as opposed to the virtual wetland model) is influenced additionally by variable groundwater heads at the upslope boundaries, which are driven largely from recharge originating from infiltration in the upslope forested areas.
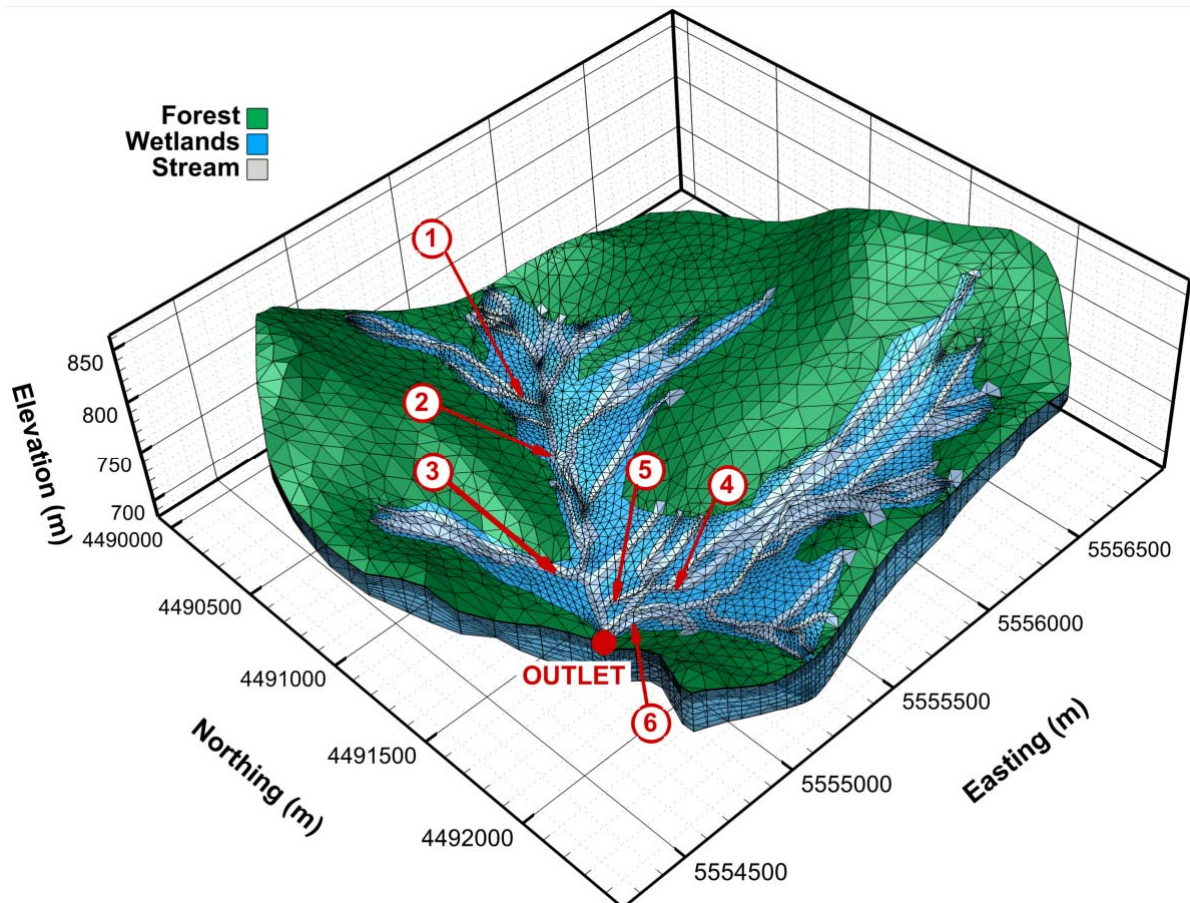

Figure 4: Model spatial discretisation for the Lehstenbach catchment and distribution of the stream, wetland and forest areas (the z-axis is exaggerated by a factor of 5). Model observation points are locations 1 to 6 and the outlet.
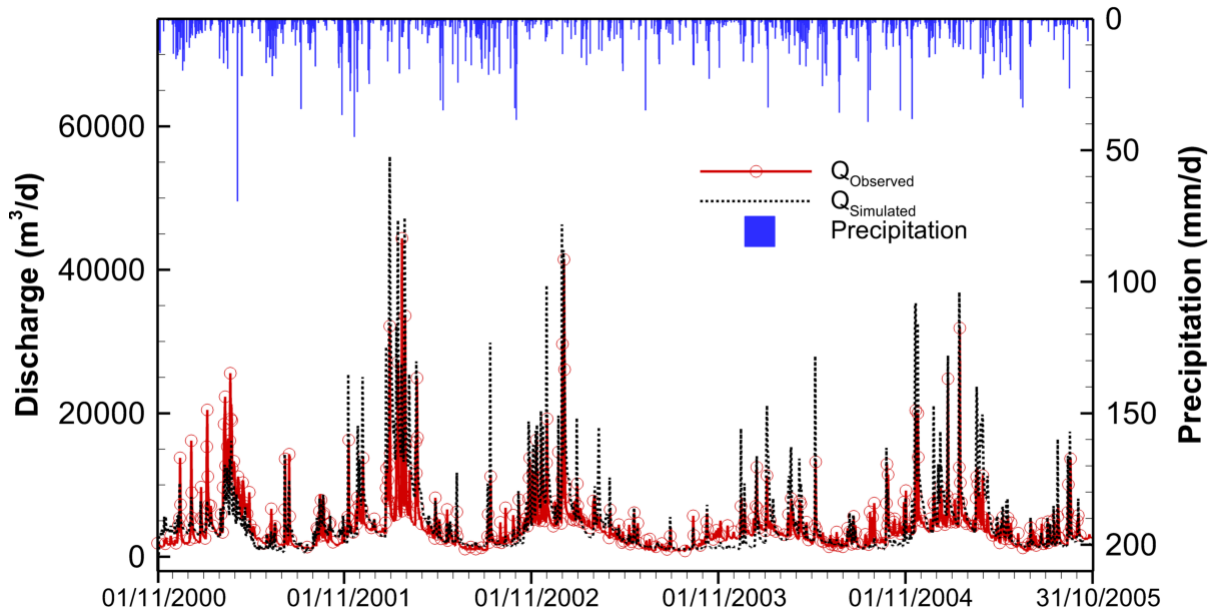
Figure 5: *Observed versus simulated discharge for the Lehstenbach catchment.*

The simulation period is the 2001 hydrological year, although a focus is placed on the large July storm simulated in the virtual wetland model. **Fehler! Verweisquelle konnte nicht gefunden werden.** shows the rainfall hyetograph and simulated streamflow hydrograph for the focus period.

4.3 HMC model analyses

The flow generation mechanisms analysed in this case study (see Figure 2) are: (1) groundwater discharge to the stream channel (GW-CH), (2) direct rainfall to the stream channel (RF-CH) and overland flow to the stream channel. The overland flow generation mechanisms analysed are: (3) groundwater discharge to wetland areas (GW-WL), (4) direct rainfall on wetlands (RF-WL) and (5) flow from forested areas (Forest).

The unique fractions *k* used in this HMC analysis are: (1) GW-CH, (2) RF-CH, (3) GW-WL, (4) RF-WL, (5) Forest, and also (6) initial water (Initial) and (7) 'reset' water (Reset). Streamflow generation mechanisms are determined based on surface node definition: i.e. stream, wetland or forest nodes. Any water flowing from forest HMCs to either wetland or stream HMCs is assigned a forest fraction of unity (i.e. f_{forest} = 1). Initial conditions for surface water in each HMC at the beginning of model simulations default to having the fraction 'initial' (i.e. $f_{initial}$ = 1). Water in the surface domain is assigned as 'reset' water if it does not meet the stability criteria defined in section 2.4.

The questions outlined in the introduction are answered by analysis of the HMC method results. Each analysis outlined below corresponds directly with questions Q1-Q3.

4.3.1   *Quantifying the stream and overland flow generation mechanisms driving flow.*

The main output from the HMC method is the different fractions of flow generation mechanisms at each HMC. Quantifying these components at the outlet is carried out by summing both the total surface outflow and surface outflow from different flow generation components across all HMCs at the select observation points.

4.3.2   *Analysing spatiotemporal variability of stream and overland flow generation.*

Spatial variability of stream and overland flow in both models is demonstrated in three ways. Firstly, visualisation of the HMC fractions across the model surface domain is shown in each model. Secondly, flow hydrographs are shown at select observation points within each of the models. Lastly, the different flow generation mechanisms driving total flow at each of the locations are summarised. The summarising of the flow components is achieved by integrating under the flow curves for each of the flow generation mechanisms, at each select observation point.

4.3.3   *Analysing 'active' and 'contributing' processes.*

The analysis of 'active' and 'contributing' processes is carried out over the entire year long simulation for the catchment scale model. In particular the components analysed are GW-CH, RF-CH and wetlands discharge to the stream channel (WL-CH = GW-WL + RF-WL). The 'active' processes were determined by summing the total fluxes (GW-CH; RF-CH, WL-CH) at each time step, and the 'contributing' processes (taken at the outlet) are determined from the outlet hydrograph and corresponding components. A long term ratio of 'contributing' to 'active' flow generation mechanisms is calculated to quantify the difference between these two. The components of GW-WL and RF-WL are not considered individually due to the slow turnover time of water within the wetlands, which creates difficulty in separating 'active' processes between the 'contributing' processes.

5   Results and discussion

5.1   Virtual wetland model.

5.1.1   Stream and overland flow generation mechanisms driving flow.

The applied rainfall and the resultant outflow and corresponding flow generation components are shown in Figure 6. From the time rainfall starts, streamflow increases slightly until day 17, at which point the rainfall rate increases significantly. This rain falling directly on the channel contributes to runoff immediately. The infiltration across the overland area increases the subsurface head, which in turn increases the groundwater discharge to the channel. The rapid response of rainfall directly on the channel (RF-CH) is clearly seen to follow the pattern of the rainfall input. During the highest rainfall period, over day 17, the groundwater discharge to the channel rises to an apparent quasi steady-state. In the four days that follow, the GW-CH component only changes slightly in relation to the total streamflow. All major changes in streamflow between days 17 to 22 are attributed to changes in overland flow to the stream. At approximately 17.6 days, the overland flow reaches the channel causing a rapid increase in stream flow. Whilst a greater proportion of rainfall to the wetland area (RF-WL) is evident, it is very interesting to note the large component of groundwater that discharged to the wetland (GW-WL). This large component of GW-WL in the outflow hydrograph appears not only to be an increase in this overland flow generation mechanism at this particular time, but also a result of the mobilisation of the ponded water generated from groundwater discharge to the wetland. The ponding of water in the wetland hollows makes up almost 100% of the surface storage (with the GW-CH and RF-CH water being relatively insignificant). Interestingly, there is only a relatively small variation in the total storage after day 18. It is interesting to note the small component of 'initial' water, which feeds the streamflow hydrograph. The 'initial' water was mobilised after the wetland hollows filled and then spilled 'initial' water toward the stream. This shows a slow rate of turnover of ponded surface water in the absence of activated flow networks.
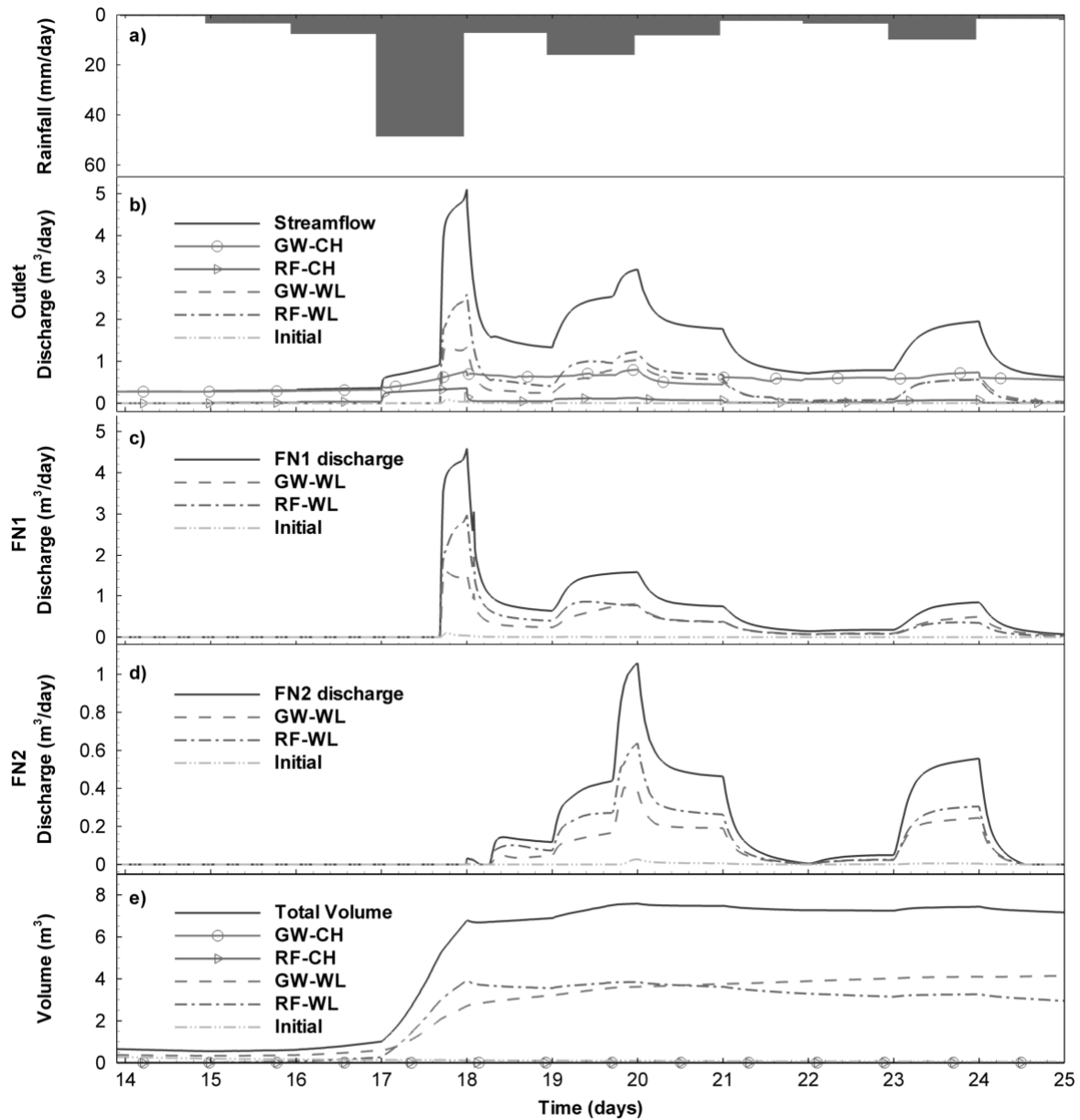
Figure 6: *Hyetograph, outlet hydrograph, FN1 hydrograph, FN2 hydrograph and total surface storage graph for the virtual wetland model during a large storm event. GW-CH and RF-CH are direct groundwater discharge and rainfall to the channel. GW-WL and RF-WL represent groundwater discharge and rainfall to the overland flow area respectively. 'Initial' represents the initial water in the surface domain at the beginning of the simulation. The 'reset' fraction of flow was negligible and hence is not shown.*

5.1.2 *Spatiotemporal variability of stream and overland flow generation.*

Two snapshots of stream and overland flow generation are shown for the virtual wetland model, just before the rainfall event at the start of day14 (Figure 7), and 6 days into the storm event at day 20 (Figure 8). Figure 7 and Figure 8 both show the distribution of: (1) GW-WL water in the hollows, and (2) GW-CH water, which is providing baseflow to the channel. At time 14 days, the rainfall event is only just beginning and therefore there is no RF-CH or RF-WL fraction of surface water (not shown in Figure 7). The reason that the fraction of GW-WL water is not equal to 1 across the hummocks and hollows is because of the persistence of 'initial' water, of which a small volume resides on the surface. The decrease in the 'initial' water is apparent in the total surface storage volume of Figure 6.
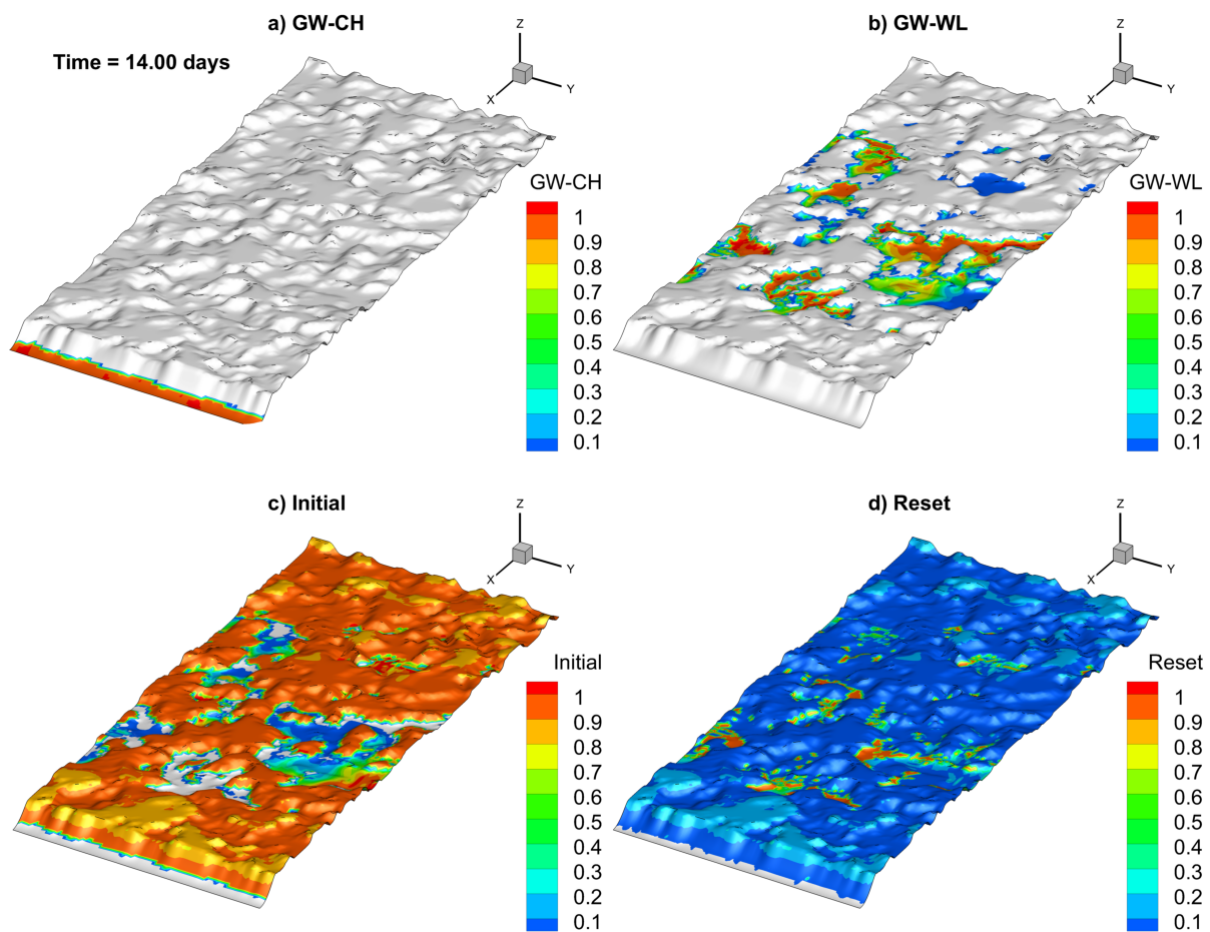

Figure 7: *Virtual wetland HMC fractions at day 14 (pre-storm event). The stream and overland flow generating mechanisms shown are: a) groundwater discharge to the channel (GW-CH), b) groundwater discharge to the wetland (GW-WL). The 'initial' and 'reset' fractions are also shown in c) and d) respectively. A GW-WL fraction of 0.5 denotes that 50% of the water at that HMC was generated from groundwater discharging to the wetland.*

[230]

The development of overland flow in the wetlands is well established by day 20. An increase in the GW-WL component of streamflow is explained by the increased subsurface heads leading to a more developed seepage face along the bank. There are two overland flow networks (identified in Frei *et al.* (2010)) that flow into the stream. Closer examination of these flow networks highlight variations in the overland flow generation across the wetland. The overland flow network on the left (herein denoted as FN1) is dominated by groundwater discharge whereas the flow network on the right (FN2) is dominated by rainfall, with clear spatial variation in each. The flow network FN2 might lend itself to a higher rainfall component because of the larger surface area of the stored water, which will therefore receive more rainfall. The RF-WL fraction is equal to unity atop the hummocks and the upper part of the stream bank because of a negligible volume of ponded water that occurs between the time at which rainfall lands and the time at which infiltration occurs.
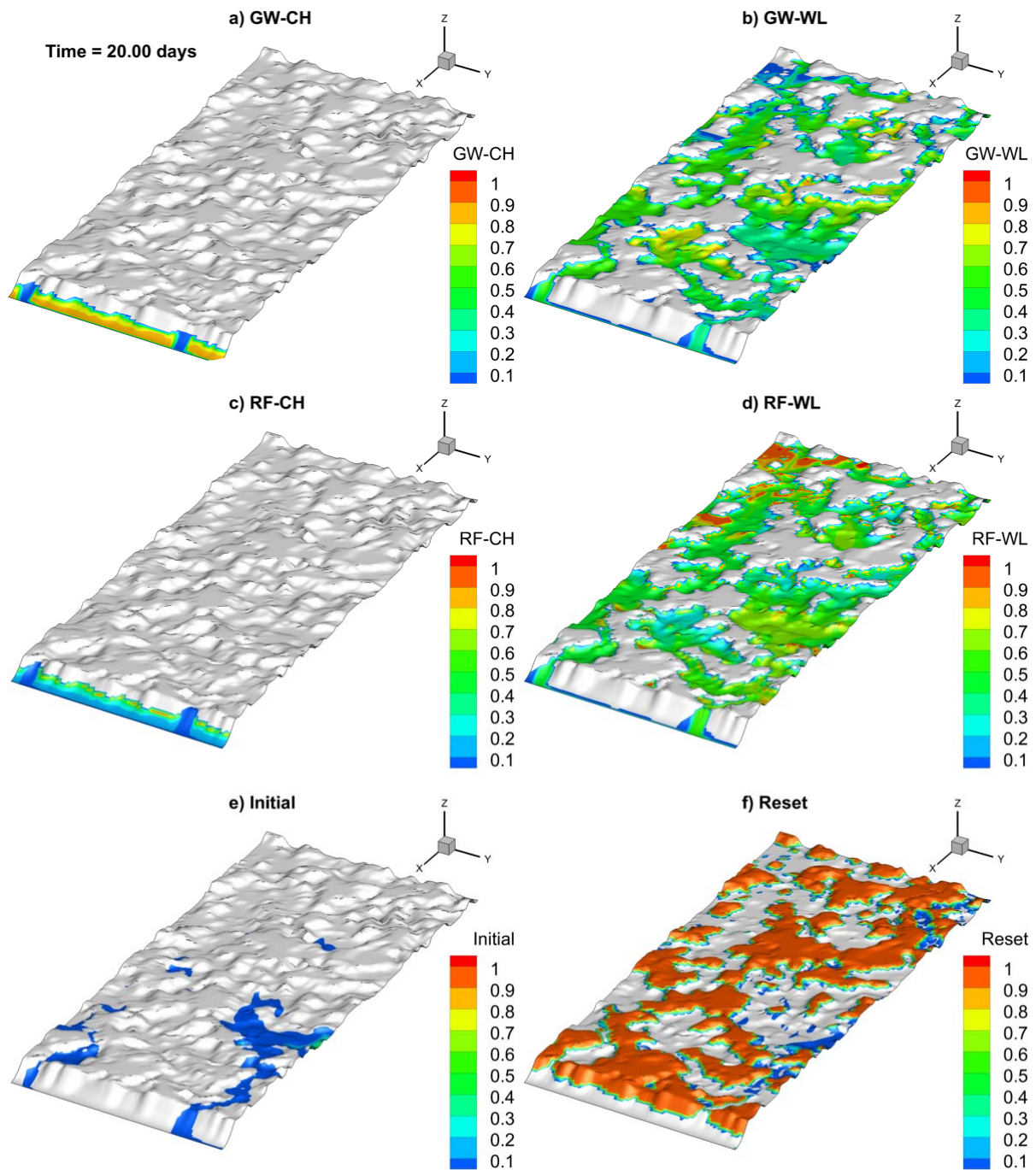
Figure 8: *Virtual wetland HMC fractions at day 20 (during the storm event). Stream and overland flow generating mechanisms shown are: a) groundwater discharge to the channel, b) groundwater discharge to the wetland, c) rainfall to the channel, d) rainfall to the wetland. The remaining 'initial' water (e) and the 'reset' fraction (f) for reset HMCs are also shown. Top right frame of figure shows the two flow networks FN1 and FN2, with the black line denoting the flow network boundary.*

Figure 9 shows a summary of the percentage of total volume of water derived from different stream and overland flow generation mechanisms. This summary is provided at the outlet and each of the flow networks (FN1 and FN2). All volumes were determined by integrating under the flow

hydrographs in Figure 6 (b-d). The contributions towards total flow from the overland flow networks were 34% and 10% for FN1 and FN2 respectively, making a total overland flow contribution of 44% over the simulation period. Not shown in Figure 9 are the components of 'initial' water and 'reset' water, which were insignificant (<1%). The volume attributed to cumulative error was insignificant (7 x 10^{-14}%).
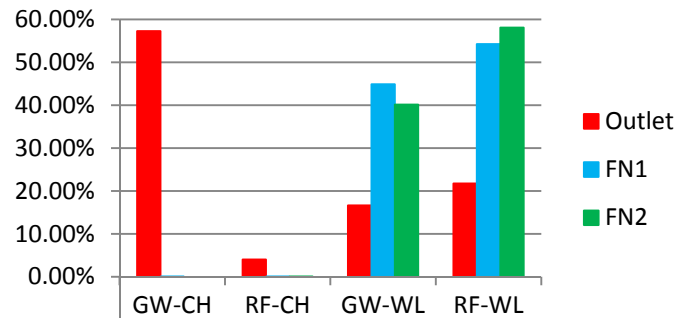

Figure 9: *Comparison of different streamflow generation mechanism contributions at the outlet, FN1 and FN2. The 'initial' and 'reset' fractions and the cumulative error in the HMCs are not shown as they were insignificant.*

The HMC analysis of the virtual wetland model highlights the degree of spatial variability of flow generation processes across the plot at fixed points in time. Similarly the HMC analysis highlights the temporal variability of flow generation processes at the outlet and discharge points of the two FNs.

HMC analysis of the virtual wetland model demonstrated clear spatial variability in overland flow generation. This variability was also clear between the two flow networks (FN1 and FN2). Conversely, direct RF-CH and GW-CH stream generation appears to have a clear functional relationship between the rainfall input and these two streamflow contributors at the outlet. The RF-CH and GW-CH relation is expected given that there are no significant time lags, no losses along the stream to the subsurface, and the subsurface is homogeneous. The GW-CH variation at the outlet appears to relate to the surface storage. The storage across the overland area shows that the relationship between overland storage and overland flow contributions to streamflow at the outlet is non-linear. This non-linear relationship is caused by the complex nature of the 'fill and spill' mechanism.

5.2 Catchment model.

Three snapshots from the model simulation for the large July storm are examined for water distribution, exchanges and flow generation mechanisms. These snapshots are taken just prior to the storm (day 216), at the peak of the storm (day 218), and 2 days after the peak (day 220). Figure 10 shows the standard HGS outputs of surface saturation, exchange flux and depth distribution across the

catchment at each of these times. Figure 10a) shows that saturation at the surface boundary increases across the catchment as the storm event progresses.

The exchange flux (Figure 10b) across the catchment shows where water is flowing from the subsurface to surface (positive values) and where water is infiltrating into the subsurface from the surface (negative numbers). Prior to the storm event there is no exchange across the forested areas, water is being lost from the wetlands to the subsurface, and groundwater is discharging to the stream (denoted by the red). At the peak of the storm, the infiltration rate peaks in the forested areas, but the infiltration from the wetlands decreases. The area of groundwater discharging to the stream is slightly increased but not significantly. At the cessation of the storm event, the infiltration rate is varied across the forested area. It can be seen on the exchange at day 220, that about two thirds of the reach on the right arm of the stream is losing.

The depth distribution (Figure 10c) across the catchment highlights the wetland areas, where most surface ponding occurs. Excluding the stream, these wetland areas lie at the lower most points of the catchment. It is these ponded wetlands that provide the overland runoff during the storm event. There is discharge of groundwater at the upper part of the right arm of the stream, however, this water is returned to the subsurface across the losing stretch of this reach of the stream (highlighted in Figure 10b).
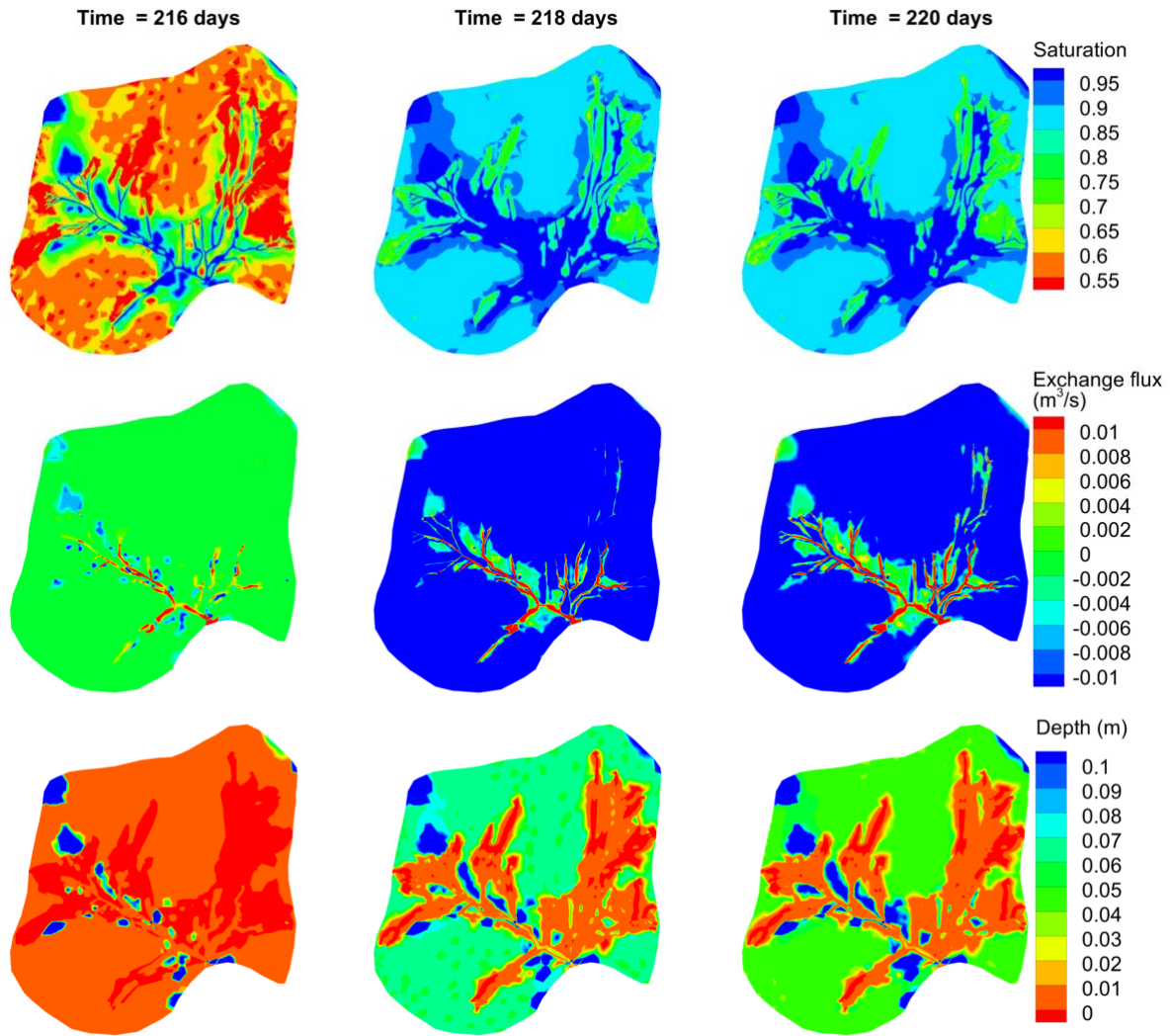
Figure 10: *Simulated surface saturation (a), exchange flux (b) and surface water depth (c), prior to the storm, at the storm peak and 2 days after the storm peak. A losing section on the right arm of the stream is highlighted in the third frame to the right of the exchange flux. Positive values of exchange flux indicate groundwater discharge and negative values indicate infiltration. Note the range of values do not include the maximum and minimum values for saturation, exchange and depth in order to highlight the differences across the catchment. All nodes with values above and below the ranges given are assigned the colour of the maximum or minimum of the range.*

5.2.1   *Stream and overland flow generation mechanisms driving flow.*

The three snapshots showing spatial distribution of the fractions of flow generation in the July storm are insightful. However, interpreting the spatiotemporal outputs with respect to their influence on the outflow hydrograph is nontrivial. Figure 11 illustrates this with a series of deconvoluted streamflow hydrographs (using the HMC method) at the points depicted in Figure 4 (i.e. the outlet and locations 1-6).

In Figure 11b) the GW-CH component of the streamflow is seen to respond immediately to rainfall events with no clear lag, possibly due to propagation of a pressure wave. As rainfall ponds on the hydraulically connected wetlands, this in turn increases the head in the underlying aquifers. The GW-CH component of streamflow is seen to make up ~97% of the flow in dry periods – the GW-WL component of streamflow contributes a very small amount to streamflow during dry periods (~3%). The RF-WL and GW-WL components of the outlet hydrograph (Figure 11b) show that the wetlands only provide a significant component to streamflow during the larger storm events (e.g. at the storm peak, day 218). Furthermore, it is evident from the other streamflow hydrographs (Figure 11c-h) that the GW-WL component is insignificant. After the large storm event from day 221, the streamflow is supported mainly by GW-CH discharge to the stream. The simulation showed the forest area had a negligible contribution to overland flow in the wetlands and hence also to streamflow, and for this reason is not shown in the hydrographs.

Figure 11i) depicts the surface water storage across Lehstenbach catchment with a breakdown of the generation mechanisms, i.e. the mechanism by which the water came into storage. This figure shows that much of the storage in the surface is ponded water in the forested areas. The second largest component of storage is rainfall stored in the wetlands. Notably, the GW-CH and RF-CH generated surface storage are relatively insignificant with respect to total storage, yet they provide the largest contribution to streamflow. The surface water volumes of 'initial', 'reset' and cumulative error are relatively insignificant (i.e. appear as horizontal lines along y = 0 in the graphs) to the flow generation mechanisms and are therefore not shown.
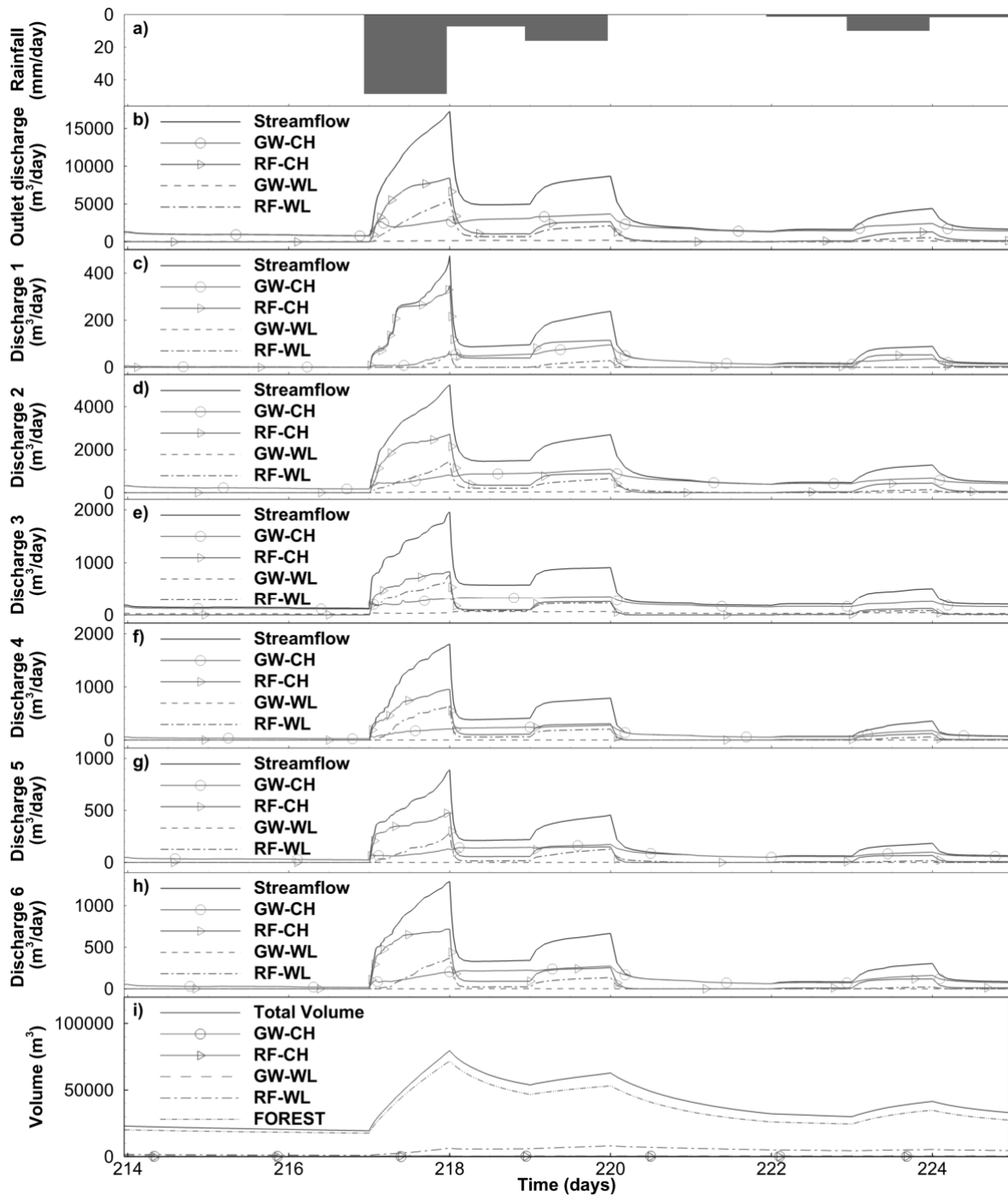
Figure 11: *Hyetograph (a), deconvoluted discharge hydrographs at: the outlet (b) and upstream points 1-6 (c to h), as well as the HMC fractions in surface-storage across the catchment (i). Note that runoff from the forest was negligible (< 1%) in contributing to streamflow and so is not shown in frames (b) to (h).*

5.2.2   *Spatiotemporal variability of stream and overland flow generation.*

The stream and overland flow generation calculated by the HMC method (at the same snapshot times as in Figure 10) for the large July storm are shown in Figure 12. Prior to the storm, the GW-CH component of streamflow over the entire stream is high and dominating. At this time, there are small patches of RF-CH generated stream water in places where little to no groundwater is discharging and where there is no upstream flow passing through. A portion of the wetland areas prior to the storm show GW-WL generated surface storage, a small portion of which is feeding into the stream, which is more clearly apparent in the hydrograph of Figure 11. The 'speckled' RF-WL water existing prior to the storm highlights areas where some ponding from rainfall has occurred that is yet to either runoff, infiltrate or evaporate. The source of this rain is attributed to smaller recent rainfall events (not shown). The bottom row of Figure 12 shows the amount of 'reset' (or unknown) fraction across the catchment during the storm. Areas where the 'reset' fraction is high correspond to areas where either no surface flow is occurring or ponding is insignificant (as defined in section 2.3). This highlights areas where ponding processes take place, but in such small quantities of water that they are not of interest, particularly in relation to the streamflow hydrograph. As noted in the HMC improvements, any reset HMC is still tracked, which means that any surface flow out of a reset HMC is also tracked so that the influence of the reset HMC is accounted for.
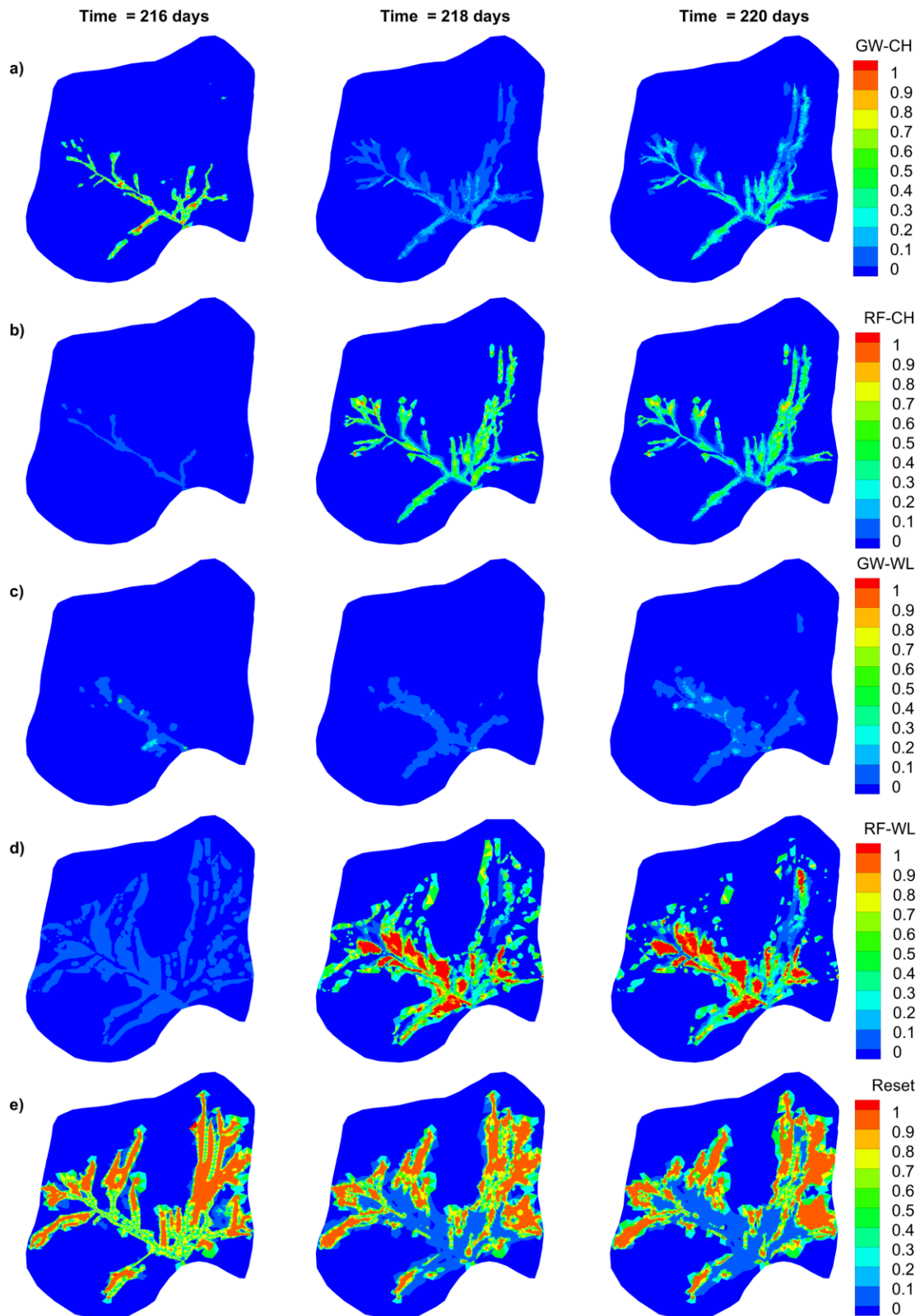
Figure 12: . *HMC calculated stream and overland flow generation for the Lehstenbach catchment – before peak (day 216), at peak (day 218) and after the peak (day 220). The flow generation components are: a) groundwater discharge to the channel (GW-CH), b) rainfall to the channel (RF-CH), c) groundwater discharge to the wetlands (GW-WL), and d) rainfall to the wetlands (RF-WL). The 'initial' fractions are not shown as all initial water has been flushed from the catchment. The 'reset' fractions are shown in row e). The 'initial' fractions are not shown as all initial water has been flushed from the catchment.*

At the peak of the large storm the GW-CH generation becomes diminished across the stream as rainfall generation mechanisms become active. The reduction of the fraction of GW-CH generation is matched by an increase in fractions of RF-CH, GW-WL and RF-WL generation. At the peak of the storm, an increase in the active part of the stream on the right arm (including upstream of the losing section) is shown in the RF-CH generation. The GW-WL generation in the wetlands at the peak of the storm is reduced. However, it is worth noting that the GW-WL water appears in the same area as where water has ponded, shown in the depth distribution in Figure 10. The RF-WL generation is more pronounced across the catchment at the peak in which all areas of ponded water are influenced. The reader is reminded that surface nodes with very little water stored ($< 10^{-10}$ m^3) were excluded from analysis when this criterion was breached (i.e. it became 'reset'), and this plays some role in the 'speckled' effect that is seen adjacent to the upper reaches of the stream. The small water storage at some wetland nodes relates to those wetland nodes not being saturated and water infiltrating quickly due to the high hydraulic conductivity near the surface.

After the peak of the storm event, the GW-CH generation component starts to increase. This increase is most apparent in the lower reaches of the stream where the RF-CH generated streamflow has been mostly flushed from the stream. The RF-CH component is still strong in small isolated areas in upstream parts of the stream that are not flowing, and instead, are ponding. The wetlands experience more groundwater discharge after the storm, which is reflected in the extent of GW-WL generation across the catchment.

Analysis of the entire 2001 hydrological year allowed comparison of the longer term flow generation across the catchment to the July large storm event. Figure 13 shows box plots of the percent contribution of each of the flow generation mechanisms across the 7 model observation points. The left plot shows the spread for the entire hydrological year and the right shows the spread for the large July storm (between 17 and 20 days). The volume of water that passed through the outlet and locations 1-6 was determined by integrating under the streamflow hydrographs for each component of flow and dividing by the total volume of streamflow that passed through. Not shown, are the fractions of 'forest' (maximum 0.3%), 'initial' (maximum 0.05%) and 'reset' (maximum 0.41%) and the cumulative error resulting from imperfect nodal fluid mass balances over the simulation (maximum -0.9%). These components are relatively insignificant in comparison to the four main flow generation mechanisms. This volumetric analysis indicates that the mechanisms for flow generation did not differ significantly across the Lehstenbach catchment, although greater variation can be seen across the focussed period of the large July storm compared to the entire year. However, it is worth noting that the 'outliers' in the 'event' plot correspond to observation point 1, which contributes less than 1% of the flow over this event.
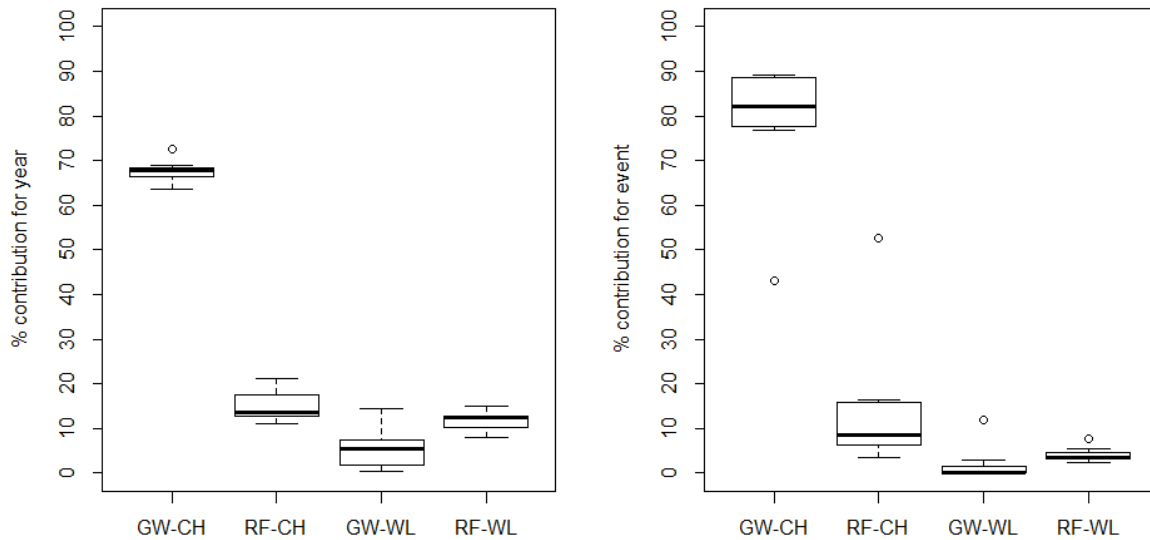
Figure 13: *Box plots showing the spread of streamflow-generation-mechanism contributions during the large storm event and over the entire year, across the 7 different model observation points.*

Comparison of the distribution of individual flow generation processes across the entire hydrological year showed surprising uniformity across the catchment. The similarities in flow generation processes over the year long time scale at the seven model observation locations, is possibly an artefact of the uniformly applied rainfall events and the simplified representation of the micro-topography across the wetlands. The distributions for the event scale showed a larger spread across the seven model observation locations, which was also evident in the individual hydrographs. This difference in the drivers of streamflow across these observation points is possibly due to timing of the activation of WL-CH flow across different areas of wetlands, and the differences in head gradient at the stream interface driving GW-CH flow.

The catchment model showed a combination of simple processes varying in space and time, which led to a complex culmination of stream and overland flow generation processes at the outlet. Rain falling in the forested areas mainly infiltrated and then recharged the underlying unconfined aquifer, which in turn fed the adjacent down-slope riparian wetlands and stream. Because of the 'rill storage' within the wetland areas, there is an aggregated 'fill and spill' mechanism that is averaged over the wetland areas. The rill storage provided a threshold to rainfall inducing runoff from the wetland areas. The GW-CH response to rainfall mimicked a dampened rainfall input. This GW-CH component appeared more sensitive than the GW-WL component, which contributed very little to streamflow. The sensitivity of the GW-CH is caused by the heads in the riparian wetlands controlling groundwater flow. As the wetlands and underlying unconfined aquifer are connected, increases in water levels in the wetlands from rainfall increases subsurface heads and hence increases the discharge of groundwater to the stream channel (i.e. GW-CH generation mechanism). Conversely, the slower, almost filtered response from the GW-WL generation mechanism is caused by: 1) the time delay in percolation recharging the unconfined aquifer from the forested areas; then 2) the slow flow of

groundwater through the unconfined aquifers into the wetlands; then 3) the mobilisation of ponded water in the wetlands into the stream once the wetlands overtop into the stream.

5.2.3   'Active' versus 'contributing' flow generation mechanisms.

A comparison of the 'active' and 'contributing' flow generation processes for GW-CH, RF-CH and WL-CH is shown in Figure 14. In Figure 14a), the 'active' component of GW-CH flow is clearly seen to be higher than the 'contributing' processes which results from losses along the stream. Similarly in Figure 14b) and c) a much larger flux is evident of 'active' RF-CH and WL-CH flow as opposed to the 'contributing' portion at the outlet. This figure highlights a clear difference between the active and contributing processes in this catchment.
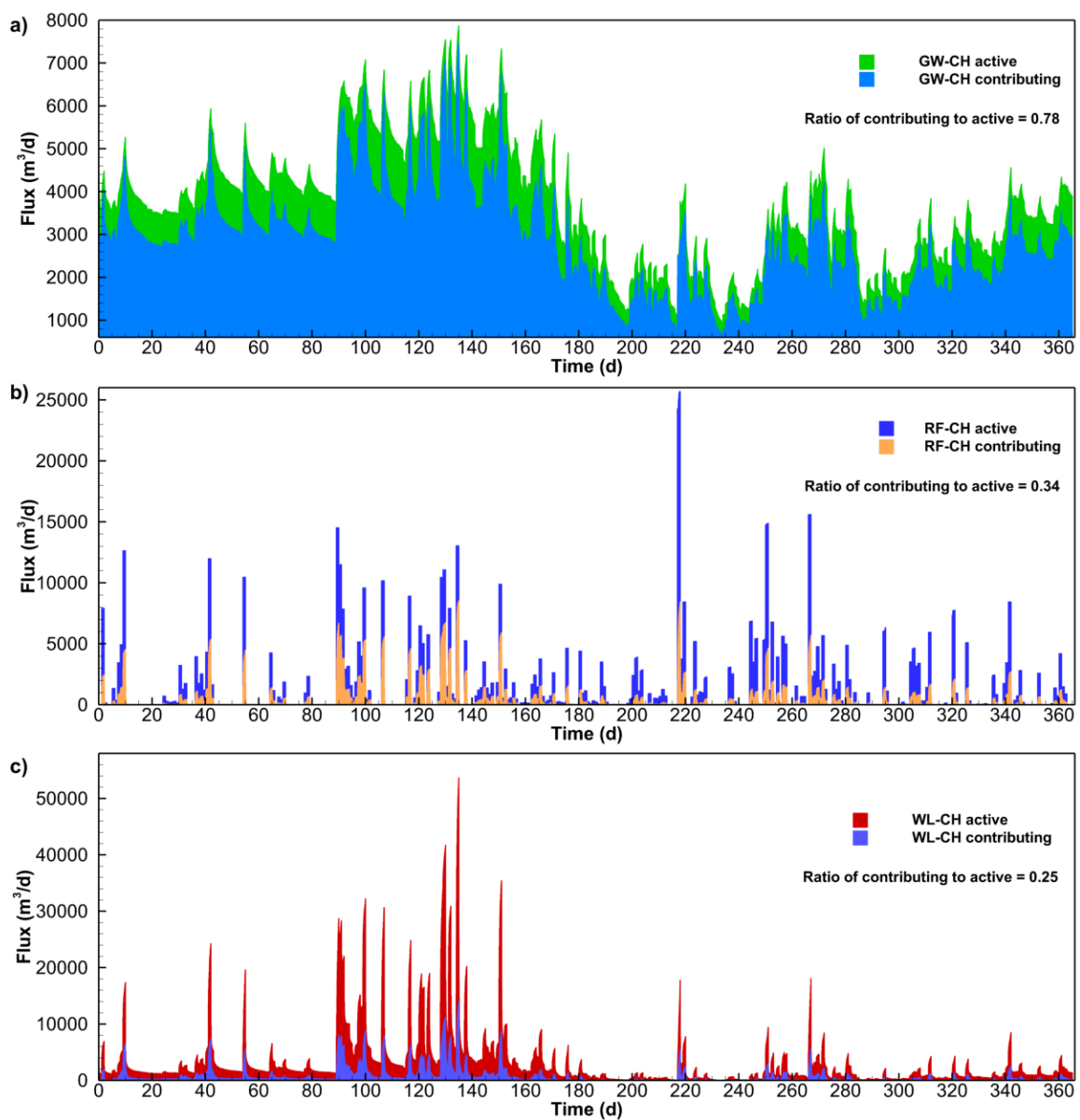

Figure 14: *Comparison of 'active' and 'contributing' processes with respect to a) GW-CH, b) RF-CH, and c) WL-CH (where WL-CH = RF-WL + GW-WL).*

The analysis of 'active' versus 'contributing' WL-CH and GW-CH processes in the catchment model highlighted significant differences between what was happening across the catchment versus what was driving the outflow. This supports the need to differentiate between these processes in interpreting streamflow hydrographs, and therefore, the need to separate the streamflow hydrograph properly. An issue was identified in identifying the 'contributing' overland flow processes, which is attributed to the storage capability of the wetlands. The relatively significant (as compared to flatter micro-topography) storage in the wetlands meant that RF-WL or GW-WL water from one event could reside for days or longer before another event mobilised this water into the stream. To track the specific event processes would require a time or event stamp for these processes, which was outside of the scope of this study, but would be a useful addition to future analysis.

5.3   Comparison of virtual wetland and catchment models.

The nature of the variability in the GW-CH component of the streamflow at the outlet of both models was similar in this modelling study. That is, the GW-CH streamflow generation was fairly consistent across storms with only minor changes relative to the total streamflow hydrograph. This GW-CH component was seen to respond immediately to rainfall with no clear lags in both of the models. Large changes in streamflow at the outlets for both of the models can be attributed to RF-CH generation and the overtopping of rills within the riparian wetlands driven by both groundwater and rainfall. However, the large RF-CH component is an artefact of the model discretisation of the stream. This discretisation doesn't capture the narrow nature of the actual channel meaning it is wider than in the catchment. This resulting increased surface area captures extra rainfall that would not usually be attributed to channel interception.

5.4   Caveats in modelling

The results of the HMC analysis in both models of this study highlight interesting interpretations of stream and overland flow generation. Unfortunately, as with all models, there are some caveats within this modelling study that limit the representation of reality, as well as any generalisations that can come from it. Firstly, this model presents a 'hypothetical reality' (see Mirus *et al*., 2009) of the Lehstenbach catchment due to parameter non-uniqueness issues. The simulations would likely have been influenced by simplification of heterogeneity within soil types, exclusion of macropore flow, and spatiotemporal resolution of rainfall and evapotranspiration inputs (spatially uniform rather than distributed, daily rather than hourly RF and ET). However, addressing these caveats would serve only to complicate the streamflow generation processes further. It is expected that additional heterogeneity and increased complexity of inputs would lead to at least the same or greater spatiotemporal variation in the different flow generation mechanisms. It is not expected that increased complexity would yield homogeneous responses in stream and overland processes, although this is yet to be tested.

5.5 Improved HMC method?

The sub-time scheme of the HMC method was an important improvement which allowed application to more complex problems than those studied in Partington *et al.* (2011 and 2012). The sub-timed HMC was necessary in both of the models, reducing the number of time steps that would have been required with the previously developed HMC method (by 10 million in the catchment year long simulation). The sub-timed scheme allowed the adaptive time-stepping scheme of the flow solution to perform as normal without tight restrictions on the maximum time-step.

The stability constraints used in the improved HMC method were able to ensure stability of the HMCs in the simulations. Interestingly, the 'reset' fractions – resulting from HMCs which were 'reset' due to no surface water flow or very small water storage – highlighted areas that were of little interest with respect to the streamflow generation. The reduction of active HMCs allowed faster computation and highlighted areas where little activity was happening relative to flow generation processes, which is reflected in the spatial distribution of the 'reset' fraction (Figure 7, Figure 8 and Figure 12) and in the actual contributing fraction of flow from reset HMCs.

The expansion of the HMC method to include overland flow generation opened it up to analysing the contributions to streamflow from overland groundwater discharge and overland rainfall. Most importantly, this expansion provided deconvolution of the flow hydrograph into the driving flow generation mechanisms at any model surface node. The HMC method also provided insight into the variability in stream and overland flow generation across both the virtual wetland and catchment model.

6 Conclusions

The shortcomings of previous HMC method implementations were overcome in this study. Specifically the following improvements to the HMC method were achieved: (1) integrating the HMC method within and ISSHM, (2) accounting for overland flow generation mechanisms, (3) developing a sub-timed scheme, and (4) implementing HMC stability constraints. These improvements allowed the analysis of both the stream and overland flow generation components of streamflow hydrographs. This analysis allowed quantification of stream and overland flow generation with respect to the streamflow hydrograph. It also allowed analysis of the variability of stream and overland flow generation at two different scales. Furthermore it allowed for a comparison between the 'active' and 'contributing' processes of stream and overland flow generation.

Through demonstration of the spatiotemporal variability of stream and overland flow generation processes as well as the difference between 'active' and 'contributing' processes, this study highlighted the difficulty in understanding how small reaches of the stream elucidate catchment-wide processes. However, uniformity in processes across larger time scales seemed apparent. Based on this

study, consideration of 'active' flow generation processes at individual hill-slopes, stream reaches or even the whole catchment provides limited insight into the makeup of the streamflow hydrograph. Hydrologists strive for the makeup of the streamflow hydrograph, as it has embedded within it, important information regarding runoff processes in large storm events and the main surface runoff mechanisms supporting streamflow in dry periods. This study demonstrated through numerical modelling, the potential variability that exists in a relatively small catchment.

Further development is recommended in expanding the HMC method to further subdivide the overland flow into saturation-excess and infiltration-excess, which is relatively straight forward. Other improvements could also track flow in the subsurface which would allow tracking of flow generated, for example from macropores and fractures. Extension to the subsurface would also allow identification of the source of recharge areas for groundwater discharge. The inclusion of event or time stamps to the HMC fractions would also serve to improve the HMC method, and allow analysis into time sources (e.g. event and pre-event water).

The HMC method as applied in this work provided a secondary way of assessing catchment functioning within the 'hypothetical reality' of the model. This is a very useful aspect of the HMC method when applied to physically distributed models that have no *a priori* assumption of flow generation processes. The use of the HMC method provides a valuable assessment of whether or not a catchment model behaves in the way desired, or more importantly, the way the catchment processes are conceptualised. In that sense it is useful for a 'soft calibration' based on understanding of catchment functioning from real observation. This can only strengthen the small arsenal of tools currently available for developing catchment models.

Acknowledgements

References

Ambroise, B., 2004. Variable 'active' versus 'contributing' areas or periods: a necessary distinction. Hydrological Processes, 18: 1149-1155.

Bishop, K., Seibert, J., Köhler, S. and Laudon, H., 2004. Resolving the double paradox of rapidly mobilized old water with highly variable responses in runoff chemistry. Hydrological Processes 18: 185–189.

Brunner, P., Cook, P.G. and Simmons, C.T., 2009. Hydrogeologic controls on disconnection between surface water and groundwater. Water Resources Research, 45.

Camporese, M., Paniconi, C., Putti, M. and Orlandini, S., 2010. Surface-subsurface flow modelling with path-based runoff routing, boundary condition-based coupling, and assimilation of multisource observation data. Water Resources Research, 46.

Carle, S.F. and Fogg, G.E., 1996. Transition Probability-Based Indicator Geostatistics. Mathematical Geology 28(4): 453–476.

Ebel, B.A. and Loague, K., 2006. Physics-based hydrologic-response simulation: Seeing through the fog of equifinality. Hydrological Processes, 20(13): 2887-2900.

Ebel, B.A., Loague, K., Montgomery, D.R., Dietrich, E., 2008. Physics-based continuous simulation of long-term near-surface hydrologic response for the Coos Bay experimental catchment. Water Resources Research, 44.

Fleckenstein, J.H., Krause, S., Hannah, D.M. and Boano, F., 2010. Groundwater-surface water interactions: New methods and models to improve understanding of processes and dynamics. Advances in Water Resources, 33(11): 1291-1295.

Freeze, R.A. and Harlan, R.L., 1969. Blue-print for a physically-based digitally simulated hydrologic response model. Journal of Hydrology, 9: 237–58.

Frei, S., Lischeid, G. and Fleckenstein, J.H., 2010. Effects of micro-topography on surface-subsurface exchange and runoff generation in a virtual riparian wetland - A modeling study. Advances in Water Resources, 33(11): 1388-1401.

Gerstberger, P. (Ed.) (2001), Waldökosystemforschung in Nordbayern: Die BITÖK-Untersuchungsflächen im Fichtelgebirge und Steigerwald. Bayreuther Forum Ökologie, (90) 1-193.

Hauck, A. , 1999. Hydrological Charakterization of the Lehstenbach Catchment. Unpublished Diploma Thesis, Department of Ecological Modelling, University of Bayreuth, Bayreuth.

HydroGeoLogic Inc., 2006. MODHMS: a comprehensive MODFLOW based hydrologic modeling system, Version 3.0, Code documentation and user's guide. HydroGeoLogic Inc., Herndon, VA.

Jacks, G., and Norrström, A. C., 2004. Hydrochemistry and hydrology of forest riparian wetlands. Forest ecology and Management, 196(2-3): 187–197.

Jones, J.P., Sudicky, E.A., Brookfield, A.E. and Park, Y.J., 2006. An assessment of the tracer-based approach to quantifying groundwater contributions to streamflow. Water Resources Research, 42(2).

Kruse, J., Lennartz, B., Leinweber, P., 2008. A modified method for measuring saturated hydraulic conductivity and anisotropy of fen peat samples. Wetlands 28(2): 527–531.

Knorr, K. H., Glaser, B. and Blodau, C. , 2008. Fluxes and 13C isotopic composition of dissolved carbon and pathways of methanogenesis in a fen soil exposed to experimental drought. Biogeosciences 5: 1457–1473.

Kollet, S.J. and Maxwell, R.M., 2006. Integrated surface-groundwater flow modeling: A free-surface overland flow boundary condition in a parallel groundwater flow model. Advances in Water Resources, 29(7): 945-958.

Kollet, S.J. and Maxwell, R.M., 2008. Demonstrating fractal scaling of baseflow residence time distributions using a fully-coupled groundwater and land surface model.Geophysical Research Letters, 35(7).

Kristensen, K. and Jensen, S., 1975. A model for estimating actual evapotranspiration from potential Evapotranspiration. Nordic Hydrology 6(3), 170–188.

Linsley, R.K., Kohler, M.A., Paulhus, J.L.H. and Wallace, J.S., 1958. Hydrology for Engineers. McGraw Hill, New York.

Li, Q., Unger, A.J.A., Sudicky, E.A., Kassenaar, D., Wexler, E.J., Shikaze, S., 2008. Simulating the multi-seasonal response of a large scale watershed with a 3D physically-based hydrologic model. Journal of Hydrology, 357: 317-336.

Lischeid, G., Kolb, A. and Alewell, C., 2002. Apparent translatory flow in groundwater recharge and runoff generation. Journal of Hydrology. 265(1-4): 195–211.

Loague, K., Vanderkwaak, J.E., 2002. Simulating hydrological response for the R-5 catchment: comparison of two models and the impact of roads. Hydrological Processes, 16: 1015-1032.

Loague, K., Heppner, C.S., Ebel, B.A., Vanderkwaak, J.E., 2010. The quixotic search for a comprehensive understanding of hydrologic response at the surface: Horton, Dunne, Dunton, and the role of concept-development simulation. Hydrological Processes, 24: 2499-2505.

Mirus, B.B., Loague,. K., Vanderkwaak, J.E., Kampf, S.K. and Burges, S.J., 2009. A hypothetical reality of Tarrawarra-like hydrologic response. Hydrological Processes, 23(7): 1093-1103.

Mirus, B.B., Ebel, B.A., Heppner, C.S. and Loague, K., 2011. Assessing the detail needed to capture rainfall-runoff dynamics with physics-based hydrologic response simulation. Water Resources Research, 47: 18.

Nathan, R.J. and McMahon, T.A., 1990. Evaluation of Automated Techniques for Base-Flow and Recession Analyses. Water Resources Research, 26(7): 1465-1473.

Panday, S. and Huyakorn, P.S., 2004. A fully coupled physically-based spatially-distributed model for evaluating surface/subsurface flow. Advances in Water Resources, 27: 361-382.

Park, Y.J., Sudicky, E.A., Panday, S. and Matanga, G., 2009. Implicit Subtime Stepping for Solving Nonlinear Flow Equations in an Integrated Surface-Subsurface System. Vadose Zone Journal, 8(4): 825-836.

Partington, D., Brunner, P., Simmons, C.T., Therrien, R., Werner, A.D., Dandy, G.C., Maier, H.R., 2011. A hydraulic mixing-cell method to quantify the groundwater component of streamflow within spatially distributed fully integrated surface water - groundwater flow models. Environmental Modelling and Software, 26:886-898.

Partington, D., Brunner, P., Simmons, C.T., Werner, A.D., Therrien, R., Maier, H.R., Dandy, G.C., 2012. Evaluation of outputs from automated baseflow separation methods against simulated baseflow from a physically-based, surface water-groundwater flow model. Journal of Hydrology, 458-459: 28-39.

Pettyjohn, W.A. and Henning, R., 1979. Preliminary estimate of ground-water recharge rates, related streamflow and water quality in Ohio. Ohio State University Water Resources Center Project Completion Report Number 552.

Pinder, G.F. and Jones, J.F., 1969 Determination of the ground-water component of peak discharge from the chemistry of total runoff. Water Resources Research, 5: 438–445.

Price, J. S., McLaren, R.G., Rudolph, D. L., 2009. Landscape restoration after oil sands mining: conceptual design and hydrological modelling for fen reconstruction. International Journal of Mining, Reclamation and Environment 99999(1):1–15.

Schlotzhauer, S. M. and Price, J. S., 1999. Soil water flow dynamics in a managed cutover peat field, Quebec: Field and laboratory investigations. Water Resources Research 35(12): 3675–3683.

Sebben, M.L., Werner, A.D., Liggett, J.E., Partington, D. and Simmons C.T., 2012. On the testing of fully integrated, surface-subsurface hydrological models. In review Hydrological Processes.

Shen, H. W. and Julien, P. Y., 1993. Erosion and sediment transport, Handbook of Hydrology.12.1-12.61.

Shen, C., Phumikar, M.S., 2010. A process-based, distributed hydrologic model based on a large-scale method for surface-subsurface coupling. Advance in Water Resources, 33: 1524-1541.

Sklash, M.G. and Farvolden, R.N., 1979. Role of Groundwater in Storm Runoff. Journal of Hydrology, 43(1-4): 45-65.

Sophocleous, M., 2002. Interactions between groundwater and surface water: the state of the science. Hydrogeology Journal, 10(1): 52-67.

Szilagyi, J., 2004. Heuristic continuous base flow separation. Journal of Hydrologic Engineering, 9(4): 311-318.

Therrien, R., McLaren, R.G., Sudicky, E.A. and Panday, S., 2009. HydroGeoSphere. A Three-dimensional Numerical Model Describing Fully-integrated Subsurface and Surface Flow and Solute Transport. 366.

Van Genuchten, M., 1980. A closed-form equation for predicting the hydraulic conductivity of unsaturated soils. Soil Science Society of America Journal 44(5): 892–898.

VanderKwaak, J.E. and Loague, K., 2001. Hydrologic-response simulations for the R-5 catchment with a comprehensive physics-based model. Water Resources Research, 37(4): 999-1013.

Vivoni, E.R., Entekhabi, D., Bras R.L., Ivanov, V.Y., 2007. Controls on runoff generation and scale-dependence in a distributed hydrological model. Hydrological Earth Systems Science, 11: 1683-1701.

Werb, S., 2009. Simulation der hydrologischen Dynamik im Einzugsgebiet des Lehstenbachs mit dem physikalisch begründeten Modell HydroGeoSphere. Diploma Thesis, University of Bayreuth, Bayreuth.

Wigmosta, M.S., Vail, L.W. and Lettenmaier, D.P., 1994. A distributed hydrology vegetation model for complex terrain. Water Resources Research, 30(6): 1665-1679.

Winter, T.C., 1999.Relation of streams, lakes, and wetlands to groundwater flow systems. Hydrogeology Journal, 7(1): 28-45.

Wittenberg, H. and Sivapalan, M., 1999. Watershed groundwater balance estimation using streamflow recession analysis and baseflow separation. Journal of Hydrology, 219(1-2): 20-33.

Erklärung

Hiermit erkläre ich, dass ich die Arbeit selbständig verfasst und keine anderen als die von mir angegebenen Hilfsmittel benutzt habe.

Ferner erkläre ich, dass ich anderweitig mit oder ohne Erfolg nicht versucht habe, diese Dissertation einzureichen. Ich habe keine gleichartige Doktorprüfung an einer anderen Hochschule endgültig nicht bestanden.

Bayreuth, den 05.10.2012   Sven Frei